Finesse in Quantum Chemistry: Accurate Energetics Relevant for Reaction Mechanisms

Thesis by
Emily Ann Carter

In Partial Fulfillment of the Requirements

for the Degree of

Doctor of Philosophy

California Institute of Technology

Pasadena, California

1987

(Submitted May 20, 1987)

This thesis is dedicated

to my parents,

Rebecca and David Carter

We shall not cease from exploration
And the end of all our exploring
Will be to arrive where we started
And know the place for the first time

T. S. Eliot — Four Quartets

Acknowledgments

I am certain that one of the best decisions I have ever made was to come to Caltech and work with Bill Goddard. From day one, he gave me the freedom to work on whatever interested me, realizing that enthusiasm and love for science must come from within. Even so, Bill's supportive attitude and utter enthusiasm for such an enormous variety of scientific problems is infectious. He challenged me with his quickness: it was always a race to see who could understand new results first and see how best to proceed! In all, he has helped me to develop into the kind of researcher and teacher that I had always hoped to be and for that I am tremendously grateful.

Before I continue, I must say that I am indebted to the National Science Foundation for a predoctoral fellowship, Gemini Industries and the International Precious Metals Institute for a research grant award, and SOHIO for a fellowship in catalysis.

I want to thank Jack Beauchamp for the many stimulating discussions we have had over the years regarding gas phase metal ion chemistry – and even positrons! Others who have made life as a graduate student much more enjoyable are Mary Selman and Greg Voth. Without Mary, my world here would be virtually womanless (a curse of the scientific community). Mary and I have taken turns venting frustrations, comrades-in-arms against subtle, residual prejudices still remaining against women in science. Simply put, she is just a great friend. Greg has not only been a terrific friend, but a stimulating verbal sparring partner. I shall miss our many animated discussions following chemical physics seminars!

I have enjoyed interacting with a number of fellow group members: Art Voter, for his friendship and wisdom; Mark McAdon, for sharing his insights into metal clusters; Jon Hurley, for his friendship and his ceaselessly sarcastic sense of humor; and Terry Coley, for his friendship and his constant barrage of questions which keep me on my toes! I especially want to thank Mark Brusich, not only for critically proofreading large parts of this thesis (for which I am immensely grateful), but for being such a good friend and safety valve, helping to ease the stress level which

tends to build around here. I must also mention Adria McMillan, without whom the Goddard group would most certainly descend into utter chaos. Thanks, Adria, for making order out of ergodicity, and especially for always having a way of brightening every day around Caltech.

Finally, I must thank my family. Thanks go first to my aunt and uncle, Murray and Ruth Blumberg, who have provided me with a home away from home, a sense of security, constancy, and love for as long as I have been at Caltech. Next, I thank my parents, who have given me more love and support than any child could possibly expect. My mother is my lifeline, the link to my emotions, the bond that will be there forever. My father is my soul-mate, I am the continuation of him and I am damn proud of it. For him, continuity is everything; I hope he knows that all he has worked for, and what his parents worked for, will continue on in me. Lastly, I want to thank my husband, Henry Weinberg, for his respect, his understanding, his sense of humor (most of the time), and most of all, his love.

Abstract

A general, systematic approach for calculating accurate energetics for chemical processes within the framework of ab initio electronic structure theory is presented. The correlation-consistent configuration interaction (CCCI) method utilizes generalized valence bond wavefunctions as the starting point for the CI, which emphasizes the inclusion of only the dominant correlations dictated by the physics of the problem. The CI expansion truncates quickly, so that processes involving polyatomic molecules, which could not be addressed with conventional CI methodology, may now be treated easily.

A variety of applications of the method are presented, including the prediction of bond energies, electronic excitation energies, and energetics of chemical reactions, for both organic and transition metal-containing molecules. In cases where experimental data are available, the agreement is generally excellent (within 1-5 kcal/mol). We have used these quantitative results, along with qualitative aspects of the wavefunctions, to assess the bonding in and reactivity of a series of organic, organometallic, and inorganic molecules. These studies have produced a number of simple concepts useful for predicting the stability and reactivity of ligands attached to transition metals. Finally, key mechanistic pathways in two transition metal-catalyzed reactions have been examined using the CCCI approach: (i) the chain initiation step for the Fischer-Tropsch synthesis of hydrocarbons; and (ii) the Ag-catalyzed olefin epoxidation reaction.

Table of Contents

Overview of the Thesis

One primary goal of the work presented herein is to construct a general, systematic approach to predicting quantitatively accurate energetics of chemical reactions. To this end, the correlation-consistent configuration interaction (CCCI) method has been developed and applied to a host of organic and inorganic molecules, with bond energies, excitation energies, and heats of reaction among the predicted energetic quantities. A subsequent, perhaps even more important, objective of this thesis is to extract simple concepts from the theoretical results which allow qualitative predictions of thermodynamic stabilities and chemical reactivity.

We begin by describing the CCCI technique (Chapter 1.A), which is based on the generalized valence bond (GVB) description of molecules. The orbitals of the GVB wavefunction comprise the basis for the CI expansion. The unique aspects of this new CI approach are: (i) the systematic incorporation of all correlations involving electrons directly affected by the process of interest; and (ii) an unbiased description of the initial and final states, maintained by including consistent amounts of correlation for both endpoints. The CCCI expansion truncates fairly swiftly, allowing the method to be applied to molecules for which traditional CI methods would be impractical. The accuracy of the technique is demonstrated for single, double, and triple bond energies in organic molecules, with excellent results for single and double bonds (generally within 1 - 5 kcal/mol of the experimental value) and less accurate results for triple bonds (errors of $\sim$ 10%).

The CCCI approach has also been applied with considerable success to electronic excitation energies. First, Chapter 1.B describes an empirical relationship between bond energies (thermochemistry) and excitation energies (spectroscopy), which is used to estimate singlet-triplet splittings in substituted carbenes from the relative bond weakening in substituted olefins and methanes. The central idea behind this empirical approach is that a carbene with a singlet ground state is nonbonding, and it must be promoted to the triplet state in order to form bonds.

As a result, bonds formed to the carbene are weakened by this promotional energy (the singlet-triplet gap). Chapters 1.C and 1.D provide predicted values from CCCI calculations of the singlet-triplet splittings in a variety of carbenes [CXY = CH_2, CF_2, CCl_2, CHF, CHCl, and $CH(SiH_3)$]. Experimental values and the empirical results of Chapter 1.B are generally in good agreement with the ab initio predictions. Qualitatively, the ground states of CXY may be understood by considering only charge transfer and steric effects, where electron withdrawing substituents with pπ lone pairs favor singlet ground states, and where electropositive, bulky groups favor triplet ground states.

Chapter 1 ends with a calculation of the bond energy in tetrafluoroethylene (Chapter 1.E), as a test of the assumptions built into Chapter 1.B and as a further test of the CCCI method. In the empirical relationship derived between bond energies and excitation energies, we assume that the *intrinsic* strengths of C-H and C=C bonds remain constant with substitution at carbon. Since C_2F_4 is expected to perturb the C=C bond (relative to ethylene) more than any other halogenated olefin, it should provide an upper limit to the error of this assumption. We find that the intrinsic C=C bond strengths (the energy required to dissociate to triplet fragments) in C_2H_4 and C_2F_4 are nearly the same, with the intrinsic C=C bond energy in C_2F_4 only $\sim$ 4 kcal/mol larger than in C_2H_4, even though their adiabatic bond strengths differ by more than 100 kcal/mol! Three conflicting experimental values for the adiabatic $F_2C{=}CF_2$ bond energy exist in the literature, ranging from 53.4 to 76.3 kcal/mol. We predict a value of D_{298} = 64.5 kcal/mol, in good agreement with the most recent experimental value (derived from the heats of formation of CF_2 and C_2F_4) of 69.0$\pm$2.7 kcal/mol.

In sum, Chapter 1 introduces the CCCI technique and presents applications for the prediction of bond energies and excitation energies in organic molecules. In addition, Chapter 1 has provided substantial support for the empirical relationship between molecular bond energies and the promotional energies in the fragments from which they are composed.

Chapter 2 discusses the fundamental aspects of the interaction between transition metal centers and their ligands. Chapters 2.A, 2.B, and 2.C discuss results for two representative early and late transition metal carbene cations, while Chapter 2.D focuses on the differences between early and late metal-oxo bonding. A postscript must be added to the bond energy reported for $Cr{=}CH_2^+$ (48.6 kcal/mol) in Chapter 2.A, which was in disagreement with the only experimental value available at the time (65±7 kcal/mol[1]). After the theoretical prediction of 49 kcal/mol was published, the experiment was repeated under different conditions. The revised experimental value is 52±3 kcal/mol,[2] in excellent agreement with the earlier theoretical result. A prediction of the electronic state splittings in $CrCH_2^+$ (Chapters 2.A and 2.C) also prompted an experimental investigation, using translational energy loss spectroscopy to determine the excitation energies. Those results are in good agreement with our early work and are presented, along with new theoretical results, in Appendix 1.

The central idea presented in Chapters 2.A - 2.C is that properties of transition metal carbenes may be predicted qualitatively merely by considering the electronic state of the metal center, as induced by the presence or lack of ancillary ligands, and by considering the electronic state of the carbene (Chapter 1). In addition to the quantitative results, Chapter 2.A points out the importance of exchange interactions for unsaturated metal centers in the determination of the properties of metal-ligand bonds, Chapter 2.B presents a new way of viewing oxidation states which is based on where the electrons physically reside (as opposed to the traditional, purely ionic convention for electron counting), and Chapter 2.C discusses the relative stabilities of covalent versus donor-acceptor bonding and terminal versus bridge bonding, as a function of the transition metal and of the substituents on the carbene (as in Chapter 1).

Chapter 2.D discusses terminal metal-oxo bonding as a function of metal, concluding that the stability and reactivity of metal-oxo systems may be understood just by considering the electronic state of the metal center. The general result is

that early metals can form strong bonds to oxygen which render the oxo ligand inert, while late metals form weaker, biradical-type bonds to oxygen, yielding an extremely reactive oxo species which may act as an oxidant or oxygen atom transfer reagent.

In order to relate the work of the previous sections to properties of coordinatively saturated metal complexes, Chapter 2.E concludes by presenting a scheme for converting the experimental or theoretical values for coordinatively unsaturated M-X bond strengths (e.g., those reported in the previous sections) to those appropriate for coordinatively saturated or low spin unsaturated complexes (which are mostly unknown). Simple additive factors, based solely on the atomic properties of the metal itself, are applied to single, double, and triple bonds.

The final two chapters are concerned with mechanisms of catalytic reactions. Chapter 3 discusses GVB/CCCI results of modeling the chain initiation step of the Fischer-Tropsch reductive polymerization of CO to hydrocarbons and oxygenates, in which a surface-bound CH_2 is thought to insert into a surface-bound H. We find that the migratory insertion of CH_2 into an adjacent metal-hydrogen bond (Ru-H, in this case) is subject to an activation barrier of $\sim$ 11 kcal/mol and is exothermic by $\sim$ 10 kcal/mol. These values were obtained by two independent approaches, with excellent agreement between the two methods (deviations of 1-2 kcal/mol). We have also estimated (from a thermodynamic cycle) the exothermicity of the chain propagation step (CH_2 inserting into an metal-alkyl bond) to be 4 kcal/mol, with a higher barrier expected due not only to the lowered exothermicity, but also due to the necessary reorientation of the alkyl group during the insertion. Consistent with these ideas, the primary product from undoped catalysts is generally methane, produced from the less activated chain initiation step.

The focus of Chapter 4 is to model the heterogeously-catalyzed ethylene epoxidation process as it occurs on supported Ag catalysts. We have carried out GVB/CCCI calculations for adsorbates on Ag clusters (primarily Ag_3) in order to accurately predict sorely needed adsorbate-surface binding energies as a function

of adsite. The binding energies, in conjunction with the qualitative features of the wavefunctions, allow us to present a new interpretation of a series of epoxidation experiments performed on single crystals of Ag, and, most importantly, we present a global picture of various reaction steps, of the nature of the oxygen species active for epoxidation, and of the role of promoters in this catalytic reaction.

Thus, we will show in the ensuing chapters that the CCCI approach to calculating energetics is accurate for a wide variety of molecular processes. The predicted energetic quantities, when used in conjunction with qualitative properties of the electronic wavefunction, provide a powerful tool for assessing the feasibility of reaction mechanisms.

References

(1) P. B. Armentrout, L. F. Halle, and J. L. Beauchamp, J. Am. Chem. Soc. **103**, 6501 (1981).

(2) N. Aristov and P. B. Armentrout, J. Am. Chem. Soc. **108**, 1806 (1986) and references therein.

Chapter 1

The Correlation-Consistent CI Approach: Theory and Applications to Bond Dissociation and Electronic Excitation in Organic Molecules

Chapter 1.A. The text of this section is a Letter coauthored with William A. Goddard III and is to be submitted to *Chemical Physics Letters.*

Correlation-Consistent Configuration Interaction: Accurate Bond Dissociation Energies from Simple Wavefunctions

Emily A. Carter and William A. Goddard III*

Contribution No. 7576 from the Arthur Amos Noyes Laboratory of Chemical Physics, California Institute of Technology, Pasadena, California 91125

Abstract: We have developed a general method employing relatively small but well-defined CI expansions for calculating accurate bond energies [e.g., errors of 1.4 kcal/mol (1.3%) for the C-H bond energy in CH_4 and 4.9 kcal/mol (2.7%) for the C=C bond energy in ethylene]. The approach includes in a systematic way all correlations involving orbitals that change significantly during bond breakage. The CI expansion truncates rapidly, enabling the application of this technique to polyatomic molecules for which normal correlation approaches would be prohibitively expensive. Thus the bond energy for BH is calculated to within 0.3 kcal/mol of the full CI value, incorporating less than 0.1% of the spin eigenfunctions. For CH_4, CH_3, CH_2, and CH this correlation-consistent CI (CCCI) method leads to accuracies of 1-7 kcal/mol. The double bond energy for C_2H_4 is excellent: $D_e^{calc}(H_2C{=}CH_2) = 174.1$ versus $D_e^{expt} = 179.0 \pm 2.3$ kcal/mol. However, the method is much less accurate for triple bonds: $D_e^{calc}(HC{\equiv}CH) = 214.3$ versus $D_e^{expt} = 236.1 \pm 0.7$ kcal/mol. The advantage of CCCI is illustrated for C_2F_4, where a full CI would involve $\sim 7 \times 10^{22}$ spatial configurations, but only 1,719 are used in CCCI. Here we obtain a C=C bond energy for C_2F_4 (where experimental values range from 53 to 76 kcal/mol) of $D_e(F_2C{=}CF_2) = 68.3 \pm 2.5$ ($D_{298} = 64.6 \pm 2.5$) kcal/mol.

I. Introduction

Accurate bond dissociation energies are essential in assessing chemical reaction mechanisms. Unfortunately, current experimental thermochemical data (especially for organic radicals and inorganic complexes) often have error bars of 5-10 kcal/mol or more.[1] We propose an approach for obtaining greater accuracy with practical ab initio calculations for systems of experimental mechanistic interest. Our goal is to develop methods equally applicable (and accurate) for molecules containing heavy atoms or transition metals as for first row molecules. In order to be useful, it is important to obtain accuracies better than 5-7 kcal/mol. Thus our efforts are directed at achieving quantitative accuracy within a small CI expansion so that the technique can be applied to a wide variety of large molecules.

Our method involves a systematic approach for treating both the molecule and the fragments after bond rupture with consistent levels of electron correlation. Thus we focus on the dominant correlations important in bond breakage. This *correlation-consistent CI* (CCCI) method[2] is also applicable to excitation energies (e.g., singlet-triplet splittings in substituted carbenes[3]) and is applied below to the doublet-quartet splitting in CH.

In the next section, we outline correlation-consistency in the calculation of bond energies. To compare the accuracy of the method to a full CI result, we find that for BH, the CCCI leads to a bond energy within 0.3 kcal/mol of the full CI,[4] although the CCCI has only one-thousandth of the configurations of the full CI. Section III reports CCCI results for the four C-H bond energies of methane, the C=C bond energy in ethylene, and the C≡C bond energy in acetylene. An illustration of the power of this CCCI approach is given for the C=C bond energy for C_2F_4, a molecule for which the experimental data vary over a range of 23 kcal/mol and for which a full CI is currently out of the question ($\sim 7 \times 10^{22}$ spatial configurations for full CI, but only 1719 spatial configurations for CCCI).

II. Theoretical Method

Generalized Valence Bond Wavefunctions

For bond breaking/making processes, the many-electron wavefunction must dissociate smoothly to fragment wavefunctions. This dictates an approach based on the valence bond wavefunction (Ψ^{VB}), which unlike the molecular orbital wavefunction (Ψ^{MO}), has the correct form for proper dissociation[5] to fragment atomic orbitals for $R_{bond} = \infty$. The variational counterparts to VB and MO wavefunctions are the self-consistent field generalized valence bond (GVB) and Hartree-Fock (HF) wavefunctions, in which the orbitals are expanded in a basis set and optimized self-consistently. Our starting point, then, for the CCCI calculations is the GVB wavefunction,[6-7] since it has the correct functional form for proper dissociation (while HF often dissociates to an ionic limit).

For the GVB calculations, only the orbitals comprising the breaking bond are treated as GVB pairs,

$$\Psi^{GVB} = [\phi_a(1)\phi_b(2) + \phi_b(1)\phi_a(2)](\alpha\beta - \beta\alpha), \tag{1}$$

where ϕ_a and ϕ_b are the variationally-optimized, overlapping, one-electron GVB orbitals. All other electrons in the molecule are treated at the HF level.

Since the number of overlapping terms in the full GVB wavefunction increases as N!, where N is the number of (overlapping) orbitals,[6] it is more effective to do the calculations in terms of orthogonal orbitals. This is accomplished by rewriting each GVB pair in (1) in the natural orbital representation

$$\Psi^{NO} = [C_g\phi_g^2 + C_u\phi_u^2](\alpha\beta - \beta\alpha), \tag{2}$$

where ϕ_g and ϕ_u are the (orthogonal) bonding and antibonding natural orbitals of a GVB pair. For a multipair system, this wavefunction

$$\Psi^{PP} = A[\Psi^{NO}(1,2)\Psi^{NO}(3,4)\ldots] \tag{2'}$$

has a product of terms as in (2) and is a special case of the full GVB wavefunction, since the full GVB wavefunction allows all possible spin couplings of the various orbitals, whereas (2′) has just a single valence bond or perfect pairing (PP) term. The GVB-PP wavefunction builds in "static correlation" between the electrons in each GVB pair, by allowing them to each occupy their own orbital, on average staying farther apart from one another than if they were restricted to occupy the same spatial orbital (as in Restricted HF theory).

Restricted CI Calculations (RCI)

Expanding the GVB-PP wavefunction (2′) in terms of natural orbitals (2) leads to a total of 2^M N-electron configurations where M is the number of GVB pairs. A close approximation to the full GVB wavefunction is obtained with the GVB-Restricted CI (RCI) wavefunction in which each pair is allowed to have all three possible occupations of the two electrons associated with that pair of orbitals, leading to 3^M configurations. The RCI lifts the spin-coupling restriction and also builds in interpair correlation (ionic configurations) in which movement of charge in one bond pair induces simultaneous movement of charge in an adjacent bond pair. In general, the RCI wavefunction provides a reasonable description of most molecules by allowing for optimization of spin-coupling and by including the dominant interpair and intrapair correlations.

In order to obtain very accurate energetics, we must go beyond a valence level CI, including correlations involving excitations to virtual (unoccupied) orbitals. In particular, the CCCI method takes into account two other important sets of correlations crucial for describing the changes in the valence orbitals during bond rupture. First we allow full correlation (within the basis) of the two electrons involved in the breaking bond (using the RCI configurations as reference states). Thus we allow all single and double excitations from each (breaking) bond pair to all other orbitals. This is denoted RCI^*SD_{bond}. Since bond dissociation generally leads to geometric and hybridization changes in the resultant fragments, we expect

that the shapes of the remaining orbitals will also be altered in the bond dissociation event. The second set of configurations included in CCCI is designed to allow for orbital shape changes among the valence orbitals not involved in the breaking bond. Thus to the RCI^*SD_{bond} configurations we add, from each RCI configuration, all single excitations from the valence space to all virtuals (RCI^*S_{val}).[8]

BH Test

These two sets of configurations supply the dominant correlations important in bond breaking processes. As a rigorous test of how well this CCCI expansion performs relative to a full CI,[4] we considered the BH molecule. The experimental D_e(B-H) = 82.3 kcal/mol,[9] while the six-electron full CI within a DZP basis (132,686 spin eigenfunctions) yields 78.9 kcal/mol.[4] The CCCI method applied to the same basis (110 spin eigenfunctions) yields D_e(B-H)=79.2 kcal/mol, in excellent agreement with the full CI (and experimental) value.[10] This indicates that CCCI, with only one-thousandth of the configurations, accounts for most of the differential correlation present in the breaking bond. This suggests CCCI as a practical method for larger systems, where full CI calculations would be impractical.

Multiple Bonds

The simplest extension of the CCCI method to double and triple bonds is to include the configurations corresponding to all single and double excitations out of each bond separately. These $RCI^*[SD_{bond\ 1} + SD_{bond\ 2} + \cdots + S_{val}]$ calculations dissociate to fragments at the HF^*S_{val} level. That is, the correlations included at the equilibrium molecular geometry for the CCCI reduce to HF*S in the limit of $R_{bond} = \infty$. Note that we do *not* allow single and double excitations from more than one bond at the same time because that calculation is *not* dissociation-consistent. It would include some double excitations on fragments, which require triple and quadruple excitations on the molecule in order to be consistent.

Basis Sets

In all calculations, the carbon atom was described by Dunning's valence double-ζ contraction[11] of Huzinaga's (9s5p) basis set,[12] augmented by one set of cartesian 3d polarization functions with the 3s combination removed ($\zeta^d = 0.64$).[13] The hydrogen atoms were described with Dunning's double-ζ contraction[11] (scaled by 1.2) of Huzinaga's[12] (4s) basis set, with one set of 2p polarization functions ($\zeta^p = 1.0$) added only to the H atom involved in the breaking bond. Dunning's valence double-ζ contraction[11] of Huzinaga's (9s5p) basis set[12] for fluorine was also used.

Geometries

Experimental geometries were used for CH_4, CH_3, the $^2\Pi$ and $^4\Sigma^-$ states of CH, C_2H_4, C_2F_4, and C_2H_2.[14] The equilibrium geometries of CH_2 ($^1A_1$) and CH_2 ($^3B_1$) were taken from the GVB-POL-CI calculations of Harding and Goddard[15] and the geometries of CF_2 ($^1A_1$) and CF_2 ($^3B_1$) were taken from the GVB(1/2) calculations (within the largest basis) of Bauschlicher *et al.*.[16]

III. Results

CH Bonds

The total energies calculated at levels ranging from HF to HF*S*D (CI-SD) to RCI*[$SD_{C-H} + S_{val}$] (CCCI) for CH_X (X = 0-4) are listed in Table I and the corresponding successive C-H bond energies are shown in Table II. The CCCI method gives excellent results (within 1-3 kcal/mol) for the first two bond energies in methane, with the agreement less good (within 5-7 kcal/mol) for the second two bond energies in CH_4. The values obtained with the present method are considerably better than the much more extensive studies of conventional CI methodology (e.g., HF*S*D), due to the errors of triple and quadruple excitations not included at R_e for HF*S*D. The exception is the C-H bond energy in CH_2 ($^3B_1$), where HF*S*D actually obtains a better bond energy than CCCI. This is due to the bias toward stabilizing high-spin states for HF*S*D. Thus CH_2 ($^3B_1$) is overstabilized

and CH ($^2\Pi$) is artificially destabilized, leading to a good bond energy through cancellation of errors. Furthermore, the range of error for HF*S*D bond energies in CH_4 is larger than for CCCI (4-10 kcal/mol), including an order of magnitude more spin eigenfunctions than CCCI.

Two multireference CI calculations of the first C-H bond energy in CH_4 have been reported previously: (i) a CASSCF/MRD-CI[17] with 63,608 configurations yielded $D_e(H_3C\text{–}H) = 104.3$ kcal/mol and (ii) a CASSCF/CCI[18] with 613,941 configurations afforded $D_e(H_3C\text{–}H) = 109.7$ kcal/mol. Our CCCI result, with only 241 (correlation-consistent) configurations, leads to $D_e(H_3C\text{–}H) = 110.5$ kcal/mol.

Since the CCCI method requires treatment of correlation equivalently at both endpoints (infinity and R_e), two sets of bond energies are listed for CH_2. The C-H bond in ground state CH_2 ($^3B_1$) is formed from the excited state of CH ($^4\Sigma^-$). However, the C-H bond in the $^1A_1$ excited state of CH_2 is formed from the ground state of CH ($^2\Pi$). The thermodynamic cycle to calculate the adiabatic bond energy [the energy to go from CH_2 ($^3B_1$) to CH ($^2\Pi$) + H (^2S)] includes:

(i) (first column entry) CH_2 ($^3B_1$) $\overset{\Delta E_{ST}}{\longrightarrow}$ CH_2 ($^1A_1$) $\overset{D(C-H)}{\longrightarrow}$ CH ($^2\Pi$) + H (^2S)

where $\Delta E_{ST}^{calc}(CH_2) = 9.0$ kcal/mol[3]

and

(ii) (second column entry) CH_2 ($^3B_1$) $\overset{D(C-H)}{\longrightarrow}$ CH ($^4\Sigma^-$) + H (^2S) $\overset{-\Delta E_{DQ}}{\longrightarrow}$ CH ($^2\Pi$) + H (^2S).

The $^4\Sigma^- - {}^2\Pi$ state-splittings of CH shown in Table III were calculated correlation-consistently using the same CI method which accurately predicts singlet-triplet gaps in substituted carbenes.[3] This is accomplished by allowing all single and double excitations to all virtuals from the electron pair involved in the excitation from doublet to quartet. These excitations are taken from RCI reference configurations where the RCI involves correlation of the C-H bond pair [GVB(1/2)]. This correlation-consistent treatment results in a $\Delta E_{DQ} = 16.4$ kcal/mol, excellent agreement with experiment ($\Delta E_{DQ}^{expt} = 16.7$ kcal/mol).[9]

Multiple Bonds

Table IV compares adiabatic C-C bond energies at various levels for ethylene and acetylene. Both HF and HF*S*D fall considerably short (20-50 kcal/mol) of the final CCCI values, which yield excellent agreement for the C-C double bond but less acceptable agreement for the triple bond. Clearly for triple bonds, simultaneous correlations (up through quadruple or even sextuple excitations to virtuals) must be necessary to approach the experimental value, while for double bonds, such simultaneous excitations appear to be much less important. The possibility of symmetric bent or "banana" bonds in C_2H_2 was explored to see if such a description could account for the correlation error. We find the CCCI bond energies with a bent bond description to be the same to within 0.3 kcal/mol as with one σ and two π bonds.[19]

$D(F_2C{=}CF_2)$

Finally, we applied the CCCI method to the bond energy of C_2F_4. The size of this system precludes full CI treatment ($\sim 10^{23}$ spatial configurations), but it requires only 1719 spatial configurations for CCCI. The experimental value for $D_{298}(F_2C{=}CF_2)$ is extremely uncertain, with values ranging from 53.4±0.7 to 76.3±3 kcal/mol.[20-22] Dissociating the σ and π bonds of C_2F_4[23] smoothly produces excited CF_2 ($^3B_1$) fragments. Thus, C=C bond cleavage can be most simply described by a CCCI of C_2F_4 dissociating to two CF_2 ($^3B_1$) fragments, followed by a CCCI deexcitation of each CF_2 ($^3B_1$) to the ground state of CF_2 ($^1A_1$). The CCCI result for $D_e(F_2C{=}CF_2)$ is 63.4 kcal/mol (Table V). Assuming the same residual correlation error occurs in C_2F_4 as in C_2H_4 ($\Delta_{corr} = D_e^{expt} - D_e^{CCCI} =$ 4.9±2.5 kcal/mol), this leads to (Table V) an estimated adiabatic bond energy of $D_e(F_2C{=}CF_2)$ = 68.3±2.5, a zero temperature value (including zero-point energy) of D_0 = 63.6±2.5, and a room temperature value of D_{298} = 64.6±2.5 kcal/mol.[24] The ubiquitous theoretical approach, HF*S*D, includes an order of magnitude more configurations than CCCI, but yields a bond energy low by 30-40 kcal/mol!

The CCCI result may be compared with three experimental values of 53.4±0.7,[20] 69.0±2.7,[21] and 76.3±3 kcal/mol.[22] The theory rules out the lowest value and agrees rather well with the intermediate value. Using $\Delta H^0_{f,298}(C_2F_4)$ = −157.4±0.7 kcal/mol,[24b] our calculations lead to $\Delta H^0_{f,298}(CF_2) = -46.5 \pm 1.6$ kcal/mol, supporting the experimental value of $\Delta H^0_{f,298}(CF_2) = -44.2 \pm 1$[1i] rather than −52. kcal/mol.[20]

IV. Conclusions

We present the simplest wavefunction emphasizing *correlation-consistency* while including the *dominant electron correlations* dictated by the physics of bond dissociation. This avoids the biases plaguing conventional CI-SD approaches, while retaining a minimum number of configurations. For single and double bonds, the method predicts bond energies in good agreement (errors of 1-7 kcal/mol) with experiment. However, for triple bonds the errors are much larger (~22 kcal/mol). An indication of the power of this approach is given for C_2F_4 where CCCI leads to an expected accuracy of 2.5 kcal/mol for 1719 configurations, while HF*SD CI utilizes 18,772 configurations, engendering an error of 30 kcal/mol, and full CI would require $\sim 10^{23}$ configurations. Thus the error of CCCI is considerably less than the dispersion in experimental values.

Acknowledgments. This work was supported by the National Science Foundation (Grant No. CHE83-18041) and the Shell Companies Foundation. EAC acknowledges a National Science Foundation predoctoral fellowship (1982-1985), a research grant award from the International Precious Metals Institute and Gemini Industries (1985-1986), and a SOHIO fellowship in Catalysis (1987).

References

(1) For inorganic complexes see, for example: a) J. L. Beauchamp, A. E. Stevens, and R. R. Corderman, Pure and Appl. Chem. **51**, 967 (1979); b) P. B. Armentrout and J. L. Beauchamp, J. Am. Chem. Soc. **103**, 784 (1981); c) P. B. Armentrout, L. F. Halle, and J. L. Beauchamp, J. Am. Chem. Soc. **103**, 6501 (1981); d) M. A. Tolbert and J. L. Beauchamp, J. Phys. Chem. **90**, 5015 (1986); e) R. L. Hettich and B. S. Freiser, J. Am. Chem. Soc. **108**, 2537 (1986). For organic radicals see, for example: f) D. F. McMillen and D. M. Golden, Ann. Rev. Phys. Chem. **33**, 493 (1982); g) S. G. Lias and P. Ausloos, Int. J. Mass Spec. Ion Phys. **23**, 273 (1977); h) P. Ausloos and S. G. Lias, J. Am. Chem. Soc. **100**, 4594 (1978); i) D. Berman, D. S. Bomse, and J. L. Beauchamp, Int. J. Mass Spec. Ion Phys. **39**, 263 (1981); j) S. G. Lias, Z. Karpas, and J. F. Liebman, J. Am. Chem. Soc. **107**, 6089 (1985).

(2) (a) R. A. Bair and W. A. Goddard III (submitted for publication) developed a somewhat more complex dissociation-consistent CI approach also based on GVB wavefunctions. (b) See R. A. Bair, Ph. D. thesis, California Institute of Technology, 1981.

(3) a) E. A. Carter and W. A. Goddard III, J. Chem. Phys. **86**, 862 (1987); b) *ibid.*, submitted for publication.

(4) R. J. Harrison and N. C. Handy, Chem. Phys. Lett. **95**, 386 (1983).

(5) W. A. Goddard III, Phys. Rev. **157**, 81 (1967).

(6) R. C. Ladner and W. A. Goddard III, J. Chem. Phys. **51**, 1073 (1969).

(7) (a) W. J. Hunt, T. H. Dunning, Jr., and W. A. Goddard III, Chem. Phys. Lett. **3**, 606 (1969); W. A. Goddard III, T. H. Dunning, Jr., and W. J. Hunt, Chem. Phys. Lett. **4**, 231 (1969); W. J. Hunt, W. A. Goddard III, and T. H. Dunning, Jr., Chem. Phys. Lett. **6**, 147 (1970); W. J. Hunt, P. J. Hay, and W. A. Goddard III, J. Chem. Phys. **57**, 738 (1972); F. W. Bobrowicz and W. A. Goddard III in "Methods of Electronic Structure Theory", H. F.

Schaefer, ed., Plenum Publishing Corporation, 1977, pp 79-127; (b) L. G. Yaffe and W. A. Goddard III, Phys. Rev. A **13**, 1682 (1976).

(8) Because the SCF calculation optimizes the shapes of orbitals and because the Brillouin theorem states that SCF wavefunctions are stable to first-order changes, single excitations (first-order changes) within a CI wavefunction correspond physically to orbital shape changes.

(9) K.-P. Huber and G. Herzberg, "Constants of Diatomic Molecules" (Van Nostrand, New York, 1979).

(10) The CCCI calculations for BH were carried out with exactly the same basis set and geometry as used in the full CI.[4] We used C_{2v} symmetry with the experimental bond distance of 2.329 bohr. The basis set for BH was the Dunning[11] double-ζ contraction of the Huzinaga[12] (9s5p) basis for boron augmented by one set of 3d polarization functions ($\zeta^d = 0.5$, with the 3s combination included) and the Dunning (4s/2s) basis for hydrogen (scaled by $\zeta^s = 1.2$) augmented by one set of 2p polarization functions (ζ^p=1.0). For BH, the total energy for RCI*[$SD_{bond} + S_{val}$] (with 110 spin eigenfunctions) is −25.15929 hartrees, while the full CI (with 132,686 spin eigenfunctions) yields −25.22763 hartrees.[4] The CCCI method dissociates to HF*S_{val} fragments, yielding a total energy for B atom of −24.53376 hartrees, while the full CI value for B is −24.60264 hartrees.[4] The total energy for H atom is −0.49928 with the (4s/2s) basis.

(11) T. H. Dunning, Jr., J. Chem. Phys. **53**, 2823 (1970).

(12) S. Huzinaga, J. Chem. Phys. **42**, 1293 (1965).

(13) The carbon d exponent was optimized for CH_4 by R. A. Bair and W. A. Goddard III (submitted for publication).[2]

(14) a) M. D. Harmony, V. W. Laurie, R. L. Kuczkowski, R. H. Schwendeman, D. A. Ramsay, F. J. Lovas, W. J. Lafferty, and A. G. Maki, J. Phys. Chem. Ref. Data **8**, 619 (1979); b) Landolt-Börnstein Tables **7**, (Springer, Berlin,

1976).

(15) L. B. Harding and W. A. Goddard III, Chem. Phys. Lett. **55**, 217 (1978).

(16) C. W. Bauschlicher, Jr., H. F. Schaefer III, and P. S. Bagus, J. Am. Chem. Soc. **99**, 7106 (1977).

(17) F. B. Brown and D. G. Truhlar, Chem. Phys. Lett. **113**, 441 (1985).

(18) P. E. M. Siegbahn, Chem. Phys. Lett. **119**, 515 (1985).

(19) The CCCI total energy [using the symmetric bent bond GVB(3/6)PP wavefunction] for C_2H_2 is -76.97901 hartrees, with 5138 spatial configurations and 9780 spin eigenfunctions. At the GVB-PP level, bent bonds are higher in energy than σ/π bonds for C_2H_2 by 0.7 kcal/mol, increasing to 1.8 kcal/mol for a six-electron full CI within the six orbitals of the triple bond [$E_{GVB-CI(3/6)}(\sigma/\pi$ bonds) $= -76.92150$ hartrees and $E_{GVB-CI(3/6)}$(symmetric bent bonds) $= -76.91857$ hartrees]. This is in contrast to GVB-PP results for C_2F_2 by R. P. Messmer and P. A. Schultz, Phys. Rev. Lett. **57**, 2653 (1986), who found bent bonds $\sim$2 kcal/mol lower than σ and π bonds.

(20) This bond energy was obtained indirectly from the heat of formation of C_2F_4 ($\Delta H^o_{f,298} = -157.4 \pm 0.7$ kcal/mol)[27b] and one experimental value for $\Delta H^o_{f,298}(CF_2) = -52.$ kcal/mol from S. G. Lias, J. F. Liebman, and R. D. Levin, J. Phys. Chem. Ref. Data **13**, 695 (1984).

(21) This bond energy was also obtained indirectly from $\Delta H^o_{f,298}(C_2F_4) = -157.4$ kcal/mol and another experimental value for $\Delta H^o_{f,298}(CF_2) = -44.2 \pm 1$ kcal/mol from Ref. 1i.

(22) K. F. Zmbov, O. M. Uy, and J. L. Margrave, J. Am. Chem. Soc. **90**, 5090 (1968). This study using Knudsen cell equilibrium at high temperature (~ 1200°K) constitutes the only directly determined bond energy for C_2F_4.

(23) We explored the possibility of bent bonds being lower in energy than σ

and π bonds for C_2F_4. We find energies equal (within 0.1 kcal/mol) at the GVB-PP level. For the four-electron full CI within the four orbitals of the double bond, the σ and π bonds are favored by 0.1 kcal/mol over symmetric bent bonds [$E_{GVB-CI(2/4)}(\sigma/\pi$ bonds) = -473.54944 hartrees and $E_{GVB-CI(2/4)}$(symmetric bent bonds) = -473.54924 hartrees].

(24) Zero point energy and temperature corrections to D_e were obtained from a) T. Shimanouchi, Tables of Molecular Vibrational Frequencies, Natl. Stand. Ref. Data Ser., Nat. Bur. Stand. **39** (1972) and b) JANAF Thermochemical Tables, Natl. Stand. Ref. Data Ser., Nat. Bur. Stand. **37** (1971).

Table I. Total Energies (hartrees) for CH_X, X=0-4.[a]

	CH_4 ($^1A_1$)	CH_3 ($^2A_2''$)		CH_2 ($^3B_1$)		CH_2 ($^1A_1$)	CH			C (^3P)
calculation[b]	(VDZDP)[c]	(VDZD)[d]	(VDZDP)	(VDZD)	(VDZDP)	(VDZDP)	$^4\Sigma^-$ (VDZD)	$^2\Pi$ (VDZDP)	$^2\Pi$ (VDZD)	(VDZD)
HF	−40.20127	−39.56032	−39.56282	−38.92254	−38.92500	−38.88382	−38.28118	−38.27215	−38.26997	−37.68452
	(1/1)	(1/1)	(1/1)	(1/1)	(1/1)	(1/1)	(1/1)	(1/1)	(1/1)	(1/1)
GVB(1/2)PP	−40.21650	"	−39.57750	"	−38.93834	−38.90032	"	−38.28918	"	"
	(2/2)		(2/2)		(2/2)	(2/2)		(2/2)		
RCI(1/2)	−40.21650	"	−39.57874	"	−38.94041	−38.90032	"	−38.29017	"	"
	(3/3)		(3/4)		(3/5)	(3/3)		(3/4)		
SD_{C-H}	−40.23107	"	−39.59498	"	−38.95869	−38.91473	"	−38.30427	"	"
	(141/141)		(134/245)		(118/286)	(106/106)		(92/164)		
CCCI[e]	−40.24497	−39.56966[f]	−39.61340	−38.93425[f]	−38.97640	−38.92646	−38.29241[f]	−38.32192	−38.27908[f]	−37.69904[f]
	(241/273)	(44/86)	(228/503)	(36/76)	(203/539)	(176/198)	(30/54)	(136/274)	(22/40)	(19/33)
HF*S*D	−40.35755	−39.68894	−39.69745	−39.02454	−39.03292	—	−38.35140	−38.37686	−38.36823	−37.75931
	(1183/1753)	(670/1903)	(929/2660)	(482/1462)	(691/2147)		(306/681)	(355/850)	(144/314)	(283/573)

a) The total energy for the hydrogen atom within the (unscaled) double-ζ basis used here is −0.49928 hartree. 1 hartree = 627.5096 kcal/mol = 27.21162 eV = 219,474.8 cm^{-1}. *b*) Calculational details are provided in Section II of the text. The corresponding number of spatial configurations/spin eigenfunctions for each wavefunction is given beneath each total energy. *c*) VDZDP basis: Huzinaga-Dunning (9s5p/3s2p) valence double-ζ basis plus one set of cartesian 3d functions ($\zeta^d = 0.64$; the 3s-combination was removed) on carbon and the Huzinaga-Dunning scaled (4s/2s) double-ζ basis for hydrogen, with one set of 2p functions ($\zeta^p = 1.0$) on the hydrogen involved in the C-H bond being broken. *d*) VDZD basis: the same basis as in *c*) but with no augmenting 2p functions for hydrogen. [Total energies for calculations using VDZD basis refer to the appropriate limit at R(C-H)= ∞, i.e., HF, HF^*S_{val}, or HF*S*D (Section II).] *e*) RCI(1/2)*[SD_{C-H} + S_{val}]. *f*) HF^*S_{val} total energy.

Table II. Adiabatic Bond Energies (D_e) in kcal/mol for CH_X–H (X = 0-3).[a]

calculation	CH_3–H	CH_2–H	CH–H[b]	C–H
HF	88.9	88.5	80.9,74.3	55.4
HF*S*D	106.3	109.0	103.8[c]	74.2
GVB(1/2)PP	98.5	97.7	91.2,82.7	66.1
RCI(1/2)	98.5	98.5	91.2,84.0	66.7
SD_{C-H}	107.3	108.7	100.3,95.4	75.6
CCCI[d]	110.5	112.9	101.9,99.5	77.6
Experiment[e]	111.9±0.3	115.8±1.4	107.4±1.3	84.5±0.2
Δ^f_{corr}	1.4±0.3	2.9±1.4	5.5,7.9±1.3	6.9±0.2
ZPE[g]	27.10	18.41	10.88±0.22	4.09

a) Calculational details are provided in Section II of the text. *b*) values of D_e(CH–H) were calculated via two thermodynamic cycles in order to treat CH_2 and CH consistently: (i) CH_2 $(^3B_1) \xrightarrow{\Delta E_{ST}} CH_2$ $(^1A_1) \xrightarrow{D(C-H)}$ CH $(^2\Pi)$ + H (^2S) (first column entry) and (ii) CH_2 $(^3B_1) \xrightarrow{D(C-H)}$ CH $(^4\Sigma^-)$ + H (^2S) $\xrightarrow{-\Delta E_{DQ}}$ CH $(^2\Pi)$ + H (^2S) (second column entry). [$\Delta E_{ST}(CH_2)$ = 9.0 and ΔE_{DQ}(CH) = 16.4 kcal/mol, from Ref. 3b and from Table III of this work. *c*) The value of D(CH-H) for HF*S*D is obtained directly from CH_2 $(^3B_1) \longrightarrow$ CH $(^2\Pi)$ + H (^2S). *d*) RCI(1/2)*[SD_{C-H} + S_{val}]. *e*) Experimental D_e's are derived from $\Delta H^o_{f,0}$ [taken from Ref. 24b and JANAF supplements in J. Phys. Chem. Ref. Data **4**, 1 (1975) and **11**, 695 (1982)], with zero point energy corrections from: Ref. 24a for CH_4; M. E. Jacox, J. Phys. Chem. Ref. Data **13**, 945 (1984) for CH_3; P. R. Bunker, P. Jensen, W. P. Kraemer, and R. Beardsworth, J. Chem. Phys. **85**, 3724 (1986) for CH_2; and Ref. 9 for CH. *f*) $\Delta_{corr} = D^{expt}$(C-H) – D^{calc}(C-H), where D^{calc} is from CCCI. *g*) ZPE = zero point energy; see footnote *e*).

Table III. Doublet-Quartet splittings (ΔE_{DQ} = $E_{^4\Sigma^-}$ − $E_{^2\Pi}$) and total energies for CH.[a]

	total energies (hartrees)		
calculation	$^4\Sigma^-$	$^2\Pi$	ΔE_{DQ} (kcal/mol)
HF	−38.28118 (1/1)	−38.26996 (1/1)	−7.0
HF*S*D	−38.35140 (160/364)	−38.36823 (144/314)	+10.6
GVB-PP	−38.29150 (2/2)	−38.30799 (4/4)	+10.3
GVB-RCI(PP)[b]	−38.29484 (3/6)	−38.30926 (6/8)	+9.0
GVB-RCI(opt)[c]	−38.29599 (3/6)	−38.30938 (6/8)	+8.4
CCCI[d]	−38.30742 (67/127)	−38.33356 (112/252)	+16.4
Experiment			+16.7[e]

a) VDZD basis. Calculational details are provided in Section II. The corresponding number of spatial configurations/spin eigenfunctions for each wavefunction is given beneath each total energy. *b*) GVB-RCI using the GVB-PP orbitals. *c*) Self-consistent GVB-RCI. *d*) RCI*$SD_{\sigma\pi_y}$(PP). *e*) Ref. 9.

Table IV. Adiabatic C-C Bond Energies (D_e) in kcal/mol for $H_2C{=}CH_2$ and $HC{\equiv}CH$.[a]

	total energies (hartrees)				$D_e(H_2C{=}CH_2)$	$D_e(HC{\equiv}CH)$	
calculation	$H_2C{=}CH_2$	CH_2 ($^3B_1$)[b]	$HC{\equiv}CH$	CH ($^4\Sigma^-$)[b]		direct[c]	using ΔE_{DQ}[d]
HF	−78.03955 (1/1)	−38.92241 (1/1)	−76.82438 (1/1)	−38.28118 (1/1)	122.2	178.5	131.6
HF*S*D	−78.29399 (1315/2092)	−39.02454 (250/732)	−77.06340 (800/1206)	−38.35140 (150/364)	153.7	205.2	193.5
GVB-PP	−78.07757 (4/4)	−38.92241 (1/1)	−76.87800 (8/8)	−38.28118 (1/1)	146.1		165.3
GVB-RCI	−78.09118 (5/6)	"	−76.92014 (14/20)	"	154.6		191.7
RCI*S_{val}	−78.12864 (239/418)	−38.93415 (20/40)	−76.95463 (536/1306)	−38.29241 (18/36)	163.4		199.3
RCI*[$SD_\sigma + SD_\pi$]	−78.11343 (465/596)	−38.92241 (1/1)	−76.95428 (1706/2926)	−38.28118 (1/1)	168.6		213.1
CCCI[e]	−78.14574 (651/944)	−38.93415 (20/40)	−76.97858 (2048/3872)	−38.29241 (18/36)	174.1		214.3
Experiment[f]					179.0±2.5	236.1±0.7	
$\Delta_{corr} = D_e^{expt} - D_e^{CCCI}$					4.9±2.5	21.8±0.7	

a) VDZD basis. Calculational details are provided in Section II of the text. The corresponding number of spatial configurations/spin eigenfunctions for each wavefunction are given beneath each total energy. *b*) Total energies for CH_2 and CH are for the appropriate limit at R(C-C) = ∞, i.e., HF, HF*S_{val}, or HF*S*D. *c*) Direct $D_e(HC{\equiv}CH)$ from $D_e(HC{\equiv}CH) = 2{\times}E(^2\Pi\ CH) - E(HC{\equiv}CH)$. *d*) $D_e(HC{\equiv}CH) = 2{\times}E(^4\Sigma^-\ CH) - E(HC{\equiv}CH) - 2{\times}\Delta E_{DQ}$, where ΔE_{DQ} = 16.4 kcal/mol (see Table III). *e*) RCI*[$SD_\sigma + SD_\pi + S_{val}$] for C_2H_4 and RCI*[$SD_\sigma + SD_{\pi_x} + SD_{\pi_y} + S_{val}$] for $HC{\equiv}CH$. *f*) Experimental D_e's are derived from $\Delta H^\circ_{f,0}$ [taken from Ref. 24b and J. Phys. Chem. Ref. Data 4, 1 (1975)] with zero point energy corrections for C_2H_4 = 30.89 kcal/mol and C_2H_2 = 16.18 kcal/mol from Ref. 24a.

Table V. Bond Energies (D_e) in kcal/mol for $F_2C{=}CF_2$.[a]

	total energies (hartrees)		$D_e^{diab}(F_2C{=}CF_2)$[c]	$D_e^{adiab}(F_2C{=}CF_2)$	
calculation	$F_2C{=}CF_2$ ($^1A_1$)	CF_2 ($^3B_1$)[b]		direct[d]	using ΔE_{ST}[e]
HF	−473.49255 (1/1)	−236.64724 (1/1)	124.3	59.4	9.3
HF*S*D	−474.07613 (18772/34184)	−236.92980 (3155/16053)	135.9	39.1	20.9
GVB-PP	−473.53219 (4/4)	−236.64724 (1/1)	149.2		34.2
GVB-RCI	−473.54868 (5/6)	"	159.5		44.5
RCI*S_{val}	−473.58045 (941/1724)	−236.65739 (63/157)	166.7		51.7
RCI*[SD_σ + SD_π]	−473.57245 (849/1098)	−236.64724 (1/1)	174.4		59.4
CCCI[f]	−473.59909 (1719/2728)	−236.65739 (63/157)	178.4		63.4
D_e^{adiab} + Δ_{corr}[g]					68.3±2.5
Experiment[h]				57.2±0.7,[i] 72.8±2.7,[j] 80.1±3[k]	

a) VDZD basis. Calculational details are provided in Section II of the text. The corresponding number of spatial configurations/spin eigenfunctions for each wavefunction are given beneath each total energy. *b*) Total energies for CF_2 are for the appropriate limit at R(C-C) = ∞, i.e., HF or HF*S_{val}. *c*) $D_e^{diab}(F_2C{=}CF_2) = 2{\times}E(^3B_1\ CF_2) - E(C_2F_4)$. *d*) Direct $D_e(F_2C{=}CF_2)$ from $2{\times}E(^1A_1\ CF_2) - E(C_2F_4)$ where the HF and HF*S*D total energies of $^1A_1$ CF_2 are −236.69898 and −237.00693 hartrees (2633 spatial configurations/4399 spin eigenfunctions). *e*) $D_e^{adiab}(F_2C{=}CF_2) = D_e^{diab}(F_2C{=}CF_2) - 2{\times}\Delta E_{ST}$, where ΔE_{ST} = 57.5 kcal/mol (Ref. 3b). *f*) RCI*[SD_σ + SD_π + S_{val}]. *g*) Δ_{corr} for C=C is taken from Table IV. *h*) Experimental D_e's are derived from D_{298}^{expt}'s by correcting for finite temperature (subtract 1.0 kcal/mol) to obtain D_0^{expt}'s and then correcting for differential zero point energy (add 4.8 kcal/mol) to obtain D_e^{expt}'s, based on the zero point energies of 13.4 kcal/mol for C_2F_4 and 4.3 kcal/mol for CF_2 (Ref. 24a). *i*) Ref. 20. *j*) Ref. 21. *k*) Ref. 22.

Chapter 1.B. The text of this section is a Letter coauthored with William A. Goddard III which appeared in the *Journal of Physical Chemistry.*

Reprinted from The Journal of Physical Chemistry, 1986, 90, 998

Relation between Singlet–Triplet Gaps and Bond Energies

Emily A. Carter[†] and William A. Goddard III*

The Arthur Amos Noyes Laboratory of Chemical Physics,[‡] California Institute of Technology, Pasadena, California 91125 *(Received: December 6, 1985)*

We propose that the dominant effect in bond energy trends of $CXYH_2$, $SiXYH_2$, and substituted olefins is the singlet–triplet energy splitting in CXY or SiXY. New predictions of singlet–triplet gaps in AXY (A = C, Si) molecules, heats of formation of substituted olefins, and Si–H bond strengths in substituted silanes are obtained.

The effects of substituents on bond energies can be quite dramatic. Thus, the C–C bond energy of ethylene (**1**) is 172 ±

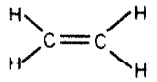

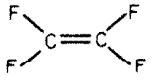

2 kcal/mol[1] whereas the C–C bond energy of tetrafluoroethylene (**2**) is only 76.3 ± 3 kcal/mol.[2] The point of this paper will be to show that these dramatic changes can be understood in terms of changes in the energetics of the fragments (CH_2 vs. CF_2) within the assumption that the actual character of the C–C double bonds is rather similar. The GVB orbitals of the C–C double bond have the form in (**3**) involving singly occupied σ and π orbitals on each

C spin-paired with a corresponding orbital on the other C.[3]

Unpairing the orbitals and separating the fragments leads then to

with each CXY fragment in the *triplet* state. However, depending upon the fragment, the ground state of CXY may be either the triplet ($\sigma\pi$) or the singlet state (σ^2)

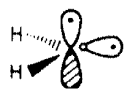

$\sigma\pi$

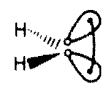

σ^2

[†] National Science Foundation Predoctoral Fellow, 1982–1985.
[‡] Contribution no. 7333.

(1) Chupka, W. A.; Lifshitz, C. *J. Chem. Phys.* **1968**, *48*, 1109.
(2) Zmbov, K. F.; Uy, O. M.; Margrave, J. L. *J. Am. Chem. Soc.* **1968**, *90*, 5090.
(3) Plots of GVB orbitals for ethylene may be found in Hay, P. J.; Hunt, W. J.; Goddard III, W. A. *J. Am. Chem. Soc.* **1972**, *94*, 8293.

0022-3654/86/2090-0998$01.50/0

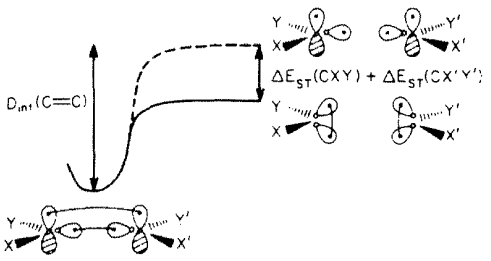

Figure 1.

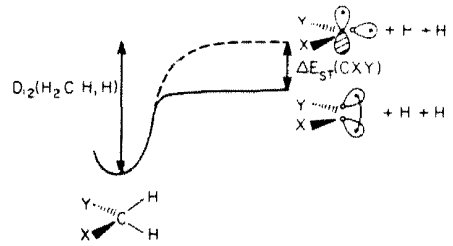

Figure 2.

Consider the simplest carbene, CH_2. It has a triplet $\sigma\pi$ ground state ($^3B_1$) with the σ^2 excited state ($^1A_1$) lying 9 kcal/mol higher.[4] Notice that while the $\sigma\pi$ ground state of CH_2 is set up to form covalent bonds, the σ^2 excited state cannot, since it has no open shell electrons. If we assume that the character of all C–C double bonds is similar at the equilibrium bond distance, a case in which the ground state of CXY is σ^2 would result in a bond energy decreased by just the sum of the σ^2 to $\sigma\pi$ excitation energies [ΔE_{ST}(CXY)] as illustrated in Figure 1. Considering the intrinsic C–C bond energy to be D_{int}(C=C) = 172 ± 2 kcal/mol (since ethylene dissociates to ground-state fragments), we obtain

$$D(XYC{=}CX'Y') = D_{int}(C{=}C) - [\Delta E_{ST}(CXY) + \Delta E_{ST}(CX'Y')] \quad (1)$$

for the bond energy in any substituted olefin in which the CXY fragments have a σ^2 ground state. Hence for CXY = CX′Y′ = CF_2, since $\Delta E_{ST} \sim 46.5$ kcal/mol,[5] we obtain

$$D(F_2C{=}CF_2) = 172 \pm 2 - 2(46.5) = 79 \pm 2 \text{ kcal/mol}^6$$

for the C–C bond energy in tetrafluoroethylene, in good agreement with the measured bond energy of 76.3 ± 3 kcal/mol. There are of course other factors (e.g. electronegativities, steric bulk, etc.) that can change with substitution; however, we will show that this $\sigma\pi$–σ^2 excitation energy of the CXY products dominates the changes in the C=C bond energy.[7]

An analogous effect occurs in the bond energies of saturated hydrocarbons. Thus for CH_4 the sum of the first two C–H bond energies is

$$D_{12}(H_2C{:}H,H) = D_1(H_3C{-}H) + D_2(H_2C{-}H)$$

as indicated schematically in Figure 2. We will argue that the sum of these two bond energies should be independent of substituent unless CXY has a σ^2 ground state. Indeed

$$D_{12}(H_2C{:}H,H) = 214.2 \pm 1.0 \text{ kcal/mol}^8$$

whereas

$$D_{12}(F_2C{:}H,H) = 168.0 \pm 1^9 = 214 - 46 \text{ kcal/mol}$$

is weaker by just the σ^2–$\sigma\pi$ excitation energy for CF_2! Thus for CXY systems with a σ^2 ground state we expect

$$D_{12}(XYC{:}H,H) = D_1(XYHC{-}H) + D_2(XYC{-}H) \sim D_{12}(H_2C{:}H,H) - \Delta E_{ST}(CXY) \quad (2)$$

for the sum of the first two C–H bond strengths in substituted methanes.

What are the physical effects which result in carbenes (or silylenes) with singlet σ^2 ground states? Two electronic factors contribute to the formation of σ^2 CXY:[10]

(a) If X and/or Y are electronegative, they will prefer to form ionic bonds. Then the C–X and C–Y bonds will utilize C p orbitals since they have the lowest valence ionization potential, leaving more s character for nonbonding C σ orbital.

(b) If X and/or Y have pπ lone pairs (which can donate electron density into the C pπ orbital), this disfavors pπ occupation by one of the C valence electrons.

Both contributions lead to relative stabilization of the σ nonbonding orbital, resulting in a singlet ground state. Thus CXY systems where X and/or Y = F, Cl, OR, NRR′, etc. are expected to have singlet ground states.

For silylenes, SiXY, the much larger s–p energy difference for second row atoms greatly favors the s^2p^2 state of Si and hence the σ^2 state of SiXY. Thus these systems are expected to have singlet ground states for the above substituents (and for X and/or Y = H, alkyl). [For carbon, the small s–p energy splitting renders sp^2 hybridization more accessible, resulting in a triplet ground state for CR_2 (R = H, alkyl).] Triplet ground states are also favored by aryl and bulky alkyl substituents (since the $\sigma\pi$ state favors a large bond angle whereas the σ^2 state prefers a small bond angle), as well as by electropositive moieties (more favorable electron donation into sp^2).

In general, then, for CXY (SiXY) with electronegative substituents such as F and Cl, the σ^2 ground state should manifest itself in weaker bonds of CXY to anything. Indeed, we can obtain a quantitative estimate for this bond weakening by assuming that two single σ bonds or one double bond should be weaker compared to the CH_2 case by just the energy cost to promote the ground-state singlet to the triplet necessary for bond formation.

Before examining trends in bond energies and their implications we will test the basic assumption that the C=C and C–H intrinsic bond energies remain approximately constant even though the actual bond energies vary over a range of ~100 kcal/mol (see Table III). From the two dissociation processes in eq 1 and 2, we obtain the following relation

$$[\Delta H_f^\circ{}_{298}(XYC{=}CX'Y') - \Delta H_f^\circ{}_{298}(CXYH_2) - \Delta H_f^\circ{}_{298}(CX'Y'H_2)] = [2D_{12}(H_2C{:}H,H) - D^\circ{}_{298}(H_2C{=}CH_2) - 4\Delta H_f^\circ{}_{298}(H)] = [\Delta H_f^\circ{}_{298}(C_2H_4) - 2[\Delta H_f^\circ{}_{298}(CH_4)]] \quad (3)$$

where $D_{12}(H_2C{:}H,H)$ and $D^\circ{}_{298}(H_2C{=}CH_2)$ are taken to be intrinsic C–H and C–C bond energies. Notice that the right-hand side is independent of X and Y, suggesting that the difference in heats of formation on the left-hand side of (3) [$\Delta(\Delta H_f^\circ{}_{298})$] should be a constant equal to 428.4 - 172.0 - 208.4[8c] = 48.0

(4) (a) Leopold, D. G.; Murray, K. K.; Lineberger, W. C. *J. Chem. Phys.* **1984**, *81*, 1048. (b) Harding, L. B.; Goddard III, W. A. *Chem. Phys. Lett.* **1978**, *55*, 217.

(5) Bauschlicher, C. W., Jr.; Schaefer III, H. F.; Bagus, P. S. *J. Am. Chem. Soc.* **1977**, *99*, 7106.

(6) The uncertainty in this number is larger than the quoted value since we have not included any estimate for the uncertainty in the theoretical singlet–triplet splitting.

(7) In CXY systems with σ^2 ground states it is possible that the ground state of the doubly bonded olefin will have banana bonds rather than σ and π bonds. Thus for $H_2Si{=}SiH_2$, Horowitz and Goddard (*J. Am. Chem. Soc.*, to be submitted) showed that the banana bond description is 3.5 kcal/mol lower than the σ and π bond description for the simple GVB-PP wave function. However, with a full GVB-CI in the double bond, they find a difference of only 0.1 kcal/mol, indicating that our assumption of the $\sigma\pi$ description is valid. [R. P. Messmer (private communication) has also shown that C_2F_4 leads to a banana bond description at the GVB-PP level.]

(8) Data for (a) $\Delta H_f^\circ{}_{298}(CH_2)$ is from ref 1; (b) $\Delta H_f^\circ{}_{298}(CH_4)$ is from Lias, S. G.; Liebman, J. F.; Levin, R. D. *J. Phys. Chem. Ref. Data* **1984**, *13*, 695; (c) $D^\circ{}_{298}$(H–H) is from McMillen, D. F.; Golden, D. M. *Annu. Rev. Phys. Chem.* **1982**, *33*, 493.

(9) Data for (a) $\Delta H_f^\circ{}_{298}(CF_2)$ is from Berman, D. W.; Bomse, D. S.; Beauchamp, J. L. *Int. J. Mass. Spectrom. Ion Phys.* **1981**, *39*, 263; (b) $\Delta H_f^\circ{}_{298}(CF_2H_2)$ is from ref 6b.

(10) Goddard III, W. A.; Harding, L. B. *Annu. Rev. Phys. Chem.* **1978**, *29*, 363.

TABLE I: Test of the Validity of Eq 3, $\Delta(\Delta H_f°_{298}) = \Delta H_f°_{298}(CXY{=}CX'Y') - \Delta H_f°_{298}(CXYH_2) - \Delta H_f°_{298}(CX'Y'H_2) = 48.0$ kcal/mol, for the Ideal Limit[a]

CXY	CX'Y'	$\Delta H_f°_{298}(CXY{=}CX'Y')$	$\Delta H_f°_{298}(CXYH_2)$	$\Delta H_f°_{298}(CX'Y'H_2)$	$\Delta(\Delta H_f°_{298})$
CH_2	CH_2	+12[b]	-18.0[b]	-18.0	+48.0
CF_2	CF_2	-164.7 ± 5[c] (-168.0)	-108.0[b]	-108.0	+51.3 ± 5
CCl_2	CCl_2	-2.7 ± 2.0[d] (+2.4)	-22.8 ± 0.2[e]	-22.8 ± 0.2	+42.9 ± 2.4
CH_2	CF_2	-82.0[b] (-78.0)	-18.0	-108.0	+44.0
CH_2	CCl_2	+0.61 ± 0.36[d] (+7.2)	-18.0	-22.8 ± 0.2	+41.4 ± 0.56
CH_2	CHF	-33.2[b] (-26.0)	-18.0	-56	+40.8
CH_2	CHCl	+8.6 ± 0.3[d] (+10.5)	-18.0	-19.5	+46.1 ± 0.3
E-CHF	CHF	-70.0[b] (-64.0)	-56[b]	-56	+42.0
E-CHCl	CHCl	+1.2 ± 2.1[d] (+9.0)	-19.5[b]	-19.5	+40.2 ± 2.1
CF_2	CHF	-117[b] (-116.0)	-108.0	-56	+47.0
CF_2	CFCl	-125 ± 4[d] (-122.6)	-108.0	-62.6 ± 3[f]	+45.6 ± 7

[a] All values in kcal/mol. [b] Reference 8b. [c] Derived from $D°_{298}(F_2C{=}CF_2)$ and $\Delta H_f°_{298}(CF_2)$ from ref 2 and 9a, respectively. [d] Cox, J. D.; Pilcher, G. *Thermochemistry of Organic and Organometallic Compounds*; Academic Press: New York, 1970. [e] Rodgers, A. S.; Chao, J.; Wilhoit, R. C.; Zwolinski, B. J. *J. Phys. Chem. Ref. Data* **1974**, *3*, 117. [f] JANAF Thermochemical Tables, *Natl. Stand. Ref. Data Ser., Natl. Bur. Stand.* **1971**, *No. 37*.

TABLE II: Predicted CXY Singlet-Triplet Gaps from Relative A-H Bond Strengths of $AXYH_2$ Molecules (kcal/mol)

			ΔE_{ST}[b]	
$AXYH_2$	$D_{12}(XYA{:}\,H,H)$[a]	AXY	this work	calcd
CH_4	214.2 ± 1	CH_2		-9.0[c]
CF_2H_2	168.0 ± 1	CF_2	46.2 ± 2	46.5[d]
CCl_2H_2	181.9 ± 2	CCl_2	32.3 ± 3	13.5,[e] 25.9[e]
$CFClH_2$	174.8 ± 3	CFCl	39.4 ± 4	
CFH_3	186.2 ± 3	CHF	28.0 ± 4	9.2[d]
$CClH_3$	194.7 ± 5	CHCl	19.5 ± 6	1.6[d]
SiH_4	180.8 ± 3.5[f]	$^3SiH_2$		16.8[g]
SiF_2H_2	107.3 ± 3.5[h]	SiF_2		73.5[g]
$SiCl_2H_2$	138.1 ± 3.6[i]	$SiCl_2$	42.7 ± 7.1	51.5 ± 6[i]
$SiFH_3$	143.1 ± 3.5[h]	SiHF		37.7[g]
$SiClH_3$	153.4 ± 6[k]	SiHCl	27.4 ± 9.5	

[a] $D_{12}(XYA{:}\,H,H)$ = the sum of the first two A-H bond energies in $AXYH_2$ at 298 K. [b] $\Delta E_{ST} = E_{triplet} - E_{singlet}$ for AXY listed in the adjacent column. [c] Reference 4 (experimental work). [d] Reference 5. [e] Reference 12. [f] Derived from ref 11a and 11b. [g] Reference 13. [h] In these cases the theoretical ΔE_{ST} was combined with eq 2 for Si and used to predict $D_{12}(XYSi{:}\,H,H)$. [i] Derived from ref 11a [$\Delta H_f°_{298}(SiCl_2H_2)$] and from Farber, M.; Srivastava, R. D. *J. Chem. Soc., Faraday Trans. 1* **1977**, *73*, 1672 [$\Delta H_f°_{298}(SiCl_2)$]. [j] Reference 11a. [k] Derived from ref 11a.

kcal/mol. This equation eliminates heats of formation and excitation energies of CXY, cancelling out substituent effects. Examination of Table I reveals that $\Delta(\Delta H_f°_{298})$ is very nearly constant, lending credence to the assumption that C=C and C-H bonds have the same character and thus the same intrinsic bond energies independent of substitution. The values deviating most from 48.0 kcal/mol all have significant uncertainties in the olefin heats of formation. Thus by assuming (3) and using $\Delta(\Delta H_f°_{298})$ = 48.0 kcal/mol, we have estimated new values for $\Delta H_f°_{298}$-$(XYC{=}CX'Y')$ listed in parentheses under the experimental values in Table I.

Given that the C=C and C-H intrinsic bond energies are essentially constant, we can utilize (1) and (2) to predict singlet-triplet energies for two very different bonding scenarios (two σ bonds to hydrogens vs. one σ and one π bond to carbon).

In Table II we display experimental values for $D_{12}(XYA{:}\,H,H)$ for a variety of substituted methanes and silanes. As the electronegativity of the substituent increases, the A-H bond energy decreases (going from Cl to F), and as two hydrogens are replaced by F or Cl, the bond energy decreases further. Equation 2 suggests

TABLE III: Predicted CXY Singlet-Triplet Gaps from Relative C=C Bond Strengths of Substituted Olefins (kcal/mol)

			ΔE_{ST}[a]	
olefin	$D_f°_{298}(C{=}C)$	CXY	this work	calcd
$CH_2{=}CH_2$	172 ± 2	CH_2		-9.0[b]
$CF_2{=}CF_2$	76.3 ± 3	CF_2	47.9 ± 2.5	46.5[c]
$CCl_2{=}CCl_2$	112.5 ± 4	CCl_2	29.8 ± 3	13.5,[c] 25.9[d]
$CH_2{=}CF_2$	129.8 ± 2	CF_2	42.2 ± 4	46.5
$CH_2{=}CCl_2$	146.3 ± 3.4	CCl_2	25.7 ± 5.4	13.5, 25.9
$CH_2{=}CHF$	151.2 ± 4	CHF	20.8 ± 6	9.2[c]
$CH_2{=}CHCl$	154.4 ± 6.3	CHCl	17.6 ± 8.3	1.6[c]
E-CHF=CHF	122.0 ± 6	CHF	25.0 ± 4	9.2
E-CHCl=CHCl	140.8 ± 12.1	CHCl	15.6 ± 7	1.6
$CF_2{=}CHF$	98.8 ± 4	CHF	26.7 ± 6[e]	9.2
$CF_2{=}CFCl$	88.8 ± 5	CFCl	36.7 ± 7[e]	

[a] $\Delta E_{ST} = E_{triplet} - E_{singlet}$ for CXY listed in the adjacent column. [b] Reference 4 (experimental work). [c] Reference 5. [d] Reference 12. [e] Derived by assuming $\Delta E_{ST}(CF_2)$ = 46.5 kcal/mol.

TABLE IV: Additional Heats of Formation Used in This Study (kcal/mol)

CXY	$\Delta H_f°_{298}(CXY)$	$SiXY/SiXYH_2$	$\Delta H_f°_{298}$-(SiXY/SiX-YH_2)
CH_2	92 ± 1[a]	$^3SiH_2$	+84.8 ± 3[f]
CF_2	-44.2 ± 1[b]	$SiCl_2$	-40.6 ± 0.6[g]
CCl_2	+54.9 ± 2[c]	SiHCl	+17.0 ± 3[f]
CFCl	+8.0[d]	SiH_4	+8.2 ± 0.5[h]
CHF	+26 ± 3[e]	$SiCl_2H_2$	-74.5 ± 3[f]
CHCl	+71 ± 5[e]	$SiClH_3$	-32.2 ± 3[f]

[a] Reference 1. [b] Reference 9a. [c] Rademann, K.; Jochims, H.-W.; Baumgärtel, H. *J. Phys. Chem.* **1985**, *89*, 3459. [d] *GMELIN Handbuch der Anorganischen Chemie*, Kohlenstoff, Teil D2, System No. 14; Springer-Verlag: Berlin, 1974. [e] Lias, S. G.; Karpas, Z.; Liebman, J. F. *J. Am. Chem. Soc.*, in press. [f] Reference 11a. [g] Farber, M., Srivastava, R. D. *J. Chem. Soc., Faraday Trans. 1* **1977**, *73*, 1672. [h] Reference 11b.

that $\Delta E_{ST}(CXY) = D_{12}(H_2C{:}H,H) - D_{12}(XYC{:}H,H)$ for the methane series and $\Delta E_{ST}(SiXY) = D_{12}(H_2Si{:}H,H) - D_{12}$-$(XYSi{:}H,H)$ for the silane series, where

$$D_{12}(H_2Si{:}H,H) = \Delta H_f°_{298}(^3SiH_2) - \Delta H_f°_{298}(SiH_4) + D°_{298}(H{-}H) =$$
$$84.8\ (\pm 3) - 8.2\ (\pm 0.5) + 104.2 = 180.8\ (\pm 3.5)\ \text{kcal/mol}^{11}$$

This leads to the predicted singlet–triplet gaps in the next to last column of Table II. As expected, increasingly electronegative X and Y lead to larger singlet–triplet gaps.

Analogous predictions are given in Table III where we show the effects of electronegative substituents on C=C (experimental) bond energies. Equation 1 allows another set of singlet–triplet gaps to be predicted. A wide variety of systems now reveals internally consistent predictions for these splittings. For instance, using (1) and (2) lead to

$$\Delta E_{ST}(CF_2) = 46.2 \pm 2,\ 47.9 \pm 2.5,\ 42.2 \pm 4 \text{ kcal/mol}$$

all in good agreement with the theoretical value of 46.5 kcal/mol.[5] On the other hand, (1) and (2) result in

$$\Delta E_{ST}(CCl_2) = 32.3 \pm 3,\ 29.8 \pm 3,\ 25.7 \pm 5.4 \text{ kcal/mol}$$

whereas the theoretical value is $\Delta E_{ST}(CCl_2) = 13.5$ kcal/mol.[5] Other predictions are

$$\Delta E_{ST}(CHF) = 28.0 \pm 4,\ 20.8 \pm 6,\ 25.0 \pm 4,\ 26.7 \pm 6 \text{ kcal/mol}$$

compared to an ab initio value of $\Delta E_{ST}(CHF) = 9.2$ kcal/mol.[5] Also predicted is

$$\Delta E_{ST}(CHCl) = 19.5 \pm 6,\ 17.6 \pm 8.3,\ 15.6 \pm 7 \text{ kcal/mol}$$

compared to a theoretical value of $\Delta E_{ST}(CHCl) = 1.8$ kcal/mol.[5] We also predict

$$\Delta E_{ST}(CFCl) = 39.4 \pm 4 \quad \text{and} \quad 36.7 \pm 7 \text{ kcal/mol}$$

which has not been previously estimated.

We are concerned that there is a difference between our predicted values for the ΔE_{ST} and some of the previously calculated values. However, these calculations were performed at a very simple level (Hartree–Fock for the $\sigma\pi$ state and GVB(1/2)PP for the σ^2 state) and we suspect that correlation effects may play an important role in obtaining ΔE_{ST}. In order to test this suspicion, we carried out ab initio GVB-CI calculations for CCl_2, the case for which values for $\Delta E_{ST}(CCl_2)$ show the greatest discrepancy ($\sim$15–20 kcal/mol) between the previous theoretical calculations and our present estimates. These new GVB-CI calculations lead to a $\Delta E_{ST}(CCl_2) = 25.9$ kcal/mol, in excellent agreement with our empirical estimates (29 ± 3 kcal/mol). The dominant correlations, which were not included in the previous theoretical work [$\Delta E_{ST}(CCl_2) = 13.5$ kcal/mol],[5] but which were found to be important in our CI calculations, were π donation from Cl pπ orbitals to the empty C pπ orbital with simultaneous σ electron transfer to the chlorines from the carbon (with excitations to virtual orbitals to allow the orbital shape readjustments needed to properly describe simultaneous electron transfer in the σ and π frameworks). These correlations stabilize the singlet state more than the triplet state of halocarbenes and hence inclusion of these charge-transfer configurations (requiring up to selected sextuple excitations) is essential for an accurate description of the ΔE_{ST} for halocarbenes.[12]

The silane thermochemical data offer further new predictions of ΔE_{ST} and Si–H bond energies. $\Delta E_{ST}(SiCl_2) = 42.7 \pm 7.1$ kcal/mol is in reasonable agreement with a previous theoretical value of 51.5 ± 6 kcal/mol.[11a] Experimental data allow the prediction of the previously unknown $\Delta E_{ST}(SiHCl) = 27.4 \pm 9.5$ kcal/mol, while reliable theoretical calculations[13] of $\Delta E_{ST}(SiXY)$ allow the predictions of two previously unreported $D_{1/2}(XYSi{:}H, H) = 143.1 \pm 3.5$ and 107.3 ± 3.5 kcal/mol for X = H, Y = F, and X = Y = F, respectively.

In conclusion, we suggest that the dominant factor in determining bond energy trends in molecules involving CXY fragments is the singlet–triplet energy splitting. In many cases the thermochemical data[14] are incomplete or controversial so that relations such as (1)–(3) can provide useful estimates of unknown data. The inverse relation of bond strength to singlet–triplet splitting has been shown to be quantitatively accurate and internally consistent for a variety of systems. The fact that many of these values for ΔE_{ST} are significantly different from those obtained from previous ab initio calculations suggests that more extensive basis sets and CI calculations are called for in these systems.[15]

Acknowledgment. This work was supported by the Shell Development Company, Houston, TX and the National Science Foundation (Grant No. CHE83-18041).

(11) Values for (a) $\Delta H_f°_{298}(^3SiH_2)$ (shorthand for SiH_2, $^3B_1$) is from Ho, P.; Coltrin, M. E.; Binkley, J. S.; Melius, C. F. *J. Phys. Chem.* **1985**, *89*, 4647; (b) $\Delta H_f°_{298}(SiH_4)$ is from JANAF Thermochemical Tables *Natl. Stand. Ref. Data Ser., Natl. Bur. Stand.* **1978** update in *J. Phys. Chem. Ref. Data* **1978**, *7*, 793–940.

(12) Carter, E. A.; Goddard III, W. A., to be submitted for publication.

(13) Colvin, M. E.; Grev, R. S.; Schaefer III, H. F.; Bicerano, J. *Chem. Phys. Lett.* **1983**, *99*, 399

(14) Additional thermochemical data used in this work are displayed in Table IV.

(15) Subsequent to the submission of this Letter, it has been brought to our attention that recent HF*S*D-CI and GVB(1/2)PP*S*D-CI calculations by Scuseria et al.[16] on CHF and CHCl yielded revised values for ΔE_{ST} of 13.2 and 5.4 kcal/mol, respectively. These results are still in substantial disagreement with our estimates, presumably due to the lack of inclusion of important charge transfer configurations.

(16) Scuseria, G. E.; Durán, M.; Maclagan, R. G. A. R.; Schaefer III, H. F., to be submitted for publication.

Chapter 1.C. The text of this section is an Article coauthored with William A. Goddard III which appeared in the *Journal of Chemical Physics*.

Electron correlation, basis sets, and the methylene singlet–triplet gap

Emily A. Carter and William A. Goddard III[a)]
Arthur Amos Noyes Laboratory of Chemical Physics,[b)] California Institute of Technology, Pasadena, California 91125

(Received 15 September 1986; accepted 9 October 1986)

The effect of basis set and electron correlation on the singlet–triplet splitting (ΔE_{ST}) of CH_2 is examined using the generalized valence bond (GVB) approach. For a standard double zeta plus polarization basis, the GVB based calculation (with only 20–25 spin eigenfunctions) approaches the full CI result (~220 000 spin eigenfunctions) of Bauschlicher and Taylor to within 0.5 kcal/mol for this basis, but both differ substantially from experiment (errors of 2.4 and 2.9 kcal/mol for GVB and full CI, respectively). We have studied the convergence of ΔE_{ST} with basis set and find that an extremely extended basis (triple zeta *sp*, diffuse *sp*, triple zeta *d*, double zeta *f*) for GVB yields $\Delta E_{ST} = 9.03$ kcal/mol, in excellent agreement with the experimental value of 9.09 ± 0.20 kcal/mol.

I. INTRODUCTION

In principle, the methods of quantum chemistry can provide exact answers to quantitative questions of physical and chemical interest such as molecular geometries, vibrational frequencies, excitation energies, bond energies, and even activation energies for chemical reactions. However, even for such small molecules as methylene, calculations must always be restricted in the basis set and level of electron correlation. Hence, it is essential to understand the level of error engendered by restrictions in basis or level of correlation. Because the relative energies of the lowest singlet and triplet states ($\Delta E_{ST} = E_{singlet} - E_{triplet}$) of substituted methylenes have been shown to be critical in determining the chemistry of such systems,[1] and because the singlet–triplet gap of methylene is now well established experimentally to be $\Delta E_{ST} = 9.09 \pm 0.20$ kcal/mol,[2] we have selected CH_2 for a study of the dependence of ΔE_{ST} on basis set and level of correlation.

There are two paradigms for including electron correlation in wave functions. One is to start with the Hartree–Fock (HF) wave function and then to include some level of excitation from occupied to virtual orbitals (commonly single and double excitations denoted HF*S*D). The problem with this approach is that a bias in the HF level of description may well remain upon any fixed level of excitation. Thus, for CH_2 using a standard basis set (valence double zeta plus polarization, VDZ*p*), the $\Delta E_{ST} = 26.1$ kcal/mol for HF and 15.3 kcal/mol for HF*S*D (see Table I). The limit of this approach is to carry out a full CI for the given basis set. Unfortunately such full CI calculations may quickly become impractical (~220 000 spin eigenfunctions for DZ*p* and ~114 000 000 spin eigenfunctions for the TZ3*p*2*f*/*n* basis discussed below).

The alternative approach, which has proved practical for moderate-sized systems, is to solve self-consistently for the orbitals of the correlated wave function. In general, such wave functions are referred to as MCSCF (multiconfigurational self-consistent field); however, to obtain energy differences, it is important to have a scheme that specifies which level of MCSCF is consistent for the two states. This is provided by the generalized valence bond (GVB) approach[3,4] in which there is one valence orbital for each valence electron. Thus, the GVB wave function for both the singlet and triplet states of CH_2 involve six optimized orbitals (in addition to the doubly occupied C 1*s*-like orbital). This wave function is often denoted GVB(3/6) to indicate that three pairs of electrons are described with six orbitals. Advantages of the GVB approach are that (i) the correlated wave function can be interpreted in terms of one-electron orbitals, and (ii) accurate excitation energies and bond energies can be obtained using rather simple wave functions.

Recently[5] there has been discussion of whether such restricted wave functions may provide energy differences more accurate than is consistent with the basis set being used. In order to understand the magnitude of any such basis set bias, we carried out systematic studies of the convergence of GVB-like wave functions as a function of basis set.

II. GVB CALCULATIONS

The full GVB wave function for $^3CH_2$ or $^1CH_2$ would involve six overlapping orbitals optimized simultaneously with the combination of all permissible spin eigenfunctions (five for $^1CH_2$, nine for $^3CH_2$).[3] Although practical for CH_2, the N! overlapping terms makes such calculations impractical for large systems, but we have found the following approach to serve quite adequately. Starting with the dominant spin eigenfunction (the valence bond or perfect-pairing spin function), the orbitals are optimized, allowing the two orbitals describing each electron pair to overlap but requiring the orbitals of different pairs to be orthogonal. These GVB orbitals are calculated in terms of the two natural orbitals for each pair to yield the GVB-PP wave function. In terms of these natural orbitals, the GVB–PP wave function of $^1CH_2$ has $2^3 = 8$ closed-shell determinants. An advantage of the GVB–PP wave function is that all two-electron interactions can be expressed in terms of Coulomb and exchange terms so that it is not necessary to transform the two-electron integrals from the atomic orbital basis to the molecular orbital representation.[4] For the VDZ*p* basis, GVB–PP

a) Author to whom correspondence should be addressed.
b) Contribution No. 6832.

 0021-9606/87/020862-04$02.10

TABLE I. The singlet-triplet energy gap (ΔE_{ST}) for CH_2 for various levels of calculation within a VDZ*p* basis.[a]

Calculation	Total energies (h)[b]		ΔE_{ST} (kcal/mol)	
	$^1A_1$	$^3B_1$	VDZ*p*	DZ*p*
HF	− 38.885 87	− 38.927 49	26.12	
	(1/1)	(1/1)		
HF*S*D	− 39.016 70	− 39.041 07	15.30	
	(415/577)	(479/1485)		
GVB–PP	− 38.938 77	− 38.953 29	9.11	
	− 38.939 40	− 38.953 90		9.10
	(8/8)	(4/4)		
GVB–RCI(PP)[c]	− 38.941 51	− 38.959 25	11.13	
	− 38.942 12	− 38.959 73		11.05
	(18/20)	(9/25)		
GVB–RCI(opt)[d]	− 38.941 89	− 38.960 35	11.59	
	− 38.942 50	− 38.960 82		11.49
	(18/20)	(9/25)		
GVB–RCI(opt)*S*D[e]	− 39.025 49	− 39.044 62		12.00
	(7759/16 674)	(5078/22 230)		
Full CI	− 39.027 18	− 39.046 26		11.97[f]
	(~44 000/~220 000)			
Experiment			9.09 ± 0.20[g]	

[a] The corresponding number of spatial configurations/spin eigenfunctions for each wave function is given below each total energy. Basis sets (DZ*p* is the same as that used for the full CI results) are described in Sec. III.

[b] 1 h = 1 hartree = 627.5096 kcal/mol = 27.211 617 eV = 219 474.65 cm^{-1}.

[c] (PP) = orbitals from the GVB perfect-pairing wave function were used for the CI basis.

[d] Orbitals were optimized for the GVB–RCI.

[e] All single and double excitations of the six valence electrons were allowed from the self-consistent GVB–RCI wave function.

[f] Reference 5.

[g] Reference 2.

yields ΔE_{ST} = 9.11 kcal/mol, but as the basis is increased, ΔE_{ST} becomes 7.01 kcal/mol (see Table II).

The major discrepancy between GVB–PP and the full GVB wave function is the lack of other spin couplings. These spin couplings are included by carrying out a restricted configuration interaction (RCI) in which the two electrons of each pair are allowed to occupy the two natural orbitals of the pair in all three ways. For $^1CH_2$, this leads to $3^3 = 27$ configurations (nine of which are not allowed by symmetry). The GVB–RCI wave function can still be interpreted in

TABLE II. ΔE_{ST} (kcal/mol) as a function of basis set.[a]

Basis set	HF	GVB–PP	GVB–RCI		Full CI
			PP[b]	Opt[c]	
DZ*p*		9.10	11.05	11.49	11.97[d]
		(− 0.000 63)	(− 0.003 35)	(− 0.003 73)	
VDZ*p*	26.11	9.11	11.13	11.59	
	(0.052 90)	(0.000 00)	(− 0.002 74)	(− 0.003 12)	
VDZ2*p*/TZ2*p*		8.15	9.98	10.42	
		(− 0.003 79)	(− 0.006 63)	(− 0.007 07)	
VDZ2*pn*/TZ2*p*		7.84	9.63	10.06	
		(− 0.004 50)	(− 0.007 38)	(− 0.007 83)	
TZ2*p*		8.01	9.69	10.07	
		(− 0.008 29)	(− 0.011 36)	(− 0.011 85)	
TZ2*pf*/TZ2*p*		7.81	9.41	9.84	
		(− 0.008 83)	(− 0.011 93)	(− 0.012 41)	
TZ3*p*2*fn*/TZ2*p*	24.87	7.01	8.60	9.03	(9.09)[e]
	(0.045 14)	(− 0.010 46)	(− 0.013 52)	(− 0.014 02)	
Change with basis	1.24	2.09	2.45	2.46	(2.88)[e]

[a] Numbers in parentheses are the energies in hartrees of the singlet state relative to the GVB-PP wavefunction within the VDZ*p* basis (total energy = − 38.938 77 h).

[b] See Table I, footnote c.

[c] See Table I, footnote d.

[d] Reference 5.

[e] Assuming that the full CI with the most extensive basis leads to the experimental value.

terms of the GVB orbital picture, and the GVB–RCI wave function is generally a good approximation to the full GVB wave function. Using the orbitals from the GVB–PP wave function, the GVB–RCI leads to $\Delta E_{ST} = 11.13$ and 11.05 kcal/mol for VDZp and DZp bases, converging to 8.60 kcal/mol for the extended TZ3p2$f$$n$ basis. Rather than using the GVB–PP orbitals, we may solve self-consistently for the orbitals of the GVB–RCI wave function,[4(b)] obtaining thereby an even better approximation to the full GVB wave function. Calculating the orbitals for the GVB–RCI self-consistently, leads to 11.59 and 11.49 kcal/mol for VDZp and DZp bases, in good agreement with the full CI result (DZp) of 11.97 kcal/mol.[5] For the largest basis set used, this self-consistent GVB–RCI yields 9.03 kcal/mol, in excellent agreement with experiment.

III. CALCULATIONAL DETAILS

A. Basis sets

We used the following basis sets:

VDZp: The Dunning valence double zeta contractions[6] of the (9s5p) and the (4s) Huzinaga Gaussian primitive bases[7] for carbon and hydrogen (exponents scaled by 1.2) are used with one set of 3d polarization functions ($\zeta^d = 0.64$) on carbon and one set of 2p polarization functions ($\zeta^p = 1.0$) on hydrogen. The s combination of the carbon 3d functions are excluded from all basis sets and all calculations, except for calculations using the DZp basis set for direct comparison to the full CI result.[5]

DZp: This basis set is given explicitly in Ref. 5. It differs from the VDZp basis by having a DZ core on carbon, different 3d polarization functions for each state, and the s combination of the d functions was included in the calculations.[8]

VDZ2p/TZ2p: For carbon, the same (9s5p/3s2p) basis was used as above, with two sets of 3d functions centered at 0.64 but scaled by 2.3 ($\zeta^d = 0.971$ and 0.422). For hydrogen, the Huzinaga[7] unscaled (6s) basis was contracted to triple zeta, with two sets of 2p functions centered at 0.91 (optimized[9] for H bonded to C) but scaled by 2.3 ($\zeta^p = 1.38$ and 0.60).

VDZ2pn/TZ2p: To the VDZ2p/TZ2p basis was added one set of diffuse s ($\zeta^s = 0.045$) and p ($\zeta^p = 0.034$) functions optimized for negative ions of carbon.[9] This is denoted as "n" for negative ion.

TZ2p: The Huzinaga (11s7p) basis[10] for carbon was contracted to (6s3p) triple zeta for both core and valence. The carbon 3d and hydrogen 2p polarization functions are the same as in VDZ2p/TZ2p.

TZ2pf/TZ2p: One set of carbon 4f functions [$\zeta^f = 0.96$, chosen to maximize overlap with the carbon d-function ($\zeta^d = 0.64$)], with the three 4p combinations removed, was added to the carbon TZ2p basis.

TZ3p2fn/TZ2p: The Huzinaga (11s7p) basis for carbon was contracted triple zeta for both core and valence as before, but diffuse s and p functions were added by scaling out (by 2.5) from the most diffuse exponents of the (11s7p) set, yielding $\zeta^s = 0.0388$ and $\zeta^p = 0.0282$. Three sets of carbon 3d-polarization functions were added, centered at 0.640 and scaled by 2.5 (leading to exponents $\zeta^d = 1.60$, 0.640, and 0.256). Two sets of carbon 4f functions were included, obtained by scaling the previous 4f exponent of 0.96 by 2.5, yielding $\zeta^f = 1.52$ and 0.607. The 3s and 4p combinations of the d and f functions were removed. For hydrogen, the same Huzinaga triple zeta basis as above was used with two sets of p-polarization functions scaled by 3.0 from $\zeta^p = 0.91$, yielding $\zeta^p = 1.58$ and 0.525.

B. Geometries

The equilibrium geometries for $^1A_1$ and $^3B_1$ CH_2 were taken from the GVB–POL–CI calculations of Harding and Goddard[11] who found $\theta_e = 133.2°$ and $R_e = 1.084$ Å for the $^3B_1$ state and $\theta_e = 101.8°$ and $R_e = 1.113$ Å for the $^1A_1$ state. For calculations involving the DZp basis set, the geometries were taken from Ref. 5.

IV. RESULTS

The ΔE_{ST} using the VDZp and DZp bases for various wave functions are shown in Table I together with experimental (corrected for relativistic effects and zero-point motion)[2] and full CI[5] values. (The full CI calculation involved all excitations of the six valence electrons in CH_2, with the C 1s frozen at the HF level.) The self-consistent GVB–RCI (with 20 to 25 spin eigenfunctions) leads to $\Delta E_{ST} = 11.5$ kcal/mol, only 0.5 kcal/mol below the value $\Delta E_{ST} = 12.0$ kcal/mol obtained from the complete CI for this basis (with ~220 000 spin eigenfunctions). Allowing all single and double excitations from the self-consistent GVB–RCI wave function (with one-tenth the number of spin eigenfunctions of the full CI wave function) yields $\Delta E_{ST} = 12.0$ kcal/mol, in complete agreement with the full CI. While a study of basis set convergence at the RCI*SD level is impractical, the small error engendered for ΔE_{ST} (0.5 kcal/mol) with the simpler GVB wave functions suggests that they may prove adequate for studying the convergence of ΔE_{ST} with basis set.

This convergence with basis set is shown in Table II, where we see that for an extremely large basis, the self-consistent GVB–RCI converges to $\Delta E_{ST} = 9.03$ kcal/mol, in excellent agreement with the experimental result. For smaller bases, the values for ΔE_{ST} decrease smoothly as the basis is extended, with the differential effects being quite similar for all three calculational levels. Solving self-consistently for the orbitals of the GVB-RCI wave function contributes ~0.43 kcal/mol energy lowering to the excitation energies. This occurs because the RCI wave function includes spin-couplings important for the triplet state which are omitted in the perfect singlet pairing wave function, resulting in orbital shape changes for the self-consistent GVB–RCI. For the uncorrelated HF wave function, the total change in ΔE_{ST} between the VDZp basis and the full basis set is -1.24 kcal/mol, while it is -2.09 kcal/mol for GVB–PP and -2.46 kcal/mol for GVB–RCI. Similar studies of convergence for full CI as a function of basis set completeness are not available. Indeed, such a full CI test on our extended basis (TZ3p2fn/TZ2p) may well be beyond the scope of current computers, since it would require ~23 million spatial configurations, ~114 million spin eigenfunctions, or ~455 million determinants! However, if we assume that the full CI would agree with experiment for the full basis

set we have used, the drop in the excitation energy would have to be 2.88 kcal/mol. This is reasonable since the corresponding quantities for lower level wave functions are 1.24 (HF), 2.09 (GVB–PP), and 2.46 (GVB–RCI) kcal/mol.

V. CONCLUSION

We have shown that the simple GVB description of the two lowest states of CH_2 ($^1A_1$ and $^3B_1$) leads to singlet–triplet gaps within 0.5 kcal/mol of the full CI result for a DZ*p* basis set (still off from experiment by 2.4 kcal/mol). However, with GVB it is practical to use extremely extended bases, leading to results within 0.1 kcal/mol of the experimental value.

ACKNOWLEDGMENTS

This work was supported by the National Science Foundation (Grant No. CHE83-18041). EAC acknowledges a National Science Foundation predoctoral fellowship (1982–1985).

[1] E. A. Carter and W. A. Goddard III, J. Phys. Chem. **90**, 998 (1986), J Am. Chem. Soc. **108**, 4746 (1986).

[2] $T_0 = 9.023 \pm 0.014$ kcal/mol is taken from P. R. Bunker, P. Jensen, W. P. Kraemer, and R. Beardsworth, J. Chem. Phys. **85**, 3724 (1986), and is corrected for relativistic effects and zero point motion by 0.07 ± 0.20 kcal/mol [I. Shavitt, Tetrahedron **41**, 1531 (1985)] to arrive at a nonrelativistic $T_e = 9.09 \pm 0.20$ kcal/mol.

[3] R. C. Ladner and W. A. Goddard III, J. Chem. Phys. **51**, 1073 (1969).

[4] (a) W. J. Hunt, T. H. Dunning, Jr., and W. A. Goddard III, Chem. Phys. Lett. **3**, 606 (1969); W. A. Goddard III, T. H. Dunning, Jr., and W. J. Hunt, *ibid.* **4**, 231 (1969); W. J. Hunt, W. A. Goddard III, and T. H. Dunning, Jr., *ibid.* **6**, 147 (1970); W. J. Hunt, P. J. Hay, and W. A. Goddard III, J. Chem. Phys. **57**, 738 (1972); F. W. Bobrowicz and W. A. Goddard III, in *Methods of Electronic Structure Theory*, edited by H. F. Schaefer (Plenum, New York, 1977), pp. 79–127; (b) L. G. Yaffe and W. A. Goddard III, Phys. Rev. A **13**, 1682 (1976).

[5] C. W. Bauschlicher, Jr. and P. R. Taylor, J. Chem. Phys. **85**, 5936 (1986).

[6] T. H. Dunning, Jr., J. Chem. Phys. **53**, 2823 (1970).

[7] S. Huzinaga, J. Chem. Phys. **42**, 1293 (1965).

[8] Excluding the *s* combination of the 3*d* functions in the DZP basis leads to an increase in ΔE_{ST} (at all levels reported in Table I) of no more than 0.02 kcal/mol and a destabilization of the total energies by no more than 0.000 28 hartrees (0.18 kcal/mol).

[9] R. A. Bair and W. A. Goddard III (submitted).

[10] S. Huzinaga and Y. Sakai, J. Chem. Phys. **50**, 1371 (1969).

[11] L. B. Harding and W. A. Goddard III, Chem. Phys. Lett. **55**, 217 (1978).

Chapter 1.D. The text of this section is an Article coauthored with William A. Goddard III and is to be submitted to the *Journal of Chemical Physics.*

Correlation-Consistent Singlet-Triplet Gaps in Substituted Carbenes

Emily A. Carter and William A. Goddard III*

Contribution No. 7568 from the Arthur Amos Noyes Laboratory of Chemical Physics, California Institute of Technology, Pasadena, California 91125

Abstract: Ab initio GVB-CI (generalized valence bond with configuration interaction) and MCSCF (multiconfiguration self-consistent field) wavefunctions are used to calculate electronic state splittings for the lowest singlet and triplet states of substituted carbenes. The calculations emphasize *correlation consistency* between the two electronic states, resulting in short CI expansions. The singlet-triplet gaps (ΔE_{ST}) for CH_2, $CH(SiH_3)$, CF_2, CCl_2, CHF, and CHCl are reported. They are in good agreement with available experimental data.

I. Introduction

The diverse reactivity among substituted carbenes, CXY, is well-known.[1] In particular, stereoselective versus nonstereoselective reactions can be understood in terms of singlet versus triplet character in the carbenes, respectively. The triplet state ($\sigma^1\pi^1$) of CXY has one valence electron in each of two nonbonding orbitals on carbon, one σ and one π as in (1), while the singlet state (σ^2) can be considered to have both of these nonbonding electrons in the σ orbital. However, GVB calculations indicate that the σ^2 state actually involves one electron in a $\sigma + \pi$ orbital with the other electron in a $\sigma - \pi$ orbital.

$\sigma\pi$ σ^2 (1)

The "biradical" character of the triplet state results in nonstereospecific reactivity (involving nonconcerted, sequential steps of bond formation), while the closed shell character of the singlet state allows concerted, one-step, stereospecific chemical reactions.[1] Thus, in order to predict the reactivity expected for a given set of substituents at carbon in CXY, it is necessary to predict the singlet-triplet splittings of CXY. Qualitative predictions of whether particular substituents will give rise to singlet or triplet ground states can be based on the following considerations. Factors favoring singlet or σ^2 ground states are:

(i) Electron-withdrawing substituents will produce ionic bonds (C^+X^-). The strongest ionic bonds will be formed to carbon orbitals with the lowest ionization potential, namely, to the carbon p-orbitals. This increase of p-character in the C-X bond induces a decrease of p-character (and hence an increase of s-character) in the nonbonding valence σ orbital. This stabilizes the σ orbital relative to the π orbital (which has no s-character) and hence favors

the σ^2 or singlet state of CXY. Thus, for strongly electron-withdrawing X or Y, the ground state of CXY is σ^2.

(ii) Substituents with pπ lone pairs can stabilize them by donation into the carbon pπ orbital. Since the pπ orbital on carbon is nearly empty in the σ^2 state, this energy lowering is larger for the singlet state than for the triplet state, resulting in a σ^2 ground state.

The above requirements are fulfilled for halogen, alkoxy, or amido substituents, since all are relatively electronegative with respect to carbon and all have pπ orbitals which can donate into an empty carbon pπ orbital. Therefore, we expect a bias toward singlet ground states for X,Y = F, Cl, OR, NRR′, etc.

Factors favoring stabilization of triplet ground states are:

(iii) For electropositive substituents (with respect to carbon), the bond to carbon will have the opposite polarity to that discussed in (i). These substituents will favor a carbon hybridization with greater *s*-character (higher electron affinity), with more carbon *s*-character in the C-X bonds and concomitantly more *p*-character in the carbon nonbonding σ orbital. This will make the relative energies of the nonbonding valence σ and π orbitals more similar (due to similar amounts of *p*-character present), favoring the triplet state of CXY.

(iv) Sterically bulky substituents favor a large X-C-Y bond angle. Since two bonds to pure *p*-orbitals favor angles of 90-105° angle, while two bonds to sp^2-like ("lobe") orbitals prefer bond angles of 115-135°,[2] the effect of increasing the X-C-Y bond angle is to increase the amount of *s*-character in the C-X bonds. As in (iii), this results in more *p*-character in the carbon nonbonding valence σ orbital, producing energetically similar nonbonding valence orbitals on carbon (σ and π), favoring the triplet state.

Thus, triplet ground states of CXY are expected for substituents which are

electropositive (with respect to carbon) and/or are bulky. Thus the following groups favor triplet ground states: X,Y = hydrogen, alkyl, aryl, SiR_3, etc. Less conventional substituents in CXY which also fulfill (iii) and (iv) are X or Y = AlR_2 or BR_2. Synthesis and subsequent reactions of the latter carbenes should yield unusual reaction chemistry due to the presence of a Lewis acid site next to the nucleophilic triplet carbene.

While these qualitative arguments help in predicting which state of CXY (σ^2 or $\sigma^1\pi^1$) is lowest, it is often important to have quantitative information on the magnitude of the singlet-triplet splittings, ΔE_{ST}, for various CXY.

Experimental Values for $\Delta E_{ST}(CXY) = E_{singlet} - E_{triplet}$

The controversies between experiment and theory regarding the singlet-triplet gap in the parent carbene, methylene, have recently been reviewed.[3-5] The first direct measurement of the methylene singlet-triplet gap was obtained from laser magnetic resonance spectra due to rotational transitions within the $v = 0$ level of the $^1A_1$ excited electronic state and to transitions from those singlet levels to vibrationally excited levels of the $^3B_1$ ground electronic state.[6] With a nonrigid bender Hamiltonian analysis of the $^3B_1$ bending potential, in combination with ab initio calculations of the spin-orbit coupling responsible for the perturbations causing the transitions, a $\Delta E_{ST}(CH_2)$ of $T_0 = 9.05 \pm 0.06$ kcal/mol was obtained.

The most recent direct measurements[7] yield a value of $T_0 = 9.023 \pm 0.014$ kcal/mol, from vibronic analysis of the photoelectron spectra of CH_2^-.[8] Electron detachment from the ground electronic state of CH_2^- ($^2B_1$) results in the formation of either $^1A_1$ or $^3B_1$ CH_2, depending on whether an electron is removed from the nonbonding carbon π (1b1) orbital or the nonbonding carbon σ (3a1) orbital, respectively. While $^2B_1$ CH_2^- and $^1A_1$ CH_2 have similar equilibrium geometries, the $^3B_1$ state of CH_2 has a bond angle $\sim 30°$ larger than the other two [θ(H-C-H)$\approx 103°$ for $^2B_1$ and $^1A_1$ versus 134° for $^3B_1$].[3,8] The photoelectron spectrum is indicative

of these differing geometries, revealing a single (0-0) peak for the $^1A_1 \leftarrow {}^2B_1$ transition and a bending vibrational progression for the $^3B_1 \leftarrow {}^2B_1$ transition. From proper identification of the (0-0) peaks for both singlet and triplet, T_0 is obtained.

Recently, Shavitt[3] has estimated the correction for the conversion of an experimental determination of $T_0(CH_2)$ to a non-relativistic theoretical calculation of $T_e(CH_2)$ (ΔE_{ST}) to be 0.07±0.20 kcal/mol. Thus, currently the best experimental value (with which to compare theoretical results) for $\Delta E_{ST}(CH_2)$ is 9.09±0.21 kcal/mol.

While CH_2 has been studied in depth, both experimentally and theoretically, ΔE_{ST}'s for substituted carbenes have, for the most part, eluded experimental determination. Only two other $\Delta E_{ST}(CXY)$ have been measured:

(i) A value of −56.6 kcal/mol for $\Delta E_{ST}(CF_2)$ has been deduced from emission spectra observed during the reaction of (^3P) oxygen atoms with tetrafluoroethylene.[9] The products of this reaction are known to be CF_2 and CF_2O, with the initial spin-allowed product being the $^3B_1$ excited state of CF_2, which is then observed to phosphoresce down to the ground state, $^1A_1$ CF_2. The vibronic transitions are well-resolved, with the expected bending progression observed, due to the greatly different bond angles predicted for the singlet and triplet states of CF_2.[10]

(ii) An approximate value of $\Delta E_{ST}(CHF)$ has been assigned from photodetachment studies from the negative ion CHF^- ($^2A''$). As for CH_2, both the $^1A'$ ground state and the $^3A''$ excited state of CHF are formed, with varying degrees of vibrational excitation. Although the spectrum is not as well resolved as in the photoelectron studies of CH_2, a tentative value of ~ -15 kcal/mol has been assigned to $T_0(CHF)$.[11]

Previous Theoretical Values for $\Delta E_{ST}(CXY)$

The first reliable ab initio study of substituted carbene singlet-triplet split-

tings was carried out by Bauschlicher *et al.*[10] Although the calculations were performed at a relatively low level [Hartree-Fock (HF) for the triplet and GVB(1/2) for the singlet], the important feature of these calculations is that the two states are treated in a *balanced* manner.[12] In particular, since the triplet nonbonding electrons on carbon occupy two orbitals, the singlet nonbonding electrons in this calculation are also allowed to occupy two orbitals [hence the GVB(1/2) calculation]. This leads to a relatively *unbiased* calculation of the electronic energy splitting, since the same number of orbitals are included in the description of both states. However, this level still has biases, with a higher degree of residual electron correlation error in the singlet than in the triplet.

Using this level of theory, Bauschlicher *et al.*[10] optimized the geometries of the lowest singlet and triplet states of CH_2, CF_2, CCl_2, CHF, CHCl, and CHBr, using double-ζ plus polarization bases, and obtained the following ΔE_{ST}'s (negative values indicate a singlet ground state): 12.8 (CH_2), −46.5 (CF_2), −13.5 (CCl_2), −9.2 (CHF), −1.6 (CHCl), and 1.1 kcal/mol (CHBr).

Other fluorine-substituted carbenes have been examined by Dixon,[13] at the same calculational level. With a valence double-ζ basis augmented by polarization functions on the central carbon and on the atoms directly attached to the central carbon, he found the following ΔE_{ST}'s: 14.0 (CH_2), −46.0 (CF_2), −8.1 (CHF), 13.0 ($CHCF_3$), −9.1 ($CFCF_3$), and 17.8 kcal/mol [$C(CF_3)_2$]. Luke *et al.*[14] used MP4 (Moller-Plesset perturbation theory through fourth order), starting from RHF (singlets) and UHF (triplets) first order wavefunctions, in order to calculate a variety of carbon and silicon based small molecules. Pertinent to our work (vide infra) are ΔE_{ST} = 16.8 (CH_2), −12.7 (CHF), and 25.7 [$CH(SiH_3)$] kcal/mol. Schaefer and co-workers,[15] using a CI-SD approach, and Köhler *et al.*,[16] using the CEPA (correlated electron pair approximation) method, have also obtained theoretical values for ΔE_{ST}[$CH(SiH_3)$] of 27.2 and 20.3 kcal/mol, respectively. Finally, Scuseria *et al.*[17] used CI-SD calculations to obtain values of −12.9 (CHF), −3.7 (CHCl), and

−3.1 (CHBr) kcal/mol, respectively.

All of the methods used above tend to *overestimate* ΔE_{ST}(CXY) for ground state triplets and to *underestimate* ΔE_{ST}(CXY) for ground state singlets. This is due to the fact that the above techniques do *not* include balanced levels of electron correlation for both singlet and triplet states: the triplet is always correlated to a greater extent than the singlet, leading to an artificially destabilized singlet.

The objective of this paper is to obtain more accurate ΔE_{ST}'s, but from simpler wavefunctions. Section II discusses several levels of correlation-consistent CI calculations designed to obtain unbiased excitation energies; Section III reports new results using the methods described in Section II to obtain ΔE_{ST} for CH_2, $CH(SiH_3)$, CF_2, CCl_2, CHF, and CHCl; Section IV discusses these predictions by comparison with experiment, previous theory, and thermochemical estimates,[18] with Section V offering concluding remarks.

II. Theoretical Method

Basis Sets

The same carbon and hydrogen basis sets were used for all of the carbenes studied. The Dunning[19] valence double-ζ (VDZ) contractions of the carbon (9s5p) and the hydrogen (4s) gaussian primitive bases of Huzinaga[20] were used (hydrogen exponents scaled by 1.2), augmented by one set of 3d polarization functions (3*s*-combination removed) on carbon ($\zeta^d = 0.64$)[21] and by one set of 2p polarization functions on hydrogen (ζ^p=1.0). Dunning's VDZ contraction[19] of Huzinaga's (9s5p) primitive basis[20] for fluorine was employed. The shape and hamiltonian consistent effective core potentials of Rappé *et al.*[22] were used for Cl and Si. The valence electrons of Cl and Si were treated explicitly, within the double-ζ basis sets of Rappé *et al.*[22] for Cl and Si, with one set of 3d polarization functions added to the Si basis (3*s*-combination removed; ζ^d=0.3247).

Geometries

The equilibrium geometries of $^1A_1$ and $^3B_1$ CH_2 were taken from the Harding and Goddard GVB-POL-CI calculations,[23] with $\theta_e = 101.8°$ and $R_e = 1.113Å$ for the $^1A_1$ state and $\theta_e = 133.2°$ and R_e=1.084Å for the $^3B_1$ state.

The optimum geometries for the $^1A_1$ and $^3B_1$ states of CF_2 and CCl_2 were taken from the HF/GVB(1/2)PP calculations of Bauschlicher *et al.*[10] For $^1A_1$ CF_2, $\theta_e = 104.7°$ and $R_e = 1.291Å$. For $^3B_1$ CF_2, $\theta_e = 118.2°$ and $R_e = 1.303Å$. For $^1A_1$ CCl_2, $\theta_e = 109.4°$ and $R_e = 1.756Å$. For $^3B_1$ CCl_2, $\theta_e = 125.5°$ and $R_e = 1.730Å$.

The equilibrium geometries used for the singlet and triplet states of CHF and CHCl were taken from the HF/GVB(1/2)PP geometry optimizations by Scuseria *et al.*[17] For $^1A'$ CHF, $\theta_e = 103.3°$, R_e(C-F) = 1.294Å, and R_e(C-H) = 1.104Å. For $^3A''$ CHF, $\theta_e = 121.1°$, R_e(C-F) = 1.304Å, and R_e(C-H) = 1.073Å. For $^1A'$ CHCl, $\theta_e = 102.1°$, R_e(C-Cl) = 1.725Å, and R_e(C-H) = 1.092Å. For $^3A''$ CHCl, θ_e = 124.4°, R_e(C-Cl) = 1.699Å, and R_e(C-H) = 1.070Å.

The geometries for the $^1A'$ and $^3A''$ states of $CH(SiH_3)$ were optimized in the present work, with the following constraints imposed: (i) overall C_s symmetry was assumed; (ii) The Si-H bond lengths were fixed at 1.487Å and the H-Si-H angles were fixed at 108.3° (with local C_{3v} symmetry imposed), which correspond to optimum values from GVB calculations[24] on Si_2H_6; and (iii) the SiH_3 group was assumed to be staggered with respect to the HC bond (as found from MINDO/3 calculations).[25] Using those parameters, the H-C-Si angle and the C-Si and C-H bond lengths were optimized at the GVB(2/4)PP level for the triplet and the GVB(3/6)PP level for the singlet (see below for a description of the calculation). The optimum values obtained are shown in Table I.

MC-SCF and CI Calculations

In order to predict accurate excitation energies, it is essential that both electronic states involved in the excitation process be treated equivalently. This

includes both the number of orbitals optimized in the SCF and the degree of electron correlation included in the wavefunction.

Several research groups[12,26] realized early on the importance of utilizing two configurations (σ^2 and π^2) in order to describe the $^1A_1$ state with the same degrees of freedom enjoyed by the single configuration description of the $^3B_1$ state ($\sigma^1\pi^1$). This two-configuration wavefunction description of the lone pair on carbon is the simplest form of the generalized valence bond (GVB) method,[27] which usually describes each of the M valence electron pairs with two natural orbitals leading to a 2^M configuration self-consistent field (MC-SCF) wavefunction. This MC-SCF wavefunction is designated **GVB(M/2M)-PP**, where M electron pairs are described by 2M natural orbitals and PP refers to the perfect singlet-pairing restriction (each electron pair optimized in the SCF is constrained to be singlet-coupled). Since a triplet state involves one pair of electrons with two orbitals as in a GVB(1/2) singlet, we will denote the HF triplet wavefunction also as GVB(1/2). The GVB(M/2M) wavefunction satisfies our requirement that the same number of orbitals are optimized in the SCF for both states. In particular, for CH_2, the six valence electrons are allowed to occupy six orbitals in both states.

While the GVB(M/2M)-PP wavefunction provides a reasonable first-order description of most molecules, lifting the restriction of singlet-pairing within GVB pairs is necessary in order to allow the other spin-couplings of a full GVB wavefunction. By allowing the two electrons in each GVB pair to occupy the two natural orbitals of the pair in all three ways, all other possible spin-couplings between the valence electrons are included. This wavefunction is referred to as **GVB-RCI(PP)** to indicate that the RCI (restricted configuration interaction) is performed within the orbitals optimized at the PP level. If the orbitals of the GVB-RCI wavefunction are calculated self-consistently, it is denoted GVB-RCI(opt). The GVB-RCI wavefunction (Ψ^{RCI}) maintains the GVB orbital picture of one electron per orbital, while obtaining optimized spin-coupling for each electronic state. In addition to

optimized spin-coupling, the RCI also incorporates ionic configurations and inter-pair correlation (i.e., dynamic correlated movement of charge within adjacent bond pairs). The effectiveness of the RCI was illustrated in a recent paper[28] on the singlet-triplet splitting in CH_2, where GVB-RCI(opt) using a DZP basis (20-25 spin eigenfunctions) calculates ΔE_{ST} to within 0.5 kcal/mol of the six electron full CI result[29] (~220,000 spin eigenfunctions). Furthermore, for an extended basis, the GVB-RCI(opt) yields ΔE_{ST} within 0.06 kcal/mol of the best experimental value.[3,7,8] Thus the GVB-RCI includes the dominant correlations important for an accurate and balanced description of electronic excitation processes, while eschewing irrelevant terms.

For substituted carbenes, the RCI with six active electrons describes the dominant σ charge transfer in the C-X and C-Y bonds and the optimal spin coupling for both the singlet and triplet states. However, for the carbenes with halogen substituents, π-donation from the halogen p lone pairs into the carbon pπ orbital is extremely important in the stabilization of the singlet state. Thus, for the halogen-substituted carbenes, we carry out the following calculations:

RCI*ΠCI(PP): starting from the GVB(M/2M)PP wavefunctions (where M = 2 for the triplets and M = 3 for the singlets), we allow a full CI within the π orbitals for each of the RCI configurations described above. This allows synergistic π-donation to the carbon and σ charge transfer from carbon to the halogens. We have also optimized this wavefunction self-consistently [denoted **RCI*ΠCI(opt)**], to evaluate possible orbital shape changes induced by the charge transfer in this CI. Since the RCI and RCI*ΠCI wavefunctions build the same correlations into both the singlet and triplet states of CXY, they are both correlation-consistent. (For CXY without lone pairs on X or Y, the RCI and the RCI*ΠCI wavefunctions are equivalent.)

The above wavefunctions only utilize valence space excitations. Since the process of interest involves an electronic excitation between the σ and π orbitals, it is

essential to allow full correlation (full freedom within the basis) of the two electrons involved in the σ and π orbitals. Therefore, to the RCI [for CH_2 and $CH(SiH_3)$] or to the RCI*ΠCI (for CHF, CHCl, CF_2, and CCl_2) configurations, we include (from each RCI configuration) all single and double excitations of the two carbon electrons in the nonbonding σ and π orbitals to all virtual orbitals [designated as **RCI*[ΠCI + $SD_{\sigma\pi}$](PP)**]. We refer to this level of CI as the correlation-consistent CI (CCCI), since it allows the same correlation and spin-coupling degrees of freedom for both singlet and triplet states, resulting in a balanced description of each. The CCCI (RCI*[ΠCI + $SD_{\sigma\pi}$(PP)]) is performed using the GVB-PP wavefunction as the first order description, since the π orbitals after the RCI*ΠCI(opt) calculation are not unique (thus single and double excitations from the carbon nonbonding electrons are not uniquely defined), which might lead to an imbalanced description of the two states.

Our overall approach is to include the dominant excitations dictated by the physical interactions in the process of interest. Namely, for an electronic excitation involving one pair of electrons, it is essential to allow the best possible description of those two electrons (i.e. a full CI within the basis). Secondly, substituents at carbon which form partially ionic bonds [either donating to carbon (e.g., $CHSiH_3$) or withdrawing charge from carbon (e.g., CHF) in the σ system] require an RCI description to allow for such σ charge transfer. Thirdly, substituents at carbon with pπ lone pairs can donate charge to the carbon pπ orbital, requiring the full CI in the π valence space. Finally, the MC-SCF solves for the optimum orbital shapes of the RCI*ΠCI wavefunction, with optimal spin-coupling included.

We have left out many second order excitations which would be included in a typical CI scheme. However, these other excitations may not treat the singlet and triplet states of CXY equivalently. Since the RHF level has much less electron correlation error in the triplet state than in the singlet state [two singly-occupied orthogonal orbitals (triplet) versus one doubly-occupied orbital (singlet)], a single

and double excitations CI (CI-SD) can fully correlate each of the C-X and C-Y bond pairs in the triplet, but not in the singlet (e.g., double excitations in the σ pair would go with an uncorrelated C-X bond, while double excitations in the C-X bond would go with an uncorrelated σ pair). For example, starting from the HF wavefunction for CH_2 ($^3B_1$) and the GVB(1/2) wavefunction for CH_2 ($^1A_1$) (using a valence double zeta basis set[19] plus one set of 3d functions on carbon[21] and a triple zeta basis set[19] plus one set of unscaled 2p functions on each H) and allowing full correlation of the two nonbonding carbon electrons (single and double excitations to all virtuals), the triplet is stabilized by only 6.8 millihartrees while the GVB(1/2) σ pair is lowered by 15.2 millihartrees. Using the HF description of the singlet, the σ pair is stabilized by 36.2 millihartrees. Therefore, the triplet nonbonding electrons have less correlation error than either description of the singlet nonbonding electrons, and thus single and double excitations from all valence orbitals will overcorrelate the triplet relative to the singlet.

In addition, CI-SD also suffers from a spin-coupling bias. Consider a double excitation from two closed shell orbitals (e.g., one single excitation from each C-X and C-Y bond pair). The triplet configuration has six open shell electrons which have nine possible spin-couplings while the singlet configuration has only four open shell electrons with only two possible spin-couplings. Therefore the triplet CI-SD wavefunction, with a maximum of six open shells can mix in up to *nine* spin eigenfunctions per spatial configuration, but the singlet CI-SD wavefunction, with a four open shell maximum, is restricted to *two* spin eigenfunctions per spatial configuration, resulting in greater flexibility for the triplet.

Both of the problems listed above (unbalanced correlation and spin-coupling) for CI-SD result in a bias in favor of the triplet state, leading to singlet-triplet splittings too high for ground state triplets and too low for ground state singlets. In contrast, the CCCI has *the same maximum number of open shells for each state (six)* and allows the same correlations for each state, treating the spin-coupling (as

well as the correlation) in an unbiased manner.

III. Results

A. CH_2

The singlet-triplet splittings in methylene are summarized in Table II. The CCCI result [RCI*$SD_{\sigma\pi}$(PP)] yields ΔE_{ST} = 9.0 kcal/mol, in excellent agreement with experiment (ΔE_{ST} = 9.1 kcal/mol). We should note that there is apparently a cancellation of errors between basis set deficiencies and inclusion of higher correlation, resulting in an extra accurate value for CCCI within a DZP type basis.

B. $CHSiH_3$

Since Si is more electropositive than H, we expect larger amounts of carbon $2s$ character in an SiC bond, leaving more $2p$ character in the carbon nonbonding σ orbital. This renders the two nonbonding orbitals on carbon close in energy, favoring the triplet state and leading to a larger singlet-triplet splitting for $CHSiH_3$ than for CH_2. Indeed, as shown in Table III, ΔE_{ST} for $CHSiH_3$ is 18.4 kcal/mol, about twice that for CH_2. As consistent with the discussion in Section II, other methods[14-16] appear to overestimate the singlet-triplet gap.

As further support for our qualitative analysis of the bonding, the GVB one electron orbitals are shown in Figs. 1 and 2 for the ground ($^3A''$) and excited ($^1A'$) states of $CHSiH_3$, respectively. A dramatic difference is visible in all valence orbitals for each state. For the triplet state, the carbon orbitals involved in the C-Si and C-H bonds have dominantly s-character, while for the singlet, these orbitals have dominantly p-character. Concomitantly, the nonbonding carbon σ orbital changes from mostly p in the triplet to mostly s in the singlet.

A quantitative indication of the s and p contributions may be evaluated using the Mulliken approximation (shown in Table IV).[30] Although Mulliken populations at best provide a qualitative indication of charge transfer, relative trends are expected to be reliable. For the triplet state, the hybridizations at carbon in the

C-Si and C-H bonds are 60.8% 2s/39.2% 2p and 45.4% 2s/54.6% 2p, respectively (more s-character in the C-Si bond, as expected), while the lone pair hybridization is 11.2% 2s/88.8% 2p. The carbon pulls off 0.37 electron from the Si, illustrating the polar nature of the carbon-silicon bond. In the singlet state, the hybridizations at carbon in the C-Si and C-H bonds are dramatically different, with 20.9% 2s/79.1% 2p and 17.1% 2s/82.9% 2p character, respectively, while the σ nonbonding orbital is 61.4% 2s/36.6% 2p. The singlet favors s-character in the nonbonding σ lone pair and concomitantly more p-character in the bonds.

C. CF_2

The singlet-triplet splittings for CF_2 are shown in Table V. In this case, the electon-withdrawing fluorines force more p-character into the C-F bonds and more s-character in the nonbonding σ orbital, favoring a singlet ground state. As seen in Table V, the singlet is stabilized greatly with respect to the triplet even at the HF level, and increasing the level of electron correlation yields $\Delta E_{ST} = -57.5$ kcal/mol, in excellent agreement with the experimental value of -56.6 kcal/mol. The only previous theory involved a GVB(1/2) calculation,[10] yielding -46.5 kcal/mol. Notice that $|\Delta E_{ST}|$ increases greatly upon the inclusion of π-donation to the carbon $p\pi$-orbital, since this stabilizes the singlet much more than the triplet. The single and double excitations from the σ and π nonbonding carbon orbitals serve to increase $|\Delta E_{ST}|$ even further. The self-consistent RCI*ΠCI(opt) calculation (for all the carbenes) yields results close to the RCI*[ΠCI + $SD_{\sigma\pi}$] calculation, even though it is a much smaller (valence level) CI, providing an independent estimate of the true ΔE_{ST}(CXY).

The orbitals for the $^3B_1$ excited state of CF_2 are shown in Fig. 3 (we do not show the $^1A_1$ orbitals since they are very similar). Comparing the bond pairs in Figs. 1 and 3 shows that the fluorines do indeed bond preferentially to the carbon p-orbitals (even more so in the $^1A_1$ state of CF_2) to form the best ionic bonds, while SiH_3 and H form bonds with much more s-character. The carbon σ

radical orbital in $^3B_1$ CF_2, displayed in Fig. 3b, has a large s-component while the same radical orbital in $^3A''$ $CHSiH_3$ is nearly all p in character. Therefore, electronegativity differences do indeed dictate the character of the C-X and C-Y bonds, thus controlling the amount of s-character in the nonbonding carbon σ orbital and hence the relative energies of the nonbonding σ and π orbitals (which determines whether the ground state of CXY is a triplet or singlet).

Analysis of the Mulliken populations for both the $^1A_1$ and $^3B_1$ states quantify the hybridization and charge transfer in the CF_2 bonds (Table IV). The $^1A_1$ ground state has 19.0% 2s/81.0% 2p character in the C-F bonds and 69.8% 2s/30.2% 2p in the carbon σ nonbonding orbital. The $^3B_1$ excited state has 45.3% 2s/54.7% 2p character in the C-F bonds and 52.7% 2s/47.3% 2p in the carbon σ nonbonding orbital. These results are consistent with the expectation that the singlet state will have mainly p-character in the bonds and dominantly s-character in the σ nonbonding orbital.

D. CCl_2

Since Cl is less electronegative than F, we expect that ΔE_{ST} will be less negative for CCl_2 than for CF_2. This is borne out in Table VI, where the singlet-triplet gaps for CCl_2 are listed as a function of increasing electron correlation. Hartree-Fock theory actually finds the triplet lower than the singlet by 0.1 kcal/mol, but GVB-PP already yields a singlet ground state. Similar to the other RCI predictions of ΔE_{ST}(CXY), the RCI results using PP orbitals stabilize the triplet slightly more than the singlet, since the optimum spin-coupling introduced by the RCI is more important for the triplet. Inclusion of the pπ donation from the Cl's increases $|\Delta E_{ST}|$ substantially, with the optimized orbitals in the RCI*ΠCI(opt) calculation increasing the gap still further. Inclusion of single and double excitations from the carbon nonbonding electrons yields our best value for $\Delta E_{ST}(CCl_2) = -25.9$ kcal/mol. The only previous theoretical result for $\Delta E_{ST}(CCl_2)$ is from GVB(1/2) calculations[10] which yielded −13.5 kcal/mol, falling in between the HF and GVB(M/2M)PP val-

ues (M = 2 for triplet and N = 3 for singlet), as expected. Clearly, inclusion of π donation and full correlation of the carbon lone pair (nonbonding electrons) is crucial for predicting the singlet-triplet splitting correctly.

Mulliken population analyses (Table IV) of the GVB(M/2M)PP wavefunctions for $^1A_1$ and $^3B_1$ CCl_2 are consistent with the fact that Cl is not as electron-withdrawing as F, so that somewhat less p-character is found in the C-Cl bonds (relative to the C-F bonds). The amount of p-character in the C-Cl bonds is still much larger in the singlet than in the triplet, as expected from arguments outlined in the introduction (19.5% s/80.5% p for $^1A_1$ and 53.5% s/46.5% p for $^3B_1$). The carbon lone pair σ orbital is primarily s-like for the singlet (72.8% s/27.2% p) and primarily p-like for the triplet (39.0% s/61.0% p), as expected. The total amount of charge transfer is the same overall (0.1 electron transferred to carbon in each state), but the partitioning is different: in the singlet, 0.20 electron is pulled off carbon in each σ bond, countered by 0.50 electron donated to carbon in the π system, while in the triplet, only 0.06 electron is removed from carbon by each σ bond, compensated by the π charge transfer of 0.23 electron. Since π-donation is larger than σ charge transfer, it is as important as the σ charge transfer in determining the separation of singlet versus triplet states.

E. CHF

The singlet-triplet splittings for CHF are displayed in Table VII. Hartree-Fock theory again predicts (incorrectly) the ground state to be $^3A''$, while GVB-PP correctly predicts the ground state to be $^1A'$. CCCI yields ΔE_{ST}(CHF) = -17.7 kcal/mol, in good agreement with a tentative experimental value of ~ -15 kcal/mol.[11] Previous theoretical values include -9.2 kcal/mol[10] from GVB(1/2) [less negative than the GVB(M/2M)PP value reported here, as expected], -12.7 kcal/mol[14] from MP4 calculations (these start with the RHF wavefunction for the singlet, building in a bias toward a smaller ΔE_{ST}), and -12.9 kcal/mol[17] from CI-SD calculations which utilized a GVB(1/2) reference state for the singlet and an

HF reference state for the triplet. Even though the CI-SD was carried out with a triple-ζ plus double polarization (TZ2P) basis set and included as many as 119,604 configurations[17] (CCCI has 1192 configurations), this method still *underestimates* ΔE_{ST}(CHF) by 5 kcal/mol.

The singlet-triplet splitting is not as large for CHF as for CCl_2 or CF_2, presumably because only one electronegative/*pi*-donating substituent is attached to carbon. The Mulliken populations (Table IV) substantiate this; while the fluorine pulls off 0.36-0.40 electron from carbon in the C-F bond, the π-donation brings the net charge at carbon back to +0.04 for $^1A'$ and +0.01 for $^3A''$. The hybridizations of the C-F and C-H bonds follow the trend, with more carbon *p*-character for the singlet than for the triplet (C-F: 79.7% p for $^1A'$ and 63.5% p for $^3A''$; C-H: 85.5% p for $^1A'$ and 40.2% p for $^3A''$). The nonbonding σ orbital at carbon has concomitantly more *s*-character for the singlet (67.4% s), whereas the triplet has more *p*-character (65.2% p).

F. CHCl

The singlet-triplet gaps for $^1A'$ and $^3A''$ CHCl are shown in Table VIII. Hartree-Fock theory again predicts a triplet ground state, while GVB-PP finds a ground state singlet, consistent with higher levels of electron correlation. ΔE_{ST}(CHCl) is smaller than for all the other substituted carbenes examined in this work, consistent with the smaller electronegativities of H and Cl. The largest correlation-consistent CI calculation yields −9.3 kcal/mol for ΔE_{ST}(CHCl), which may be compared with previous theoretical values of −1.6 [GVB(1/2)][10] and −3.7 kcal/mol [GVB(1/2)*SD with a TZ2P basis].[17] Again, even though the CI-SD calculation involved up to 74,546 configurations and used a TZ2P basis,[17] the correlation-consistent CI method yields a more accurate value for ΔE_{ST} (based on the results for CHF), with only 1192 configurations.

Much less charge transfer is found for CHCl than for the other halogen-substituted carbenes (Table IV). Chlorine pulls off 0.10 and 0.22 electron from

arbon in the C-Cl bond of CHCl in the $^3A''$ and $^1A'$ states, respectively, but this is completely countered in π system (leaving the Cl with +0.02 and +0.03 total charge in the $^1A'$ and $^3A''$ states, respectively). As found for all of the halogen-substituted carbenes, $^1A'$ CHCl has mostly p-character in the C-H and C-Cl bonds (C-H: 82.6% p and C-Cl: 78.5% p) and mostly s-character in the nonbonding σ orbital (67.8% s), while $^3A''$ CHCl has less p-character in the C-H and C-Cl bonds (C-H: 44.4% p and C-Cl: 51.4% p) and more p-character in the nonbonding σ orbital (70.3% p).

IV. Discussion

Our results for the singlet-triplet splittings in six carbenes are summarized in Table IX for the three highest calculational levels, along with comparisons to a full CI value[29] for $\Delta E_{ST}(CH_2)$, experimental data for ΔE_{ST} (CH_2,[3,7,8] CF_2,[9] and CHF[11]), and thermochemical estimates for ΔE_{ST} (CF_2, CCl_2, CHF, and CHCl).[18] The agreement between CCCI and experiment is excellent, where experimental ΔE_{ST}'s are available (CH_2, CF_2, and CHF).

As reported previously,[28] the RCI(opt) method with only 20-25 spin eigenfunctions yields a ΔE_{ST} for CH_2 which is within 0.5 kcal/mol of the full CI result for a DZP basis. Using the correlation error incurred by all three calculational levels relative to this full CI result, we can estimate the full CI results for the other carbenes studied here (ignoring differential correlation errors for substituted carbenes). These full CI estimates are shown in parentheses.

The CCCI wavefunction yields a $\Delta E_{ST}(CH_2)$ value close to experiment, and assuming the residual correlation error present in CCCI for CH_2 is the same in other systems, we have estimated "experimental" values for ΔE_{ST} of the substituted carbenes (shown in parentheses). The agreement is good where experimental data are available.

We have shown in previous work[18a] that the dominant contribution to the bond weakening in substituted olefins and methanes (relative to the parent com-

pounds C_2H_4 and CH_4) is the promotional cost to excite CXY from a ground state singlet (nonbonding) to the excited state triplet (bonding). This relationship was used to derive thermochemical estimates for ΔE_{ST}(CXY) by evaluating C=C and C-H bond weakening in various substituted olefins and methanes.[18a] The estimates for ΔE_{ST} shown in Table IX are different than those derived in Ref. 18a, since more than one value for the heats of formation of CXY are used in the present work (Table X). The large uncertainties associated with our thermochemical estimates of ΔE_{ST} are a direct result of the uncertainties associated with the experimental heats of formation and bond energies (Table X).

For instance, the estimated ΔE_{ST} for CF_2 in Ref. 18a was based solely on a value for the C=C bond energy in C_2F_4 (76.3±3 kcal/mol), measured by Margrave and co-workers[31] from the heat of the reaction $C_2F_4 \rightleftharpoons 2\ CF_2$. The thermal decomposition of C_2F_4 to form CF_2 was followed at temperatures between 1127 and 1220°K in a Knudsen cell to obtain the equilibrium constant as a function of temperature from the appearance potential (AP) intensities of $C_2F_4^+$ and CF_2^+. Errors in the equilibrium constant may be due to the assumptions needed to convert the AP intensities to partial pressures or to the lack of a true thermal equilibrium (C_2F_4 was formed by pyrolysis of Teflon and an equilibrium was assumed since CF_2^+ was observed in the mass spectrometer). Indeed, a third law analysis of shock-tube experiments yields $\Delta H^o_{f,298} = 67.5$ kcal/mol for the $C_2F_4 \rightleftharpoons 2\ CF_2$ equilibrium.[31,32] The discrepancies between these two direct measurements of the C=C bond energy in C_2F_4 (67.5 versus 76.3 kcal/mol) suggests that a more reliable estimate of this bond energy might be obtained from independent measurements of the heats of formation of C_2F_4 and CF_2. Unfortunately, while three independent measurements for $\Delta H^o_{f,298}(C_2F_4)$ agree to within 0.7 kcal/mol (-157.4 ± 0.7 kcal/mol),[33] the heat of formation of CF_2 is much less certain. The two most recent values are -52.[34] and -44.2 ± 1[35] kcal/mol, leading to $D^{expt}_{298}(F_2C{=}CF_2) = 53.4{\pm}0.7$ and $69.0{\pm}2.7$ kcal/mol, considerably different from Margrave's determination. If these

two estimates are used for the C=C bond energy, then the thermochemical estimate for $\Delta E_{ST}(CF_2)$ becomes -55.4 ± 3.9 kcal/mol, in much better agreement with both theory and experiment.

Table X displays new predictions for C=C bond energies in substituted olefins, based on the premise[18a] that when CXY has a singlet ground state, the C=C bond in the corresponding olefins will be weakened relative to the C=C bond in ethylene by $\Delta E_{ST}(CXY)$. We obtain the new predictions by subtracting our best ab initio values for ΔE_{ST} (the CCCI calculations in Table IX) from 172.2 ± 2.1 kcal/mol (the C=C bond energy in ethylene):[33]

$$D^o_{f,298}(XYC=CX'Y') = D^o_{f,298}(H_2C=CH_2) - \Delta E_{ST}(CXY) - \Delta E_{ST}(CX'Y')$$
$$= 172.2 \pm 2.1 - \Delta E_{ST}(CXY) - \Delta E_{ST}(CX'Y'), \qquad (2)$$

where ΔE_{ST} (CH_2) is set to zero in Eq. (2) (ground state triplets incur no promotional costs).[18a] These new estimates for $D^o_{f,298}(XYC{=}CX'Y')$ compare favorably in most cases with the experimental bond dissociation energies also shown in Table X. While the discrepancies are due in part to uncertainties in the experimental heats of formation of CXY, Eq. (2) assumes the intrinsic C=C bond strength for all olefins to be constant (that of C_2H_4).[18a] Recent calculations on the intrinsic C=C bond strength (to dissociate to triplet fragments) of C_2F_4 reveal that $D^{int}_{298}(F_2C{=}CF_2)$ is greater than $D^{int}_{298}(H_2C{=}CH_2)$ by 6.9 kcal/mol.[36] Since C_2F_4 should perturb $D^{int}_{298}(C{=}C)$ more than any other halogenated olefin, $\Delta D^{int}_{298} = 6.9$ kcal/mol should be an upper bound on the error of our predicted C=C bond energies.

V. Conclusions

Ab initio GVB-CI calculations have been carried out to determine the singlet-triplet splittings for a variety of substituted carbenes. Emphasizing *correlation-consistency* and including the dominant charge transfer processes in the choice of the CI expansion leads to accurate values for $\Delta E_{ST}(CXY)$ using quite small CI

calculations. Explanations have been offered as to why other methods tend to *overestimate* ΔE_{ST} for ground state triplets and *underestimate* ΔE_{ST} for ground state singlets. The new values for ΔE_{ST} obtained in the present work are used to predict new C=C bond energies in substituted olefins.

Acknowledgments. This work was supported by the National Science Foundation (Grant No. CHE83-18041) and the Shell Companies Foundation. EAC acknowledges a National Science Foundation predoctoral fellowship (1982-1985), a research grant award from the International Precious Metals Institute and Gemini Industries (1985-1986), and a SOHIO fellowship in Catalysis (1987).

References

(1) a) W. Kirmse, "Carbene Chemistry" (Academic, New York, 1971); b) P. P. Gaspar and G. S. Hammond, in "Carbenes", R. A. Moss and M. Jones, Eds. (Wiley, New York, 1975), Vol. 2; c) R. A. Moss and M. Jones, in "Reactive Intermediates", M. Jones and R. A. Moss, Eds. (Wiley, New York, 1981), Vol. 2; d) *ibid.* (Wiley, New York, 1985), Vol. 3; e) E. R. Davidson, in "Diradicals", W. T. Borden, Ed. (Wiley, New York, 1982).

(2) W. A. Goddard III and L. B. Harding, Ann. Rev. Phys. Chem. **29,** 363 (1978).

(3) I. Shavitt, Tetrahedron **41**, 1531 (1985).

(4) W. A. Goddard III, Science **227**, 917 (1985).

(5) H. F. Schaefer III, Science **231**, 1100 (1986).

(6) A. R. W. McKellar, P. R. Bunker, T. J. Sears, K. M. Evenson, R. J. Saykally, S. R. Langhoff, J. Chem. Phys. **79**, 5251 (1983).

(7) a) D. G. Leopold, K. K. Murray, and W. C. Lineberger, J. Chem. Phys. **81**, 1048 (1984); b) D. G. Leopold, K. K. Murray, A. E. S. Miller, W. C. Lineberger, J. Chem. Phys. **83**, 4849 (1985).

(8) a) P. R. Bunker and T. J. Sears, J. Chem. Phys. **83**, 4866 (1985); b) P. R. Bunker, P. Jensen, W. P. Kraemer, and R. Beardsworth, J. Chem. Phys. **85**, 3724 (1986).

(9) a) S. Koda, Chem. Phys. Lett. **55**, 353 (1978); b) *idem*, Chem. Phys. **66**, 383 (1982).

(10) C. W. Bauschlicher, Jr., H. F. Schaefer III, and P. S. Bagus, J. Am. Chem. Soc. **99**, 7106 (1977).

(11) D. G. Leopold, K. K. Murray, and W. C. Lineberger, private communication.

(12) Earlier work which focused on the necessity of a balanced description of

correlation to provide unbiased excitation energies may be found in P. J. Hay, W. J. Hunt, and W. A. Goddard III, Chem. Phys. Lett. **13**, 30 (1972).

(13) D. A. Dixon, J. Phys. Chem. **90**, 54 (1986).

(14) B. T. Luke, J. A. Pople, M.-B. Krogh-Jespersen, Y. Apeloig, M. Karni, J. Chandrasekhar, and P. v. R. Schleyer, J. Am. Chem. Soc. **108**, 270 (1986).

(15) J. D. Goddard, Y. Yoshioka, H. F. Schaefer III, J. Am. Chem. Soc. **102**, 7644 (1980).

(16) H. J. Köhler and H. Lischka, J. Am. Chem. Soc. **104**, 5884 (1982).

(17) G. E. Scuseria, M. Durán, R. G. A. R. Maclagan, and H. F. Schaefer III, J. Am. Chem. Soc. **108**, 3248 (1986).

(18) (a) E. A. Carter and W. A. Goddard III, J. Phys. Chem. **90**, 998 (1986); (b) These values have been revised here to reflect the latest experimental values for $\Delta H^0_{f,298}$ (Table X).

(19) T. H. Dunning, Jr., J. Chem. Phys. **53**, 2823 (1970).

(20) S. Huzinaga, J. Chem. Phys. **42**, 1293 (1965).

(21) Optimized for CH_4 by R. A. Bair and W. A. Goddard III, submitted for publication.

(22) A. K. Rappé, T. A. Smedley, and W. A. Goddard III, J. Phys. Chem. **85**, 1662 (1981). Note that the second p exponent for the Cl basis listed in Table I of this reference should read 0.641, not 0.691, and the s orbital energy for Cl in Table IV of this reference should read -1.0675, not -0.1068.

(23) L. B. Harding and W. A. Goddard III, Chem. Phys. Lett. **55**, 217 (1978).

(24) D. S. Horowitz and W. A. Goddard III, to be published.

(25) R. Noyori, M. Yamakawa, and W. Ando, Bull. Chem. Soc. Jap. **51**, 811 (1978).

(26) C. F. Bender, H. F. Schaefer III, D. R. Franceschetti, and L. C. Allen, J.

Am. Chem. Soc. **94**, 6888 (1972).

(27) (a) W. J. Hunt, T. H. Dunning, Jr., and W. A. Goddard III, Chem. Phys. Lett. **3**, 606 (1969); W. A. Goddard III, T. H. Dunning, Jr., and W. J. Hunt, Chem. Phys. Lett. **4**, 231 (1969); W. J. Hunt, W. A. Goddard III, and T. H. Dunning, Jr., Chem. Phys. Lett. **6**, 147 (1970); W. J. Hunt, P. J. Hay, and W. A. Goddard III, J. Chem. Phys. **57**, 738 (1972); F. W. Bobrowicz and W. A. Goddard III in "Methods of Electronic Structure Theory", H. F. Schaefer, ed., Plenum Publishing Corporation, 1977, pp 79-127; (b) L. G. Yaffe and W. A. Goddard III, Phys. Rev. A **13**, 1682 (1976).

(28) E. A. Carter and W. A. Goddard III, J. Chem. Phys. **86**, 862 (1987).

(29) C. W. Bauschlicher, Jr. and P. R. Taylor, J. Chem. Phys. **85**, 5936 (1986).

(30) Mulliken populations were obtained by summing over the electron populations of each carbon s and p basis function within each natural orbital for each GVB pair.

(31) K. F. Zmbov, O. M. Uy, and J. L. Margrave, J. Am. Chem. Soc. **90**, 5090 (1968).

(32) A. P. Modica and J. E. LaGraff, J. Chem. Phys. **43**, 3383 (1965).

(33) "JANAF Thermochemical Tables", Natl. Stand. Ref. Data Ser., Natl. Bur. Stand. **37** (1971) and supplements to JANAF in: J. Phys. Chem. Ref. Data **3**, 311 (1974); *ibid.* **4**, 1 (1975); *ibid.* **7**, 797 (1978); and *ibid.* **11**, 695 (1982).

(34) S. G. Lias, J. F. Liebman, and R. D. Levin, J. Phys. Chem. Ref. Data **13**, 695 (1984).

(35) D. W. Berman, D. S. Bomse, and J. L. Beauchamp, Int. J. Mass. Spectrom. Ion Phys. **39**, 263 (1981).

(36) E. A. Carter and W. A. Goddard III, J. Am. Chem. Soc., submitted for publication.

Table I. Optimum geometries for the $^1A'$ and $^3A''$ states of $CH(SiH_3)$.

geometrical parameters	$^1A'$	$^3A''$
Θ_e(H-C-Si)[a]	106.1°	140.4°
R_e(C-Si)[a]	1.951Å	1.867Å
R_e(C-H)[a]	1.123Å	1.091Å
R(Si-H)[b]	1.487Å	
Θ(H-Si-H)[b]	108.3°	
Θ_D(H-C-Si-H)[c]	60.0°	

a) Optimization carried out at the GVB(3/6)-PP level. *b*) Ref. 24. *c*) Ref. 25.

Table II. Singlet-triplet splittings (ΔE_{ST}) and total energies for the $^1A_1$ and $^3B_1$ states of CH_2.

	total energies(h)[b]		
calculation[a]	$^1A_1$	$^3B_1$	ΔE_{ST}(kcal/mol)[c]
HF	−38.88587 (1/1)	−38.92749 (1/1)	26.1
GVB-PP	−38.93877 (8/8)	−38.95329 (4/4)	9.1
GVB-RCI(PP)	−38.94151 (18/20)	−38.95925 (9/25)	11.1
GVB-RCI(opt)	−38.94189 (18/20)	−38.96035 (9/25)	11.6
Full CI[d]	−39.02718 (∼44,000/∼220,000)	−39.04626	12.0
CCCI[e]	−38.96706 (1174/1989)	−38.98135 (774/2070)	9.0
Previous Theory			13.5(CI-SD),[f] 16.8(MP4)[g]
Experiment[h]			9.1±0.2

a) Calculational details are provided in Section II. The corresponding number of spatial configurations/spin eigenfunctions for each wavefunction is given beneath each total energy. *b*) 1 h = 1 hartree = 627.5096 kcal/mol = 27.211617 eV = 219,474.75 cm^{-1}. *c*) $\Delta E_{ST} = E_{singlet} - E_{triplet}$. *d*) Ref. 29. *e*) RCI*$SD_{\sigma\pi}$(PP). *f*) R. R. Lucchese and H. F. Schaefer III, J. Am. Chem. Soc. **99**, 6765 (1977). *g*) B. T. Luke, J. A. Pople, M.-B. Krogh-Jespersen, Y. Apeloig, J. Chandrasekhar, and P. v. R. Schleyer, J. Am. Chem. Soc. **108**, 260 (1986). *h*) Ref. 3, 7, and 8.

Table III. Singlet-triplet splittings (ΔE_{ST}) and total energies for the $^1A'$ and $^3A''$ states of $CH(SiH_3)$.

	total energies(h)		
calculation	$^1A'$	$^3A''$	ΔE_{ST}(kcal/mol)
HF	−328.96121 (1/1)	−329.01652 (1/1)	34.7
GVB-PP	−329.01135 (8/8)	−329.04047 (4/4)	18.3
GVB-RCI(PP)	−329.01551 (18/20)	−329.04698 (9/25)	19.7
GVB-RCI(opt)	−329.01614 (18/20)	−329.04857 (9/25)	20.4
CCCI[a]	−329.04260 (4180/7447)	−329.07199 (3318/9030)	18.4
Previous Theory			20.3(CEPA),[b]25.7(MP4),[c]27.2(CI-SD)[d]

a) RCI*$SD_{\sigma\pi}$(PP). *b*) Ref. 16. *c*) Ref. 14. *d*) Ref. 15.

Table IV. Bond populations, total charges, and carbon hybridization for CXY.[a]

CXY	State	C-X Bond	Bond Population on Carbon[b]	Total Charges C	Total Charges X	Hybridization C-X Bond % 2s	Hybridization C-X Bond % 2p	C σ[c] % 2s	C σ[c] % 2p
CH_2	$^3B_1$	C-H	1.16	6.30	0.85	51.0	49.0	19.0	81.0
CH_2	$^1A_1$	C-H	1.06	6.21	0.89	17.5	82.5	62.1	37.9
$CHSiH_3$	$^3A''$	C-H	1.13	6.40	0.86	45.4	54.6	11.2	88.8
		C-Si	1.37		13.45[d]	60.8	39.2		
$CHSiH_3$	$^1A'$	C-H	1.02	6.29	0.90	17.1	82.9	61.4	38.6
		C-Si	1.23		13.53[d]	20.9	79.1		
CF_2	$^3B_1$	C-F	0.67	5.72	9.14	45.3	54.7	52.7	47.3
CF_2	$^1A_1$	C-F	0.59	5.80	9.10	19.0	81.0	69.8	30.2
CCl_2	$^3B_1$	C-Cl	0.94	6.11	16.94	53.5	46.5	39.0	61.0
CCl_2	$^1A_1$	C-Cl	0.80	6.10	16.95	19.5	80.5	72.8	27.2
CHF	$^3A''$	C-H	1.18	5.99	0.86	59.8	40.2	34.8	65.2
		C-F	0.64		9.15	36.5	63.5		
CHF	$^1A'$	C-H	1.00	5.96	0.92	14.5	85.5	67.4	32.6
		C-F	0.60		9.12	20.3	79.7		
CHCl	$^3A''$	C-H	1.18	6.20	0.83	55.6	44.4	29.7	70.3
		C-Cl	0.90		16.97	48.6	51.4		
CHCl	$^1A'$	C-H	1.06	6.16	0.86	17.4	82.6	67.8	32.2
		C-Cl	0.78		16.98	21.5	78.5		

a) Based on Mulliken populations (Ref. 30). *b*) Perfect covalent bonding would lead to a carbon bond population of 1.00. *c*) Carbon σ nonbonding orbital. *d*) Each H on SiH_3 pulls 0.10 electron off of Si.

Table V. Singlet-triplet splittings (ΔE_{ST}) and total energies for the $^1A_1$ and $^3B_1$ states of CF_2.

	total energies(h)		
calculation	$^1A_1$	$^3B_1$	ΔE_{ST}(kcal/mol)
HF	−236.69898 (1/1)	−236.64724 (1/1)	−32.5
GVB-PP	−236.75904 (8/8)	−236.68387 (4/4)	−47.2
GVB-RCI(PP)	−236.75979 (18/20)	−236.68597 (9/25)	−46.3
RCI*ΠCI(PP)	−236.77747 (63/91)	−236.69470 (27/75)	−51.9
RCI*ΠCI(opt)	−236.79045 (63/91)	−236.69510 (27/75)	−59.8
CCCI[a]	−236.80127 (1219/2060)	−236.70966 (792/2120)	−57.5
Previous Theory			−46.5[GVB(1/2)][b]
Experiment			−56.6[c]

a) RCI*[ΠCI + $SD_{\sigma\pi}$](PP). *b*) Ref. 10. *c*) Ref. 9.

Table VI. Singlet-triplet splittings (ΔE_{ST}) and total energies for the $^1A_1$ and $^3B_1$ states of CCl_2.

	total energies(h)		
calculation	$^1A_1$	$^3B_1$	ΔE_{ST}(kcal/mol)
HF	−956.67142 (1/1)	−956.67156 (1/1)	0.1
GVB-PP	−956.72841 (8/8)	−956.70211 (4/4)	−16.5
GVB-RCI(PP)	−956.73338 (18/20)	−956.70863 (9/25)	−15.5
RCI*ΠCI(PP)	−956.74827 (63/91)	−956.71457 (27/75)	−21.1
RCI*ΠCI(opt)	−956.75250 (63/91)	−956.71550 (27/75)	−23.2
CCCI[a]	−956.77628 (1219/2060)	−956.73495 (792/2120)	−25.9
Previous Theory			−13.5[GVB(1/2)][b]

a) RCI*[ΠCI + $SD_{\sigma\pi}$](PP). *b*) Ref. 10.

Table VII. Singlet-triplet splittings (ΔE_{ST}) and total energies for the $^1A'$ and $^3A''$ states of CHF.

	total energies(h)		
calculation	$^1A'$	$^3A''$	ΔE_{ST}(kcal/mol)
HF	−137.78206 (1/1)	−137.78916 (1/1)	4.5
GVB-PP	−137.83874 (8/8)	−137.82013 (4/4)	−11.7
GVB-RCI(PP)	−137.84018 (18/20)	−137.82333 (9/25)	−10.6
RCI*ΠCI(PP)	−137.85094 (36/47)	−137.82858 (18/50)	−14.0
RCI*ΠCI(opt)	−137.86149 (36/47)	−137.82931 (18/50)	−20.2
CCCI[a]	−137.87560 (1192/2016)	−137.84740 (783/2095)	−17.7
Previous Theory			−9.2[GVB(1/2)],[b] −12.7(MP4),[c] −12.9(CI-SD)[d]
Experiment			∼ −15[e]

a) RCI*[ΠCI + $SD_{\sigma\pi}$](PP). *b*) Ref. 10. *c*) Ref. 14. *d*) Ref. 17. *e*) Ref. 11.

Table VIII. Singlet-triplet splittings (ΔE_{ST}) and total energies for the $^1A'$ and $^3A''$ states of CHCl.

	total energies(h)		
calculation	$^1A'$	$^3A''$	ΔE_{ST}(kcal/mol)
HF	−497.78302 (1/1)	−497.80255 (1/1)	12.3
GVB-PP	−497.83563 (8/8)	−497.82949 (4/4)	−3.9
GVB-RCI(PP)	−497.83910 (18/20)	−497.83502 (9/25)	−2.6
RCI*ΠCI(PP)	−497.84773 (36/47)	−497.83843 (18/50)	−5.8
RCI*ΠCI(opt)	−497.85006 (36/47)	−497.83943 (18/50)	−6.7
CCCI[a]	−497.87415 (1192/2016)	−497.85933 (783/2095)	−9.3
Previous Theory			−1.6[GVB(1/2)],[b] −3.7(CI-SD)[c]

a) RCI*[ΠCI + $SD_{\sigma\pi}$](PP). *b*) Ref. 10. *c*) Ref. 17.

Table IX. Singlet-triplet splittings ($\Delta E_{ST} = E_{singlet} - E_{triplet}$) in CXY for three correlation-consistent levels of CI (kcal/mol).[a]

CXY	Theory[b]				Experiment[b]	Thermochemical
	RCI*ΠCI(PP)	RCI*ΠCI(opt)	Full CI	CCCI[c]		Estimate[d]
CH_2	11.1	11.6	12.0[e]	9.0	9.09±0.21[f]	—
$CHSiH_3$	19.7	20.4	(21.0±0.4)	18.4	(18.5±0.2)	—
CF_2	−51.9	−59.8	(−55.2±4.2)	−57.5	−56.6,[g](−57.4±0.2)	−50.0±10.8
CCl_2	−21.1	−23.2	(−21.6±1.4)	−25.9	(−25.8±0.2)	−31.0±10.7
CHF	−14.0	−20.2	(−16.5±3.4)	−17.7	∼ −15,[h](−17.6±0.2)	−22.4±6.6
CHCl	−5.8	−6.7	(−5.6±0.7)	−9.3	(−9.2±0.2)	−16.7±8.2

a) Details of the basis sets and MCSCF/CI calculations are given in Section II. *b*) Values in parentheses represent our best estimates for ΔE_{ST} for both a full CI within a DZP basis and experimental values, based on comparisons of the present CI calculations with full CI and experimental values for CH_2. *c*) RCI*[ΠCI + $SD_{\sigma\pi}$](PP). *d*) Based on the theoretical relationship between D(C=C) and ΔE_{ST}(CXY) (Ref. 18). Values revised according to new thermochemical data (see Section IV). *e*) Ref. 29. *f*) Refs. 3, 7, and 8. *g*) Ref. 9. *h*) Ref. 11.

Table X. Predicted bond energies for XYC=CX'Y' from $D^{\circ}_{f,298}(XYC{=}CX'Y') = D^{\circ}_{f,298}(H_2C{=}CH_2) - \Delta E_{ST}(CXY) - \Delta E_{ST}(C'Y')$ (kcal/mol).[a,b]

CXY	CX'Y'	D^{pred}_{298}(C=C)[c]	D^{expt}_{298}(C=C)[d]	$\Delta H^{\circ}_{f,298}$(XYC=CX'Y')	$\Delta H^{\circ}_{f,298}$(CXY)	$\Delta H^{\circ}_{f,298}$(CX'Y')
CH_2	CF_2	114.7±2.1	122±1, 129.8±2	−82.0	92±1[h]	−52., −44.2 ± 1[e]
CF_2	CF_2	57.2±2.1	53.4±0.7,69.0±2.7	−157.4 ± 0.7[f]	−52., −44.2 ± 1	−52.,−44.2 ± 1
CF_2	CF_2	57.2±2.1	64.5±2.5,[g]76.3±3[h]	−157.4 ± 0.7	−46.5 ± 1.6[g]	−46.5 ± 1.6
CH_2	CCl_2	146.3±2.1	146.3±3.4,136.4±1.4	0.61±0.36[i]	92±1	54.9±2,[j]45.
CCl_2	CCl_2	120.4±2.1	112.5±6, 92.7±2.0	−2.7 ± 2.0[i]	54.9±2,45.	54.9±2,45.
CH_2	CHF	154.5±2.1	151.2±4	−33.2	92±1	26±3[h]
CHF	CHF	136.8±2.1	122.0±6	−70.0	26±3	26±3
CF_2	CHF	97.0±2.1	91.0±3,98.8±4	−117.	−52.,−44.2±1	26±3
CH_2	CHCl	162.9±2.1	154.4±6.3	8.6±0.3[i]	92±1	71±5[h]
CHCl	CHCl	153.6±2.1	140.9±12.1	1.1±2.1[i]	71±5	71±5
CCl_2	CHCl	137.0±2.1	127.9±8.6,118±6.6	−2.0 ± 1.6[i]	54.9±2, 45.	71±5

a) Experimental heats of formation and bond energies are from Ref. 34 unless otherwise noted. *b*) $D^{\circ}_{f,298}(H_2C{=}CH_2)$ = 172.2±2.1 kcal/mol (Ref. 33). *c*) Using the $T_e = \Delta E_{ST}$ values from column 5 of Table IX. These should be corrected to T_0 using differential zero point energies of 0.1±0.1 kcal/mol for CHX and CCl_2 and 0.2±0.1 kcal/mol for CF_2, however these corrections have been omitted since they are small. *d*) Obtained from the heats of formation listed here unless otherwise noted. *e*) Ref. 35. *f*) Ref. 33. *g*) Ab initio theoretical value (E. A. Carter and W. A. Goddard III, submitted for publication). *h*) Ref. 31. *i*) J. D. Cox and G. Pilcher, "Thermochemistry of Organic and Organometallic Compounds" (Academic, New York, 1970). *j*) K. Rademann, H.-W. Jochims, and H. Baumgärtel, J. Phys. Chem. **89**, 3459 (1985). *k*) S. G. Lias, Z. Karpas, and J. F. Liebman, J. Am. Chem. Soc. **107**, 6089 (1985).

Figure Captions

Fig. 1. The GVB(2/4)-PP one-electron orbitals for $^3A''$ $CHSiH_3$: a) the C-Si bond pair; b) the C nonbonding σ orbital (singly-occupied); and c) the C-H bond pair. Contours are from -0.5 to +0.5 a.u., with increments every 0.05 a.u.

Fig. 2. The GVB(3/6)-PP one-electron orbitals for $^1A'$ $CHSiH_3$: a) the C-Si bond pair; b) the C nonbonding σ natural orbital (nearly doubly-occupied); and c) the C-H bond pair.

Fig. 3. The GVB(2/4)-PP one-electron orbitals for $^3B_1$ CF_2: a) a C-F bond pair; b) the C nonbonding σ orbital (singly-occupied); and c) a C-F bond pair.

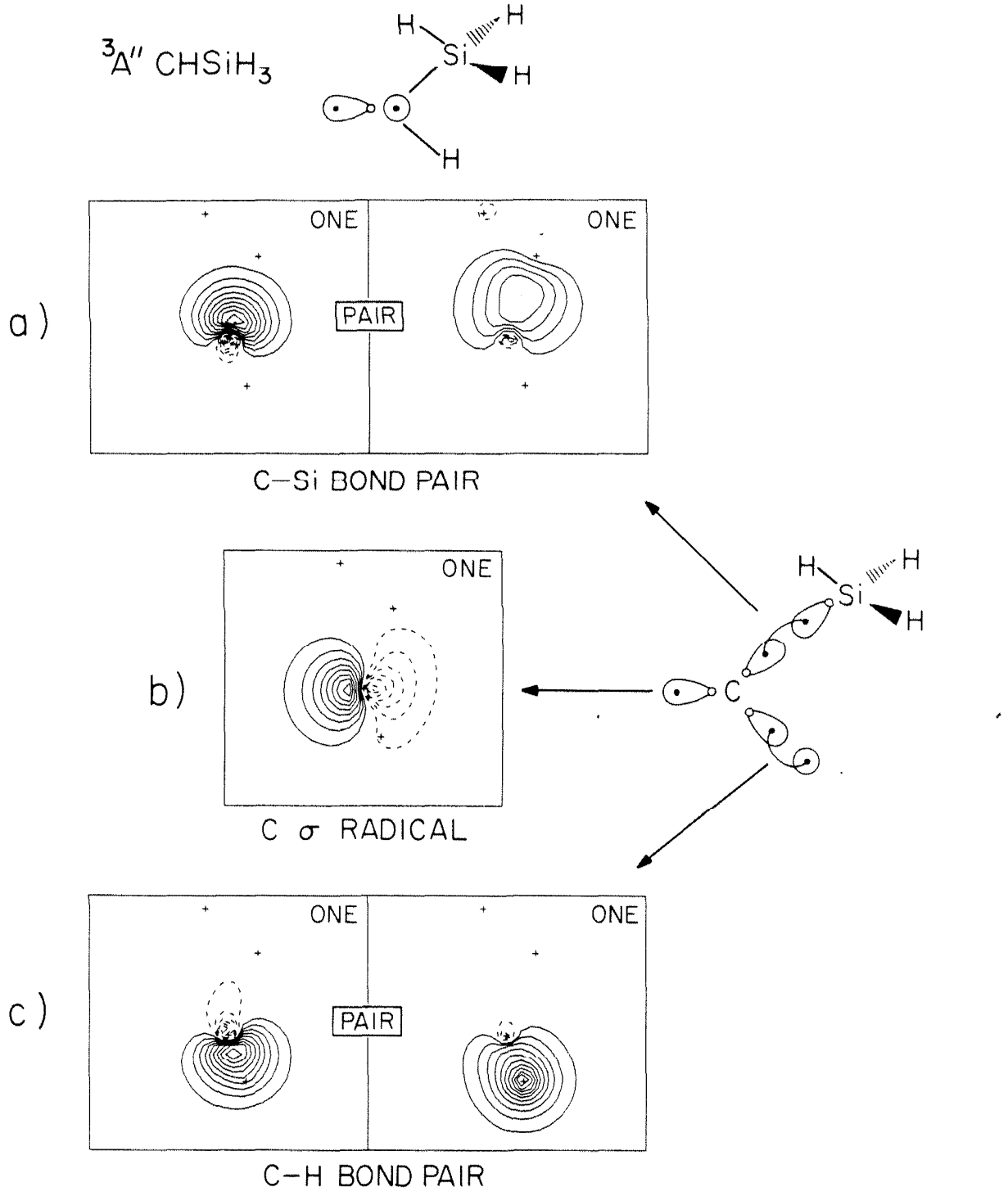
$^3A''$ $CHSiH_3$
H
Si
H
H
H
a)
ONE
ONE
PAIR
C–Si BOND PAIR
b)
ONE
C σ RADICAL
c)
ONE
ONE
PAIR
C–H BOND PAIR

Figure 1.

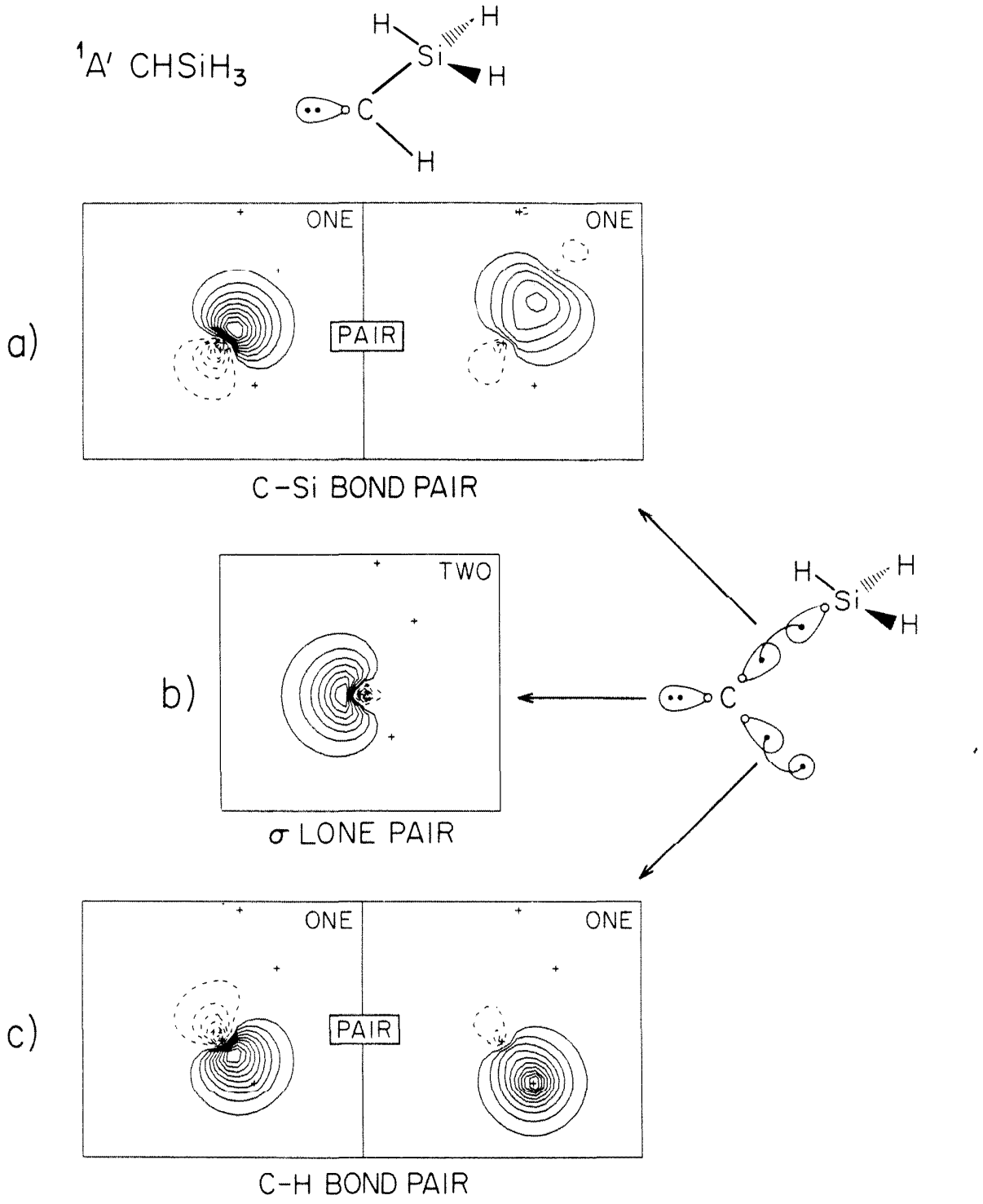
^{1}A′ CHSiH$_3$
H
H
Si
H
C
H
a)
ONE
ONE
PAIR
C-Si BOND PAIR
b)
TWO
σ LONE PAIR
H
H
Si
H
C
c)
ONE
ONE
PAIR
C-H BOND PAIR

Figure 2.

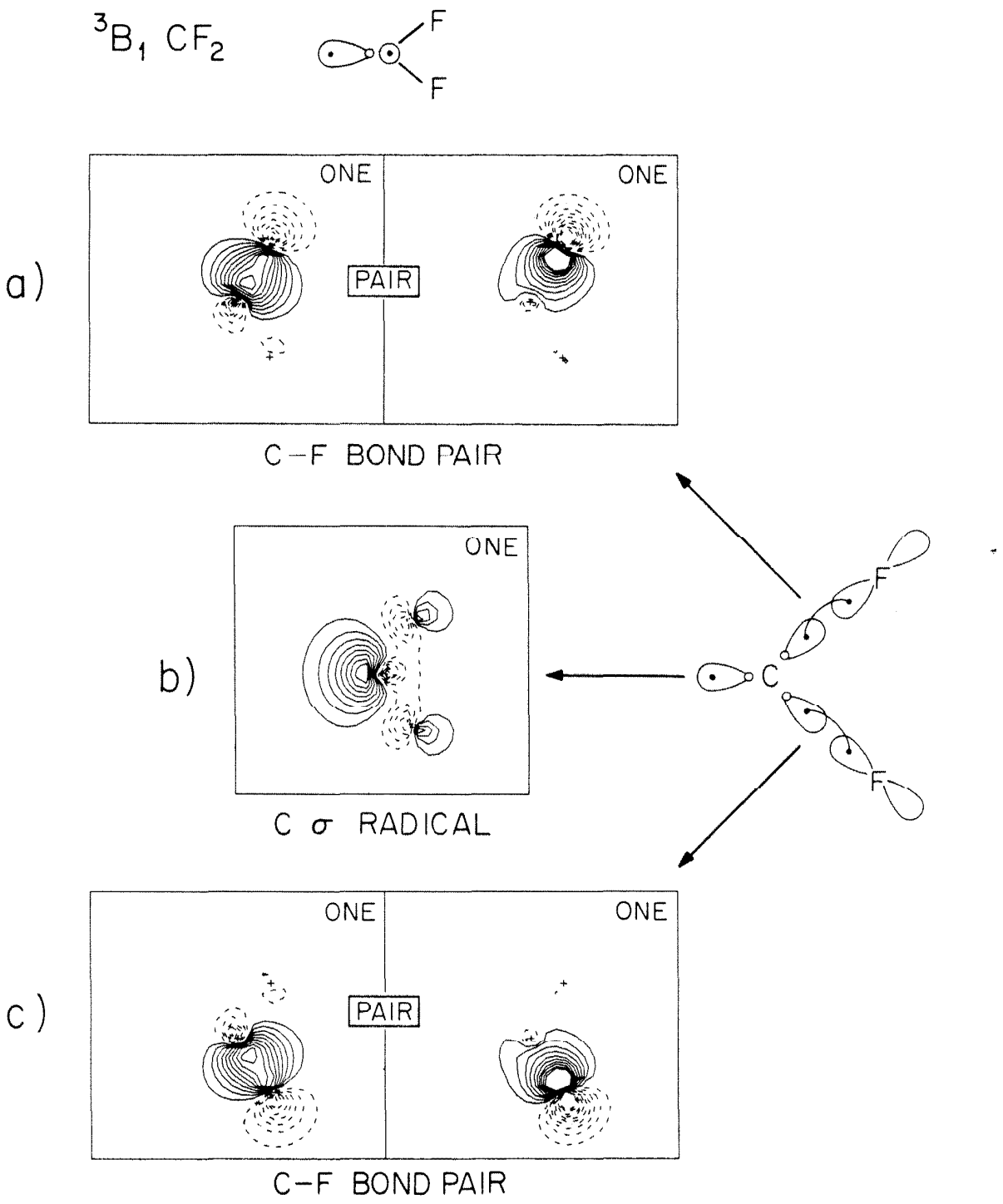
$^3B_1$ CF_2
F
F
a)
ONE
ONE
PAIR
C–F BOND PAIR
b)
ONE
C σ RADICAL
C
F
F
c)
ONE
ONE
PAIR
C–F BOND PAIR

Figure 3.

Chapter 1.E. The text of this section is a Communication coauthored with William A. Goddard III which has been submitted to the *Journal of the American Chemical Society*.

The C=C Double Bond of Tetrafluoroethylene

Emily A. Carter and William A. Goddard III*

Contribution No. 7577 from the Arthur Amos Noyes Laboratory of Chemical Physics, California Institute of Technology, Pasadena, California 91125.

Abstract: Current experimental values for the C=C bond dissociation energy of tetrafluoroethylene (C_2F_4) range from 53.4 to 76.3 kcal/mol. Since traditional theoretical approaches for calculating accurate bond energies would be impractical for a system as large as C_2F_4 (a full CI for a double zeta plus polarization basis would be $\sim 10^{23}$ spatial configurations), we have applied the recently developed correlation-consistent configuration interaction (CCCI) method to C_2F_4 [requiring only 1719 configurations but obtaining $D_e(H_2C{=}CH_2)$ to an accuracy of 4.9 kcal/mol]. We find: (i) $D_{298}(F_2C{=}CF_2) = 64.5 \pm 2.5$ kcal/mol; (ii) the CCCI value for $D_{298}(F_2C{=}CF_2)$ implies a new value for the heat of formation of CF_2: $\Delta H^0_{f,298}\,(CF_2) = -46.5 \pm 1.6$ kcal/mol [recent experimental values for $\Delta H^0_{f,298}\,(CF_2)$ range from $-52.$ to -44.2 ± 1 kcal/mol]; (iii) the intrinsic C=C bond strengths to dissociate to triplet fragments are nearly constant (within 4 kcal/mol) in C_2H_4 and C_2F_4, even though their adiabatic bond strengths differ by over 100 kcal/mol; and (iv) σ and π bonds are favored over bent bonds in C_2F_4.

Tetrafluoroethylene is an unusual olefin, with one of the weakest carbon-carbon double bonds known [D(C=C) $\sim$ 60 kcal/mol]. Unfortunately, the experimental C=C bond energy for C_2F_4 remains quite uncertain, with values ranging from 53 to 76 kcal/mol.[1-3] In addition, the nature of the double bond in C_2F_4 has also been disputed: the importance of bent or "banana" bonds versus the conventional σ and π bonds has not been addressed quantitatively, although a recent paper has suggested that bent bonds may be preferred in C_2F_2.[4] In order to settle these issues, we carried out ab initio generalized valence bond with configuration interaction (GVB-CI) calculations, utilizing a new approach in the CI expansion which systematically includes all correlations likely to change appreciably in the bond cleavage process. This *correlation-consistent CI* (CCCI), so named to indicate that no biases are built into the wavefunctions of either reactant or product, truncates much more rapidly than traditional singles and doubles CI approaches, yet gives much more accurate results.[5]

Table I provides a systematic study of the C_2F_4 bond strength as a function of electron correlation.[6] Hartree-Fock (variational MO) theory predicts a direct bond energy of 59.4 kcal/mol, using $\Delta E^{HF} = 2 \times E^{HF}(^1A_1\ CF_2) - E^{HF}(C_2F_4)$. This is close to our best estimate of 68.3 kcal/mol, but only as an artifact of the incapability of HF theory to properly describe the singlet states of carbenes [e.g., $\Delta E_{ST}(CF_2)$ = 32.5 kcal/mol for HF, whereas the CCCI value is 57.5 kcal/mol[7] and the experimental value is 56.6 kcal/mol[8]], leading to an artificially destabilized dissociation limit.

Including singles and doubles CI (HF*S*D) leads to a bond 20 kcal/mol *weaker* than HF because it leads to a good description of singlet CF_2 but cannot remove all problems in the HF description of C_2F_4, even though as many as 34,184 spin eigenfunctions are included in the CI calculation. The problem with HF*S*D is that the triple and quadruple excitations required to properly describe the fragments are not accounted for in the molecule, resulting in a low bond energy.

The GVB-CCCI method yields much more accurate bond energies (despite

using only one-tenth of the configurations), due to its correlation-consistent nature and emphasis on including the dominant correlations important for describing bond rupture. Indeed, with increasing amounts of correlation starting from GVB-PP through RCI*[$SD_\sigma + SD_\pi + S_{val}$], the bond energy smoothly converges to a value of 63.4 kcal/mol. Briefly, the GVB-CCCI method begins with the generalized valence bond wavefunction which allows the electrons in the breaking bond to each occupy their own orbital (rather than doubly-occupied as in restricted HF theory). Two sets of correlations are included in the CCCI: (i) full correlation of the electrons in the breaking bond (i.e., all single and double excitations to all unoccupied orbitals) and (ii) all single excitations from all valence orbitals to allow for orbital shape changes which accompany bond scission as the fragments relax.[5]

CCCI calculations on ethylene[5] lead to a residual correlation error of 4.9±2.5 kcal/mol in describing the double bond energy (Table I). Assuming the same error for C_2F_4 yields a final prediction of $D_e(F_2C{=}CF_2)$ = 68.3±2.5 kcal/mol. Using experimental values for the zero-point energies of C_2F_4 (13.4 kcal/mol) and CF_2 (4.3 kcal/mol),[9] along with the temperature correction (1.0 kcal/mol) to the bond energy of C_2F_4,[10] we calculate $D_{298}(C_2F_4)$ = 64.5±2.5 kcal/mol.

Of the three experimental values for $D_{298}(C_2F_4)$ listed in Table I, we can rule out the lowest value of 53.4±0.7 kcal/mol, since the CCCI method provides a lower bound on the bond energy (electron correlation error is larger in the molecule than in the fragments). Our theoretical prediction agrees most closely to the intermediate value of 69.0±2.7 kcal/mol.[2] From our prediction of $D_{298}(C_2F_4)$ plus the experimental $\Delta H_{f,298}(C_2F_4)$ = −157.4±0.7 kcal/mol, we derive $\Delta H^0_{f,298}(CF_2)$ = −46.5±1.6 kcal/mol, in good agreement with the most recent experimental value. This suggests that the 1977 value[1] of −52. kcal/mol for the heat of formation of CF_2 is in error and that the 1981 value[2] of −44.2±1 kcal/mol is correct.

Recently, we reported a simple relationship between bond energies [D(C=C)] in substituted olefins or methanes and singlet-triplet excitation energies (ΔE_{ST}) in substituted carbenes.[11] We showed that trends in C=C bond strengths in halo-

genated olefins could be explained by considering only whether the CXY fragments comprising the olefin have singlet or triplet ground states. Diabatically breaking the σ and π bonds in an olefin results in triplet fragments, but if the ground state of CXY is a singlet, the adiabatic bond energy is weaker by the electronic relaxation energy, ΔE_{ST}. Assuming that the diabatic C=C bond energy (to dissociate to triplet fragments) is independent of substitution, we used experimental adiabatic olefin bond energies to estimate the singlet-triplet splittings of substituted carbenes.[11] In turn, we used CCCI calculations of ΔE_{ST} to obtain new estimates of the adiabatic bond energies, $D_{298}(C=C)$.[7]

Since ethylene dissociates to triplet fragments adiabatically, these estimates were based on the assumption that the *intrinsic* olefin C=C bond strength is $D_{298}(H_2C=CH_2) = 172.2 \pm 2.1$ kcal/mol.[10] As a quantitative test of this premise, we have calculated the intrinsic bond energies in ethylene and tetrafluoroethylene (Table I). The CCCI calculations yield intrinsic bond energies [to CX_2 ($^3B_1$) fragments] of D_e = 178.4 kcal/mol for C_2F_4 and D_e = 174.1 kcal/mol for C_2H_4.[5] Thus the assumption that the diabatic bond energy is independent of substitution is correct to 4.3 kcal/mol (2%). When zero point energy and heat capacity corrections are included[9,10,12] to arrive at D_{298} for each olefin, the intrinsic bond energy for C_2F_4 is larger than for C_2H_4 by 6.9 kcal/mol. Thus the error in using the relationship between D(C=C) and ΔE_{ST} as presented in ref 11 is 6.9 kcal/mol. Considering that the observed *adiabatic* bond strengths differ by more than 100 kcal/mol, the change in the intrinsic bond strengths is very small.

Recently there has been some concern whether the CC double bond in C_2F_4 is better described as a sigma bond plus a pi bond or as two "banana" or bent bonds.[4] To address this issue, we calculated the relative energies of three C=C bonding configurations: (i) σ and π C-C bonds; (ii) skewed σ and π bonds with no symmetry restrictions; and (iii) symmetric bent bonds. The one-electron GVB orbitals for (i)-(iii) are shown in fig 1. At the self-consistent GVB-PP level, all three descriptions are within 0.1 kcal/mol in energy, with the unsymmetrical wavefunction

(ii) lowest. When the four electrons involved in the C=C bond are allowed any occupation of the four bonding orbitals (GVB-CI), the three descriptions remain very close in energy (within 0.3 kcal/mol), but the σ and π bond wavefunction prevails as the lowest energy structure.[13] Thus we believe that the double bond is best thought of in terms of the σ and π bond description.

In conclusion, we report an accurate ab initio theoretical prediction of the bond energy of C_2F_4 [$D_{298}(C{=}C)$ = 64.5±2.5 kcal/mol] and of the heat of formation of CF_2 ($\Delta H^o_{f,298} = -46.5 \pm 1.6$ kcal/mol), using the newly-developed CCCI methods. The predicted bond energy helps distinguish between the large discrepancies in existing experimental values for $D_{298}(C_2F_4)$, ruling out one estimate (53.4 kcal/mol) and strongly supporting the 69.0 kcal/mol value. Furthermore, *intrinsic* C=C bond energies are found to be nearly constant (within 7 kcal/mol), even though the observed bond strengths differ by up to $\sim$ 100 kcal/mol, supporting the previously proposed approach for estimating $\Delta E_{ST}(CXY)$ based on C=C bond weakening.[11] Finally, we find that the traditional picture of multiple bonds (σ and π bonds) is correct for C_2F_4.

Acknowledgments. This work was supported by the National Science Foundation (Grant No. CHE83-18041) and the Shell Companies Foundation. EAC acknowledges a National Science Foundation predoctoral fellowship (1982-1985), a research grant award from the International Precious Metals Institute and Gemini Industries (1985-1986), and a SOHIO fellowship in Catalysis (1987). We also thank M. H. McAdon for help with the convergence of the skewed σ and π bond wavefunction.

References

(1) An indirect determination of $D(F_2C{=}CF_2)$ from the heat of formation of C_2F_4 ($\Delta H^0_{f,298} = -157.4 \pm 0.7$ kcal/mol) and a 1977 experimental value for $\Delta H^o_{f,298}(CF_2) = -52.$ kcal/mol (Lias, S. G.; Liebman, J. F.; Levin, R. D. *J. Phys. Chem. Ref. Data* **1984**, *13*, 695) yields $D_{298} = 53.4 \pm 0.7$ kcal/mol.

(2) Using another (more recent) determination of $\Delta H^o_{f,298}(CF_2) = -44.2 \pm 1$ kcal/mol (Berman, D.; Bomse, D. S.; Beauchamp, J. L. *Int. J. Mass Spec. Ion Phys.* **1981**, *39*, 263) yields $D_{298} = 69.0 \pm 2.7$ kcal/mol.

(3) This value constitutes the only directly determined bond energy ($D_{298} = 76.3 \pm 3$ kcal/mol) for C_2F_4 in a Knudsen cell equilibrium study at high temperature ($\sim 1200^o$K) by Zmbov, K. F.; Uy, O. M.; Margrave, J. L. *J. Am. Chem. Soc.* **1968**, *90*, 5090.

(4) Messmer, R. P.; Schultz, P. A. *Phys. Rev. Lett.* **1986**, *57*, 2653.

(5) Carter, E. A.; Goddard III, W. A. *Chem. Phys. Lett.*, submitted for publication.

(6) The Dunning valence double-ζ contraction (Dunning, Jr., T. H. *J. Chem. Phys.* **1970**, *53*, 2823) of the Huzinaga (9s5p) gaussian bases for carbon and fluorine (Huzinaga, S. *J. Chem. Phys.* **1965**, *42*, 1293) were used, with one set of cartesian 3d polarization functions added to the carbon basis [$\zeta^d = 0.64$; optimized for CH_4 by R. A. Bair and W. A. Goddard III (submitted for publication)], with the 3s combination omitted. The experimental geometry of C_2F_4 was taken from the "Landolt-Börnstein Tables"; Springer: Berlin, 1976; Vol. 7.

(7) Carter, E. A.; Goddard III, W. A. *J. Chem. Phys.*, submitted for publication.

(8) a) Koda, S. *Chem. Phys. Lett.* **1978**, *55*, 353; b) *idem*, *Chem. Phys.* **1982**, *66*, 383.

(9) a) Shimanouchi, T. Tables of Molecular Vibrational Frequencies, *Natl. Stand. Ref. Data Ser., Nat. Bur. Stand.* **1972**, *1*; b) Jacox, M. E. *J. Phys. Chem. Ref. Data* **1984**, *13*, 945.

(10) a) JANAF Thermochemical Tables, *Natl. Stand. Ref. Data Ser., Nat. Bur. Stand.* **1971**, *37*; b) JANAF Thermochemical Tables, 1982 Supplement, *J. Phys. Chem. Ref. Data* **1982**, *11*, 695.

(11) Carter, E. A.; Goddard III, W. A. *J. Phys. Chem.* **1986**, *90*, 998.

(12) Zero point energies for CF_2 were taken from ref 9b (4.3 kcal/mol) for the $^1A_1$ state, while the zero point motion of the $^3B_1$ state was estimated (4.1±0.1 kcal/mol) from the frequency shifts in C_2D_4[9a] going to CD_2 (Bunker, P. R.; Jensen, P.; Kraemer, W. P.; Beardsworth, R. *J. Chem. Phys.* **1986**, *85*, 3724) and the frequencies in C_2F_4. This leads to $T_0(CF_2)$ = 57.3±0.1 kcal/mol [$\Delta E_{ST} = T_e(CF_2)$ = 57.5 kcal/mol].

(13) The calculations on FC≡CF (ref 4), which find bent bonds ~2 kcal/mol lower than $\sigma\pi$ bonds, did not go beyond the GVB-PP description.

Table I. C=C Bond Energies (D_e) in kcal/mol for $F_2C{=}CF_2$.[a]

	total energies (hartrees)		$D_e^{diab}(F_2C{=}CF_2)$[c]	$D_e(H_2C{=}CH_2)$[d]	$D_e^{adiab}(F_2C{=}CF_2)$	
calculation	$F_2C{=}CF_2$ ($^1A_1$)	CF_2 ($^3B_1$)[b]			direct[e]	using ΔE_{ST}[f]
HF	−473.49255 (1/1)	−236.64724 (1/1)	124.3	122.2	59.4	9.3
HF*S*D	−474.07613 (18772/34184)	−236.92980 (3155/16053)	135.9	153.7	39.1	20.9
GVB-PP	−473.53219 (4/4)	−236.64724 (1/1)	149.2	146.1		34.2
GVB-RCI	−473.54868 (5/6)	"	159.5	154.6		44.5
RCI*S_{val}	−473.58045 (941/1724)	−236.65739 (63/157)	166.7	163.4		51.7
RCI*[SD_σ + SD_π]	−473.57245 (849/1098)	−236.64724 (1/1)	174.4	168.6		59.4
CCCI[g]	−473.59909 (1719/2728)	−236.65739 (63/157)	178.4	174.1		63.4
$D_e^{adiab} + \Delta_{corr}^{h}$						68.3±2.5
D_{298}[i]						64.5±2.5
Experiment (D_{298})					53.4±0.7[j] 69.0±2.7,[k] 76.3±3[l]	

a) VDZD basis on C and VDZ basis on F. See ref 5 for details of the calculations. The corresponding number of spatial configurations/spin eigenfunctions for each wavefunction are given beneath each total energy. *b*) Total energies for CF_2 are for the appropriate limit at R(C-C) = ∞, i.e., HF or HF*S_{val}. *c*) $D_e^{diab}(F_2C{=}CF_2) = 2{\times}E(^3B_1\ CF_2) - E(C_2F_4)$. *d*) Included for comparison to $D_e^{diab}(F_2C{=}CF_2)$ to indicate convergence [$D_e^{expt}(H_2C{=}CH_2) = 179.0{\pm}2.5$ kcal/mol]; ref 5. *e*) Direct $D_e(F_2C{=}CF_2)$ from $2{\times}E(^1A_1\ CF_2) - E(C_2F_4)$ where the HF and HF*S*D total energies of $^1A_1$ CF_2 are −236.69898 and −237.00693 hartrees (2633 spatial configurations/4399 spin eigenfunctions). *f*) $D_e^{adiab}(F_2C{=}CF_2) = D_e^{diab}(F_2C{=}CF_2) - 2{\times}\Delta E_{ST}$, where ΔE_{ST} = 57.5 kcal/mol (ref 7). *g*) RCI*[SD_σ + SD_π + S_{val}]. *h*) Δ_{corr} = 4.9 kcal/mol is the correlation error inherent to the CCCI method for double bonds (obtained from $D_e^{expt} - D_e^{calc} = 179.0{\pm}2.5 - 174.1 = 4.9{\pm}2.5$ kcal/mol for C_2H_4); see ref 5. *i*) The predicted D_e is converted to D_{298} by using the temperature and zero point energy corrections for C_2F_4 from refs 9 and 10. *j*) ref 1. *k*) ref 2. *l*) ref 3.

Figure Caption

Fig. 1. The GVB(2/4)PP one-electron orbitals of the C=C bond in C_2F_4 are shown for (i) (symmetry-constrained) σ and π bonds, $E_{PP(2/4)} = -473.53219$ hartrees, $E_{GVB-CI(2/4)} = -473.54944$ hartrees; (ii) skewed σ and π bonds (no symmetry constraints), $E_{PP(2/4)} = -473.53242$ hartrees, $E_{GVB-CI(2/4)} = -473.54899$ hartrees; and (iii) symmetric bent or "banana" bonds, $E_{PP(2/4)} = -473.53226$ hartrees, $E_{GVB-CI(2/4)} = -473.54924$ hartrees. Contours are plotted from -0.5 to $+0.5$ a.u., with increments every 0.05 a.u.

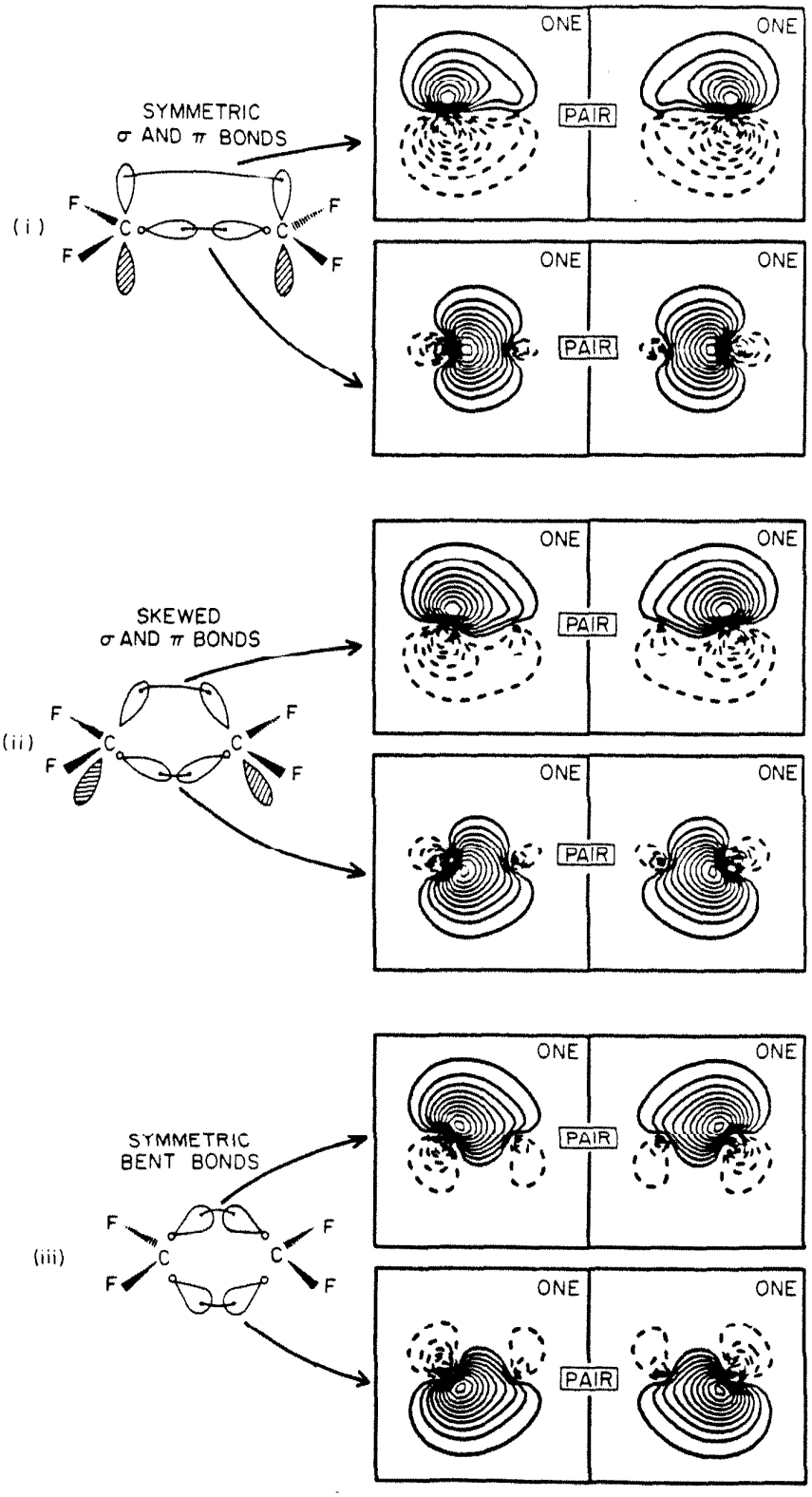
SYMMETRIC
σ AND π BONDS
(i)
F
C
C
F
ONE
PAIR
ONE
SKEWED
σ AND π BONDS
(ii)
SYMMETRIC
BENT BONDS
(iii)

Figure 1.

Chapter 2

Fundamental Studies of Transition Metal-Ligand Bonding

Chapter 2.A. The text of this section is an Article coauthored with William A. Goddard III which appeared in the *Journal of Physical Chemistry.*

Reprinted from The Journal of Physical Chemistry, 1984, *88*, 1485.

The Chromium Methylidene Cation: $CrCH_2^+$

Emily A. Carter[†] and William A. Goddard III*

Arthur Amos Noyes Laboratory of Chemical Physics,[‡] California Institute of Technology, Pasadena, California 91125 *(Received: October 26, 1983)*

We have examined the electronic structure and bonding characteristics of the experimentally observed cation $CrCH_2^+$. We find a $^4B_1$ ground state with a covalent double bond between ^6S Cr^+ and $^3B_1$ CH_2. These results are in contrast to previous theoretical studies which found a lowest state with $^6B_1$ symmetry and a single Cr–C bond. We calculate a direct bond energy of 44 kcal/mol and estimate the fully correlated limit to be 49 kcal/mol, which may be compared with the experimental value of 65 ± 7 kcal/mol and the previous theoretical results of 18.3 and 22.3 kcal/mol. The differences in results between the two theoretical studies on $CrCH_2^+$ are discussed.

Introduction

Although the bonding and thermodynamic properties of organic molecules are reasonably well understood, little reliable thermochemical information is available for organo-transition-metal complexes. Metal–carbon bond strengths are of particular interest because of the possible role of metal–alkyl, metal–alkylidene, and metal–alkylidyne intermediates in the mechanisms of both homogeneous and heterogeneous reactions, e.g., the elucidation of the mechanisms of reductive polymerization of CO by H_2 (Fischer Tropsch synthesis of hydrocarbons), olefin metathesis by early transition-metal alkylidene complexes, Ziegler–Natta polymerization of olefins, and many other industrially important catalytic processes.

In the past few years, advances in both theoretical and experimental characterization of metal–carbon species have been attained. GVB calculations of bond energies for several transition-metal alkylidene complexes led to bond strengths of 48–86 kcal/mol.[1,2] Experimental bond dissociation energies for gas-phase, first-row transition-metal–methylene positive ions, ranging in value from 65 ± 7 to 96 ± 5 kcal/mol, have been determined by Beauchamp and co-workers.[3] Schaefer and co-workers have

[†] National Science Foundation Predoctoral Fellow, 1982–85.
[‡] Contribution No. 6936.

(1) Rappé, A. K.; Goddard III, W. A. *J. Am. Chem. Soc.* **1982**, *104*, 448.
(2) Carter, E. A.; Goddard III, W. A. *Organometallics*, submitted for publication.

0022-3654/84/2088-1485$01.50/0

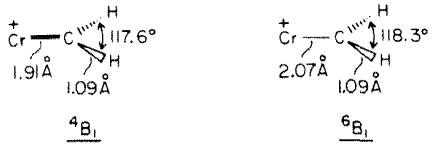

Figure 1. Equilibrium geometries for $^4B_1$ $CrCH_2^+$ and $^6B_1$ $CrCH_2^+$.

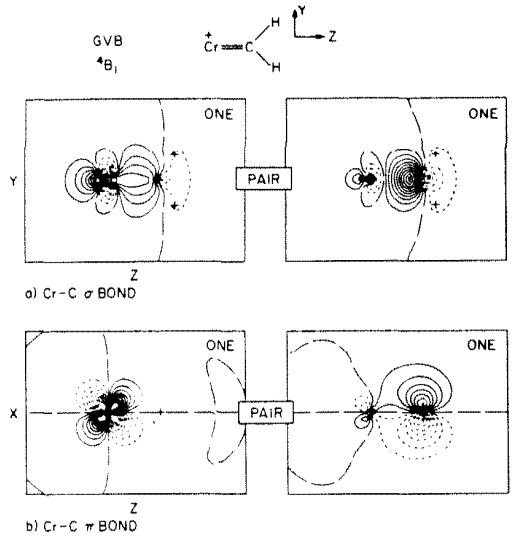

Figure 2. GVB orbitals for $^4B_1$ $CrCH_2^+$ at its equilibrium geometry: (a) GVB orbitals for the Cr–C σ bond; (b) GVB orbitals for the Cr–C π bond. Long dashes indicate zero amplitude; the spacing between contours is 0.05 au. The same convention is used in all plots.

carried out Hartree–Fock and configuration interaction calculations on two of the metal–methylene cations observed by Beauchamp, $CrCH_2^+$ and $MnCH_2^+$.[4] However, the calculations lead to a bond energy of 18.3 kcal/mol for $CrCH_2^+$, whereas Beauchamp's result is 65 ± 7 kcal/mol for $CrCH_2^+$. (Similarly, for $MnCH_2^+$, theory and experiment yield 36.0 and 94 ± 7 kcal/mol, respectively.) The current study was undertaken partly to resolve this large disagreement in bond energies and partly to elucidate the nature of metal–carbon double bonds.

Results and Discussion

Orbitals, Geometry, and Vibrational Frequencies for the Ground State ($^4B_1$). Starting with the ground state of Cr^+, $(3d)^5$ or ^6S, with its five singly occupied orbitals and the ground state ($^3B_1$) of CH_2 with its two singly occupied orbitals (σ,π), we might

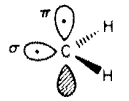

expect to find a double bond by simply spin pairing the Cr d_{z^2} orbital with the CH_2 σ orbital and the Cr d_{xz} orbital with the CH_2 π orbital. Indeed, we find the ground state to have exactly this

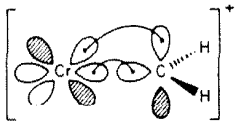

(3) Armentrout, P. B.; Halle, L. F.; Beauchamp, J. L. *J. Am. Chem. Soc.* **1981**, *103*, 6501.
(4) Vincent, M. A.; Yoshioka, Y.; Schaefer III, H. F. *J. Phys. Chem.* **1982**, *86*, 3905.

TABLE I: Vibrational Frequencies (cm^{-1}) for $^4B_1$ and $^6B_1$ $CrCH_2^+$ [a]

state	ν_{Cr-C}	ν_{C-H}	$\nu_{HCH\ scissors}$
$^4B_1$	542	3339	1316
$^6B_1$	495	3336	1336

[a] Frequencies are calculated from the harmonic force constants obtained from spline fits to $(RCI^*S)_{valence}$ calculations.

character, as indicated in Figure 1. Thus the ground state has a Cr–C double bond with orbitals as shown in Figure 2. Each bond pair is quite covalent, involving one electron in an orbital localized on Cr and one electron in an orbital localized on C. Analyzing the orbital character in the Cr σ bond[5] indicates that although the available σ orbital in the ground state of Cr^+ $[(3d)^5]$ is $d\sigma$, the Cr σ orbital of the Cr–C σ bond is 47% 4sp and 53% 3d. The reason for the large amount of s character in the σ bond is analyzed below. As would be expected from these descriptions, we find C_{2v} symmetry (stable with respect to both in-plane and out-of-plane distortions) in the equilibrium geometry for the ground state.

The geometry for this state is given in Figure 1 where we see that the HCH bond angle is identical with that in ethylene (117.6°). The calculated Cr=C bond length (1.91 Å) cannot be directly compared with experiment since no chromium–alkylidene complexes have been structurally characterized. The Cr–C bond length may be compared with theoretical values for $MnCH_2^+$ [R(Mn=C) = 2.01 Å] and $FeCH_2^+$ [R(Fe=C) = 1.96 Å].[6] The Mn–C bond is substantially longer than the Cr–C bond because Mn(I) bonds to CH_2 in its $(4s)^1(3d)^5$ ground state, using the larger 4s orbital to make the σ bond and a 3d orbital to make the π bond, whereas the σ bond in $CrCH_2^+$ is only 47% sp and hence is much smaller than in $MnCH_2^+$. For the same reason, a Cr^0=CH_2 (s^1d^5 Cr) would have a much longer bond (the σ bond would involve primarily the 4s orbital on Cr) than our Cr^I=CH_2, whereas a Cr^{II}=CH_2 (d^4 Cr^{2+}) complex should have a much shorter bond (since the σ bond would involve a pure Cr 3d orbital).

The vibrational frequencies for both the $^4B_1$ ground state and the $^6B_1$ excited state are listed in Table I. To our knowledge, no experimental metal–carbon double bond vibrational frequencies have been reported; however, these values (542 and 495 cm^{-1}) can be compared with calculations on $ClRuH(CH_2)$, where the Ru–C stretching frequencies were calculated to be 746 and 798 cm^{-1} for the two states examined.[2] Given the much stronger bond strength in the Ru complex (91 kcal) compared with the Cr system (49 kcal), coupled with similar M–C distances, leads to the prediction of a higher vibrational frequency in the Ru system, as observed. The C–H stretching frequencies (3339 and 3336 cm^{-1}) are a bit high when compared with the C–H stretch in CH_2=CH_2 (3056 cm^{-1}). However, Schaefer has noted that theoretical X–H vibrational frequencies are generally high by 10%.[7] The H–C–H scissors mode (1316 and 1336 cm^{-1}) is similar to the value for the same mode in ethylene (1393 cm^{-1}), as expected for an H–C–H bend of an sp^2-hybridized center.

The Sextet Excited State ($^6B_1$). As discussed below, the sextet ground state of Cr^+ results from the large number of (negative) exchange interactions engendered by this high spin state (the basis of Hund's rule). *Spin pairing* of the CH_2 and Cr^+ orbitals has the effect of *decreasing* this exchange stabilization, and thus for sufficiently small overlap, bond pairing will not be able to overcome the spin stabilization. Thus we find a low-lying excited state consisting of a σ bond (CH_2 σ with Cr d_{z^2}) but *no* π bond. In this case the CH_2 π orbital is coupled high spin with the remaining four Cr d orbitals to yield an S = 5/2 or sextet state ($^6B_1$). The *geometry for the $^6B_1$ state is shown in Figure 1.* The Cr–C bond length has increased from 1.91 to 2.07 Å, as expected from the

(5) Analyses of orbital character in the GVB orbitals are carried out by summing over Mulliken populations for the first and second NO's of each GVB pair.
(6) Brusich, M. J.; Goddard III, W. A., to be submitted for publication.
(7) Schaefer III, H. F. "The Electronic Structure of Atoms and Molecules"; Addison-Wesley: Reading, MA, 1972.

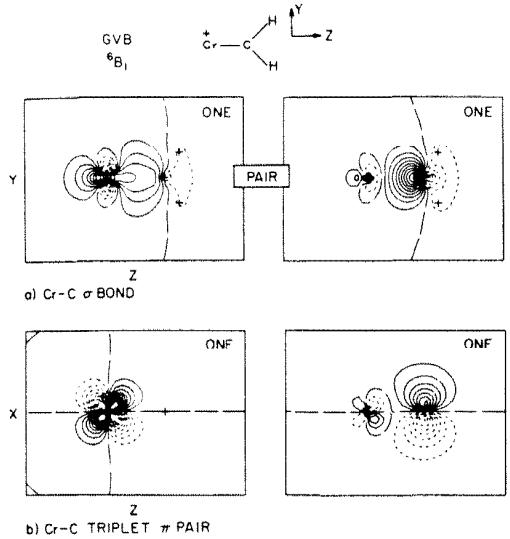

Figure 3. GVB orbitals for $^6B_1$ $CrCH_2^+$ at its equilibrium geometry: (a) GVB orbitals for the Cr–C σ bond; (b) GVB orbitals for the Cr–C π bond.

TABLE II: d–d and s–d Exchange Integrals[a] for Cr^+ (kcal/mol)

state	K_{sd}	K_{dd}
^6S (d^5)		16.5
^6D (s^1d^4)	5.0	18.4

[a] Averaged over the various d orbitals.

repulsion induced by triplet coupling of the π electron pair. The C–H bond length and the H–C–H angle are approximately the same for both states, indicating that the hybridization of the carbon orbitals has not changed. We find C_{2v} symmetry for the equilibrium geometry of the $^6B_1$ state, again stable with respect to in-plane and out-of-plane distortions. The Cr–C bonding orbitals for the sextet state are shown in Figure 3. Again, the Cr–C σ bond is quite covalent, with one electron in a Cr d orbital and one electron in a C sp hybrid orbital. The triplet-coupled π orbitals of the sextet state look similar to the π pair in the quartet state, except that the triplet π orbitals must get orthogonal to one another, as evidenced from the node around Cr built into the carbon pπ orbital.

Exchange Couplings. Before proceeding, it is appropriate to be a bit more explicit about the role of exchange interactions in Cr^+ and $CrCH_2^+$. Cr^+ has a high-spin, $(3d)^5$, ^6S ground state and a high-spin, $(4s)^1(3d)^4$, ^6D first excited state which lies 1.52 eV (35.1 kcal/mol higher in energy.[8] The ^6S state is lower than the ^6D state because the magnitude of the exchange terms is larger for the high-spin d^5 case. The ^6S state has ten d–d exchange terms (K_{dd}) between the five d electrons, whereas the ^6D has six K_{dd} and four K_{sd} terms between the four d electrons and the s electron.

$$E_{ex}(d^5) = -10K_{dd}$$

$$E_{ex}(s^1d^4) = -6K_{dd} - 4K_{sd}$$

The d–d exchange terms are larger than the s–d exchange terms (see Table II), leading to a larger overall exchange energy contribution in the ^6S state.

Using the average d–d and d–s exchange terms from Table II, we can now predict the nature of the bonding in $CrCH_2^+$. Indeed, analyzing the differential loss of exchange terms (see Figure 4) expected upon bonding CH_2 to Cr^+ in either the $(3d)^5$ ground state or the $(4s)^1(3d)^4$ excited state allows a prediction of the fraction

(8) Moore, C. E. *Natl. Stand. Ref. Data Sec., Natl. Bur. Stand.* **1971**, *No. 35*, Vol. 2, p 10.

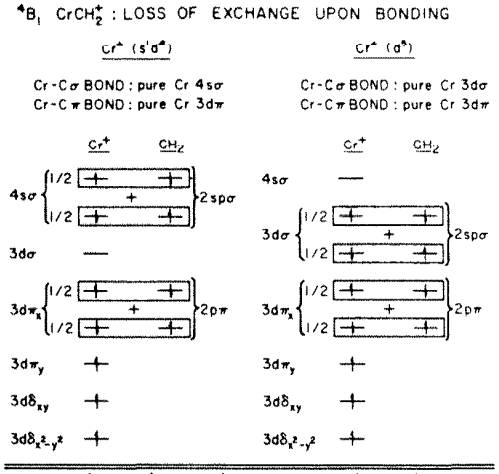

	$K_i^{Cr^+}$	$K_f^{Cr^+}$	ΔK^{Cr^+}	$K_i^{Cr^+}$	$K_f^{Cr^+}$	ΔK^{Cr^+}
K_{dd}	−6	−4.5	+1.5	−10	−6.5	+3.5
K_{sd}	−4	−2	+2	0	0	0

$K_i^{Cr^+}$ = Number of exchange terms (K_{dd} and K_{sd}) for Cr^+ before bonding to CH_2.

$K_f^{Cr^+}$ = Number of exchange terms (K_{dd} and K_{sd}) for Cr^+ after bonding to CH_2.

ΔK^{Cr^+} = Differential loss of exchange for Cr^+ upon bonding to CH_2.

Figure 4. Diagram depicting the origin of the differential loss of exchange upon bonding CH_2 to a $4s\sigma/3d\pi$ combination or to a $3d\sigma/3d\pi$ combination on Cr.

TABLE III: $^6B_1$–$^4B_1$ Excitation Energies for $CrCH_2^+$[a]

calculations	($^4B_1$), no. config/ no. SEF[b]	($^6B_1$), no. config/ no. SEF	ΔE-($^6B_1$–$^4B_1$), kcal	ground state
HF	1/1	1/1	−53.7	$^6B_1$
GVB-PP	4/4	2/2	−11.3	$^6B_1$
GVB-RCI	9/34	5/10	+12.5	$^4B_1$
$(GVB\text{-}RCI^*S)_{valence}$	507/3912	327/1501	+18.0	$^4B_1$
$RCI_\pi{}^*D_\sigma$ $+RCI_\sigma{}^*D_\pi$ $+(RCI^*S)_{valence}$	1415/8928	482/2146	+19.0	$^4B_1$

[a] The geometries used were the optimum values calculated at the $(GVB\text{-}RCI^*S)_{valence}$ level. [b] no. config = number of spatial configurations. SEF = spin eigenfunctions.

of 4s and 3d character in the Cr–C σ bond. Pairing the orbitals of Cr^+ and CH_2 into a simple, doubly bonded $^4B_1$ state for $CrCH_2^+$ leads to a loss of favorable (negative) exchange terms due to spin pairing in the bond.[9] If both the Cr–C bonds are to Cr d orbitals, $3.5K_{dd}$ are lost upon bonding (57.8 kcal/mol). If the σ bond involves the Cr 4s orbital instead of a 3d orbital, $1.5K_{dd}$ and $2K_{sd}$ are lost (27.6 kcal/mol). Thus it is intrinsically (30.2 kcal/mol) more favorable to bond methylene to one Cr s orbital and one Cr d orbital than to two Cr d orbitals. However, the excitation energy to the $(4s)^1(3d)^4$ state of Cr^+ is 33.9 kcal/mol.[10] Thus one expects an almost 50/50 mix of s and d (instead of pure d) in the σ orbital, as observed.

$^6B_1$–$^4B_1$ State Splitting: The Importance of Correlation. The energy difference between the sextet state and the quartet state

(9) This simple analysis is true only for perfect singlet pairing in each bond. If we include other spin-coupling terms (e.g., in an RCI wave function), we gain back some of the exchange energy we lose by singlet pairing each bond pair, complicating the hybridization analysis.

(10) Our calculations on Cr^+ lead to 33.9 kcal/mol as the state splitting for $Cr^+(d^5)$–$Cr^+(s^1d^4)$. The experimental result is 35.1 kcal/mol, averaged over total angular momentum states. See ref 8.

as a function of the level of electron correlation is given in Table III. Note that Hartree–Fock prefers the $^6B_1$ state by *54 kcal*, whereas the basic GVB description (GVB-RCI, including the spin-coupling configurations) leads to a $^4B_1$ ground state by 12.5 kcal. The highest level calculated leads to a $^4B_1$ ground state by 19.0 kcal. Why is there such a dramatic effect of electron correlation upon the stability of these spin states? In Brooks and Schaefer's previous work on $MnCH_2$,[11] Hund's rules were assumed valid for these systems, which would then suggest a sextet ground state for $CrCH_2^+$. However, Hund's rules only apply in cases of *mutually orthogonal* orbitals, where the exchange terms necessarily favor a high-spin ground state. For orbitals that overlap, one-electron terms generally dominate exchange terms, so that low-spin ground states are expected. Thus the $^4B_1$ state is the expected ground state for $CrCH_2^+$.

Why does Hartree–Fock theory not lead to the correct ground state? The reason is that Hartree–Fock cannot describe the doubly bonded state properly. This state involves a π bond with low overlap ($S_{Cr-C\pi} = 0.33$), whereas in Hartree–Fock the two orbitals in the bond pair must have unit overlap. To resolve this conflict, the optimum Hartree–Fock orbitals become very ionic (π electrons on the metal; σ electrons on the CH_2) so as to be consistent with the doubly occupied orbitals. This charge separation is highly

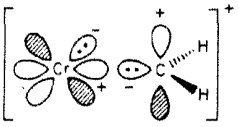

unfavorable, forcing the Hartree–Fock $^4B_1$ state very high in energy. On the other hand, for the $^6B_1$ state, triplet pairing of the Cr π_x and C π_x electrons forces these π electrons to be in separate, mutually orthogonal orbitals. To whatever the CH_2 π_x and Cr π_x atomic orbitals overlap, there will be an antibonding interaction. However, for $^+Cr–CH_2$ this overlap is small so that Hartree–Fock predicts a high-spin ground state, with a single Cr–C σ bond.

In the GVB wave function, we allow the two orbitals of each pair to have their optimum overlap, removing the restriction that causes Hartree–Fock to yield an ionic description of the π bond for the $^4B_1$ state. For a purely covalent bond, the GVB wave function would have the form $\Psi = lr + rl$, except that the GVB wave function allow l and r to have whatever shape minimizes the energy of the wave function.

$$\psi_{HF} = \phi_a\phi_a$$

$$\psi_{covalent} = \phi_l\phi_r + \phi_r\phi_l$$

$$\psi_{GVB} = \varphi_a\varphi_b + \varphi_b\varphi_a$$

Generally the optimum wave function is about ~90% covalent and ~10% ionic. In the GVB wave function for a double bond, there are two possible spin couplings (VB structures) that should be optimized along with the orbitals. However, for computational convenience, we generally optimize the orbitals only for one structure (perfect pairing), leading to the GVB-PP wave function. These spin coupling terms are then included by a CI in which the two electrons in each pair are allowed to have all three possible occupations of the two orbitals for that pair. This wave function, the GVB-RCI, has nine spatial configurations for a double bond. In addition to the GVB spin coupling, this wave function allows for interpair correlation and atomic high-spin coupling. The interpair correlation allows for correlated movement of electrons in one pair to one side of a bond, while electrons in another pair move to the other side of a bond, for an overall covalent structure:

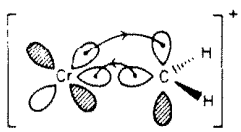

(11) Brooks, B. R.; Schaefer III, H. F. *Mol. Phys.* **1977**, *34*, 193.

TABLE IV: Cr–C Bond Energies (kcal/mol) of $CrCH_2^+$

calculation	$^4B_1$ state total energy, hartree	$^4B_1$ state bond energy	$^6B_1$ state total energy, hartree	$^6B_1$ state bond energy
HF	−1 080.829 94	−60.9	−1 080.915 49	−7.2
GVB(2/4)-PP	−1 080.915 49	−7.2	−1 080.933 53	+4.1
GVB-RCI	−1 080.956 18	+18.3	−1 080.936 22	+5.8
$RCI_\pi{}^*D_\sigma$ + $RCI_\sigma{}^*D_\pi$	−1 080.983 98	+35.8		
$(RCI^*S)_{valence}$	−1 081.000 43	+38.8	−1 080.971 67	+20.8
$RCI_\pi{}^*D_\sigma$ + $RCI_\sigma{}^*D_\pi$ + $(RCI^*S)_{valence}$	−1 081.008 68	+44.0	−1 080.978 39	+25.0

The RCI wave function allows the Cr d electrons in bond pairs to gain back some of the exchange energy they have lost in bonding by including the atomic high-spin coupling. These spin-coupling effects are expected to be more important for the $^4B_1$ state than for the $^6B_1$ state, since more exchange terms are lost by bond pairing two Cr orbitals to CH_2 to form a double bond instead of a single bond. The $^6B_1$ state gains little back from atomic high-spin coupling since it already has five electrons high-spin coupled. Thus the major element that brings about the inversion of ground states is including optimal spin coupling in the GVB wave function. Allowing Cr to have both favorable exchange interactions as well as favorable bonding interactions results in the doubly bonded $^4B_1$ ground state for $CrCH_2^+$.

Bond Energies. Calculating the Cr–C bond strength dissociation consistently[12] (vide infra) leads to a direct bond energy of 44.0 kcal/mol for $^4B_1$ $CrCH_2^+$, dissociating into ground-state fragments, ^6S Cr^+ and $^3B_1$ CH_2. An indication of the importance of electron correlation in transition-metal systems is exhibited in Table IV. As the level electron correlation accounted for increases, so does the bond energy, as expected when a more accurate description of the bound molecule is obtained.

All bond energies for $CrCH_2^+$ are calculated in a "dissociation-consistent" manner. This means that we calculate a wave function at R_e(Cr–C) which smoothly dissociates to the proper covalent limits at R(Cr–C) = ∞, retaining the same description of electron correlation in the wave function for $R = \infty$ that existed for R_e. Thus our bond energies are said to be "dissociation-consistent".

Such dissociation consistent wave functions should be expected to yield bond energies that are too small, although the bond energies will increase as the level of electron correlation is increased. In order to estimate the role of reduced correlation energy at our best level of calculation, we will compare the results of the same calculational level on a known bond energy of CH_2, namely, in $H_2C{=}CH_2$. The results for various levels of dissociation-consistent calculations on ethylene (using the same bases as for $CrCH_2^+$) are shown in Table V. Using the same basis set for carbon and hydrogen as was used for the $CrCH_2^+$ calculations (vide infra) and the same level of dissociation-consistent CI leads to a direct bond energy for $CH_2{=}CH_2$ of D_e = 175.4 kcal/mol as compared with the experimental value of 180.0 kcal/mol. This 4.6 kcal/mol of residual correlation energy for $CH_2{=}CH_2$ is expected to be a lower bound on the residual error in our calculation of the $CrCH_2^+$ bond energy (since Cr may have additional correlation errors from the other Cr d orbitals). Thus, our best (probably conservative) estimate for the bond energy for $CrCH_2^+$ is D_e = 48.6 kcal/mol.

Comparisons with Previous Theoretical Studies. Vincent et al.[4] carried out Hartree–Fock calculations on the $^6B_1$ state, leading to an optimum geometry with R_{Cr-C} = 2.064 Å and θ_{H-C-H} = 113.5°, whereas using correlated wave functions we find R_{Cr-C} = 1.91 Å and θ_{H-C-H} = 117.6° for the $^4B_1$ state and R_{Cr-C} = 2.07 Å and θ_{H-C-H} = 118.3° for the $^6B_1$ state. The smaller θ_{H-C-H} in the Hartree–Fock geometry is indicative of a larger amount of

(12) Bair, R. A.; Goddard III, W. A. *J. Phys. Chem.*, submitted for publication. See Bair, R. A. Ph.D. Thesis, California Institute of Technology, June 1981.

TABLE V: C–C Bond Energies for Ethylene (kcal/mol)

calculation	total energy, hartree		no. config/SEF[a]		$D_e(CH_2{=}CH_2)$	
	VDZ[b]	VDZd[c]	VDZ	VDZd	VDZ	VDZd
HF	−78.011 30	−78.040 81[d]	1/1	1/1	115.7	122.8[d]
GVB(2/4)-PP	−78.051 39	−78.079 57[e]	4/4	4/4	140.8	147.0[e]
GVB-RCI(4)	−78.066 51	−78.092 50[d]	5/6	5/6	150.3	155.3[d]
$(GVB\text{-}RCI^*S)_{valence}$	−78.096 61	−78.130 16[d]	167/292	263/460	160.2	164.2[d]
$D_\pi{}^*RCI_\sigma + D_\sigma{}^*RCI_\pi + (RCI^*S)_{valence}$	−78.101 80	−78.148 01[e]	367/544	759/1096	163.4	175.4[e]
expt						180.0[f]

[a] Given for $CH_2{=}CH_2$ only. [b] VDZ = valence double ζ bases for C and H. Reference 18. [c] VDZd = VDZ + one set of C d polarization functions. [d] Reference 6. [e] This work. Reference 19. [f] "JANAF Thermochemical Tables", *Natl. Stand. Ref. Data Sec., Natl. Bur. Stand.* 1970, *No. 37*.

TABLE VI: Davidson's Correction for $^4B_1$ and $^6B_1$ $CrCH_2^+$

state	limit of CI[a]	no. config/SEF	total energy, hartree	quadruples contribn, kcal/mol	Davidson's cor, kcal/mol
$^4B_1$	doubles	502/2197	−1 080.984 89		12.1
$^4B_1$	quadruples	1373/8829	−1 081.008 61	14.9	
$^4B_1$	unlimited	1415/8928	−1 081.008 68		
$^6B_1$	doubles	320/1699	−1 080.977 70		2.2
$^6B_1$	quadruples[b]	482/2146	−1 080.978 39	0.4	

[a] The "unlimited" CI is our dissociation-consistent $D_\pi{}^*RCI_\sigma + D_\sigma{}^*RCI_\pi + (RCI^*S)_{valence}$. This CI is then limited to doubles or quadruples. [b] "Quadruples" is the same as the unlimited CI in this orbital space.

$^1A_1$ character in the CH_2 part of the wave function (θ^{opt} = 104°) as opposed to $^3B_1$ character (θ^{opt} = 133°).

At the optimum Hartree–Fock geometry, Vincent et al. carried out a singles and doubles CI (SD-CI) calculation leading to a bond energy of 18.3 kcal/mol. Including Davidson's correction[13] for quadruple excitations yielded a bond energy of 22.3 kcal/mol. Since Davidson's correction is only an estimate, we decided to test the calculation of the quadruples correction by carrying out our best level of calculation restricted first to doubles and then to quadruples to directly calculate the correlation energy gained by including excitations up to quadruples. The results are shown in Table VI. Davidson's correction was also calculated from the formula, $\Delta E_Q = (1 - C_0^2)\Delta E_D$ (where C_0 refers to the CI coefficient for the dominant configuration in the singles and doubles CI calculation, ΔE_D is the difference in total energies of the SCF wave function—in this case a GVB-PP wave function—and the singles and doubles CI wave function, and ΔE_Q is the estimated difference in the total energies of the SD-CI wave function and the wave function that includes up through quadruple excitations). By knowing C_0 and ΔE_D, we have calculated ΔE_Q for comparison with the ab initio "Davidson's correction". The results show that Davidson's formula underestimates the amount of correlation for low-spin states and overestimates the correlation error for high-spin states. Thus, the Vincent et al. estimate of the bond energy in $^6B_1$ $CrCH_2^+$ may be slightly high, due to an overestimate of Davidson's correction. Perhaps a more accurate estimate of their bond energy would be 18.3 (SD-CI result) + 0.4 = 18.7 kcal/mol.

Vincent et al. also carried out Hartree–Fock calculations on the $^4B_1$ state; however, the $^4B_1$ state is not bound in this description. The major problem here is that the Hartree–Fock description of the $^4B_1$ state is extremely high in energy (54 kcal above $^6B_1$) with quite distorted orbitals (see Figure 5). The Hartree–Fock σ MO is localized primarily on the CH_2 ligand, while the Hartree–Fock π MO is localized primarily on Cr, with a small amount of delocalization onto the CH_2 ligand. Thus the Hartree–Fock description is not a covalent description where each bond has one electron localized near each nucleus. Even with HFSD-CI, the $^4B_1$ state is not bound. Thus double excitations are not sufficient both to change the shape of the orbitals and to include correlation effects. Starting with a Hartree–Fock wave function, we should include at least triple excitations and preferably quadruple excitations in order to get a description comparable to GVB. The strength of the GVB approach is that the correlation effects are included self-consistently so that the orbital shapes are optimum for various electron correlation terms. This allows a small CI to obtain a high-quality result.

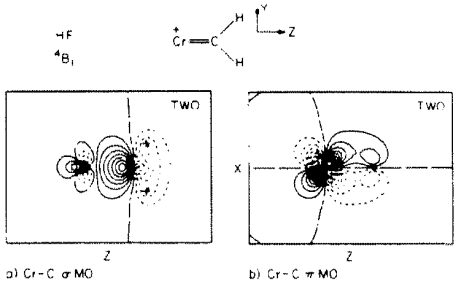

Figure 5. Hartree–Fock orbitals for $^4B_1$ $CrCH_2^+$ at its equilibrium geometry: (a) the Cr–C σ bond; (b) the Cr–C π bond.

Comparison with Experiment. Experimental bond energies for metal–carbon doubly bonded species have only recently become available through the ion beam studies by Beauchamp and coworkers.[3] The bond energies were determined from measuring the reaction cross section for the reaction of $CH_2{=}CH_2$ with first-row transition-metal ions.

$$M^+ + CH_2{=}CH_2 \rightarrow MCH_2^+ + CH_2$$

Although these values are for isolated gas-phase ions, they have provided the only clue into a thermochemical description of solution organometallic chemistry. Beauchamp and co-workers have determined $M{=}CH_2^+$ bond strengths for Cr^+ through Ni^+ that range from 65 to 96 kcal/mol, with $D(Cr{=}C) = 65 \pm 7$ kcal/mol. The weak point of the ion beam technique is lack of structural information. It is not possible to decide between two isomeric structures. Our results suggest a weaker bond energy (49 kcal) for $Cr^+{=}CH_2$; however, it is conceivable that another isomer could have a stronger bond.

As mentioned previously, there are no examples of structurally characterized chromium–alkylidene complexes with which to compare. Fischer has characterized chromium singlet carbene complexes with typical Cr–C bond lengths of 2.00–2.15 Å,[14]

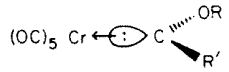

(13) (a) Davidson, E. R. In "The World of Quantum Chemistry"; Daudel, R.; Pullman, B.; Eds.; Reidel: Dordrecht, Holland, 1974; p 17. (b) Langhoff, S. R.; Davidson, E. R. *Int. J. Quant. Chem.* **1974**, *8*, 61.

(14) Fischer, E. O. *Pure Appl. Chem.* **1972**, *30*, 353.

somewhat longer than the results presented above. However, since Fischer carbenes have a single dative bond from a doubly occupied σ orbital on the carbene ligand, they are expected to have longer bonds than those found for doubly bonded Cr–C systems. Most known metal–alkylidene complexes are found among third-row transition metals. Two examples of third-row, terminal alkylidene complexes are Schrock's $Cp_2Ta(CH_2)CH_3$ ($Cp = \eta^5$-C_5H_5) with a Ta–CH_2 bond length of 2.03 Å[15] and $W(O)(CHCMe_3)(PEt_3)Cl_2$ with a W–CH_2 bond length of 1.88 Å.[16] Both systems are expected to have M=CH_2 double bonds with primarily d character in the σ bond. As a result, the W=C bond is shorter than our Cr=C bond!

Summary. We find that the ground state of $CrCH_2^+$ consists of a covalent Cr–C double bond, where the Cr–C σ bond has nearly equal parts 4s and 3d character. The hybridization and nature of the ground state has been explained in terms of differential changes in exchange terms, K_{dd} and K_{sd}. The $^6B_1$–$^4B_1$ energy difference as a function of correlation has been discussed. In addition, we find a direct bond energy of 44 kcal and an estimated bond energy of 48.6 kcal/mol, in fair agreement with experiment, 65 ± 7 kcal.

Calculational Details

Basis Sets. We explicitly considered all electrons for Cr, C, and H. We used a valence double ζ basis for Cr (10s8p5d/5s4p2d)[17] and the Dunning–Huzinaga valence double ζ bases for carbon (9s5p/3s2p) and for hydrogen (4s/2s).[18] One set of d polarization functions was added to the carbon basis, optimized for $CrCH_2^+$ ($\zeta = 0.69$).[19]

Wave Functions. The geometry optimizations for both the $^6B_1$ and $^4B_1$ states of $CrCH_2^+$ were carried out by utilizing a (GVB-RCI*S)$_{valence}$ wave function (generalized valence bond restricted configuration interaction times singles from all valence orbitals).

(a) For the $^4B_1$ state, the GVB(2/4) wave function corresponds to correlating the Cr–C σ and Cr–C π bond, each with a second natural orbital, leading to four natural orbitals in all. The C–H pairs were left uncorrelated but solved for self-consistently. The RCI allows all configurations arising from different occupations of each pair of natural orbitals for each GVB bond pair ($3^2 = 9$ spatial configurations and 34 spin eigenfunctions), allowing for interpair correlation and GF coupling. Then we allow all single excitations from all valence orbitals of the nine spatial configurations of the RCI wave function to all virtual orbitals (this includes single excitations from the CH pairs and the singly occupied Cr d orbitals), for a total of 507 spatial configurations and 3912 spin eigenfunctions. The single excitations allow for orbital readjustment upon stretching or bending the molecule.

(b) For the $^6B_1$ state, the GVB(1/2) wave function corresponds to correlating the Cr–C σ bond pair with a second natural orbital, while the Cr–C π system is described by two high-spin-coupled orbitals. This is comparable to the GVB(2/4) wave function for the $^4B_1$ state. Both have four valence orbitals, with two Cr–C σ natural orbitals and two Cr–C π natural orbitals. The RCI allows all single and double excitations within the GVB σ pair and within the two singly occupied Cr–C π natural orbitals (the valence bond orbitals that compose the π bond in the ground state, $^4B_1$), resulting in five spatial configurations and ten spin eigenfunctions. For the GVB-RCI*S wave function, we start with each of the five spatial configurations of the RCI wave function and allow all single excitations from all valence orbitals to all virtual orbitals, for a total of 327 spatial configurations and 1501 spin eigenfunctions.

To calculate the Cr–C bond energy in $CrCH_2^+$, we used several different dissociation-consistent CI[12] wave functions at the equilibrium geometries of $CrCH_2^+$ and of $^3B_1$ CH_2 [$\theta_{H-C-H} = 133°$, R(C–H) = 1.078 Å].[20] In addition to calculating the Cr–C bond energy at the HF level,[21] the GVB-PP (generalized valence bond with perfect pairing restriction) level, the GVB-RCI level (vide supra), and the (GVB-RCI*S)$_{valence}$ level (vide supra), we also carried out two further dissociation-consistent CI's on the $^4B_1$ ground state and one further dissociation-consistent CI on the $^6B_1$ excited state.

(a) $RCI_\pi{}^*D_\sigma + RCI_\sigma{}^*D_\pi$: This CI (for $^4B_1$ $CrCH_2^+$ only) consists of all single and double excitations from the three RCI configurations of the Cr–C σ bond pair, simultaneous with an RCI in the Cr–C π bond pair plus the opposite—all singles and doubles from the Cr–C π bond RCI configurations, simultaneous with an RCI in the Cr–C σ bond pair. Note the excitations are from the Cr–C bond pairs to all virtuals, including excitations to Cr singly occupied d orbitals and to the other GVB pair. This leads to a total of 1025 spatial configurations and 5810 spin eigenfunctions for the $^4B_1$ state (note that this includes the generic "GVB-CI" configurations). This wave function dissociates correctly to HF fragments, ^6S Cr^+ and $^3B_1$ CH_2.

(b) $RCI_\pi{}^*D_\sigma + RCI_\sigma{}^*D_\pi + (RCI^*S)_{valence}$: This CI wave function includes all the configurations for the wave function described directly above, but, in addition, includes the RCI*S configurations (same as described for the geometry optimization) not present in the previous wave function, leading to 1415 spatial configurations and 8928 spin eigenfunctions for the $^4B_1$ state and 482 spatial configurations and 2146 spin eigenfunctions for the $^6B_1$ state. This wave function correctly dissociates to HF*S (all single excitations from the HF wave function) fragments.

The C–C bond energy of ethylene was calculated at the HF, GVB(2/4)-PP, GVB-RCI(4), (GVB-RCI*S)$_{valence}$, and $RCI_\pi{}^*D_\sigma + RCI_\sigma{}^*D_\pi + (RCI^*S)_{valence}$ levels, as described above, using VDZ bases for C and H.[18] The effect of C d functions on the C–C bond energy was examined by using the d function optimized for $CrCH_2^+$.[19] The $^3B_1$ CH_2 fragment was calculated at the equilibrium geometry ($\theta = 133°$, R(C–H) = 1.078 Å)[20] at the HF and HF*S levels.

The $^6B_1$–$^4B_1$ state splittings were calculated by using all of the above methods. The ^6D–^6S state splittings for Cr^+ were calculated at the Hartree–Fock level, using an averaged-field Hamiltonian to represent the four d electrons in ^6D Cr^+. The exchange integrals for ^6D Cr^+ and ^6S Cr^+ were taken from Hartree–Fock calculations.

Acknowledgment. This work was supported in part by grants from the National Science Foundation (No. DMR82-15650) and the Shell Development Company.

Registry No. $CrCH_2^+$, 88968-58-5.

(15) Guggenberger, L. J.; Schrock, R. R. *J. Am. Chem. Soc.* **1975**, *97*, 6578.
(16) Wengrovius, J. H.; Schrock, R. R.; Churchill, M. R.; Missert, J. R.; Youngs, W. J. *J. Am. Chem. Soc.* **1980**, *102*, 4515.
(17) Rappé, A. K.; Goddard III, W. A., unpublished results. See, for example, Rappé, A. K.; Smedley, T. A.; Goddard III, W. A. *J. Phys. Chem.* **1981**, *85*, 2607.
(18) Huzinaga, S. *J. Chem. Phys.* **1965**, *42*, 1293. Dunning, Jr., T. H. *Ibid.* **1970**, *53*, 2823.
(19) The C d function ($\zeta = 0.69$) was optimized by using a fixed geometry [R(Cr–C) = 2.10 Å, $\theta_{H-C-H} = 120°$, R(C–H) = 1.078 Å) at the RCI*S level.
(20) Shih, S.-K.; Peyerimhoff, S. D.; Buenker, R. J.; Peric, M. *Chem. Phys. Lett.* **1978**, *55*, 206.
(21) Although Hartree–Fock does not dissociate correctly, we include this calculation for completeness.

Chapter 2.B. The text of this section is an Article coauthored with William A. Goddard III which appeared in the *Journal of the American Chemical Society.*

Reprinted from the Journal of the American Chemical Society, 1986, *108*, 2180.

Bonding in Transition-Metal–Methylene Complexes. 2. $(RuCH_2)^+$, a Complex Exhibiting Low-Lying Methylidene-like and Carbene-like States[1]

Emily A. Carter[†] and William A. Goddard III*

Contribution No. 7266 from the Arthur Amos Noyes Laboratory of Chemical Physics, California Institute of Technology, Pasadena, California 91125. *Received August 15, 1985*

Abstract: The electronic structure for a representative late-transition-metal–methylene complex, $Ru{=}CH_2^+$, has been studied by ab initio methods (generalized valence bond/configuration interaction). The electronic-state spectrum reveals five states close in energy (spread of 12.9 kcal/mol) that partition into two groups in terms of energy separation and mode of metal–carbon bonding. The ground state has $^2A_2$ symmetry and contains covalent M–C σ and π bonds ("metal–methylidene"); a $^2A_1$ state of the same bond character is only 1.2 kcal/mol higher. A cluster of three degenerate excited states ($^4A_2$, $^4B_1$, and $^4B_2$) 12.9 kcal/mol above the ground state exhibits completely different bonding character, namely, σ-donor/π-acceptor M–C bonds are formed ("metal–carbene"). We conclude that for highly unsaturated, late-transition-metal systems, metal–carbene bonding may be competitive with metal–alkylidene bonding, leading to donor/acceptor bonds comparable in strength to that of covalent double bonds!

I. Introduction

Metal complexes containing CH_2 ligands have been postulated as intermediates for numerous catalytic reactions (e.g., Fischer–Tropsch reductive polymerization of CO and olefin metathesis) and have been isolated in a number of cases including[2a,b]

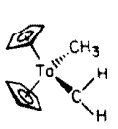

1

and

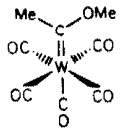

2

In the simple oxidation-state formalism, the CH_2 is thought of as $(CH_2)^{2-}$, with the metal oxidized by two units; however, the chemistry of these systems tends to fall into one of two distinct classes, one of which is nucleophilic and the other electrophilic.

A series of generalized valence bond (GVB) studies on high-oxidation-state metal complexes such as[3] $Cl_2Ti{=}CH_2$ (**3**), $Cl_4Cr{=}CH_2$ (**4**), and $Cl_4Mo{=}CH_2$ (**5**) showed that these systems all have the form **6** with a *covalent metal–carbon double bond*

6

involving a π bond composed of one electron in a metal dπ orbital spin-paired with one electron in a C pπ orbital, and a σ bond consisting of one electron in a metal dσ orbital spin-paired with one electron in a C sp^2 σ orbital. Similar studies[1,4] on $(Cr{=}CH_2)^+$ (**7**), $(Mn{=}CH_2)^+$ (**8**), and $(Fe{=}CH_2)^+$ (**9**) lead also to a double bond with a similar covalent M dπ–C pπ bond but a σ bond having varying amounts of dσ and sσ character on the metal.

Such studies suggest the following valence bond view of metal–methylene bonds. The metal is considered to be in the atomic configuration (s^1d^{n-1}, d^n, etc.) appropriate for its charge and environment (no formal charge transfer to the CH_2), and the CH_2 is considered to be neutral and in one of its two most stable forms, the triplet $\sigma\pi$ ground state **10** or the singlet σ^2 excited state (9 kcal/mol higher[5]) **11**. The ground state and low-lying excited states of the system are formed by combining the various low-lying metal atomic configurations with **10** and **11** to form various bonding states.

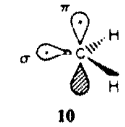

10

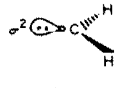

11

Metal–methylene complexes involving **10** have covalent metal–carbon double bonds and are termed metal methylidenes to emphasize the double-bond character. Examples include the so-called Schrock complexes **1**. Metal–methylene complexes involving **11** require empty dσ or s orbitals on the metal (that can accommodate the CH_2 σ pair) and prefer a doubly occupied dπ orbital on the metal that can overlap the empty π orbital of σ^2 CH_2. This leads to a metal–carbon bond best described in terms of donor–acceptor or Lewis acid–Lewis base concepts (as in "Fischer"-type carbenes such as **2**, or, in general, as **12**). We

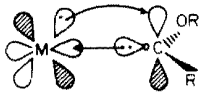

12

will refer to such systems as metal carbenes. Supporting evidence for such differences in the metal–carbon bond character is the drastic contrast in chemical reactivity of **6** with **12**. Metal methylidenes such as **3**–**5** are precatalysts for metathesis[6] and polymerization reactions with olefins,[7] whereas metal carbenes such as **2** generally exhibit stoichiometric reactivity with olefins, leading to the formation of cyclopropanes.[8]

[†] National Science Foundation Predoctoral Fellow, 1982–1985.

(1) Paper 1 in this series: Carter, E. A.; Goddard, W. A., III. *J. Phys. Chem.* **1984**, *88*, 1485.

(2) (a) Schrock, R. R. *J. Am. Chem. Soc.* **1975**, *97*, 6577. Guggenberger, L. J.; Schrock, R. R. *Ibid.* **1975**, *97*, 6578. (b) Fischer, E. O. *Adv. Organomet. Chem.* **1976**, *14*, 1. For an extensive review of both Fischer- and Schrock-type carbenes, Dötz, K. H.; Fischer, H.; Hofmann, P.; Kreissl, F. R.; Schubert, U.; Weiss, K. *Transition Metal Carbene Complexes*; Verlag Chemie: Deerfield Beach, FL, 1984.

(3) (a) Rappé, A. K.; Goddard, W. A., III. In *Potential Energy Surfaces and Dynamics Calculations*; Truhlar, D. G., Ed.; Plenum: New York, 1981; pp 661–684. (b) *J. Am. Chem. Soc.* **1982**, *104*, 297. (c) *Ibid.* **1982**, *104*, 448. (d) *Ibid.* **1980**, *102*, 5114.

(4) $MnCH_2^+$ and $FeCH_2^+$ work: Brusich, M. J.; Goddard, W. A., III, to be published. For another recent paper on $CrCH_2^+$ concurring with our earlier results (ref 1), see Alvarado-Swaisgood, A. E.; Allison, J.; Harrison, J. F. *J. Phys. Chem.* **1985**, *89*, 2517.

(5) Leopold, D. G.; Murray, K. K.; Lineberger, W. C. *J. Chem. Phys.* **1984**, *81*, 1048.

(6) (a) Lee, I. B.; Ott, K. C.; Grubbs, R. H. *J. Am. Chem. Soc.* **1982**, *104*, 7491. (b) Wengrovius, I. A.; Schrock, R. R.; Churchill, M. R.; Missert, I. R.; Youngs, W. J. *Ibid.* **1980**, *102*, 4515. (c) Gilet, M.; Mortreux, A.; Folest, J.-C.; Petit, F. *Ibid.* **1983**, *105*, 3876. (d) Kress, J.; Osborn, J. A. *Ibid.* **1983**, *105*, 6346. (e) Katz, T. J.; Han, C.-C. *Organometallics* **1982**, *1*, 1093. (f) Howard, T. R.; Lee, J. B.; Grubbs, R. H. *J. Am. Chem. Soc.* **1980**, *102*, 6876.

(7) (a) Turner, H. W.; Schrock, R. R. *J. Am. Chem. Soc.* **1982**, *104*, 2331. (b) Levisalles, J.; Rose-Munch, F.; Rudler, H.; Daran, J.-C.; Dromzée, Y.; Jeannin, Y. *J. Chem. Soc., Chem. Commun.* **1981**, 152.

0002-7863/86/1508-2180$01.50/0

This gestalt view of bonding in terms of combining complete many-electron states is a characteristic distinguishing the valence bond viewpoint from the molecular orbital viewpoint in which one-electron orbitals are constructed (from the same atomic orbitals), but where distinctions between atomic configurations such as σ^2 vs. $\sigma\pi$ methylene or s^1d^4 vs. d^5 Cr^+ become blurred. Although this valence bond view of bonding has been implicit in several papers, no examples of the metal–carbene bonding (as in **12**) have been examined with GVB techniques. In this paper we report all-electron ab initio GVB calculations on a system $(RuCH_2)^+$ (**13**) that exhibits both methylidene- and carbene-like states having comparable bond strengths. Indeed, the lowest carbene-like state

13

($^4A_2$) is only 12.9 kcal/mol above the lowest methylidene-like state ($^2A_2$). The results for the $^2A_2$ ground state of **13** (methylidene) are examined in section II, while the wave function for the $^4A_2$ excited state of **13** (carbene) is described in section III. A summary of our conclusions is presented in section IV, while further details of the calculations are outlined in section V.

II. The Ground State of $RuCH_2^+$: Methylidene Bonding

A. Low-Lying Covalent States. Using the coordinate system

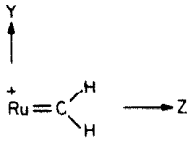

we will denote the five valence d orbitals of Ru as

$$d\sigma = d_{z^2} \quad (a_1)$$

$$d\pi_x = d_{xz} \quad (b_1)$$

$$d\pi_y = d_{yz} \quad (b_2)$$

$$d\delta_{xy} = d_{xy} \quad (a_2)$$

$$d\bar{\delta}_{x^2-y^2} = d_{x^2-y^2} \quad (a_1)$$

In C_{2v} symmetry, $d\bar{\delta}$ and $d\sigma$ have the same symmetry (shown in parentheses); however, the $d\sigma$ and $d\bar{\delta}$ character perseveres. To predict low-lying states of the metal–methylene complex, we utilize the valence bond picture in which the ground-state molecular or atomic fragments are brought together to form two-electron bond pairs in the resulting complex. Starting with the high-spin d^7 configuration associated with the ^4F ground state of Ru^+ and the ground state of CH_2 (**10**), we see that singly occupied $d\sigma$ and $d\pi$ orbitals are required on Ru^+. This leaves three orbitals ($d\delta$, $d\bar{\delta}$, and $d\bar{\pi}$) for the remaining five valence electrons on Ru^+. Thus, double-bonded $RuCH_2^+$ leads to three low-lying states with the following occupations of the nonbonding Ru d orbitals.

$$^2B_2\ (d\delta)^2(d\bar{\delta})^2(d\bar{\pi})^1 \text{ (20.0 kcal/mol above } ^2A_2)$$

$$^2A_1\ (d\delta)^2(d\bar{\delta})^2(d\bar{\pi})^2 \text{ (1.2 kcal/mol above } ^2A_2) \qquad (1)$$

$$^2A_2\ (d\delta)^1(d\bar{\delta})^2(d\bar{\pi})^2 \text{ (ground state)}$$

Using simple ligand-field considerations, one might argue that the $^2B_2$ state would be the lowest, since the $d\bar{\pi}$ orbital, which overlaps the CH bonds, is singly occupied (less electron–electron repulsion in the molecular plane than for the other two states). However, this state is 20.0 kcal/mol above the ground state. In order to consistently predict such ordering of states in the bound complex, it is useful to examine the energies for the corresponding atomic configurations of Ru^+. As shown in Table I, the three configurations in (1) lead to the following atomic energies:

$$^2B_2\ (d\sigma)^1(d\pi)^1(d\delta)^2(d\bar{\delta})^2(d\bar{\pi})^1 \text{ (20.1 kcal/mol above } ^2A_2)$$

$$^2A_1\ (d\sigma)^1(d\pi)^1(d\delta)^2(d\bar{\delta})^1(d\bar{\pi})^2 \text{ (degenerate with } ^2A_2) \qquad (2)$$

$$^2A_2\ (d\sigma)^1(d\pi)^1(d\delta)^1(d\bar{\delta})^2(d\bar{\pi})^2$$

Although all three configurations are d^7 Ru^+, they have different electron repulsion energies (even when the orbital shapes are identical), and we see by examination of (2) that it is this *atomic-electron repulsion energy* that *determines the relative energies* in (1). For example, $^2B_2$ has four electrons in the xy plane ($\delta^2\bar{\delta}^2$), whereas $^2A_1$ and $^2A_2$ have the doubly occupied orbitals in different planes ($\bar{\delta}^2\bar{\pi}^2$ or $\delta^2\bar{\pi}^2$), leading to lower electron repulsion. Thus, in predicting the ground configuration of $RuCH_2^+$ we need only consider two factors:

(i) which states of Ru^+ can form two covalent bonds, and

(ii) of the states satisfying (i), which occupation of the nonbonding d orbitals has the lowest atomic energy (lowest electron repulsion).

B. Bonding in the Ground State, $RuCH_2^+$ ($^2A_2$). The generalized valence bond (GVB) one-electron orbitals for the Ru–C σ and π bonds are shown in Figure 1 where we see that both bonds are quite covalent. The Ru–C σ bond pair has an overlap of 0.68, with 1.04 electrons ascribed to Ru^+ and 0.96 electron associated with CH_2.[9] The Ru–C π bond pair has an overlap of 0.48, with 1.16 electrons localized on Ru^+ and the other 0.84 electron on CH_2. The bonding orbitals on Ru are almost entirely 4d in character (the Ru σ bonding orbital is 87.8% 4d and 12.2% 5sp, while the Ru π bonding orbital is 99.1% 4d and 0.9% 5p). Thus the $RuCH_2^+$ complex is best described as d^7 Ru^+, forming a covalent double bond with triplet methylene.

The covalent nature of the Ru=CH_2 bond is further supported by comparison with the bonds in ethylene. The GVB orbitals for the σ and π bonds of CH_2=CH_2 are shown in Figure 1, where it is evident that the carbon σ and π character in both $RuCH_2^+$ and CH_2=CH_2 are very similar. The C–C σ overlap in ethylene is 0.88, while the C–C π bond overlap is 0.65. The overlaps are lower in $RuCH_2^+$ due to the longer bond lengths [R(Ru=C) = 1.88 Å vs. R(C=C) = 1.34 Å;[10] see Figure 2] and some mismatch in orbital extent for Ru 4d vs. C 2sp. However, the trends in overlap (σ vs. π) compare well: S_σ–S_π = 0.23 for CH_2=CH_2 and S_σ–S_π = 0.20 for $RuCH_2^+$ ($^2A_2$).

One further indication of covalent bonding becomes evident as we pull the molecule apart, breaking the double bond. For covalent bonds, the overlap in each bond decreases monotonically as the bond length is increased from its equilibrium position, and this is indeed observed for $RuCH_2^+$ ($^2A_2$) (see Figure 3). The opposite behavior of the bond pair overlap observed for the low-lying $^4A_2$ excited state of $RuCH_2^+$ will be discussed in section III.

C. Oxidation-State Formalisms. The result of a *covalent* double bond between a metal atom and CH_2 is in *direct contradiction* with the literal interpretation of the popular oxidation-state formalism, which denotes the methylidene ligand as CH_2^{2-} when bound to transition metals. The oxidation formalism *implies ionic bonding*; our theoretical results show clearly that bonds between transition metals and CH_2 are often *covalent*, not ionic.

From these and other GVB calculations, the following alternatives formalism has evolved:

(1) Consider every ligand as neutral and start with the appropriate charge state of the metal (Ti^0 for **3**, Cr^0 for **4**, Mo^0 for

(8) (a) Fischer, E. O.; Dötz, K. H. *Chem. Ber.* **1970**, *103*, 1273. (b) Dötz, K. H.; Fischer, E. O. *Ibid.* **1972**, *1356*. (c) Stevens, A. E.; Beauchamp, J. L. *J. Am. Chem. Soc.* **1979**, *101*, 6449. (d) Brandt, S.; Helquist, P. J. *Ibid.* **1979**, *101*, 6473. (e) Brookhart, M.; Humphrey, M. B.; Katzer, H. J.; Nelson, G. O. *Ibid.* **1980**, *102*, 7803. (f) Brookhart, M.; Tucker, J. R.; Husk, G. R. *Ibid.* **1981**, *103*, 979. (g) Casey, C. P.; Vollendorf, N. W.; Haller, K. J. *Ibid.* **1984**, *106*, 3754. (h) Casey, C. P.; Shusterman, A. J. *Organometallics* **1985**, *4*, 736. (i) Brookhart, M.; Studabaker, W. B.; Husk, G. R. *Ibid.* **1985**, *4*, 943. (j) Casey, C. P.; Miles, W. H.; Tukada, H. *J. Am. Chem. Soc.* **1985**, *107*, 2924. (k) Stevens, A. E.; Beauchamp, J. L. *Ibid.* **1978**, *100*, 2584.

(9) The electron populations and hybrid character are determined by summing the Mulliken populations from both natural orbitals (weighted by occupation) of each GVB bond pair.

(10) Harmony, M. D.; Laurie, V. W.; Kuczkowski, R. L.; Schwendeman, R. H.; Ramsay, D. A.; Lovas, F. J.; Lafferty, W. J.; Maki, A. G. *J. Phys. Chem. Ref. Data* **1979**, *8*, 676.

Table I. Single Configuration SCF and CI Energies for d^7 Ru^+

relevant $RuCH_2^+$ symmetry[a]	Ru^+ hole config[b]			Ru^+ full config					Ru^+ SCF total energy, hartrees	Ru^+ $H(i,i)$[c] total energy, hartrees	ΔE(SCF),[d] kcal/mol	ΔE(CI),[e] kcal/mol
				σ	π	π^*	δ	δ^*				
$^2B_2$	σ	π	π^*	1	1	1	2	2	−4437.140 79	−4437.139 59	+26.8	+27.4
–	π^*	δ	δ^*	2	2	1	1	1		−4437.150 49		+20.5
–	π	δ	δ^*	2	1	2	1	1	−4437.151 45	−4437.150 49	+20.1	+20.5
$^4A_2$	σ	δ	δ^*	1	2	2	1	1	−4437.172 83	−4437.172 29	+6.7	+6.8
$^4B_2$	σ	π^*	δ^*	1	2	1	2	1	−4437.172 82	−4437.172 29	+6.7	+6.8
$^2A_1$, $^4B_1$[f]	σ	π	δ^*	1	1	2	2	1	−4437.172 82	−4437.172 29	+6.7	+6.8
$^4B_1$	σ	π^*	δ	1	2	1	1	2	−4437.172 82	−4437.172 29	+6.7	+6.8
$^2A_2$	σ	π	δ	1	1	2	1	2	−4437.172 82	−4437.172 29	+6.7	+6.8
–	π	π^*	δ^*	2	1	1	2	1		−4437.183 19		0.0
–	π^*	π^*	δ	2	1	1	1	2	−4437.183 54	−4437.183 19	0.0	0.0

[a] The C_{2v} symmetries listed for $RuCH_2^+$ doublet states correspond to $^3B_1$ CH_2 bound to the configuration of Ru^+ listed in the next column. The quartet states of $RuCH_2^+$ correspond to $^1A_1$ CH_2 bound to the configuration of Ru^+ listed in the next column. [b] The doubly occupied orbitals have been omitted for clarity in discussions. Our convention for d-orbital symmetries has $\sigma = 4d_{z^2}$, $\pi = 4d_{xz}$, $\pi^* = 4d_{yz}$, $\delta = 4d_{xy}$, $\delta^* = 4d_{x^2-y^2}$, where the Ru–C axis is z and the $RuCH_2^+$ plane is yz. Thus, π and δ are "pi-like" (antisymmetric) with respect to the molecular plane. [c] Using field-averaged orbitals from the SCF wave function ($^7/_5$ electrons per d orbital to obtain equivalently shaped d orbitals), we constructed all 10 states corresponding to the d^7 configuration of Ru^+. A 10-configuration CI leads to seven states corresponding to ^4F (each with total energy −4437.183 19 hartrees) and three states corresponding to ^4P (higher by 34.2 kcal/mol). When real orbitals are used, only two of these 10 configurations ($\pi\pi^*\delta$) and ($\pi\pi^*\delta^*$) have pure ^4F symmetry and none has pure ^4P symmetry. The diagonal energies for these configurations are given by $H(i,i)$. For some configurations we solved for the SCF wave function (rather than using field-averaged orbitals); this leads to energies lower by 0.1–0.6 kcal. The energy differences in $H(i,i)$ are a measure of the increased electron repulsion energy (exchange energies) in these states. [d] SCF excitation energy (in kcal/mol) from the $\pi\pi^*\delta$ ground state of Ru^+. [e] CI excitation energy (in kcal/mol) from the $\pi\pi^*\delta$ ground state of Ru^+. [f] $RuCH_2^+$ ($^4B_1$) excited state with a single σ-donor bond.

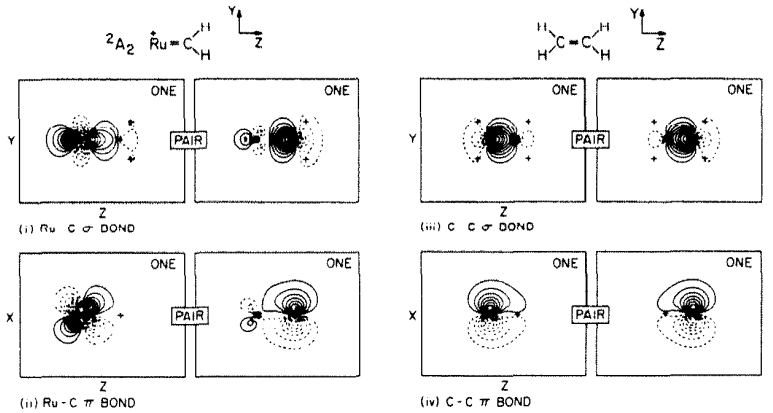

Figure 1. GVB orbitals for the methylidene complex $RuCH_2^+$ ($^2A_2$) [(i) and (ii)] and for $CH_2{=}CH_2$ [(iii) and (iv)]. (i) Ru–C σ bond; (ii) Ru–C π bond; (iii) C–C σ bond; (iv) C–C π bond. Contours reflect regions of constant amplitude ranging from −0.5 to +0.5 a.u., with increments of 0.05 a.u.

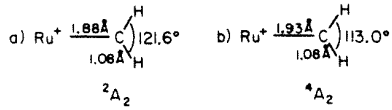

Figure 2. Optimum geometries at the GVB(2/4)-RCI level for (a) ground-state $RuCH_2^+$ ($^2A_2$) and (b) excited-state $RuCH_2^+$ ($^4A_2$).

5, and Ru^+ for **13**), and consider first the ground atomic configuration for the metal (s^2d^2 for Ti, s^1d^5 for Cr and Mo, and d^7 for Ru^+).

(2) Ligands such as cyclopentadienyl (Cp) or Cl prefer larger amounts of ionic character in the bond and consequently prefer to bond to s-like metal orbitals rather than d orbitals (lower ionization potential (IP) for s than d and hence easier charge transfer). For a qualitative analysis it is just as well to consider these ligands as reduced (e.g., Cp^- or Cl^-) and the metal oxidized. For two such electronegative ligands to both obtain partial ionic bonds requires an s^2 metal configuration. In the GVB description, an s^2 pair is described by (s + pz) and (s − pz) hybrid orbitals, and each plays the role of bonding to one electronegative ligand (thus preferring a 180° bond angle). If there are more than two such electronegative ligands, the ionic bonds must involve metal d electrons (since s^3 is not allowed and s^2p is generally quite high) and consequently the bonds become less ionic.

(3) Bonds to alkyl, aryl, and hydride ligands prefer covalent bonding, particularly if the metal has enough electronegative ligands to utilize the s electrons on the metal.

(4) More subtle effects can be involved for groups with active p-like lone pairs such as oxo or alkoxide groups, but we will eschew them here.

Although more cumbersome than the usual oxidation-state formalism, we find that this VB formalism provides a simple means of correctly predicting the character of numerous quite different states of organometallic complexes. Some examples follow:

(1) For $RuCH_2^+$ we label the Ru atom as Ru(I) and consider the ground d^7 configuration, since the bonds are covalent and there is a +1 charge on the metal.

(2) Since neutral Ru atom has an s^1d^7 ground state and Cl is very electronegative, we expect RuCl to have a very ionic bond,[11] and hence the Ru in RuCl is labeled as Ru(I). Further, ligands added to Ru^ICl should form covalent bonds, since all remaining unpaired Ru electrons are in d orbitals, as in $Ru^I{=}CH_2^+$.

(3) GVB calculations on $ClRu(H)(CH_3)$[12] show the metal to have the same electronic character as in $Ru^I{=}CH_2^+$; namely, the

(11) Carter, E. A.; Goddard, W. A., III, unpublished.
(12) Carter, E. A.; Goddard, W. A., III, manuscript in preparation.

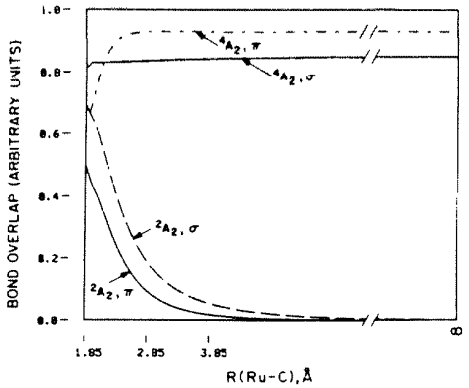

Figure 3. Ru–C σ and π bond overlaps for the $^4A_2$ (donor–acceptor or carbene-like bond) and $^2A_2$ (covalent or methylidene-like bond) states of $RuCH_2^+$ as a function of distance. Overlap decreases with distance for covalent bonds but is approximately constant for donor–acceptor bonds.

bonds to H and CH_2 are quite covalent and the CH_2 bonds in both Ru(I) systems are nearly identical in character. **14** depicts the

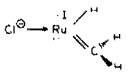

14

electronic character at Ru(I) as three covalent bonds drawn as lines, one dative bond from Cl^- as an arrow, and two doubly occupied d orbitals by two pairs of dots.

(4) $(Cl)(NO)(PPh_3)_2Os(CH_2)$[13] is written as

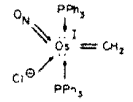

15

indicating that the metal is thought of as a d^7 Os(I) (after making an ionic bond to Cl to form Cl^-) with three covalent d bonds (two to CH_2 and one to the π orbital of NO), leaving two double occupied d orbitals. In addition to the five d orbitals of Os(I), the four arrows indicate the ligands overlapping the four empty Os 6s and 6p orbitals to yield a total of 18 electrons associated with the metal (four in doubly occupied d orbitals, six in three covalent metal–ligand bonds, and eight in the pairs indicated with arrows).

(5) $(Cp^*)(NO)(PPh_3)Re(CH_2)^+$[14] is written as

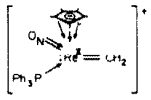

16

to show that the Cp^* ($Cp^* = C_5Me_5$) has formed an ionic bond and thus the metal should be thought of as d^5 Re(II). In this case there are five ligand-to-metal donor bonds, requiring an empty 5d orbital in addition to the four empty 6s and 6p orbitals, so that the d^5 configuration of Re(II) has one doubly occupied d orbital plus three singly occupied d orbitals (which are used in the three covalent bonds).

Examples 1–5 illustrate how to designate and predict the character of metal–ligand bonds, the nonbonding electron configuration at the metal, and the overall degree of saturation of the metal complex. This new VB oxidation-state formalism provides logical explanations and predictions for bond character trends in the forthcoming sections.

(13) Hill, A. F.; Roper, W. R.; Waters, J. M., Wright, A. H. *J. Am. Chem. Soc.* **1983**, *105*, 5939.

(14) Patton, A. T.; Strause, C. E.; Kuobler, C. B.; Gladysz, J. A. *J. Am. Chem. Soc.* **1983**, *105*, 5804.

Table II. Vibrational Frequencies (cm^{-1}) for the $^2A_2$ and $^4A_2$ States of $RuCH_2^+$[a]

state	ν_{Ru-C}	ν_{C-H}	$\nu_{HCH\,bending}$
$^2A_2$	665	3245	1461
$^4A_2$	464	3256	1437

[a] Based on ω_e from cubic spline fits to results from GVB(2/4)-RCI calculations.

D. Geometries. The optimum calculated geometry for $RuCH_2^+$ ($^2A_2$) is shown in Figure 2a. The Ru–C bond length of 1.88 Å may be compared with experimental values for metal–methylidene bond lengths such as $R(Os^I{=}CH_2)$ = 1.92 Å in **15**[13] and $R(Re^{II}{=}CH_2)$ = 1.898 Å in **16**.[14] The Ru^I–C bond length is expected to be shorter than the Os^I–C bond length since the d-orbital extent for Ru(I) is smaller than that for Os(I) (4d for Ru vs. 5d for Os). For d^5 Re(II), the greater orbital extent due to a higher n quantum number is nearly canceled by the higher effective nuclear charge, which causes a greater contraction of the orbitals for Re(II) than for Ru(I). Consistent with our expectations, covalent d bonds involving d orbitals of similar size result in very similar bond lengths.

The other geometrical parameters of $RuCH_2^+$ are not unusual. The C–H bond lengths (1.08 Å) are typical for sp^2 C–H bonds. The HCH bond angle of 121.6° is characteristic of a triplet methylene forming two covalent bonds to another moiety (a metal or another CH_2). For instance, $CrCH_2^+$ ($^4B_1$) has θ(HCH) = 117.6° and $CH_2{=}CH_2$ has θ(HCH) = 117.6°.[1,10] On the other hand, θ(HCH) = 133° for free CH_2 ($^3B_1$),[15] indicating that electron pair–pair repulsions decrease θ(HCH) upon complexation.

E. Vibrational Frequencies. The vibrational frequencies for $RuCH_2^+$ ($^2A_2$) are shown in Table II. The Ru–CH_2 stretching frequency is 665 cm^{-1}, which may be compared with theoretical values for $CrCH_2^+$ ($^4B_1$) of ν_{Cr-C} = 542 cm^{-1} and the values obtained for two rotamers of $ClRu^IH(CH_2)$ of ν_{Ru-C} = 746 and 798 cm^{-1}.[1,12] The M=C frequencies correlate well with bond strength in order of $Cr^+ < Ru^+ < ClRuH$. The $D_0(M^I{=}CH_2)$ are 44.0, 68.0 (vide infra), and 85.5 kcal/mol for M = Cr^+, Ru^+, and ClRuH, respectively. A recent matrix isolation study[16] on $FeCH_2$ provides the first experimental M–CH_2 stretching frequency, 623.6 cm^{-1}, in good agreement with our value for $RuCH_2^+$. The C–H symmetric stretch at 3245 cm^{-1} and the HCH scissors mode at 1461 cm^{-1} are in reasonable agreement with those expected for sp^2 C–H bonds. (The corresponding values in $CH_2{=}CH_2$ are 3056 and 1393 cm^{-1}, respectively.[17])

F. The Ru=C Bond Strength in $RuCH_2^+$ ($^2A_2$). Few metal–ligand bond strengths for saturated organometallic complexes are known, either experimentally or theoretically. The majority of those that have been measured are for gas-phase, highly unsaturated bare metal cations with just one ligand.[18] In this section we will consider the relationship expected between the bond energies in such unsaturated species as compared with saturated organometallic complexes.

All calculations carried out on $RuCH_2^+$ are such that the wave function for $RuCH_2^+$ at its equilibrium geometry (given in Figure 2a) dissociates smoothly to the appropriate covalent fragments, retaining the same level of electron correlation in the fragments as that included for the complex. In addition, we allow the fragments to relax to their equilibrium geometries, thus obtaining

(15) Shih, S.-K.; Peyerimhoff, S. D.; Buenker, R. J.; Peric, M. *Chem. Phys. Lett.* **1978**, *55*, 206.

(16) Chang, S.-C.; Kafafi, Z. H.; Hauge, R. H.; Billups, W. E.; Margrave, J. L. *J. Am. Chem. Soc.* **1985**, *107*, 1447.

(17) Shimanouchi, T. *Tables of Molecular Vibrational Frequencies*; U. S. Government Printing Office: Washington, DC, 1972, NSRDS-NBS-92.

(18) See, for example, (a) Armentrout, P. B.; Beauchamp, J. L. *J. Am. Chem. Soc.* **1981**, *103*, 784. (b) Armentrout, P. B.; Halle, L. F.; Beauchamp, J. L. *Ibid.* **1981**, *103*, 6501. (c) Mandich, M. L.; Halle, L. F.; Beauchamp, J. L. *Ibid.* **1984**, *106*, 4403.

Table III. Bond Dissociation Energies (kcal/mol) for the Methylidene State of $RuCH_2^+$ ($^2A_2$)

calculational level[a]	D_e(Ru=C)	$RuCH_2^+(^2A_2)$ total energy, hartrees[b]	fragment total energies, hartrees	
			Ru^+	$CH_2(^3B_1)$
HF	-11.5	-4476.088 67	-4437.183 54	-38.923 41
		(1/1)	(1/1)	(1/1)
GVB(2/4)-PP	27.6	-4476.151 00	-4437.183 54	-38.923 41
		(4/4)	(1/1)	(1/1)
RCI(2/4)	45.4	-4476.179 23	-4437.183 54	-38.923 41
		(9/17)	(1/1)	(1/1)
$RCI_v{}^*D_v + RCI_v{}^*D_v$	55.2	-4476.194 88	-4437.183 54	-38.923 41
		(989/2627)	(1/1)	(1/1)
$(RCI(2/4)^*S)_{val,Ru}$	59.5	-4476.202 74	-4437.184 49	-38.923 41
		(321/1233)	(21/48)	(1/1)
$(RCI(2/4)^*S)_{val,full}$	63.3	-4476.220 28	-4437.184 49	-38.934 99
		(507/2091)	(21/48)	(22/44)
$RCI_v{}^*D_v + RCI_v{}^*D_v + (RCI(2/4)^*S)_{val,full}$	68.0	-4476.227 77	-4437.184 49	-38.934 99
		(1379/4377)	(21/48)	(22/44)

[a] Each of these calculations is explained in detail in section V. [b] The number of spatial configurations/number of spin eigenfunctions are given in parentheses.

the adiabatic, dissociation-consistent[19] bond energy.

The Ru=C bond energies for $RuCH_2^+$ ($^2A_2$) as a function of electron correlation are shown in Table III. At the highest level, we find a direct, adiabatic Ru=C bond energy of D_e = 68.0 kcal/mol, for $RuCH_2^+$ ($^2A_2$) dissociating into ground-state fragments Ru^+ (^4F) ($\pi\bar{\pi}\delta$ and $\pi\bar{\pi}\bar{\delta}$ in Table I) and CH_2 ($^3B_1$). Note that although the metal is in a promoted state at R_e (6.7 kcal/mol above ^4F; see Table I), the metal relaxes to ^4F Ru^+ as the bond breaks.[20] This direct bond energy is expected to be a lower limit since electron-correlation effects increase when more electrons are in the same regions of space. Analogous calculations for the double bond of CH_2=CH_2 (using the same basis sets and level of CI as in $RuCH_2^+$) lead to a calculated bond energy of 174.4 kcal/mol,[1] which is 5.6 kcal/mol smaller than the experimental value of $D_e(CH_2{=}CH_2)$ = 180.0.[21] We expect the residual correlation error in $Ru{=}CH_2^+$ to be at least as high as in $CH_2{=}CH_2$ (due to the presence of the other valence d electrons on Ru); hence, we estimate the exact bond energy for $RuCH_2^+$ ($^2A_2$) to be

$$D_e^{exact}(Ru^+{=}CH_2) = 73.6 \text{ kcal/mol}$$

G. Correlation between Saturated and Unsaturated M=CH_2 Bond Energies. Since gas-phase $RuCH_2^+$ has not yet been observed, a direct comparison cannot be made with experiment. However, we have carried out equivalent calculations on the larger $Ru^I{=}CH_2$ complex, $ClRu^IH(CH_2)$, **14**, which in the $^1A'$ state should model coordinatively saturated, 18-electron ruthenium–alkylidene complexes such as $CpRu^I(L)(R)(CH_2)$ (where L = CO or PR_3 and R = alkyl, aryl, or H), which has been postulated as an intermediate in the isomerization of a dimethylruthenium complex to an olefin hydride complex.[22] For **14**, at the same level of electron correlation and the same basis sets as used in the present study, we find a direct, adiabatic Ru=C bond energy of D_e(Ru=C) = 85.5 kcal/mol (vs. 68.0 for $RuCH_2^+$).[12]

Why is the bond stronger in the more highly saturated system even though the metal–carbon bond has not changed character? The answer involves the change in spin coupling necessarily associated with covalent-bond formation. For atoms, the ground state has the singly occupied orbitals coupled to form the highest spin state (Hund's rule). This results from the exchange energy terms

$$E^{ex} = -\sum_{i>j} K_{i\alpha,j\alpha} - \sum_{i>j} K_{i\beta,j\beta}$$

which arise (from the Pauli principle) *only* for orbitals with the same spin. For d^7 Ru^+, the quartet state ($S = {}^3/_2$) with five α spins and two β spins leads to 11 exchange interactions, each of which contributes an average of negative 15 kcal/mol to the energy.[23] In contrast, the atomic doublet state ($S = {}^1/_2$) with four α spins and three β spins leads to only nine exchange interactions and an energy about 30 kcal/mol higher. However, formation of a covalent bond (perfect pairing) between a ligand and a singly occupied d orbital necessarily requires that the bond pair be coupled into a singlet (low-spin) with the result that the metal d orbital is half the time α and half the time β. This results in a decrease in atomic exchange stabilization that goes hand in hand with covalent bonding to singly occupied d orbitals. The magnitude of this effect increases with the number of other singly occupied high-spin-paired d orbitals and hence it depends on how saturated the bonding to the metal is.

In forming a covalent double bond to CH_2 in (singlet) ClRu-(CH_2)H, the two metal orbitals that were originally high-spin ($\alpha\alpha$, leading to a $-K_{dd}$ exchange term) in the (triplet) ClRuH fragment must now each become α half the time and β half the time, with the result that they have the same spin only half the time (i.e., $\alpha\alpha + \alpha\beta + \beta\alpha + \beta\beta$ leads to a $-{}^1/_2K_{dd}$ average exchange term). The result is that the atomic exchange energy becomes less negative by ${}^1/_2K_{dd}$ = 7.5 kcal/mol. Thus

$$D_e[(Cl)(H)Ru{=}CH_2] = D_{int}(Ru{=}CH_2) - 7.5 \text{ kcal/mol}$$

where $D_{int}(Ru{=}CH_2)$ is the intrinsic (exchangeless) metal–methylene bond strength (for any $RuCH_2$ system). If there is a third unpaired d orbital on the metal (as in Ru^+), the spin of the free atom is $\alpha\alpha\alpha$, leading to $-3K_{dd}$ among those three electrons, but after bonding to two of the d orbitals, the spins on the metal are $\alpha\alpha\alpha + \alpha\beta\alpha + \beta\alpha\alpha + \beta\beta\alpha$, leading to an average of (1/4)(3 + 1 + 1 + 1) = $3/2K_{dd}$. Thus, in $RuCH_2^+$, the M=CH_2 bond loses $3/2K_{dd}$ = 22.5 kcal/mol. Thus

$$D_e(Ru^+{=}CH_2) = D_{int}(Ru{=}CH_2) - 22.5 \text{ kcal/mol}$$

and we expect

$$D_e[(Cl)(H)Ru{=}CH_2] - D_e(Ru^+{=}CH_2) = 15 \text{ kcal/mol} \quad (3)$$

Indeed, from the calculated bond energies (85.5 and 68.0), we obtain 17.5 kcal/mol for the quantity in (3). Thus *the differences in bond strengths for saturated vs. unsaturated metal complexes are dominated by the differential loss of exchange coupling on the metal.* Hence, we obtain

$$D_{int}(Ru{=}CH_2) = 68.0 + 22.5 = 90.5 \text{ kcal/mol} \quad (4)$$

$$D_{sat}(Ru{=}CH_2) = D_{int} - {}^1/_2K_{dd} = 83.0 \text{ kcal/mol} \quad (5)$$

(19) Bair, R. A.; Goddard, W. A., III, submitted for publication in *J. Phys. Chem.*

(20) At R_e, $RuCH_2^+$ ($^2A_2$) has the Ru$^+$ configuration $\sigma^1_{z^2}\pi^1_{xz}\bar{\pi}^2_{yz}\delta^2_{x^2-y^2,xy}\delta^1_{x^2-y^2,xy}$ which, under C_{2v} symmetry, relaxes as the bond breaks by mixing d_{z^2} and $d_{x^2-y^2}$ to form $\sigma^1_{x^2-y^2}\pi^1_{xz}\bar{\pi}^2_{yz}\delta^2_{z^2,x^2-y^2}\delta^1_{x^2-y^2}\delta^1_{xy}$. This latter configuration has ^4F symmetry with respect to the x axis.

(21) *JANAF Thermochemical Tables*; U.S. Government Printing Office: Washington, DC, 1970, NSRDS-NBS-37.

(22) Kletzin, H.; Werner, H.; Serhadli, O.; Ziegler, M. L. *Angew. Chem., Int. Ed. Engl.* **1983**, *22*, 46.

(23) K_{dd} = average exchange energy between two d orbitals. $K_{dd}(Ru^+)$ = 15 kcal/mol and K_{dd} = 7.5 kcal/mol from our ab initio Hartree–Fock calculations on Ru^+.

(where D_{sat} is the bond energy expected for a saturated Ru=CH_2 complex) from our direct GVB calculations. Including the estimated correction of 5.6 kcal/mol, (4) and (5) become

$$D_{int}^{exact}(Ru{=}CH_2) = 96.1 \text{ kcal/mol} \quad (6)$$

$$D_{sat}^{exact}(Ru{=}CH_2) = 88.6 \text{ kcal/mol} \quad (7)$$

We expect $D_{int}(Ru{=}CH_2)$ to remain fairly constant, regardless of the nature or existence of ancillary ligands, for a given electronic state of the metal atom. This is borne out in the cases above, $RuCH_2^+$ and $ClRuH(CH_2)$, for which D_{int} = 90.5 and 93.0 kcal/mol, respectively.

To see how to use these quantities for predicting bond energies, consider the 18-electron complex, $Cp(dppe)Ru{=}CH_2^+$ (the Fe analogue is known[24]): Ru(II) is d^6, but this complex requires

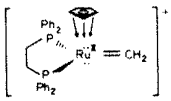

five empty acceptor orbitals (the 5s, three 5p, and one 4d) on the metal (as indicated by the arrows). The requirement of a d hole plus two singly occupied d's that can bond to CH_2 forces the other four electrons to occupy the two remaining d orbitals, leading to the intermediate triplet spin state of Ru(II). Thus, in bonding CH_2 to the fragment $Cp(dppe)Ru^+$, the two unpaired electrons in the intermediate spin state lose $^1/_2K_{dd}$, and we predict a bond energy of

$$D_e^{exact}[Cp(dppe)Ru{=}CH_2^+] = D_{int}(Ru{=}CH_2) - 7.5 = 96.1 - 7.5 = 88.6 \text{ kcal/mol}$$

In contrast, removal of the chelating phosphine should lower the bond energy, since $CpRu{=}CH_2^+$, does not require a d hole for

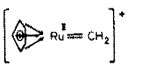

donation from the Cp^- ligand, leading to a high-spin d^6 Ru(II). In this case, the fragment $CpRu^+$ has four unpaired spins with $-6K_{dd}$ between them, while $CpRuCH_2^+$ with two unpaired electrons has only $-3^1/_2K_{dd}$ involving these four electrons (after forming the bond). Therefore, we expect

$$D_e^{exact}(CpRu^+{=}CH_2) = 96.1 - (\tfrac{7}{2})(15) = 58.6 \text{ kcal/mol}$$

Thus, dramatic differences in bond energies are expected bewteen unsaturated vs. saturated complexes, *even as the nature of the bond being broken remains constant*.

This leads to the exchange moderated ligand effect: Added ligands serve to quench many of the intraatomic exchange terms (due either to covalent bond formation or to coordinated Lewis bases forcing the metal into a lower spin state). The differential-exchange energy lost in the more saturated complex will be less than that lost in a highly unsaturated system, leading to a larger observed Ru=CH_2 bond energy.

As another example, consider the saturated system $(Cl)(NO)Ru^I(PPh_3)_2{=}CH_2$. Although $RuCH_2^+$ has an estimated Ru–C bond energy of 73.6 kcal/mol, here we expect to have an Ru–C bond energy of $96.1 - {}^1/_2K_{dd}$ = 88.6 kcal/mol, the same as predicted for our model compound $ClRuH(CH_2)$ and for $Cp(dppe)Ru{=}CH_2^+$. Thus, *saturated metal complexes are expected to have substantially larger bond energies than those of their unsaturated counterparts.*

This result suggests two further extensions. First, the fact that the intrinsic bond strengths of these two ruthenium(I)–alkylidene systems are essentially identical implies that the character of the bonding is also the same for both systems. Thus, by understanding the simple case of $RuCH_2^+$, we can understand the bonding in the larger Ru(I) complex, $ClRuH(CH_2)$, and in other electronically analogous systems. Second, the simplicity (and generality) of the expression for the intrinsic bond strength is provocative; it suggests that we may be able to estimate the bond energies of saturated organometallic (or any other) complexes from bond energies known for unsaturated complexes containing the same ligand. Calculation of $D_{int} = D_e(\text{unsaturated}) + \Delta K_{dd}$ yields

$$D_e(\text{saturated}) = D_e(\text{unsaturated}) + \Delta K_{dd} - {}^1/_2K_{dd}$$

assuming covalent bonds to d orbitals are formed in the saturated complex. (This does require that the metal atoms have the same electronic state in both complexes.)

H. Summary. We see that each property of the $^2A_2$ state of $RuCH_2^+$ taken separately or together, implicates one possible description of the bonding between Ru^+ and CH_2. Thus, we may best think of this complex as consisting of high-spin d^7 Ru^+ forming two covalent bonds to $^3B_1$ CH_2.

III. A Low-Lying Excited State of $RuCH_2^+$: Carbene Bonding

A. Covalent vs. Donor–Acceptor Bonding. As discussed in section II.G, the intraatomic exchange stabilization of a free metal ion necessarily weakens metal–ligand bonds, since this stabilization is at least partially quenched upon complexation. In section II, we examined the lowest spin state of $RuCH_2^+$, formed from ground-state fragments, and found a $^2A_2$ ground state. However, higher spin states may be important if they lead to less exchange energy quenching in the complex. Thus we investigated the possible existence of low-lying quartet states of $RuCH_2^+$.

There are three ways in which quartet states may be formed for $RuCH_2^+$. First, we can form a quartet state directly from the ground $^2A_2$ state by triplet-coupling the weakest bond, namely, the π bond. This leads to a singly bonded $^4A_2$ state of Ru^+–CH_2, which suffers less exchange loss than the doublet ground state (only 1 K_{dd} = 15 kcal/mol), but it is destabilized by forcing the overlapping Ru dπ orbital and the C pπ orbital to be orthogonal. The $^4A_2$ state formed in this manner lies above the $^2A_2$ ground state by 50.9 kcal/mol.

A second way to form a quartet state of $RuCH_2^+$ is to promote d^7 Ru^+ to s^1d^6 before bonding to triplet CH_2. This costs 28.4 kcal/mol,[25] but in return we can form two covalent bonds to CH_2, thus avoiding the π repulsions which caused the above quartet to fail.

Promoting Ru^+ to the s^1d^6 excited state leads to five equivalent states (the ^6D state). When the same labeling scheme as in section II.A (the corresponding $RuCH_2^+$ symmetries are shown in parentheses) is used, these become

$$(5s)^1(d\sigma)^2(\underline{d\pi})^1(d\bar{\pi})^1(d\delta)^1(d\bar{\delta})^1 \quad (^4B_1)$$

$$(5s)^1(d\sigma)^1(d\pi)^2(d\bar{\pi})^1(d\delta)^1(d\bar{\delta})^1 \quad (^6A_1)$$

$$(5s)^1(\underline{d\sigma})^1(\underline{d\bar{\pi}})^1(d\pi)^2(d\delta)^1(d\bar{\delta})^1 \quad (^4A_2)$$

$$(5s)^1(\underline{d\sigma})^1(\underline{d\pi})^1(d\bar{\pi})^1(d\delta)^2(d\bar{\delta})^1 \quad (^4B_2)$$

$$(5s)^1(\underline{d\sigma})^1(\underline{d\pi})^1(d\bar{\pi})^1(d\delta)^1(d\bar{\delta})^2 \quad (^4B_1)$$

Bringing up the CH_2 in the *yz* plane, we can form a double bond involving 4dσ and 4dπ orbitals for the last three ($^4A_2$, $^4B_2$, and $^4B_1$), and we can form a double bond involving 5s and 4dπ for the last three and the first (also $^4B_1$). Thus we expect three nearly degenerate, doubly bonded quartet states (symmetries $^4A_2$, $^4B_2$, and $^4B_1$) to arise from binding Ru^+ (s^1d^6) to CH_2 ($^3B_1$). The σ bond is allowed to be either s- or d-like on the metal.

In addition to the promotional energy ($d^7 \rightarrow s^1d^6$), we must also consider the loss of intraatomic exchange interactions for s^1d^6 Ru^+ in order to fully assess the energetics of complexation. Assuming pure dσ and pure dπ orbitals are utilized on the metal, forming

(24) Brookhart, M.; Tucker, J. R.; Flood, T. C.; Jensen, J. *J. Am. Chem. Soc.* **1980**, *102*, 1203.

(25) Our calculations at the HF level lead to $E_p(^4F \rightarrow {}^4D)$ = 28.4 kcal/mol, while the experimental E_p = 25.1 kcal/mol averaged over angular momentum states (E_p = promotional energy). Moore, C. E. *Atomic Energy Levels*; NSRDS-NBS-35, 1971, Vol. 3, p 25.

Table IV. Comparison of Related State Splittings in $RuCH_2^+$ and Ru^+[a]

	$RuCH_2^+$		corresponding Ru^+ states				
			hole config				
state	total energy, hartrees	excitation energy, kcal/mol				$H(i,i)$, hartrees	excitation energy, kcal/mol
$^4B_1$	−4476.163 98	+9.6	σ	π^*	δ	−4437.172 29	0.0
$^4B_2$	−4476.164 13	+9.5	σ	π^*	$\bar{\delta}$	−4437.172 29	+0.0
$^4A_2$	−4476.164 19	+9.4	σ	δ	$\bar{\delta}$	−4437.172 29	+0.0
$^2B_2$	−4476.147 38	+20.0	σ	π	π^*	−4437.139 59	+20.6
$^2A_1$	−4476.177 31	+1.2	σ	π	$\bar{\delta}$	−4437.172 29	+0.0
$^2A_2$	−4476.179 23	0.0	σ	π	δ	−4437.172 29	0.0

[a] These $RuCH_2^+$ results are based on calculations at the GVB(2/4)-RCI level. All quartet states were calculated by using the optimum geometry for $^4A_2$ $RuCH_2^+$, while all doublet-state calculations utilized the optimum geometry for $^2A_2$ $RuCH_2^+$. Ru^+ results are taken from the CI described in Table I, footnote *c*. More accurate $^4A_2$–$^2A_2$ energy splittings are reported in Table V.

a double bond leads to a differential loss of exchange energy of $\Delta K = 1\,K_{sd} + 2.5K_{dd}$. The average s–d exchange interaction in Ru^+ is $K_{sd} = 7.5$ kcal/mol and the average $K_{dd} = 15$ kcal/mol, leading to a loss of 45.0 kcal/mol upon forming a double bond. Adding this loss to the promotional energy of 28.4 kcal/mol results in a weakening of the double bond by 73.4 kcal/mol! This suggests that such a state would be high above the ground state.

Repeating the analysis for a double bond comprised of a 5sσ orbital and a 4dπ_{xz} orbital on Ru^+, we find that formation of a double bond to triplet CH_2 leads to a differential exchange energy loss of $\Delta K = 2K_{sd} + 1.5\,K_{dd} = 37.5$ kcal/mol. Adding the promotional energy yields an inherent weakening of the Ru–C double bond of 65.9 kcal/mol. Thus, if this quartet state is formed at all, we would expect a *weak* $Ru^+{=}CH_2$ bond in which the σ bond involves primarily the 5s orbital on Ru^+.

Summarizing, the formation of covalent bonds to s^1d^6 Ru^+ leads to highly excited states for $Ru{=}CH_2^+$. However, all is not lost: there is yet another possibly favorable manner to form a quartet state. We now consider binding singlet CH_2 to d^7Ru^+. The questions which must be answered for this new case include what sort of bonding is possible, what the costs are concerning promotional and exchange energies, and how these quartet states are related (by symmetry) to our previous constructs.

The bond of singlet CH_2 (**11**, with its doubly occupied sp orbital (σ) in the molecular plane and empty pπ_x orbital perpendicular to the molecular plane) and Ru^+ involves a σ-donor bond from CH_2 to Ru^+ and a possible dπ–pπ "back-bond" from Ru^+ to CH_2. The situation here is slightly more complicated than the usual concept of σ-donor/π-acceptor bonding in which the σ lone pair of the ligand is thought to donate into an empty dσ orbital on the metal, while the metal dπ lone pair delocalizes or "back-bonds" into the empty CH_2 pπ orbital. The complication is that d^7 Ru^+ wishes to be high-spin; the cost in energy to force Ru^+ to have an empty dσ orbital is $2K_{dd} = 30$ kcal/mol. Thus, it is less favorable to force d^7 Ru^+ into its low-spin configuration than to promote d^7 Ru^+ to s^1d^6 Ru^+. However, promoting Ru^+ does not alleviate the problem, since now the singly occupied 5s orbital is in the σ space, inhibiting σ donation. In addition, high-spin s^1d^6 Ru^+ (^6D) (with all d orbitals occupied) is favored over intermediate-spin s^1d^6 Ru^+ (with a dσ hole) by $1K_{sd} + 3K_{dd} = 52.5$ kcal/mol. Thus, forcing Ru^+ to have an empty σ orbital is unfavorable by at least 30 kcal/mol. (Furthermore, the $RuCH_2^+$ states formed from such Ru^+ configurations with singlet CH_2 lead to doublet states, whereas we seek quartet states.)

The question now is whether singlet CH_2 can form a good bond to a state with an occupied dσ orbital. Perhaps by mixing in the s^1d^6 excited state, Ru^+ can form a singly occupied 5s–4d$_{z^2}$ hybrid σ orbital which is localized away from the Ru–C bonding area, leaving negligible electron density in the molecular sigma system and thus allowing σ donation from CH_2 ($^1A_1$) into the "vacant" σ space of Ru^+, as shown below. If so, we expect the favorable

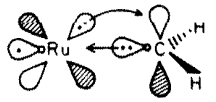

state to have a doubly occupied dπ_{xz} orbital (to allow dπ–pπ back-bonding) and a singly occupied dσ_{z^2} orbital (to allow s–d hybridzation out the back of the complex so as not to interfere with the σ-donor bond). This leads to three plausible (high-spin) Ru^+ configurations (degenerate for the free ion),

$$(sd\sigma)^1(d\pi)^2(d\pi^*)^2(d\delta)^1(d\bar{\delta})^1 \quad (^4A_2)$$

$$(sd\sigma)^1(d\pi)^2(d\pi^*)^1(d\delta)^2(d\bar{\delta})^1 \quad (^4B_2)$$

$$(sd\sigma)^1(d\pi)^2(d\pi^*)^1(d\delta)^1(d\bar{\delta})^2 \quad (^4B_1)$$

(where the symmetries are for $RuCH_2^+$). These (degenerate) quartet states predicted for Ru^+ (d^7) forming a σ-donor/π-acceptor bond to singlet CH_2 have the same symmetries as for Ru^+ (s^1d^6), forming two covalent bonds to CH_2 $^3(B_1)$! Hence, by calculating the $^4A_2$, $^4B_2$, and $^4B_1$ wave functions for $RuCH_2^+$, we will determine which mode of bonding (donor–acceptor vs. covalent) is preferred.

Of course we can in fact predict a priori which bonding mode is preferred by comparing the promotional and exchange costs for both systems. For covalent bonding we found a total destabilization of 65.9 kcal/mol for forming σ and π bonds utilizing the Ru^+ 5s and 4d$_{xz}$ orbitals. For donor–acceptor bonding, the mixing of some s^1d^6 character into ground-state d^7 Ru^+ will cost no more than the s^1d^6–d^7 promotional energy of 28.4 kcal/mol, and the promotion of CH_2 from triplet to singlet costs 9 kcal/mol,[5] for a total promotional energy of ≤38 kcal/mol. Since no covalent bonds have been formed with Ru^+, we *retain all intraatomic exchange stabilization* on Ru^+. Thus, donor–acceptor bonding is predicted to be more favorable than covalent bonding by 66 − 38 ≥ 28 kcal/mol for the quartet states. This simplistic analysis does not address the probable differences in intrinsic bond stengths of covalent vs. donor–acceptor bonds, as well as the cost of orthogonalizing the singly occupied sdσ orbital away from the donor σ bond. However, with such a large bias toward donor–acceptor bonding due to the retention of exchange terms on Ru^+, we expect that donor–acceptor bonding will be the preferred mode of bonding for the quartet state. The question of where this donor–acceptor state lies relative to the ground state will depend on the two factors neglected in the above analysis: (i) the intrinsic strength of a σ-donor/π-acceptor bond relative to the intrinsic strength of a covalent double bond and (ii) the magnitude of the repulsive interaction in the three-electron σ system.

B. The Quartet State Spectrum for $RuCH_2^+$. From the results in Table IV, we find that the quartet states ($^4A_2$, $^4B_1$, and $^4B_2$) of $RuCH_2^+$ are indeed degenerate, as predicted. In addition, we see that they are not far above the $^2A_2$ ground state of $RuCH_2^+$. The $^4A_2$–$^2A_2$ state splitting as a function of electron correlation is given in Table V, where we see that further inclusion of electron correlation yields a $^4A_2$–$^2A_2$ state splitting of 12.9 kcal/mol. This small state splitting is suggestive of at least two conclusions. First, $RuCH_2^+$ ($^4A_2$) makes use of the least destabilizing mode of bonding available, namely, donor–acceptor bonding, in which little promotional energy and no exchange energy are lost on Ru^+ and only 9 kcal/mol promotional energy is lost by exciting CH_2 from $^3B_1$ to $^1A_1$. Thus we propose that the bonding in $RuCH_2^+$ ($^4A_2$) consists of a σ-donor–π-acceptor bond between CH_2 ($^1A_1$) and Ru^+ (d^7), a description consistent with its molecular properties (vide infra).

The second major conclusion to be drawn from the $^4A_2$ – $^2A_2$ state splitting of 12.9 kcal/mol is that donor/acceptor bond en-

Table V. $^4A_2$–$^2A_2$ Excitation Energies (kcal/mol) for $RuCH_2^+$ [a]

calculational level	no. of config/SEF [b] $^4A_2$	$^2A_2$	$\Delta E(^4A_2–^2A_2)$
HF	1/1	1/1	−20.1
GVB-PP	4/4	8/8	4.9
GVB-RCI	9/34	27/76	15.0
$RCI_\sigma{}^*D_\sigma + RCI_\sigma{}^*D_\pi$	1065/5886	2875/11 486	8.9
$(GVB\text{-}RCI^*S)_{val,Ru}$	442/2570	816/4150	13.0
$(GVB\text{-}RCI^*S)_{val,full}$	637/4962	1365/8156	14.2
$RCI_\sigma{}^*D_\sigma + RCI_\sigma{}^*D_\pi + (RCI^*S)_{val,full}$	1579/10042	3895/18 102	12.9

[a] Optimum geometries at the GVB(2/4)-RCI level were used for $^2A_2$ and $^4A_2$ $RuCH_2^+$. For excitation energy calculations, the GVB(3/6) level is used for $^2A_2$, while the GVB(2/4) level is used for $^4A_2$, to maintain an "orbitally balanced" description (see section V). [b] No. of config./SEF is the no. of spatial configurations/number of spin eigenfunctions.

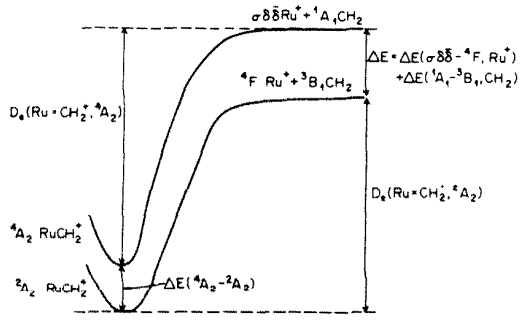

Figure 4. Qualitative potential curves for $^4A_2$ and $^2A_2$ $RuCH_2^+$. Our theoretical values are D_e ($^2A_2$) = 68.0 kcal/mol, D_e ($^4A_2$) = 65.9 kcal/mol, and $\Delta E(^4A_2–^2A_2)$ = 12.9 kcal/mol. Our best estimate for D_e^{exact} ($^2A_2$) = 73.2 kcal/mol.

ergies can be comparable in strength to covalent bond energies. That is, $D_e(Ru{=}CH_2^+, {}^4A_2)$ can be predicted from the cycle illustrated in Figure 4 to be

$$D_e(Ru{=}CH_2^+, {}^4A_2) = D_e(Ru{=}CH_2^+, {}^2A_2) + \Delta E(\sigma\delta\bar{\delta} - {}^4F, Ru^+) + \Delta E({}^1A_1–{}^3B_1, CH_2) - \Delta E({}^4A_2–{}^2A_2)$$

This calculation is explicitly for the *diabatic* bond strength of CH_2 complexes, however, this would be the *adiabatic* bond strength for metal–carbene systems in which the free carbene has a singlet ground state (e.g., CF_2, C(OR)R, etc.) and thus is the relevant quantity to use for comparison with currently observed metal carbenes. The above equation leads to a predicted $D_e(Ru{=}CH_2^+, {}^4A_2)$ of 68.0 + 6.9 + 7.3 − 12.9 = 69.3 kcal/mol,[26] which is of the same magnitude as the covalent $Ru{=}CH_2$ bond strength. Calculated bond energies for $RuCH_2^+$ ($^4A_2$) dissociating to d^7 Ru^+ and CH_2 ($^1A_1$) are discussed in detail in section III.D.

C. Properties of the Low-Lying Excited State, $RuCH_2^+$ ($^4A_2$). It is important to emphasize that it suffices to examine any one of the three degenerate quartet states of $RuCH_2^+$, since they all exhibit the same properties, with the only physical difference between them being the configuration of electrons in nonbonding d orbitals. We choose to examine the $^4A_2$ state simply because it is of the same spatial symmetry as the ground $^2A_2$ state, which allows a more direct comparison of the two spin states.

The optimum geometry for the $RuCH_2^+$ ($^4A_2$) excited state (at the GVB(2/4)-RCI level) is shown in Figure 2b. The Ru–C bond length of 1.93 Å is 0.05 Å longer than the Ru–C bond length in the covalently bonded $^2A_2$ ground state, suggestive of a change in the bonding scheme for the $^4A_2$ state. Supporting evidence that this bond lengthening is due to a change from a covalent (triplet) alkylidene structure to a donor–acceptor (singlet) carbene structure is given by examination of the following experimental example.

(26) At the highest level of calculation used herein, we find $\Delta E(\sigma\delta\bar{\delta} - {}^4F, Ru^+)$ = 6.9 kcal/mol and $\Delta E({}^1A_1–{}^3B_1, CH_2)$ = 7.3 kcal/mol.

Roper and co-workers[27] have synthesized and obtained X-ray structures of

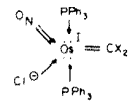

where X = H or F. We would expect the CH_2 case to have an Os=C covalent double bond and thus to have nucleophilic, alkylidene character. However, the triplet state of CF_2 is about 46 kcal/mol above the singlet,[28] and hence we would expect electrophilic, carbene character in the latter. The $Os{=}CH_2$ bond length is 1.92 Å,[27a] whereas the $Os{=}CF_2$ bond length is 1.967 Å,[27b] a bond lengthening of 0.047 Å upon going from an alkylidene to a carbene bonding structure. This is in excellent agreement with the bond lengthening of 0.05 Å we find for Ru, lending credence to the assignment of $RuCH_2^+$ ($^4A_2$) as a singlet carbene bound to Ru^+.

Further indication of the singlet nature of the CH_2 ligand in $RuCH_2^+$ ($^4A_2$) is seen in the decrease in HCH bond angle from 121.7° to 113.0°, going from $^2A_2$ to $^4A_2$ $RuCH_2^+$. (The HCH bond angle in CH_2 ($^1A_1$) is 103°, whereas in CH_2 ($^3B_1$) the angle is 133°.[28]) The C–H bond lengths in $RuCH_2^+$ ($^4A_2$) remain the same as in the ground state, R(C–H) = 1.08 Å.

The GVB orbitals for the Ru–C σ and π bonds as well as for the nonbonding singly occupied σ orbital ($5s/4dz^2$) are shown in Figure 5a. Notice the difference in character of the σ and π bonds of Figure 5a from the covalent σ and π bonds of Figure 1a. The σ bond for $RuCH_2^+$ ($^4A_2$) resembles an "in/out" correlated σ pair of CH_2 ($^1A_1$) (1.27 electrons are localized on CH_2, while the other 0.73 electron is donated to Ru^+), as can be seen by comparing Figure 5a with Figure 5b, which depicts the two σ donor electrons of free CH_2 ($^1A_1$). By comparing Figures 5a and 1a we see also that the π bond for $RuCH_2^+$ ($^4A_2$) has much more character on Ru^+ (1.58 electrons) than does the $RuCH_2^+$ ($^2A_2$) π bond (1.16 electrons). This is consistent with the description of the $RuCH_2^+$ ($^4A_2$) π bond as an "in/out" correlated Ru^+ $d\pi$-orbital back-bonding into the empty CH_2 $p\pi$ orbital. By comparing the π bond of Figure 5a with the "in/out" correlated two-electron $d\pi$ pair in free Ru^+ depicted in Figure 5c, we see that the π bond of $RuCH_2^+$ ($^4A_2$) is indeed a $d\pi$ pair on Ru^+ delocalizing onto CH_2. Thus, the σ- and π-bonding orbitals of $RuCH_2^+$ ($^4A_2$) indicate σ-donor/π-acceptor bonding as in **12**. However, recall that high-spin d^7 Ru^+ does not have an empty $d\sigma$ orbital ready for σ donating by CH_2 ($^1A_1$). The discussion in section III.A proposes that if the singly occupied $4d\sigma$ orbital can mix in 5s character to rehybridize away from the Ru–C bond, Ru^+ may simulate an empty $d\sigma$ orbital by having no electron density in the σ region between Ru and C. The bottom plot of Figure 5a shows this singly occupied Ru^+ orbital, which indeed rehybridizes out the back of the molecule to minimize repulsions with the Ru–C bonds. The Mulliken population of this singly occupied valence orbital show the predicted mixing of the s^1d^6 excited state into the d^7 ground state in order to effect this rehybridization (28% 5s, 72% 4d).

This donor–acceptor bonding mode is further indicated by the Mulliken populations of each bond pair. For the σ bond, there is considerable charge tranfer (0.73 electron) from the CH_2 σ orbital to Ru^+, indicating a strong donor–acceptor interaction. This is complemented in the π system with a "π back-bond" which transfers 0.43 electron back to the CH_2 $p\pi_x$ orbital. Because Ru^+ is positively charged, the back-donation from Ru^+ is not as effective as it is expected to be in a saturated, neutral $Ru{=}CH_2$ complex, resulting in a slight overall charge transfer to the metal.

The σ and π bond overlaps in $RuCH_2^+$ ($^4A_2$) provide further verification of our bonding description. In marked contrast to

(27) (a) Hill, A. F.; Roper, W. R.; Waters, J. M.; Wright, A. H. *J. Am. Chem. Soc.* **1983**, *105*, 5939. (b) Roper, W. R. "Group VIII Transition Metal Complexes of CH_2, CF_2, and Other Simple Carbenes". Presented at a Seminar at the California Institute of Technology, July 23, 1984.

(28) Bauschlicher, C. W., Jr.; Schaefer, H. F., III; Bagus, P. S. *J. Am. Chem. Soc.* **1977**, *99*, 7106.

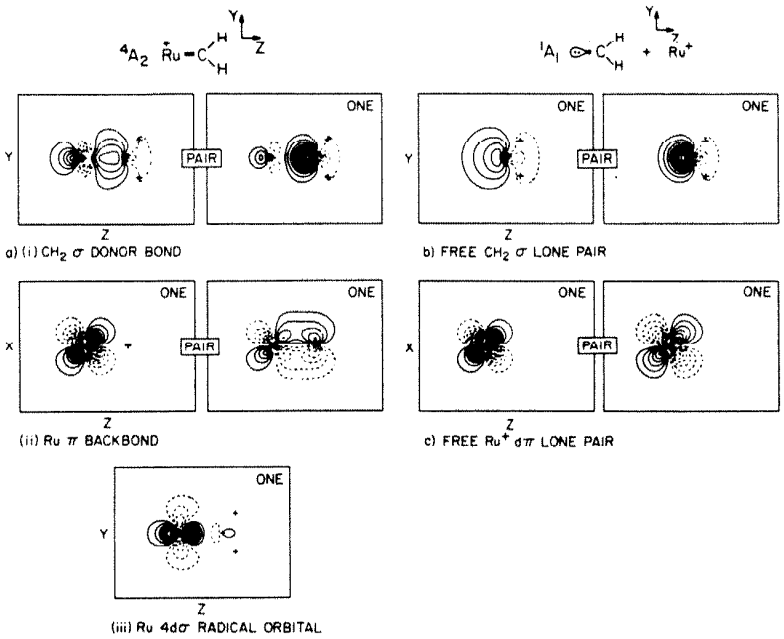

Figure 5. GVB orbitals for (a) the carbene complex $RuCH_2^+$ ($^4A_2$): (i) Ru–C σ bond, (ii) Ru–C π bond, and (iii) Ru sd_{z^2} singly occupied; (b) CH_2 ($^1A_1$) $sp\sigma$ pair; (c) Ru^+ (d^7) $d\pi_{xz}$ pair.

the covalently bonded state of $RuCH_2^+$ ($^2A_2$), which has σ and π bond overlaps of 0.68 and 0.48, respectively, the $RuCH_2^+$ ($^4A_2$) σ and π overlaps are significantly larger, 0.83 for the σ bond and 0.69 for the π bond. This fact by itself is suggestive of bonds more localized over only one center, since an "in/out" correlated σ lone pair on CH_2 ($^1A_1$) has an overlap of 0.85 and a 4d lone pair on Ru^+ has an overlap of 0.93. Thus, the "σ bond" has almost the same overlap as the σ orbital in free CH_2 ($^1A_1$), highly suggestive of a localized σ pair on CH_2 along with a localized π pair on Ru^+ in $RuCH_2^+$ ($^4A_2$).

Even stronger evidence for this donor–acceptor model is provided from the behavior of the overlaps as we stretch the Ru–C bonds, shown in Figure 3. As discussed in section II.B, the overlaps in covalent bonds are expected to decrease monotonically to zero at infinite separation. The overlaps of the Ru–C bond pairs for the $^4A_2$ state exhibit the opposite behavior. Here the overlaps increase as the bond is stretched, with the maximum values reached at the infinite limit [corresponding to the overlaps of the lone pairs in the fragments Ru^+ and CH_2 ($^1A_1$)]. This behavior is completely consistent with our formulation of two lone pairs which delocalize at R_e to form donor–acceptor bonds and relocalize as the bond is broken.

The vibrational frequencies of the $^4A_2$ state are shown in Table II, where we see that the C–H symmetric stretching and scissors bending frequencies are nearly identical with those for the ground state. The only true indicator of a bonding change comes from the much smaller Ru–CH_2 stretching frequency (464 cm^{-1} for the $^4A_2$ state vs. 665 cm^{-1} for the $^2A_2$ ground state). This suggests a looser, if not a weaker, bond (as discussed in the next section), as might be expected intuitively from the nature of a donor–acceptor interaction (not a strong function of distance).

To summarize, all of the properties of the low-lying $^4A_2$ excited state of $RuCH_2^+$ are in sharp contrast to those of the ground-state structure, with the orbitals, geometry, Mulliken populations, $d\pi$–$p\pi$ back-bonding interactions, orbital-overlap behavior, and vibrational frequencies completely supporting the description of the bonding in $RuCH_2^+$ ($^4A_2$) as a σ-donor/π-acceptor situation.

D. Bond Energies for $RuCH_2^+$ ($^4A_2$). Donor–acceptor bond strengths for transition-metal systems have presently been limited experimentally to M–CO bond dissociation enthalpies (which range from 37 to 46 kcal/mol[29]). Previous theoretical calculations for transition-metal carbenes have been limited to low-level calculations (HF) using experimental geometries with an MBS (minimum basis set) description of $(CO)_4Cr{=}CH(OH)$ and $(CO)_4Fe{=}CH(OH)$.[30] HF calculations are expected to describe covalent bonds poorly, but may provide acceptable descriptions of donor–acceptor bonds in which the doubly occupied donor orbitals have high overlap. Nakatsuji et al.[30] found bond energies for the above two hydroxycarbenes of 44.4 kcal/mol for the Cr system and 36.8 kcal/mol for the Fe complex at the HF level.

The present bond-energy calculations as a function of electron correlation are given in Table VI. We have chosen here to calculate the (nonadiabatic) bond energy for $RuCH_2^+$ ($^4A_2$) dissociating to the $\sigma\delta\bar{\delta}$ state of Ru^+ (see Table I) and CH_2 ($^1A_1$). Since Ru^+ and CH_2 adopt these electronic states in the complex, dissociation with geometrical relaxation (i.e., to the equilibrium geometry of singlet CH_2) but no electronic relaxation (e.g., from $\sigma\delta\bar{\delta}$ to ^6F Ru^+) will yield an intrinsic (promotionless) donor–acceptor bond energy. For comparison with experimental metal–carbene bond energies, this (promotionless) bond energy is the important one, since the metal–carbene bond energy in a saturated metal complex is very likely to involve no electronic relaxation of fragments. For instance, the bond energy in a Fischer carbene complex, e.g., $(CO)_5W{=}C(OMe)Me$, involves the reaction

$$(CO)_5W{=}C(OMe)Me \rightarrow (CO)_5W + :C(OMe)Me.$$

Since both $W(CO)_5$ (low-spin d^6) and C(OMe)Me are expected to be singlets, no electronic relaxation is expected to occur (i.e., $W(CO)_5$ is not likely to relax to a triplet or change its low-spin d^6 orbital occupation). Thus, the bond energy measured for $W{=}C(OMe)Me$ will involve no promotional energies in the fragments and will therefore be an intrinsic donor–acceptor bond energy. To make a comparison with bond energies for saturated systems, we report electronically nonadiabatic bond energies that (due to the lack of electronic relaxation) correspond to intrinsic

(29) Lewis, K. E.; Golden, D. M.; Smith, G. P. *J. Am. Chem. Soc.* **1984**, *106*, 3905.

(30) Nakatsuji, H.; Ushio, J.; Han, S.; Yonezawa, T. *J. Am. Chem. Soc.* **1983**, *105*, 426.

Table VI. Bond Dissociation Energies (kcal/mol) for the Carbene State of $RuCH_2^+$ ($^4A_2$)

calculational level	$D_e(Ru{=}C)^a$	$RuCH_2^+(^4A_2)$ total energy, hartrees[b]	fragment total energies, hartrees	
			Ru^+	$CH_2(^1A_1)$
HF	41.3	−4476.120 76	−4437.173 31	−38.881 64
		(1/1)	(1/1)	(1/1)
GVB(2/4)-PP	42.5	−4476.147 40	−4437.177 41	−38.902 31
		(4/4)	(2/2)	(2/2)
RCI(2/4)	52.9	−4476.164 19	−4437.177 63	−38.902 31
		(9/34)	(3/6)	(2/2)
$RCI_\sigma{}^*D_\sigma + RCI_\pi{}^*D_\pi$	61.7	−4476.194 80	−4437.179 09	−38.917 42
		(1065/5886)	(51/123)	(53/53)
$(RCI(2/4)^*S)_{val,Ru}$	64.0	−4476.200 96	4437.196 59	38.902 31
		(442/2570)	(57/168)	(2/2)
$(RCI(2/4)^*S)_{val,full}$	70.3[c]	−4476.216 96	−4437.196 59	−38.908 31
		(637/4962)	(57/168)	(37/40)
$RCI_\sigma{}^*D_\sigma + RCI_\pi{}^*D_\pi$ + $(RCI(2/4)^*S)_{val,full}$	65.8	−4476.226 38	−4437.198 08	−38.923 42
		(1579/10 042)	(101/269)	(79/82)

[a] Bond energy (D_e) dissociating to the $\sigma\bar{\sigma}\delta\bar{\delta}$ state of Ru^+ (see Table I) and the $^1A_1$ state of CH_2 [using the optimal GVB(1/2) description for CH_2 (σ/π correlated σ pair)]. [b] The number of spatial configurations/number of spin eigenfunctions are given in parentheses. [c] We believe this value is an overestimate; see discussion in section III.D.

donor–acceptor bond energies.[31,32]

Examination of Table VI reveals that the σ-donor/π-acceptor bond strength (65.8 kcal/mol) in $RuCH_2^+$ ($^4A_2$) is predicted to be nearly as strong as the covalent $D_e(Ru{=}CH_2, {}^2A_2)$ of 68.0 kcal/mol. However, the covalent D_e predicted for a saturated $Ru{=}CH_2$ complex (68.0 + 15 = 83.0 kcal/mol) is larger than the donor–acceptor saturated complex D_e, because the donor–acceptor bond energy as defined does not depend on the degree of saturation (since the metal and CH_2 fragments do not electronically reorganize or change spin couplings).

The progression of bond energies as a function of electron correlation in Table VI indicates a convergence to $D_e(Ru^+{=}CH_2, {}^4A_2)$ = 65.8 kcal/mol as our best value for the donor–acceptor intrinsic bond energy of Ru^+ bonding to any carbene (CF_2, CR(OR), CCl_2, etc.). We consider the value of 70.3 kcal/mol for $RCI^*S_{val,full}$ to be an overestimate of the true bond energy due to an artifact of this particular calculation for donor–acceptor bonding configurations. This level leads to an imbalanced inclusion of electron correlation in which the complex is correlated to a greater degree than the fragments. This is consistent with the large $^1A_1$–$^3B_1$ splitting for CH_2 at this level (16.7 kcal/mol rather than 13.2 kcal/mol as found for other levels), leading to a bond energy which is too high. For covalent bonds, however, this calculational level leads to a fairly balanced description at R_e and $R = \infty$, as borne out in the convergence of covalent bond energies for both $Cr{=}CH_2^+$ ($^4B_1$)[1] and $Ru{=}CH_2^+$ ($^2A_2$).

In summary, we predict donor–acceptor bonds of typical (singlet) carbenes such as $:CF_2$, $:CCl_2$, :CR(OR), etc., to Ru to have bond strengths of ~65 kcal/mol, while covalent Ru=C alkylidene bond strengths in saturated complexes are expected to be ~85 kcal/mol. In addition, since $Ru{=}CF_2$ and other ruthenium–carbene complexes have been synthesized by Roper and co-workers,[33] while terminal $Ru{-}CR_2$ alkylidene systems are as yet unknown (although postulated by Knox,[34] Werner,[22] and Shapley[35]), this suggests a lower bound on an Ru–C single (covalent) bond energy of ≥43 kcal/mol. We conclude this simply by observing that many μ-CR_2–Ru complexes exist, with two Ru–C σ bonds in preference to terminal $Ru{=}CR_2$ complexes.[34-36] Thus, two Ru–C σ bonds are more stable than one 86 kcal/mol Ru=C terminal double bond, which implies D(Ru–C) ≥ 43 kcal/mol.

IV. Summary

Ab initio electronic structure calculations on $RuCH_2^+$ reveal the following conclusions:

i) $RuCH_2^+$ has a $^2A_2$ ground state with two covalent Ru–C bonds, resulting in a bond energy of 68.0 kcal/mol for the unsaturated metal–CH_2 complex.

ii) From the present calculations and others on more saturated complexes, a means of estimating covalent-bond energies for fully saturated metal complexes from bond energies known for unsaturated complexes is put forth, with the result

$$D_{saturated} = D_{intrinsic} - \tfrac{1}{2}K_{dd} = D_{unsaturated} + \Delta K_{lost} - \tfrac{1}{2}K_{dd}$$

In particular, this yields an estimate for an $Ru{=}CH_2$ bond energy in a coordinatively saturated complex of 83.0 kcal/mol, which agrees well with a model saturated $Ru{=}CH_2$ complex (with a calculated bond energy of 85.5 kcal/mol).

iii) A low-lying (12.9 kcal/mol up) triply degenerate excited state exists ($^4A_2$, $^4B_1$, $^4B_2$) with an Ru–C double bond of completely different structure from the ground state; namely, the excited state exhibits metal–carbene σ-donor/π-acceptor bonding. This donor/acceptor bond is worth 65.8 kcal/mol for both unsaturated and saturated complexes.

iv) A lower bound of 43 kcal/mol is obtained for the covalent Ru–C single bond strength in a saturated complex.

V. Calculational Details

A. Basis Sets. All atoms were described with all-electron valence double-ζ (VDZ) basis sets. In addition, one set of d-polarization functions (ζ_d = 0.69) was added to the C basis set.[1] A Four's level VDZ basis set was used for Ru with the (16s13p7d/6s5p3d) contraction, shown in Table VII.[37] The Ru and Ru^+ state splittings obtained with this basis set contraction at the HF level are given in Table VIII. The standard Huzinaga–Dunning VDZ bases were used for C (9s5p/3s2p) and H (4s/2s).[38]

B. Geometry Optimizations. All geometrical parameters of the $^4A_2$ and $^2A_2$ states of $RuCH_2^+$ were optimized at the GVB-RCI(2/4) level (generalized valence bond–restricted configuration interaction). The GVB–RCI(2/4) description allows a full CI within each pair of natural orbitals (NO's, two natural orbitals

(31) No exchange energy is lost upon bonding in these complexes. Thus the intrinsic bond energy for a donor–acceptor bond is "promotionless" instead of "exchangeless".

(32) To calculate an adiabatic bond energy for $RuCH_2^+$ ($^4A_2$) merely involves $D_e(^2A_2) - \Delta E(^4A_2{-}{}^2A_2)$ (see Figure 4).

(33) (a) Clark, G. R.; Hoskins, S. V.; Jones, T. C.; Roper, W. R. *J. Chem. Soc., Chem. Commun.* **1983**, *719*. (b) Clark, G. R.; Hoskins, S. V.; Roper, W. R. *J. Organomet. Chem.* **1982**, *234*, C9. (c) Hoskins, S. V.; Pauptit, R. A.; Roper, W. R.; Waters, J. M. *Ibid.* **1984**, *269*, C55. (d) Roper, W. R.; Wright, A. H. *Ibid.* **1982**, *233*, C59.

(34) Dyke, A. F.; Knox, S. A. R.; Mead, K. A.; Woodward, P. *J. Chem. Soc., Chem. Commun.* **1981**, *861*; and paper immediately following.

(35) Holmgren, J. S.; Shapley, J. R. *Organometallics* **1985**, *4*, 793.

(36) Lin, Y. C.; Wreford, S. S. *J. Am. Chem. Soc.* **1983**, *105*, 1679.

(37) Rappé, A. K.; Goddard, W. A., III, to be published. This basis set was optimized for the d^n configuration of the metal as laid out in Rappé, A. K.; Smedley, T. A.; Goddard, W. A., III *J. Phys. Chem.* **1981**, *85*, 2607. The 4d VDZ basis optimized in this manner is an adequate description of the valence space.

(38) (a) Huzinaga, S. *J. Chem. Phys.* **1965**, *42*, 1293; (b) Dunning, T. H., Jr. *Ibid.* **1970**, *53*, 2823.

Table VII. The Ru Basis Set (ref. 37): Cartesian Gaussian Functions with Exponents (α_i) and Contraction Coefficients (C_i)

function type	α_i	C_i
s	24 880.0	0.020 012 7
s	3752.0	0.138 963 2
s	848.1	0.483 648 9
s	231.5	0.495 299 4
s	331.7	−0.133 155 3
s	60.94	0.421 658 9
s	24.01	0.672 702 2
s	35.38	−0.305 490 3
s	9.385	0.405 974 8
s	3.929	0.772 575 7
s	5.203	−0.404 813 7
s	1.285	0.690 500 8
s	0.4972	0.549 049 6
s	0.7682	−0.531 792 9
s	0.097 77	1.155 993 9
s	0.034 88	1.000 000 0
p	1212.0	0.028 609 8
p	284.7	0.187 631 2
p	88.76	0.522 389 5
p	30.9	0.427 965 0
p	20.06	0.063 944 4
p	11.68	0.500 460 4
p	4.489	0.512 729 1
p	9.097	−0.040 937 7
p	1.534	0.631 716 1
p	0.5207	0.462 236 4
p	0.8698	−0.202 323 5
p	0.1292	1.056 815 3
p	0.040 51	1.000 000 0
d	136.9	0.044 666 1
d	39.33	0.241 463 0
d	13.58	0.527 230 7
d	4.817	0.411 489 5
d	3.873	0.195 821 5
d	1.281	0.870 102 4
d	0.3139	1.000 000 0

Table VIII. Hartree–Fock State Splittings for Ru and Ru^+ [a]

state	total energy, hartrees	excitation energies (eV) this work	NHF[b]	expt[c]
Ru(^{5}F)	−4437.301 90	2.61	1.69	1.09
Ru(^{5}D)	−4437.350 33	1.30	1.42	0.87
Ru(^{5}F)	−4437.397 94	0.00	0.00	0.00
Ru^+(^{6}D)	−4437.138 66	7.06	7.10	8.46
Ru^+(^{4}F)	−4437.183 54	5.83	5.92	7.37

[a] Results are for the Ru basis set contraction shown in Table VII. [b] Numerical Hartree–Fock results from ref 39. [c] Experimental data from ref 25, averaged over angular momentum states.

per M–C bond) describing the Ru–C σ and π bonds, resulting in nine spatial configurations. For $^2A_2$ $RuCH_2^+$ these nine configurations have 17 associated spin eigenfunctions (SEF's), while for the $^4A_2$ state the nine configurations have 34 associated SEF's. The physical interpretation of the RCI wave function involves inclusion of interpair correlation and high-spin coupling on the metal atom.

C. Bond Energies. 1. $RuCH_2^+$ ($^2A_2$): Covalent Bonds. Bond energies for $RuCH_2^+$ were calculated at the Hartree–Fock (HF), generalized valence bond with perfect-pairing restriction [GVB](2/4)-PP, GVB-RCI(2/4), $RCI_\sigma{}^*D_\sigma + RCI_\pi{}^*D_\pi$, RCI-(2/4)$^*S_{val,Ru}$, RCI(2/4)$^*S_{val,full}$, and $[(RCI_\sigma{}^*D_\sigma + RCI_\pi{}^*D_\pi) + RCI(2/4)^*S_{val,full}]$ levels. The bond energies given in Table III are for the adiabatic dissociation pathway

$$Ru{=}CH_2^+ (^2A_2) \rightarrow Ru^+ (^4F) + CH_2 (^3B_1)$$

Calculations at large R(Ru–C) distances (e.g., 5.00 Å) indicate that the $\sigma^1\pi^1\delta^1$ configuration of Ru^+ at R_e smoothly converts into ^4F Ru^+ at large R, giving rise to a truly adiabatic potential energy pathway. We now define the higher order CI's listed above:

1) $RCI_\sigma{}^*D_\sigma + RCI_\sigma{}^*D_\pi$: From the nine RCI configurations for $RuCH_2^+$ ($^2A_2$), we allow all single and double excitations to all virtuals from one Ru–C bond pair at a time, while maintaining the RCI description in the other bond pair. In particular, while the Ru–C π bond is described at the RCI level, we simultaneously allow all single and double excitations from the Ru–C σ bond pair and then vice versa, hence the name $RCI_\sigma{}^*D_\sigma + RCI_\sigma{}^*D_\pi$. This CI dissociates properly to HF fragments. (Note that all single and double excitations from both bond pairs simultaneously do not dissociate to a cleanly described limit.)

2) RCI(2/4)$^*S_{val,Ru}$: From the nine RCI configurations we allow all single excitations from the valence Ru orbitals and the Ru–C bonds to all virtuals. This CI is also dissociation-consistent, dissociating to $HF^*S_{valence}$ for Ru^+ and HF for CH_2.

3) RCI(2/4)$^*S_{val,full}$: From the nine RCI configurations we allow all single excitations from all valence orbitals (including CH pairs) to all virtuals. We allow this CI to dissociate to HF^*S_{val} fragments, although this is overcorrelating the dissociated limit and thus will give too small a bond energy. Test calculations indicate this leads to at most a 0.2 kcal/mol underestimate of the bond energy.

4) $[(RCI_\sigma{}^*D_\sigma + RCI_\sigma{}^*D_\pi) + (RCI(2/4)^*S_{val,full})]$: This CI is merely the superposition of the previous two CI's listed above, dissociating to HF^*S_{val} fragments, with the same slight overcorrelation problem resulting in ~0.2 kcal/mol too low a bond energy.

2. $RuCH_2^+$ ($^4A_2$): Donor/Acceptor Bonds. The bond energies for the $^4A_2$ state were calculated at the same levels as the ground state; thus the CI's are identical at R_e for both states. However, this state dissociates to CH_2 ($^1A_1$) and $\sigma\delta\bar{\delta}$ Ru^+ (since the electronic configuration of Ru^+ at R_e does not change upon stretching this type of bond). We allow the CH_2 σ pair to use a π-correlating orbital as a second natural orbital, since this is the optimum GVB(1/2) description of singlet CH_2. Note that at R_e, π back-bonding from Ru^+ forces the dominant correlating orbital to be σ^* for the CH_2 σ pair. Thus the dominant correlation changes from R_e to $R = \infty$, and we allow the optimal correlation for both limits. We now discuss the CI's in terms of their dissociation limits, since these limits are different from the covalent case.

1) $RCI_\sigma{}^*D_\sigma + RCI_\sigma{}^*D_\pi$: This CI dissociates to a GVB(1/2)-correlated Ru^+ dπ pair and a GVB(1/2)-correlated CH_2 σ pair, from each of which all single and double excitations to all virtuals are allowed. This overcorrelates the infinite limit (since simultaneous double excitations on both fragments result in overall quadruples), leading to a lower bound on the bond energy. However, test calculations at $R = \infty$ show these quadruple excitations do not contribute to the bond energy. Thus the bond energy is effectively dissociation-consistent.

2) RCI(2/4)$^*S_{val,Ru}$: This wave function dissociates properly to RCI(1/2)$^*S_{val}$ on Ru^+ and RCI(1/2) on CH_2 ($^1A_1$).

3) RCI(2/4)$^*S_{val,full}$: This wave function dissociates to RCI-(1/2)$^*S_{val}$ Ru^+ and RCI(1/2)$^*S_{val}$ CH_2, which provides a lower bound on the bond energy, but in practice, test calculations suggest this overcorrelation is negligible (<0.02 kcal/mol).

4) $[(RCI_\sigma{}^*D_\sigma + RCI_\sigma{}^*D_\pi) + (RCI(2/4)^*S_{val,full})]$: The superposition of the two CI's above dissociates to $[(RCI(1/2)^*D_\pi) + (RCI(1/2)^*S_{val})]$ Ru^+ and $[(RCI(1/2)^*D_\sigma) + (RCI(1/2)^*S_{val})]$ CH_2. Again this wave function involves higher order excitations at $R = \infty$ that are not included at R_e, resulting in a net overcorrelation of 0.3 kcal/mol from test calculations.

5) "Test Calculations": We superimpose the two fragment wave functions without allowing any electronic interaction between them, to simulate the infinitely far apart fragments. Then we perform the same CI's for this superimposed fragment wave function as were calculated at R_e. This provides a check on potential overcorrelation problems. The largest difference between the "test" bond energies and the bond energies calculated from the (sometimes overcorrelated) fragments was 0.3 kcal/mol.

D. State Splitings. The $^4A_2$ state at the GVB(2/4)-PP level has a valence space consisting of two C–H doubly occupied orbitals

(39) Martin, R. L.; Hay, P. J. *J. Chem. Phys.* **1981**, *75*, 4539.

(treated as HF MO's), two Ru–C bond pairs each with a second NO for a total of four Ru–C bonding orbitals, one doubly occupied nonbonding $d\pi_{yz}$ orbital, and three singly occupied $d\sigma$, $d\delta$, $d\bar{\delta}$ orbitals, for a total of 10 orbitals in the valence space. At the GVB(2/4)-PP level for $RuCH_2^+$ ($^2A_2$), there is the same orbital space for CH_2 and for the Ru–C bonds, but there are two doubly occupied nonbonding d orbitals ($d\pi_{yz}$ and $d\delta_{x^2-y^2}$) plus one singly occupied $d\delta_{xy}$ orbital, for a total of nine valence orbitals. To treat the states of $RuCH_2^+$ with the same degree of flexibility, we must have the same number of valence orbitals in the SCF calculations. Therefore, for $RuCH_2^+$ ($^2A_2$) we correlate the $d\delta_{x^2-y^2}$ with a second natural orbital (leading to a GVB(3/6)-PP description) in order to compare with the GVB(2/4)-PP description of $RuCH_2^+$ ($^4A_2$).

Acknowledgment. This work was supported by the Shell Development Company, Houston, TX, and the National Science Foundation (Grant No. DMR82-15650).

Registry No. $Ru{=}CH_2^+$, 101031-94-1.

Chapter 2.C. The text of this section is an Article coauthored with William A. Goddard III which appeared in the *Journal of the American Chemical Society.*

Reprinted from the Journal of the American Chemical Society, 1986, *108*, 4746.

Bonding in Transition-Metal Methylene Complexes. 3. Comparison of Cr and Ru Carbenes; Prediction of Stable $L_nM(CXY)$ Systems[1]

Emily A. Carter[†] and William A. Goddard III*

Contribution No. 7336 from the Arthur Amos Noyes Laboratory of Chemical Physics, California Institute of Technology, Pasadena, California 91125. *Received December 9, 1985*

Abstract: The electronic structure of the lowest carbene state of a representative early-transition-metal complex, $CrCH_2^+$ ($^6A_1$ symmetry), has been examined by using ab initio techniques. Its properties reveal a complex with a single σ-donor bond from singlet CH_2 to high-spin (d^5) Cr^+ and no π-back-bond, resulting in a low bond energy (38.7 kcal/mol) and a large carbene–alkylidene state splitting (18.8 kcal/mol). These results are contrasted with Ru carbene (possessing both σ- and π-donor bonds) properties [D_e(Ru=C) = 65.8 kcal/mol and ΔE(carbene–alkylidene) = 12.9 kcal/mol]. This comparison enables, for the first time, a separation of σ-donor bond strengths from π-donor bond strengths. Finally, using only valence electron properties, we are able to predict stabilities of $L_nM(CXY)$ complexes (e.g., how substituents at carbon affect the preference for bridging vs. terminal CXY), discussing trends for the entire transition series.

I. Introduction

Terminal metal carbene and alkylidene complexes are ubiquitous throughout the transition elements.[2] The nomenclatural distinction between "carbene" and "alkylidene" represents a fundamental difference in reactivity.[3] Metal carbene complexes usually behave as electrophiles, with typical reactions including Lewis base adduct formation via attack at the carbon center[4]

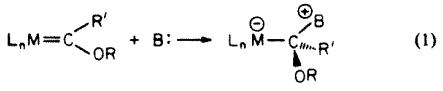

(1)

and stoichiometric cyclopropanation of olefins[5]

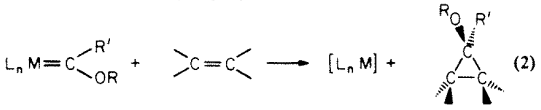

(2)

On the other hand, metal alkylidene complexes are nucleophilic, undergoing Wittig-type alkylations,[6,7] Lewis acid adduct formation,[8]

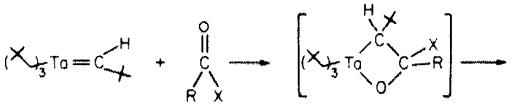

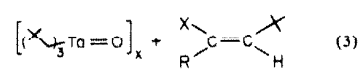

(3)

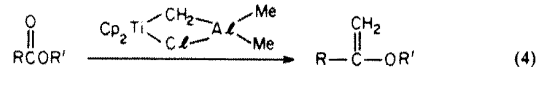

(4)

[†] National Science Foundation Predoctoral Fellow, 1982–1985.

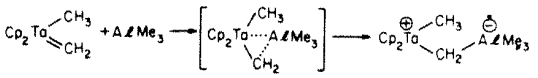

(5)

and olefin metathesis.[9]

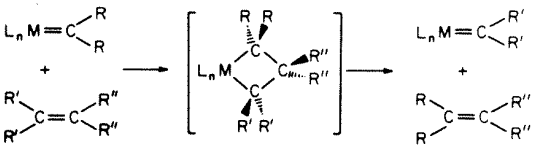

(6)

These two greatly different modes of reactivity reflect a dra-

(1) (a) Paper 1 of this series: Carter, E. A.; Goddard, W. A., III *J. Phys. Chem.* **1984**, *88*, 1485. (b) Paper 2: Carter, E. A.; Goddard, W. A., III *J. Am. Chem. Soc.* **1986**, *108*, 2180. (c) Earlier work on high-valent alkylidene complexes includes: Rappé, A. K.; Goddard W. A., III *J. Am. Chem. Soc.* **1982**, *104*, 297; **1982**, *104*, 448; **1980**, *102*, 5114.

(2) For a comprehensive review, see: Dötz, K. H.; Fischer, H.; Hofmann, P.; Kreissl, F. R.; Schubert, U.; Weiss, K. *Transition Metal Carbene Complexes*; Verlag Chemie: Deerfield Beach, FL, 1984.

(3) Collman, J. P.; Hegedus, L. S. *Principles and Applications of Organotransition Metal Chemistry*; University Science Books: Mill Valley, Ca, 1980; Chapter 3.

(4) (a) Wong, W.-K.; Tam, W.; Gladysz, J. A. *J. Am. Chem. Soc.* **1979**, *101*, 5440. (b) Yu, Y. S.; Angelici, R. J. *Organometallics* **1983**, *2*, 1018. (c) Kuo, G.-H.; Helquist, P.; Kerber, R. C. *Ibid.* **1984**, *3*, 806.

(5) (a) Fischer, E. O.; Dötz, K. H. *Chem. Ber.* **1970**, *103*, 1273. (b) Dötz, K. H.; Fischer, E. O. *Ibid.* **1972**, *105*, 1356. (c) Stevens, A. E.; Beauchamp, J. L. *J. Am. Chem. Soc.* **1979**, *101*, 6449. (d) Brandt, S.; Helquist, P. J. *Ibid.* **1979**, *101*, 6473. (e) Brookhart, M.; Humphrey, M. B.; Kratzer, H. J.; Nelson, G. O. *Ibid.* **1980**, *102*, 7803. (f) Brookhart, M.; Tucker, J. R.; Husk, G. R. *Ibid.* **1981**, *103*, 979. (g) Casey, C. P.; Vollendorf, N. W.; Haller, K. J. *Ibid.* **1984**, *106*, 3754. (h) Casey, C. P.; Shusterman, A. J. *Organometallics* **1985**, *4*, 736. (i) Brookhart, M.; Studabaker, W. B.; Husk, G. R. *Ibid.* **1985**, *4*, 943. (j) Casey, C. P.; Miles, W. H.; Tukada, H. *J. Am. Chem. Soc.* **1985**, *107*, 2924. (k) Stevens, A. E.; Beauchamp, J. L. *Ibid.* **1978**, *100*, 2584.

(6) Schrock, R. R. *J. Am. Chem. Soc.* **1976**, *98*, 5399.

(7) (a) Tebbe, F. N.; Parshall, G. W.; Reddy, G. S. *J. Am. Chem. Soc.* **1978**, *100*, 3611. (b) Pine, S. H.; Zahler, R.; Evans, D. A.; Grubbs, R. H. *Ibid.* **1980**, *102*, 3270.

(8) Schrock, R. R. *J. Am. Chem. Soc.* **1975**, *97*, 6577.

0002-7863/86/1508-4746$01.50/0

matic difference in the metal–carbon bonding. Conventional design prescriptions call for "low-valent" metal fragments [e.g., $W(CO)_5$] for carbenes and "high-valent" metal moieties (e.g., Cp_2TaR) for alkylidenes in order to maximize stability of the resultant complex. In addition, the presence of a heteroatom on the CXY ligand is known to stabilize carbenes, while alkyl or hydrogen groups are thought to stabilize alkylidene ligands. The combination of a "low-valent" metal fragment with a C(OR)R′ [or $C(NR_2)R'$, etc.] carbene ligand translates into the now-familiar σ-donor bond from the carbene and donor π-back-bond from the "low-valent" metal. As we have shown previously,[1] "high-valent" metals interacting with an alkyl-only-substituted CXY ligand results in an olefinic-type, *covalent* double bond.

These contrasting bonding structures (donor/acceptor for carbene and covalent for alkylidene) are given physical justification via the *valence bond view* of metal–carbene (alkylidene) bonds.

1. Metal Carbenes. The "low-valent" metal fragment is generally surrounded by closed-shell ligands (such as CO or PR_3). In this environment, the metal atom is forced into a *low-spin, d^n electronic state* to minimize Pauli repulsions (orthogonality) with ligand lone pairs. A low-spin, d^n metal atom has doubly occupied d-orbitals set up for π-back-bonding to a carbene (or other ancillary ligands with low-lying acceptor orbitals). The carbene fragment will be a σ-donor as desired, if the *singlet* state of the CXY ligand is the ground state. The purpose of the electronegative heteroatom linkage (e.g., X = OR, NR_2, F, Cl) is to stabilize the singlet (σ^2) state of CXY. The two lowest states of CXY are triplet ($\sigma\pi$) and singlet (σ^2).

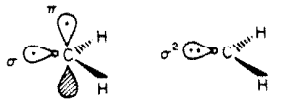

1 **2**

If either X or Y is electron-withdrawing, then the C–X and C–Y bonds will involve mostly p-character on carbon [lower ionization potential (IP) than s]. In addition, the pπ lone pairs on X (or Y) will donate electron density into the C pπ-orbital. Both of these effects work to destabilize the carbon pπ and to stabilize the carbon σ-orbital, resulting in a σ^2 (singlet) ground state. Thus the requirement of "low-valent" metals and "heterocarbenes" for the formation of stable metal–carbenes physically means that doubly occupied metal d-orbitals and a ground-state singlet carbene will result in σ-donor/π-acceptor metal–carbene bonds.

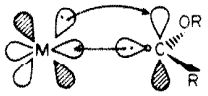

2. Metal Alkylidenes. The "high-valent" metal fragment generally has a ligand set consisting of one or more ionic ligands (Cp, Cl, O(*t*-Bu), etc.) and alkyl ligands (odd-electron fragments). The ionic ligands prefer to bond to s-electrons (lower IP than d-electrons) on the metal, while the alkyl ligands require singly occupied metal d-orbitals to bond to. As described previously,[1b] the ionic ligands effectively oxidize the metal (e.g., $Cp_2Ta^{II}CH_3$, where "II" indicates Ta is oxidized by two units in essentially transferring the metal s-electrons to the Cp ligands), leaving a d^n metal ion. Without closed-shell ligands to force a low-spin metal configuration, the metal adopts the lowest energy configuration available, namely, the highest spin state allowed within the five d-orbitals. This metal atom (ion) is now set up to covalently bond to any ligand with unpaired electrons, be it alkyls or the triplet ($\sigma\pi$) state of the CXY ligand (two unpaired electrons). A triplet ground state of CXY will be favored when X and Y are not heteroatoms but rather are alkyl (or hydrogen) substituents. Hence, the statement that "high-valent" metal fragments and alkylcarbenes are necessary for stable metal–alkylidene formation translates physically to high-spin metal atoms (in which the s-electrons are utilized in ionic bonds), forming covalent metal–carbon double bonds to ground-state triplet CRR′ ligands.

In this paper we compare and contrast properties of simple metal carbenes, $(M{=}CH_2)^+$, involving an early, first-row transition metal (Cr) and a late, second-row transition metal (Ru). In particular, their relative stabilities and M–C bond strengths are examined, with the emphasis on how early transition metals are expected to differ from late transition metals in these unsaturated systems. Section II discusses new results of ab initio calculations on the lowest carbene state of $CrCH_2^+$ ($^6A_1$), while section III briefly reviews previous work on the lowest carbene state of $RuCH_2^+$ ($^4A_2$). The comparison of Cr and Ru carbenes allows, for the first time, donor/acceptor bond strengths to be separated into σ-donor and π-donor single bond strengths (section IV). Finally, using information gleaned from our present and previous work on both carbenes and alkylidenes, we predict stabilities of $L_nM(CXY)$ complexes, discussing trends for the entire transition series (section V). Section VI contains a summary, while section VII supplies calculational details.

II. Carbene Bonding for $CrCH_2^+$: The $^6A_1$ State

The lowest (two) states of $CrCH_2^+$ are formed by combining the ground state of CH_2 ($^3B_1$; see **1**) with the ground state of Cr^+ (^6S). This combination of spins ($S = 1$ with $S = {}^5/_2$) leads to three possible values of total spin: $S = {}^3/_2$ (with a double bond), $S = {}^5/_2$ (with a single bond), and $S = {}^7/_2$ (with no bond). Thus the ground state of $CrCH_2^+$ is $^4B_1$ with covalent σ and π bonds [leading to a total bond energy of $D_e(Cr{=}C,{}^4B_1) = 44.0$ kcal/mol (49.6 kcal/mol at the fully correlated limit)], leaving three unpaired d-electrons on the Cr center. The first excited state is $^6B_1$ with a covalent σ bond, leaving four unpaired d-electrons on Cr and the unpaired C pπ-electron all coupled high spin to yield $S = {}^5/_2$ [leading to a total bond energy of $D_e(Cr{-}C,{}^6B_1) = 25.0$ kcal/mol (30.6 kcal/mol at the fully correlated limit)]. The other combination of ground-state Cr^+ and CH_2 where $S = {}^7/_2$ has no bond, leading to a repulsive potential curve.[1a]

A simple-minded interpretation of the above results would suggest a σ bond worth 30.6 kcal/mol and a π bond of 19 kcal/mol, both seemingly quite weak. In fact, the *inter*atomic spin pairing essential to covalent bond formation necessarily leads to a reduction in the *intra*atomic high-spin coupling favored for each atom (Hund's rule), so that the observed bond is much weaker than it would be if no extra unpaired orbitals were available. Indeed, the spin pairing for the double bond of $^4B_1$ leads to a loss of 57.8 kcal/mol in exchange energy. Thus, the *intrinsic* strength of the double bond is 107.4 kcal/mol even though the observed bond strength is only 49.6 kcal/mol. On the other hand, for the $^6B_1$ excited state, with only one covalent bond, the loss of intraatomic exchange is only 33 kcal/mol, so that the *intrinsic* strength of the σ bond is calculated to be 63.6 kcal/mol.

This enormous loss of intraatomic exchange energy engendered by covalent bond formation to ground state CH_2 (methylidene bonding) leads to the possibility that states involving the singlet excited state (**2**) of CH_2 might be low-lying. In this case, the bonding is dominated by overlap of the σ pair of CH_2 with Cr^+

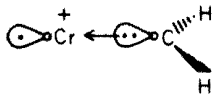

(9) (a) Lee, I. B.; Ott, K. C.; Grubbs, R. H. *J. Am. Chem. Soc.* **1982**, *104*, 7491. (b) Wengrovius, I. A.; Schrock, R. R.; Churchill, M. R.; Missert, I. R.; Youngs, W. I. *Ibid.* **1980**, *102*, 4515. (c) Gilet, M.; Mortreux, A.; Folest, J.-C.; Petit, F. *Ibid.* **1983**, *105*, 3876. (d) Kress, J.; Osborn, J. A. *Ibid.* **1983**, *105*, 6346. (e) Katz, T. J.; Han, C.-C. *Organometallics* **1982**, *1*, 1093. (f) Howard, T. R.; Lee, J. B.; Grubbs, R. H. *J. Am. Chem. Soc.* **1980**, *102*, 6876.

Table I. $CrCH_2^+$ State Splittings[a] and Bond Dissociation Energies (kcal/mol) for the Carbene State of $CrCH_2^+$ ($^6A_1$)

calculational level	D_e(Cr–C)	$^6A_1$ $CrCH_2^+$ total energy, hartree[b]	$\Delta E(^6A_1-^6B_1)$[c]	$\Delta E(^6A_1-^4B_1)$[c]
HF	35.8	−1080.942 26 (1/1)	−16.8	−70.5
GVB(1/2)PP	29.9	−1080.953 62 (2/2)	−12.6	−23.9
GVB-RCI(2)	30.3	−1080.954 27 (3/8)	−11.3	+1.2
RCI(2)*D_σ	33.4	−1080.974 03 (184/759)		
RCI(2)*S_{val}	36.7	−1080.970 48 (211/1184)	+0.8	+18.8
RCI(2)*D_σ + RCI(2)*S_{val}	38.7	−1080.988 48 (366/1799)		

[a] The $^6B_1$ and $^4B_1$ $CrCH_2^+$ total energies are reported in ref 1a. [b] Total energy in hartrees where 1 hartree = 27.2116 eV = 627.5096 kcal/mol. The values in parentheses are (number of spatial configurations)/(number of spin eigenfunctions). [c] The values shown are at the correlationally consistent calculational levels for $^6A_1$, $^6B_1$, and $^4B_1$, as discussed in section VII.

with no loss of intraatomic exchange energy.[10] This requires the promotion of CH_2 from $^3B_1$ to $^1A_1$, at an energy cost of 9 kcal/mol,[11] followed by complexation via a σ-donor bond to ground-state, high-spin d^5 Cr^+ to form the $^6A_1$ (carbene) state. In contrast to the $^4B_1$ and $^6B_1$ states, no exchange terms are lost on Cr^+, since all five high-spin paired electrons on Cr^+ remain high spin. Since the C pπ-orbital is empty, this donor–acceptor state could be stabilized by dπ–pπ-back-bonding. However, we find that with only one electron in the Cr dπ-orbital, this back-bonding provides negligible stabilization.

The $^6A_1$(carbene)–$^4B_1$(methylidene) state splitting as a function of electron correlation is given in Table I. The three GVB calculational levels used here to obtain $\Delta E(^6A_1-^4B_1)$ are correlationally and orbitally consistent. That is, at each level, the same number of orbitals and the same types of excitations are included for both the $^6A_1$ and the $^4B_1$ states. [Other levels of calculation examined in evaluating the Cr–C bond energies (see Table I) do not treat these two states comparably and are not used in considering the state splitting.]

From Table I, we see that the state splitting is sensitive to the level of electron correlation. Notice the complete about-face of $\Delta E(^6A_1-^4B_1)$ upon relaxation of the perfect pairing restriction, as in the GVB-RCI wavefunction. At the best level of calculation, we find that the carbene state ($^6A_1$) lies 18.8 kcal/mol above the methylidene ($^4B_1$) ground state. Thus, $^6A_1$ is only 0.8 kcal/mol above the $^6B_1$ state at the same level of theory.[12]

Supporting evidence for the presence of *two* excited states of $CrCH_2^+$ lying about 18–19 kcal/mol above the ground state comes from recent experiments by Beauchamp and co-workers[13] in which translational energy loss spectroscopy was used to search for excited states of $CrCH_2^+$ formed from Cr^+ colliding with CH_4 in a molecular beam. The spectrum indicates a wide weak peak consistent with at least one spin-forbidden transition at an energy of ~24 kcal/mol less than the elastic peak. Given an energy resolution of 0.2 eV (~5 kcal/mol), our theoretical values for the sextet–quartet energy gaps are within the experimental error. The relative energies of the three low-lying states of $CrCH_2^+$ as well as their respective limits at infinite R(Cr–C) are displayed in Figure 1.

The optimum geometry of the single-bonded donor/acceptor $^6A_1$ state [see Figure 2a: R(Cr–C) = 2.32 Å, θ(HCH) = 108.9°] differs considerably from the covalently single-bonded $^6B_1$ state [R(Cr–C,$^6B_1$) = 2.07 Å, θ(HCH,$^6B_1$) = 118.3°], with a Cr–C bond length longer by 0.3 Å and a much smaller HCH bond angle, close to that in free singlet CH_2 (102°).[14,15a] The long Cr–C bond

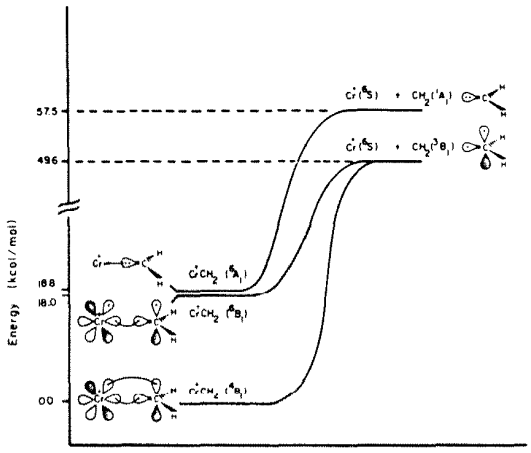

Figure 1. Electronic state correlation diagram for the three lowest states of $CrCH_2^+$: $^6A_1$, $^6B_1$, and $^4B_1$. The two B_1 states dissociate to ^6S Cr^+ and $^3B_1$ CH_2, while the $^6A_1$ state dissociates to ^6S Cr^+ and $^1A_1$ CH_2.

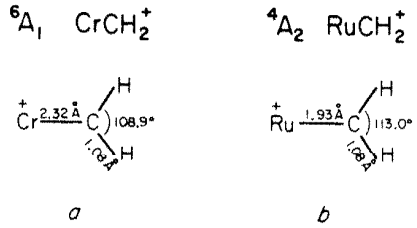

Figure 2. Optimum geometries for the carbene states of (a) $CrCH_2^+$ ($^6A_1$) and (b) $RuCH_2^+$ ($^4A_2$).

length and the small HCH angle are expected for a σ-donor bond with negligible dπ–pπ-back-bonding from the singly occupied Cr dπ_{yy}-orbital, a description that is also indicated by Mulliken populations and orbital plots.

The orbitals for the carbene state, $CrCH_2^+$ ($^6A_1$), are shown in Figure 3a where we see a Cr–C σ bond consisting of an "in/out" correlated CH_2 σ pair (1.75 electrons on CH_2 with a high bond orbital overlap of 0.83) delocalizing toward the Cr cation (0.25 electrons transferred to Cr^+), similar in character to the σ-donor bond for the carbene state of $RuCH_2^+$ ($^4A_2$), as shown in Figure 3b.i. In contrast to the carbene state of $RuCH_2^+$, however, we find no dπ–pπ-back-bonding for the carbene state of $CrCH_2^+$. Thus, Mulliken populations indicate only 0.01 electrons donated from the Cr 3dπ_{xz} singly occupied orbital to the CH_2 2p_x orbital, and even at the much shorter Cr–C bond length of 2.07 Å, the dπ delocalization is only 0.05 electrons for $CrCH_2^+$ ($^6A_1$). In contrast, for the carbene state of $RuCH_2^+$, there are 0.43 electrons transferred from the Ru dπ *doubly occupied* orbital into the C

(10) An exception to this statement exists if enough ligand donor bonds force the orbital into a lower spin state in order to allow more effective σ-donation. In this case, the spin coupling is indeed affected, and some exchange energy is lost. For $CrCH_2^+$, however, we need not force the metal into a lower spin state.

(11) Leopold, D. F.; Murray, K. K.; Lineberger, W. C. *J. Chem. Phys.* **1984**, *81*, 1048.

(12) There is no correlationally consistent calculational analogue for $^6A_1$ $CrCH_2^+$ at the RCI*S_{val} + [RCI,*D_σ + RCI,*D_σ] calculational level (see ref 1a) which yielded $\Delta E(^6B_1-^4B_1)$ = 19.0 kcal/mol. Therefore we compare excitation energies at the highest *correlation-consistent* level, RCI*$S_{valence}$.

(13) Hanratty, M. A.; Carter, E. A.; Beauchamp, J. L.; Goddard III, W. A.; Illies, A. J.; Bowers, M. T. *Chem. Phys. Lett.* **1986**, *123*, 239.

(14) The C–H bond length is insensitive to mode of bonding and was kept fixed at 1.078 Å. θ(H–C–H) for $^1A_1$ CH_2: Harding, L. B.; Goddard, W. A., III *Chem. Phys. Lett.* **1978**, *55*, 217.

(15) (a) Bauschlicher, C. W., Jr.; Schaefer, H. F., III; Bagus, P. S. *J. Am. Chem. Soc.* **1977**, *99*, 7106. (b) Carter, E. A.; Goddard, W. A., III *J. Phys. Chem.* **1986**, *90*, 998. (c) Koda, S. *Ibid.* **1979**, *83*, 2065.

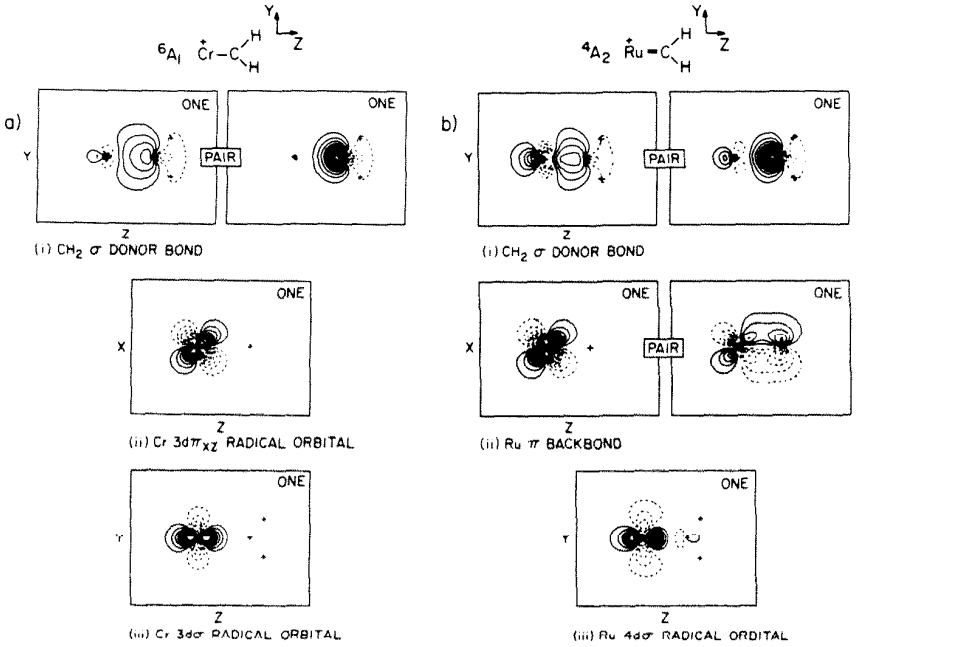

Figure 3. GVB one-electron orbitals for the carbene states of (a) $CrCH_2^+$ ($^6A_1$) [(i) CH_2 σ-donor bond; (ii) Cr 3dπ singly occupied orbital; (iii) Cr 3dσ singly occupied orbital] and (b) $RuCH_2^+$ ($^4A_2$) [(i) CH_2 σ donor bond; (ii) Ru 4dπ-back-bond; (iii) Ru 4dσ singly occupied orbital]. Contours represent regions of constant amplitude ranging from −0.5 to +0.5 au, with increments of 0.05 au.

pπ empty orbital. The difference here is that electron repulsion in the doubly occupied orbital drives one of the electrons toward delocalization, as displayed in Figure 3b.ii. The lack of a π-back-bond leads to the long bond length of 2.32 Å for Cr—carbene and a low Cr—C carbene stretching frequency of 295 cm^{-1} (in comparison with 464 cm^{-1} calculated for the doubly bonded Ru=C carbene stretching frequency).

Another difference between the bonding in the carbene states of $CrCH_2^+$ and $RuCH_2^+$ is in the behavior of the singly occupied metal dσ-orbital, illustrated in Figure 3, parts a.iii and b.iii. For $CrCH_2^+$ ($^6A_1$), there is minimal s–d mixing into the singly occupied Cr σ orbital (94.1% 3d/5.9% 4s) because the small size of the 3d orbital and the long Cr–C bond length leads to little overlap between Cr 3d and the σ pair of CH_2. However, for $RuCH_2^+$, the M–C bond length is much shorter (due to the π-back-bond) and the Ru^+ 4d-orbital is larger (than Cr 3d), leading to a high overlap with the σ pair of CH_2. As a result, the singly occupied Ru dσ-orbital must s–d hybridize in order to minimize repulsive interactions (the singly occupied Ru σ orbital has hybridization 72% 4d/28% 5s).

Summarizing, the various properties (orbital character, long bond length, small vibrational frequency, and small HCH bond angle) in the carbene state $CrCH_2^+$ ($^6A_1$) reveals a bond involving a donor σ bond from singlet CH_2 to high-spin, d^5 Cr^+. The carbene–methylidene state splitting ($^6A_1$–$^4B_1$) is larger for $CrCH_2^+$ than for $RuCH_2^+$ ($^4A_2$–$^2A_2$) due to the presence of a strong two-electron π back-bond for $RuCH_2^+$ ($^4A_2$) and no π-back-bond for $CrCH_2^+$ ($^6A_1$).

III. Carbene State of $RuCH_2^+$: A Review

Ground-state high-spin d^7 Ru^+ forms three degenerate carbene states upon interaction with CH_2 ($^1A_1$). These three states ($^4A_2$, $^4B_1$, $^4B_2$) arise from degenerate valence electron configurations[1b] on Ru^+ and differ in the CH_2 complex only in the occupation of the nonbonding d-orbitals. They have equivalent bonding descriptions, namely, that of a Ru–C σ-donor/π-acceptor double bond. We chose to examine the $^4A_2$ state in the most detail simply because it has the same spatial symmetry as the ground ($^2A_2$) alkylidene-type state.

The basic properties of the carbene state of $RuCH_2^+$ necessary for comparison with the Cr carbene system include the following:

(i) The carbene–alkylidene energy gap [$\Delta E(^4A_2$–$^2A_2)$] is 12.9 kcal/mol at our highest level of theory.

(ii) The optimum geometry at the GVB-RCI(2/4) level is shown in Figure 2b. The carbene nature of the Ru–C bond is supported by the small H–C–H bond angle of 113° and the longer bond length of 1.93 Å compared to that of the ground alkylidene state (1.88 Å).

(iii) The GVB orbitals are shown in Figure 3b where we see that the CH_2 forms a σ-donor bond to Ru^+ involving an in/out correlated, sp^2 hybrid, while the Ru^+ forms a π-back-bond to the empty C pπ orbital. The charge transfers involved in these bonds work in concert (electroneutrality principle). Thus, the Mulliken populations indicate 0.73 electrons donated to Ru^+ in the σ system and 0.43 electrons donated to CH_2 in the π system.

(iv) The Ru=C carbene bond energy is 65.8 kcal/mol in $RuCH_2^+$ ($^4A_2$), probably a representative bond energy for coordinatively saturated, low-valent metal heterocarbenes. The Ru=C alkylidene bond energy in $RuCH_2^+$ ($^2A_2$) is 68.0 kcal/mol, leading to an estimated[1b] Ru=CH_2 alkylidene bond energy of 83.0 kcal/mol for a saturated complex. (An independent, direct calculation on a model saturated system yielded 84.7 kcal/mol for the Ru=C bond strength.)

IV. Partitioning the Double Bond into σ- and π-Donor Contributions

π-Back-bonding is commonly involved in discussions of organometallic metal–ligand bonds having ligands with low-lying π-acceptor orbitals (e.g., CO or CXY, where X and/or Y are electron-withdrawing groups), but little quantative evidence is available regarding the strength of and the extent of charge transfer in such a π-bond. The only experimental verification of this effect is obtained indirectly by assigning changes in bond lengths and vibrational frequencies in M–CO or M=CXY systems as due to changes in the extent of back-bonding. The calculation outlined below provides a direct, quantitative assessment regarding such bonds.

From two independent analyses, we find that the π-back-bond in the carbene state of $RuCH_2^+$ ($^4A_2$) is worth approximately 30 kcal/mol. Our approach was to eliminate the C $2p_x$ and $3d_{xz}$ basis functions from the SCF calculation, thereby prohibiting π-back-bonding since no delocalization into the C π system is possible. This results in an energy destabilization of 27.4 kcal/mol. Since the rest of the bonding remains the same as in the full basis set description, this destabilization may be attributed solely to the strength of the π-back-bond. A more reliable estimate for the π bond strength is obtained by examining the $^4B_1$ carbene state of $RuCH_2^+$ which differs from $RuCH_2^+$ ($^4A_2$) only in having reversed $d\pi_{xz}$- and $d\delta_{xy}$-orbital occupations [$(d\pi_{xz})^1(d\delta_{xy})^2$ for $^4B_1$ and $(d\pi_{xz})^2(d\delta_{xy})^1$ for $^4A_2$].[16] Since the $^4B_1$ state has a negligible one-electron π-back-bond (vide infra) and the $^4A_2$ state has a significant two-electron π-back-bond, the $^4B_1$–$^4A_2$ splitting is a measure of the Ru–C π bond strength. This energy splitting was calculated to be 31.5 kcal/mol, in close agreement with the other π bond strength estimate of 27.4 kcal/mol. Thus, we conclude that the strength of the π-back-bond for $RuCH_2^+$ ($^4A_2$) is ~30 kcal/mol. For neutral, less electrophilic metal centers, we expect π-back-bond strengths to be higher than 30 kcal/mol, since delocalization into the carbene π system should be more facile.

Both the $RuCH_2^+$ ($^4B_1$) excited state with its singly occupied $d\pi$-orbital and the $CrCH_2^+$ ($^6A_1$) excited state (high-spin d^5 Cr^+) can only provide *one*-electron $d\pi$–$p\pi$-back-bonding to CH_2 ($^1A_1$). The extent of charge transfer is negligible in both cases, with 0.10 electrons transferred by Ru^+ and 0.01 electrons transferred by Cr^+. (We expect slightly more electron transfer for Ru^+ since 4d-orbitals are larger than 3d-orbitals and can thus delocalize more effectively.) Thus, for both first- and second-row transition-metal ions, the *one*-electron $d\pi$–$p\pi$-back-bond is negligible in comparison with a *two*-electron $d\pi$–$p\pi$-back-bond.

The bond energy of the $CrCH_2^+$ ($^6A_1$) is interesting because it provides quantitative determination of the strength of a single σ-donor bond, unlike the case of $RuCH_2^+$ ($^4A_2$), in which there is both a σ- and a π-donor bond, making it difficult to determine the energy partitioning in the Ru–C double bond. Table I contains an analysis of the Cr–C bond energy for $CrCH_2^+$ ($^6A_1$) as a function of electron correlation. [The Cr–C bond energy is for the symmetry-allowed process

$$(^6A_1)\ CrCH_2^+ \rightarrow (^6S)\ Cr^+ + (^1A_1)\ CH_2$$

yielding an intrinsic σ-donor bond strength.] At our highest calculational level, we find a bond energy of 38.7 kcal/mol. Hence, we estimate the strength of a C to Cr σ-donor bond with no π-back-bond to be worth ~39 kcal/mol.

Since the total bond energy for the carbene state of $RuCH_2^+$ ($^4A_2$) is $D_e = 65.8$ kcal/mol, then we estimate the σ-donor bond energy to be $D_e^\sigma = D_e - D_e^\pi = 65.8 - 31.5 = 34.3$ kcal/mol. This value is quite close to the value (39 kcal/mol) obtained for Cr–carbene. For systems with a singly occupied nonbonding $d\sigma$-orbital, we would expect the values for σ-donor bond strengths to *decrease* going from first row to second row due to the higher metal 4d/carbene σ overlap for the more diffuse 4d electrons. Our value of 30 kcal/mol for the two-electron π-back-bond of a second-row transition metal is probably a lower limit on the strength of such a bond in a neutral complex. However, the strength of such a two-electron π-back-bond for low-spin d^n first-row metals is probably less than 30 kcal/mol (due to the small radial extent of the 3d-orbitals).

V. Transition-Metal–Ligand Bonding Trends: Control of Reactivity

In the above sections, we found that, with proper choices of metal and ligands, one can obtain complexes in which the ground and excited states exhibit vastly different bonding character. Given the opportunity of added ligands to perturb the electronic state splittings at the metal center, we have the potential for designing complexes either with covalently bonded alkylidene ligands or with σ-donor/π-back-bonding carbene ligands depending upon the choice of metal and ligand environment.

The purpose of this section is to discuss how to use such valence bond ideas to control metal–ligand bond character, thus opening up the possibility for distinctive changes in chemical reactivity of organotransition-metal systems. Our premise is that control of the electronic configuration of the metal center—not merely oxidation state—is the key to controlling both the bond *type* and bond *strength* for a given metal–ligand system. For the sake of brevity we will illustrate such effects only for M–CXY systems, but the arguments expressed may be applied to any other metal-ligand system with overall covalent character.

First, we discuss how intraatomic exchange stabilization and promotional energies affect metal–orbital hybridization, bond character (covalent vs. donor/acceptor), and bond strengths in metal–carbon bonds. Second, we describe how ligand type affects the nature of the metal–carbon bond. Third, we conclude with a general prescription of how to bias the outcome in favor of alkylidene, carbene, or intermediate bonding in M–CXY complexes.

A. Metal Exchange and Promotional Effects on M–CXY Bonds. Due to the greater number and larger magnitude of favorable exchange interactions between valence electrons in a transition metal as compared with a main-group or nonmetal atom,[17] the loss of exchange energy upon forming covalent bonds with ligands (via spin pairing in the bonds) plays a much more significant role in determining bond properties for transition metals than for other atoms. If this exchange loss destabilization is large enough, promotion of the metal atom to an excited state may be favorable if it results in less exchange loss. These two effects are evidenced by changes in hybridization of metal bonding orbitals, bond character, and bond strength. Since these effects are most dramatic in bare metal systems, we will discuss only bare M–CXY systems.

1. Hybridization. Metal orbital hybridization in M–CXY bonds can be predicted qualitatively by comparing the relative metal destabilization upon bonding the ligand to an s- vs. a d-orbital. Valence s → p and d → p excitations for transition metals are sufficiently high in energy that valence p-orbitals make little contribution to bonding. Thus the hybridization changes are greatest in the M–C σ bond, with little d–p mixing in the π bond (>90% d). Therefore we will describe only hybridization effects in the σ bond.

For a ground-state metal atom or ion with an *occupied* valence s orbital (s^1d^{n-1} or s^2d^{n-2} state), the CXY covalent σ bond will have a large amount of s character in the metal-bonding orbital. This is due to spin pairing of the metal s-electron with the ligand electron in the bond, resulting in the loss of *only* s–d exchange terms (K_{sd}), each typically ~5 kcal/mol (10–15 kcal/mol smaller than d–d exchange terms). In cases where the metal has a choice between s and d, the s-orbital is preferred since it loses less exchange energy upon forming the metal–ligand bond. For example, binding Mn^+ (s^1d^5 ground state) to CH_2 ($^3B_1$) leads to a σ bond which has 87% s character.[18] This is due to the reluctance of Mn^+ to destroy the stabilization of the half-filled d-shell (i.e., a large loss in exchange energy).

If the metal has a d^n ground state, then to form a bond to a metal s-orbital will require the d → s promotional energy in addition to various s–d + d–d exchange losses ($E_p^{d\rightarrow s} + \Delta K_{sd+dd}$).[19] To decide whether bonding to an s orbital will occur, we must compare this sum with the d–d exchange loss incurred upon bonding to the d^n ground state (ΔK_{dd}). These relative energies will determine the dominant hybridization. In other words, for $E_p^{d\rightarrow s} + \Delta K_{sd+dd} > \Delta K_{dd}$, we expect >50% d-character in the M–C σ bond and vice versa. As the difference between these two values grows, so does the dominant orbital contribution to the metal σ-orbital.

(16) The corresponding Ru^+ occupations are degenerate, leading to no added promotional effects. See Table I in ref 1b.

(17) Typical values: K_{dd} ~ 15–20 kcal/mol and K_{sd} ~ 5–8 kcal/mol for transition metals; K_{pp} ~ 10 kcal/mol for non-transition metals.

(18) Brusich, M. J.; Goddard, W. A., III, unpublished results.

(19) $E_p^{d\rightarrow s}$ designates the $d^n \rightarrow s^1d^{n-1}$ promotional energy. ΔK_{sd+dd} refers to a loss of both s–d and d–d exchange terms when forming both σ and π bonds.

As an illustration of this competition, consider that the σ bond in $CrCH_2^+$ is 53% d/47% sp on the metal, arising from $E_p^{d\rightarrow s} + \Delta K_{sd+dd} - \Delta K_{dd} = 13.7$ kcal/mol.[1a] The difference in destabilization energy suggests that metal d-character should dominate. However, the large difference in the size of the 3d and 4s orbitals favors s-bonding, leading to rather balanced d vs. s character. The case of covalently bonded $RuCH_2^+$ ($^2A_1$) provides an example at the opposite extreme. Forming two covalent bonds to d^7 Ru^+ costs $1.5K_{dd} = 22.5$ kcal/mol, while forming one s bond and one d bond to s^1d^6 Ru^+ costs $E_p^{d\rightarrow s} + 2K_{sd} + 1.5K_{dd} = 65.9$ kcal/mol.[1b] Thus a dσ bond is favored over an sσ bond by 43.4 kcal/mol. This is borne out convincingly in the actual Ru–C σ-bond hybridization of 88% 4d/12% 5s character on the metal.

Thus we see that knowledge of the ground-state configuration of the metal, coupled with values for promotional and exchange energies, allows qualitative prediction of the hybridization in metal–ligand covalent σ bonds for all ranges of cases: mostly s character ($MnCH_2^+$), a 50/50 mixture of s and d ($CrCH_2^+$), and mostly d character ($RuCH_2^+$).

2. Bond Character. The same analysis also yields predictions about donor/acceptor vs. covalent bond character. Donor/acceptor bonds will be favored when the exchange and promotional destabilizations for forming covalent bonds are prohibitively large and when two-electron π-back-bonds are achievable. Covalent bonds will be favored when little promotional or exchange energy is lost upon bonding or when a π-back-bond is not possible (reducing the prospective donor bond order from two to one). A competition between covalent and donor/acceptor bonding will be expected when the exchange loss is intermediate and π-back-bonds are possible.

We expect group 8–10 metals to be good candidates for carbene bonding, since two-electron π-back-bonds may be formed without requiring intermediate or low-spin metal centers. We expect those metals that can have a σ hole (allowing formation of a σ-donor bond from the ligand) to be even more likely to exhibit carbene bonding. In addition, carbene bonding is also favored for those systems where covalent bonding costs too much in exchange loss. For example, the loss of exchange and promotional energies for forming two covalent bonds in $FeCH_2^+$ is ~40 kcal/mol, bonding to either the s^1d^6 ground state of Fe^+ (^6D) or to the low-lying ($E_p^{s\rightarrow d} = 6.7$ kcal/mol)[20] d^7 excited state of Fe^+ (^4F).[21] Since ^6D and ^4F Fe^+ have both singly and doubly occupied d-orbitals, π-back-bonding from Fe^+ and σ-donation from CH_2 can both be achieved as in $RuCH_2^+$ ($^4A_2$). Since the loss of exchange and/or promotion is greater for Fe^+ than for Ru^+ [ΔK_{dd} (Ru^+,d^7) = $1.5K_{dd}$ = (1.5)(15) = 22.5 kcal/mol], we expect carbene bonding to be favored for Fe^+. This is nicely illustrated by the experiments of Brandt and Helquist who isolated the dimethyl sulfide adduct of the $FeCH_2^+$ complex $[(Cp(CO)_2FeCH_2SMe_2]^+$. This complex, or perhaps the free $L_nFeCH_2^+$ species, was found to directly cyclopropanate olefins, as expected for the reaction chemistry of an electrophilic carbene.[5d] Gas-phase work of Stevens and Beauchamp[5k] also implies cyclopropanation chemistry by $CpFe(CO)_2CH_2^+$.

Covalently bonded metal alkylidenes are most favorable for early transition metals, since two-electron π-back-bonding is not possible (no doubly occupied valence d-orbitals in the ground state) and only a minor loss of exchange and promotional energy is incurred (due to the small number of valence electrons). A classic example of this is the first-isolated M=CH_2 complex, $Cp_2(CH_3)Ta{=}CH_2$, which exhibits nucleophilic alkylidene character.[8] This can be understood by an exchange energy analysis modified by the presence of other ligands. Ta has an s^2d^3 ground state in which the s electrons and one d electron are involved in bonding to the Cp and CH_3 ligands, leaving two high-spin d-electrons to bond to CH_2. Binding CH_2 to the 16-electron $Cp_2(CH_3)Ta$ fragment results in only $0.5K_{dd}$ loss (~7 kcal/mol). The small exchange loss coupled with no π-back-bonding possibilities leads to the formation of a covalent, nucleophilic metal–alkylidene bond.

Competitive carbene and alkylidene bonding should occur when π-back-bonding is possible and there is an intermediate loss of exchange in forming covalent bonds. We expect this behavior in second- and third-row group 8–10 metals, since π-back-bonding is possible and the exchange loss is not as large (the average K_{dd}'s for second- and third-row group 8–10 metals are ~5 kcal/mol smaller than for their first-row congeners[22]). $RuCH_2^+$ is one example of this, in which the dπ–pπ back-bonding is great enough (30 kcal/mol) and exchange loss is large enough (66 kcal/mol) to allow competitive carbene/alkylidene states. Binding CH_2 ($^3B_1$) to the ground-state d^7 Ru^+ leads directly to a stable alkylidene. Due to the lack of exchange loss and the strength of the donor/acceptor bond, a CH_2 ($^1A_1$) bound to d^7 Ru^+ results in a carbene of nearly the same stability as the alkylidene. Experimental examples from group 8–10 second- and third-row metals span the range of behavior from nucleophilic to electrophilic. Roper and co-workers[23] have shown that the complexes $Cl(NO)(PPh_3)_2M{=}CH_2$ (M = Ru, Os) are nucleophilic, reacting with acids not bases, while Thorn and Tulip[24] isolated the pyridine adduct of the electrophilic $Br(PMe_3)_3(CH_3)Ir^+{=}CH_2$.

3. Bond Strengths. Although conventional wisdom correlates bond strengths with orbital overlaps, other factors contribute significantly to bond energy trends. M–CXY bond strengths are weakened by both exchange loss and possible promotion of the metal and/or the ligand. In general, due to small exchange loss, early transition-metal alkylidenes are expected to have strong bonds, with the bond strengths *increasing* down a column due to the *decreasing* size of the exchange terms.[22] The bond strengths in metal–carbenes depend on the effectiveness of σ-donor/π-back-bonding, since the metal need not incur exchange loss. Promotional effects may sometimes be required for effective σ-donor/π-acceptor bonding. Hence the bond strengths in unsaturated late-transition-metal carbene systems are expected to be stronger than for early-transition-metal carbene systems due to more effective π-back-bonding. In addition, we expect these bond strengths to *increase* down a column since the *increasing size* of the d-orbitals may allow more effective delocalization for the π-back-bond. The intermediate cases suggest metal–carbene bond strengths can be as strong as the corresponding metal–alkylidene bond strengths (for the unsaturated systems).

The trends for saturated metal complexes are even simpler to analyze. For a given set of ligands, the valence electron configuration at the metal is expected to be *constant* for metals in the same column. Thus, there is no need to consider promotional energy (since the constant ligand set induces the same ground-state valence electron configuration for each metal) and the same *number* of exchange terms is lost as we go down a column. Since $\Delta E_p = 0$ and ΔK_{dd} = (constant)K_{dd}, then the only variable in determining the bond energies is the *magnitude* of the intraatomic exchange integral, which decreases as we go down a column.[22] This *decreases* the destabilization due to exchange loss and hence *increases* the bond energy as we go down a column. Conventional wisdom attributes this trend solely to the increasing size of the d orbitals inducing larger overlap and hence stronger bonds

B. Effect of Ligand Type on the M–CXY Bond. Metal–carbon bond character is determined not only by electronic interactions on the metal but also by the nature of the CXY ligand. The substituents on the carbon ligand can greatly influence the stability of alkylidene vs. carbene bonding. We have shown that alkylidenes involve triplet CXY fragments forming *covalent* bonds, whereas carbenes involve singlet CXY fragments forming *donor/acceptor* bonds to a metal center. Therefore, if X and Y are chosen to stabilize the triplet, alkylidene bonding will be favored, while if

(20) Moore, C. E. *Natl. Stand. Ref. Data Ser. (U.S., Natl. Bur. Stand.)* **1971**, *3*, (35).

(21) Since $K_{dd}(Fe^+) = 20.7$ kcal/mol and $K_{sd}(Fe^+) = 5.0$ kcal/mol, ΔK-($Fe{=}CH_2^+$, $s^1d^6Fe^+$) = $1.5K_{dd} + 2K_{sd} = 41$ kcal/mol. ΔK_{dd}($FeCH_2^+$, d^7Fe^+) + $E_p^{s\rightarrow d}(Fe^+) = 1.5K_{dd} + E_p = 31.05 + 6.7 = 37.75$ kcal/mol.

(22) Froese Fischer, C. *The Hartree-Fock Method for Atoms—A Numerical* Approach; Wiley-Interscience: New York, 1977

(23) (a) Hill, A. F.; Roper, W. R.; Waters, J. M.; Wright, A. H. *J. Am. Chem. Soc.* **1983**, *105*, 5939. (b) Roper, W. R. *Group VIII Transition Metal Complexes of CH_2, CF_2, and Other Simple Carbenes*; Seminar at the California Institute of Technology, 23 July 1984

(24) Thorn, D. L.; Tulip, T. H. *J. Am. Chem. Soc.* **1981**, *103*, 5984.

X and Y are chosen to stabilize the singlet, carbene bonding will be favored (ignoring the metal's electronic interaction already discussed in section V.A).

In general, electronegative substituents (e.g., F, Cl, OR) on the carbon ligand stabilize the singlet carbene state,[15] whereas electron-donating substituents favor the triplet alkylidene state of CXY.[25] For instance, while CH_2 has a *triplet* ground state (with $^1A_1$ lying ~9 kcal/mol higher[12]), CF_2 has a *singlet* ground state with the triplet state lying ~57 kcal/mol higher.[15c] Thus, replacing CH_2 with CF_2 will lead to a bias of ~66 kcal/mol toward formation of a metal–carbene! If carbene bonding is desired, a CXY ligand (X,Y = F, Cl, OR, H; R = alkyl) in conjunction with a metal from groups 8–10 increases the driving force for formation of a terminal σ-donor/π-acceptor bond. Examples of such bonding in group 8–10 systems included CH_2 complexes of Fe[26] and Ir[24] and CF_2, CCl_2, C(F)(Cl), and C(F)(O-*t*-Bu) complexes of Fe, Ru, and Os, all of which exhibit the expected electrophilic, singlet carbene character (e.g., facile reactions with nucleophiles).[27] The only exception is found in CF_2 complexes of Ru(0) and Os(0) where the π-back-bonding is so effective as to inhibit the electrophilicity of these carbenes, rendering them slightly nucleophilic.[28]

It is well-known that group 6 metals readily form the so-called Fischer carbenes in which a low-valent metal, usually surrounded by five carbonyl ligands, is bonded to an alkoxycarbene ligand in a donor/acceptor fashion.[2] These systems are metal carbenes partly because the alkoxycarbene has a singlet ground state and partly because the closed-shell ancillary ligands (e.g., PR_3, CO) force the metal into a low-spin d^n configuration primed for forming donor/acceptor bonds (with doubly occupied $d\pi$-orbitals). A dramatic example of how the chemistry (and, we believe, the bond character) changes going from an unsaturated to a saturated metal complex (with closed-shell ligands) is found in the work of Stevens and Beauchamp[5c] who demonstrated that $MnCH_2^+$ undergoes metathesis reactions, while $(CO)_5MnCH_2^+$ yields only cyclopropanation products. The unsaturated system s^1d^5 Mn^+, being unable to form a π-back-bond, is forced to form a covalent alkylidene bond which, as such, undergoes metathesis. Attaching the CO's forces Mn^+ into a low-spin d^6 state which can now form π-back-bonds, leading to a donor/acceptor carbene bond that can undergo cyclopropanation.

In order to prepare stable alkylidenes, we require CXY to have a triplet ground state or a low-lying triplet excited state. This requirement is fulfilled by methylene and mono- or dialkyl or aryl carbenes. Examples are prevalent among the early transition metals, as evidenced by their nucleophilic chemistry. For instance, Ta neopentylidene complexes are catalysts for ethylene polymerization,[29] Ti alkylidene complexes are postulated intermediates in olefin metathesis,[9] and other early transition metals participate in the reactions shown in (3)–(5).[6-8] This predominance of alkylidenes in the early metals is due to small exchange losses, strong M–C π bonds (large d-orbitals for early metals), and the lack of doubly occupied d orbitals (disfavoring donor/acceptor bond formation). The late transition metals generally prefer not to form terminal alkylidene bonds in a mononuclear complex. Late transition metals form weak covalent π bonds since d-orbitals contract as we go across a row. Thus reactions which would form $M{=}CR_2$ complexes in early transition metals lead instead to dinuclear *bridging* CR_2 complexes in late transition metals.[30]

C. Design Prescription of Carbenes and Alkylidenes. From sections V.A and V.B, we see that the electronic state of a metal and its ligands greatly influences its bond character and reactivity. Using the ideas presented thus far, we can now predict, based solely on the electronic structure of the metal complex, what elements are necessary to form stable carbenes and alkylidenes.

To ensure the formation of a metal–alkylidene with nucleophilic character, we require the CXY ligand to be a triplet so that it can form two covalent bonds to a metal atom. This suggests CXY ligands where X and Y are σ-donating or electropositive. Then the C–X and C–Y bonds will use more C s character to lower the energy of the carbene, destabilizing the C σ nonbonding orbital. Second, use of substituents X and Y without pπ lone pairs will favor occupation of the C π nonbonding orbital. Third, use of bulky X and/or Y will force sp^2 hybridization on the C to obtain larger X–C–Y bond angles to relieve steric (Pauli) repulsion. The increased s character in the C–X/C–Y bonds results in increased p character in the nonbonding carbon σ-orbital. These three factors leading to the destabilization of the carbon σ-orbital and the stabilization of the carbon π-orbital favor $\sigma\pi$ (triplet) alkylidene (**1**) over σ^2 (singlet) carbene (**2**).

Indeed, the metal alkylidenes which have been synthesized to date contain hydrogen, alkyl, or aryl substituents on the carbon, which are σ-donating (H and R), do not possess pπ lone pairs (H, R, and Ar), and may be bulky (R and Ar). As a further synthetic extension, we suggest that X and/or Y = SiR_3, AlR_2, and BR_2 should be effective in stabilizing triplet CXY (and hence metal alkylidenes), since all three are electropositive, are σ-donating, lack pπ lone pairs, and are bulky. While a tungsten $C(H)(SiMe_3)$ alkylidene system has been synthesized,[31] $CX(AlR_2)$ and $CX(BR_2)$ alkylidenes are unknown. However, $M{-}C(X)(AlR_2)$ and $M{-}C(X)(BR_2)$ should exhibit unusual reactivity due to the presence of a Lewis acid adjacent to a nucleophilic carbon center. In particular, such systems may show enhanced reactivity as olefin polymerization or metathesis catalysts, since those reactions often require Lewis acid cocatalysts. The formation of a temporary olefin adduct at the Lewis acid site may promote reaction at the M=C bond.

To form a stable alkylidene, the metal center must incur little exchange loss upon bonding to the CXY ligand. This requirement is satisfied best by early transition metals, where the small number of valence d electrons results in small exchange losses. It is also important that these metals can form stable, coordinatively unsaturated complexes (e.g., 14- and 16-electron complexes) in which the metal has unpaired electrons set up for bonding to triplet CXY.[32] Thus stable terminal alkylidenes are expected (and found) for early-transition-metal mono- and dialkyl or aryl alkylidenes, with the most stable alkylidenes found among the third-row elements (due to a smaller K_{dd} and a stronger π bond). Terminal alkylidene complexes involving late transition metals will generally be less stable due to weaker covalent π bonds, and thus late transition metals will prefer to make two σ bonds to CXY, resulting in the formation of *bridging* alkylidenes (as is found experimentally).[30] Those few examples of terminal CR_2 complexes bound to group 8–10 metals all indicate *carbene* character (most of these examples involve CH_2, since the small $^1A_1$–^3B splitting

(25) (a) Ab initio theoretical calculations on CLiH and CLi_2 (extreme electron-donating substituents) yield triplet ground states. See: Harrison, J. F.; Liedtke, R. C.; Liebman, J. F. *J. Am. Chem. Soc.* **1979**, *101*, 7162. (b) GVB-CI calculations yield a triplet ground state for $CH(SiH_3)$: Carter, E. A.; Goddard III, W. A., unpublished results.

(26) Brookhart, M.; Tucker, J. R.; Flood, T. C.; Jensen, J. *J. Am. Chem. Soc.* **1980**, *102*, 1203.

(27) (a) Clark, G. R.; Hoskins, S. V.; Roper, W. R. *J. Organomet. Chem.* **1982**, *234*, C9. (b) Mansuy, D.; Lange, M.; Chottard, J. C.; Bartoli, J. F.; Chevrier, B.; Weiss, R. *Angew. Chem., Int. Ed. Engl.* **1978**, *17*, 781. (c) Roper, W. R.; Wright, A. H. *J. Organomet. Chem.* **1982**, *233*, C59. (d) Clark, G. R.; Marsden, K.; Roper, W. R.; Wright, L. J. *J. Am. Chem. Soc.* **1980**, *102*, 1206. (e) Hoskins, S. V.; Pauptit, R. A.; Roper, W. R.; Waters, J. M. *J. Organomet. Chem.* **1984**, *269*, C55.

(28) Clark, G. R.; Hoskins, S. V.; Jones, T. C.; Roper, W. R. *J. Chem. Soc., Chem. Commun* **1983**, 719.

(29) Turner, H. W.; Schrock, R. R.; Fellmann, J. D.; Holmes, S. J. *J. Am. Chem. Soc* **1983**, *105*, 4942.

(30) (a) For a comprehensive review, see: Herrmann, W. A. *Adv. Organomet. Chem.* **1982**, *20*, 159. See also: (b) Theopold, K. H.; Bergman, R. G. *J. Am. Chem. Soc.* **1981**, *103*, 2489. (c) Isobe, K.; Andrews, D. G.; Mann, B. E.; Maitlis, P. M. *J. Chem. Soc., Chem. Commun* **1981**, 809. (d) Herrmann, W. A.; Bauer, C.; Plank, J.; Kalcher, W.; Speth, D.; Ziegler, M. L. *Angew. Chem., Int. Ed. Engl.* **1981**, *20*, 193. (e) Sumner, C. E., Jr.; Collier, J. A.; Pettit, R. *Organometallics* **1982**, *1*, 1350. (f) Lin, Y. C.; Calabrese, J. C.; Wreford, S. S. *J. Am. Chem. Soc.* **1983**, *105*, 1679. (g) Laws, W. J.; Puddephatt, R. J. *J. Chem. Soc., Chem. Commun* **1983**, 1020. (h) Holmgren, J. S.; Shapley, J. R. *Organometallics* **1985**, *48* 793. (i) Morrison, E. D.; Geoffroy, G. L.; Rheingold, A. L. *J. Am. Chem. Soc* **1985**, *107*, 254.

(31) Legzdins, P.; Rettig, S. J.; Sanchez, L. *Organometallics* **1985**, *4*, 1470.

(32) See, for example: Green, J. C.; Payne, M. P.; Teuben, J. H. *Organometallics* **1983**, *2*, 203.

in CH_2 makes the carbene more accessible).[24,26]

For a strong metal–carbene bond, we require a singlet ground state (or low-lying singlet excited state) of the CXY ligand in order to form a σ-donor/π-acceptor bond to the metal center. When X or Y in the CXY ligand are electronegative, the C–X/C–Y bonds utilize C p-orbitals, since the lower ionization potential of the C 2p allows more charge transfer to the electronegative substituents. More p character in the C–X/C–Y bonds stabilizes the nonbonding C σ-orbital by introducing more s character into it. In addition, pπ lone pairs on X or Y may delocalize into the nonbonding C pπ, disfavoring pπ occupation by one of the carbon valence electrons. Both high electronegativity and the presence of pπ lone pairs act to stabilize the σ^2(carbene) state of CXY **2**.[15b,33]

To favor a stable metal–carbene, we would like either a late transition metal with doubly occupied d-orbitals to induce π-back-bonding [e.g., Cp(dppe)Fe=CH_2^+][26] or an early transition metal with ancillary closed-shell ligands that force the metal to be low-spin d^n [e.g., $(CO)_5Cr{=}C(OMe)(Me)$][2] such that dπ–pπ back-bonding is possible. Examples of such metal–carbene complexes include many group 6 carbonyl alkylalkoxy carbenes as well as late transition metal CH_2, CF_2, CCl_2, and CF(OtBu) complexes, all exhibiting varying degrees of electrophilic character.[27]

Strong preference for carbene bonding is expected in the first-row group 8–10 metals since the exchange loss incurred in forming covalent (alkylidene) bonds is particularly high (due to large K_{dd}). However, for second- and third-row late transition metals, the more moderate exchange losses lead to more *competitive* alkylidene and carbene bonding when the CXY ligand has a *small* $^1A_1$–$^3B_1$ splitting (namely, for CH_2), just as found for $RuCH_2^+$. Bridging carbenes with electronegative substituents at carbon should be (and are) rare, since donor/acceptor (terminal) bonding is preferred.[30a] Indeed, the M–C bonds in a μ-CF_2 complex should be weaker than those in a μ-CR_2 system by the singlet-triplet gap of CF_2 (57 kcal/mol), since excitation to $^3B_1$ CF_2 is necessary in order to form the bridged species.

In sum, a desired bonding/reactivity scenario, be it carbene, alkylidene, or an intermediate case, can be designed by appropriate choice of both metal and ligand to meet the electronic requirements dictated by the character of each mode of bonding.

VI. Summary

Ab initio electronic structure calculations on simple metal carbenes reveal the following conclusions.

(i) Relative stabilities of metal carbenes vs. metal alkylidenes are predicted to be most sensitive to choice of metal for the first-row transition-metal CH_2 complexes (alkylidene state lowest for the early metals and the carbene state more favored for the late metals).

(ii) Second- and third-row metals lead to situations where both states may be competetive and where the ground state may be determined by other factors (e.g., substituents on CXY and/or ancillary ligands).

(iii) M–CH_2 σ-donor bonds are calculated to be worth 35–40 kcal/mol while π-back-bonds are found to be ~30 kcal/mol. These values are expected to vary systematically depending on the electronegativity of the metal complex, with the σ bond becoming stronger and the π bond becoming weaker as the metal becomes more electrophilic.

(iv) The above ideas are utilized in formulating a general design prescription for the synthesis of $L_nM(CXY)$ complexes, based on quantitative electronic properties. For example, terminal CXY groups will be favored by electronegative substituents at carbon (X, Y = F, Cl, OR, NR_2), while bridging CXY will be favored when X and/or Y are electropositive (X, Y = R, H, SiR_3).

VII. Calculational Details

A. Basis Sets. All atoms were described with all-electron valence double-ζ (VDZ) basis sets. The Four's level VDZ basis sets[34] were used for Cr, contracted (10s8p5d/5s4p2d), and for Ru, contracted (16s13p7d/6s5p3d).[34b] The standard Huzinaga–Dunning VDZ bases[35] for C (9s5p/3s2p) and H (4s/2s) were used, with one set of d-polarization functions (ζ_d = 0.69)[18a] added to the carbon basis set.

B. Wavefunctions. The generalized valence bond (GVB) method was used in all calculations. The GVB perfect pairing wavefunction is an MCSCF (multiconfigurational self-consistent field) wavefunction in which each bond pair is described with two GVB one-electron orbitals

$$\varphi(1)\varphi(2) \rightarrow \varphi_a(1)\varphi_b(2) + \varphi_b(1)\varphi_a(2)$$

whose shapes are optimized. As a bond is broken, the overlap, S_{ab}, of the two GVB orbitals describing the bond goes to zero, but for a strong bond near R_e, or for a lone pair, the overlap is near unity. In the limit that $S_{ab} \rightarrow 1$, the GVB description degenerates to the HF description. Generally it is only necessary to use the GVB description for electron pairs where the overlap differs significantly from unity. This applies most strongly to M–X bonds in which the mismatch in orbital sizes results in overlaps ranging from 0.3 to 0.7 between metal and ligand orbitals, while the doubly occupied core orbitals and C–H bonds (each pair with nearly unit overlap) are treated at the Hartree–Fock level. Thus, the general wavefunction has the form

$$\mathcal{A}|\Phi_{CORE}(\varphi_{1a}\varphi_{1b} + \varphi_{1b}\varphi_{1a})(\varphi_{2a}\varphi_{2b} + \varphi_{2b}\varphi_{2a})\cdots\chi_{SPIN}| \qquad (1)$$

where the doubly occupied orbitals are in Φ_{CORE} but calculated self-consistently with the GVB orbitals (φ_{1a},φ_{1b}), (φ_{2a},φ_{2b}), etc.

In order to indicate how many electrons are correlated, we denote the wavefunction as

$$GVB(n/m)$$

where n is the number of GVB electron pairs and m (usually $m = 2n$) is the total number of natural orbitals within the GVB space. The wavefunction (1) is denoted as PP (for perfect pairing) because the electrons in orbitals φ_{1a} and φ_{1b} have their spins coupled into a singlet, the electrons in orbitals φ_{2a} and φ_{2b} have their spins coupled into a singlet, etc.

C. Geometry Optimization. The geometry of the $^6A_1$ state of $CrCH_2^+$ was optimized at the GVB-RCI(1/2)*S_{val} level (generalized valence-bond-restricted configuration interaction times all single excitations from all valence orbitals to all virtual orbitals). The GVB-RCI(1/2) description allows a full CI within the pair of natural orbitals describing the Cr–C σ bond, resulting in three spatial configurations. For $^6A_1$ $CrCH_2^+$ these three configurations have eight associated spin eigenfunctions (SEF's), while for the $^4B_1$ state, the GVB(2/4)-RCI description (two bond pairs with four natural orbitals to describe both σ and π bonds) has nine configurations with 34 associated SEF's. The physical interpretation of the RCI wavefunction involves inclusion of interpair correlation and high-spin coupling on the metal atom. Single excitations from the valence orbitals to all virtuals allows orbital shapes to relax as the geometry is optimized. Note we kept the C–H bond distance fixed at 1.078 Å, while optimizing the H–C–H angle and the Cr–C distance.

D. Bond Energies. The bond energies for the $^6A_1$ state of $CrCH_2^+$ were calculated at the GVB(1/2)-PP, GVB-RCI(2), GVB-RCI(2)*D_e, GVB-RCI*S_{val}, and GVB-RCI(2)*S_{val} + GVB RCI(2)*D_e levels. Since the PP, RCI, and RCI*S levels are explained above, we will now outline the two calculations which allow double excitations to the virtual space. While the GVB-RCI wavefunction generally leads to a good description of potential surfaces as bonds are formed and broken, we find that it is systematically low for bond energies. The reason is that at R_e there are a number of ways that the electrons correlate their motion, only part of which can be described with the two GVB orbitals (per bond pair). Thus, to obtain good bond energies, we must allow the two electrons of the bond pair to use any orbital of the basis (double excitations out of the bond pair are thus required). This CI, denoted as GVB-RCI(2)*D_e, includes all single and double excitations from the Cr–C σ bond pair starting from the set of RCI configurations. The other (higher level) calculation is just a sum of the RCI*S and the RCI*D_e calculations. We calculate the energy to dissociate to ground-state Cr^+ (^6S) and excited state CH_2 ($^1A_1$), since this process corresponds to the experimentally observable metal–carbene dissociation pathway in which no electronic relaxation from singlet fragments is expected (e.g., for low-valent $M(CO)_5$ and hetero-carbene fragments). At infinite Cr–C separation, we allow the CH_2 σ pair to use a π-correlating orbital as a second natural orbital, since this

(33) Carter, E. A.; Goddard, W. A., III, unpublished results.

(34) (a) Rappé, A. K.; Goddard, W. A., III, unpublished results. These basis sets were optimized for the d^n configuration of the metal as laid out in: Rappé, A. K.; Smedley, T. A.; Goddard, W. A., III *J. Phys. Chem.* **1981**, *85*, 2607. (b) The Ru basis set may be found in ref 1b.

(35) (a) Huzinaga, S. *J. Chem. Phys.* **1965**, *42*, 1293. (b) Dunning, T. H., Jr. *Ibid.* **1970**, *53*, 2823.

provides the best correlation for singlet CH_2 described as a GVB(1/2) orbital pair. (The CH_2 σ pair at R_e(Cr–C) prefers a σ-correlating orbital.)

We now discuss the CI's in terms of their dissociation limits.

(1) GVB(1/2)-PP and GVB-RCI(2) both dissociate to Hartree–Fock (HF) Cr^+ (total energy = −1042.004 30 hartree) and GVB(1/2)CH_2 (total energy = −38.901 64 hartree). [We calculate an HF bond energy by dissociating to HF Cr^+ and HF CH_2 (total energy = −38.880 98 hartree).]

(2) RCI(2)*D_e dissociates to HF Cr^+ and RCI(2)*D_e CH_2 (total energy = −38.916 49 hartree; 45 spatial configurations/45 spin eigenfunctions).

(3) RCI(2)*S_{val} dissociates to HF*S_{val} Cr^+ (equivalent to HF here) and RCI(2)*S_{val} CH_2 (total energy = −38.907 64 hartree, 34 spatial configurations/37 spin eigenfunctions). The RCI*$S_{valence}$ CI in general not dissociation-consistent, but due to the equivalence of HF to HF*S for d^5 Cr^+, this CI, as are all the ones discussed here, is indeed dissociation-consistent.[1]

(4) RCI(2)*S_{val} + RCI(2)*D_e dissociates to HF (or equivalently, HF*S_{val}) Cr^+ and {RCI(2)*S_{val} + RCI(2)*D_e} CH_2 (total energy = −38.922 49 hartree; 69 spatial configurations/72 spin eigenfunctions), since the σ bond localizes back on CH_2 at $R = \infty$.

E. State Splittings. In order to preserve a balanced description of the $^6A_1$ and $^4B_1$ states of $CrCH_2^+$, we must allow the same degree of freedom for both states in order to ensure we are treating both states equivalently (no artificial biases). We can accomplish this by maintaining the same number of occupied orbitals included in the SCF description of both states. The $^6A_1$ state, with a GVB(1/2) description, has a valence space consisting of two C–H doubly occupied orbitals (treated as HF MO's), one Cr–C bond pair with two natural orbitals (NO's), and five singly occupied nonbonding 3d-orbitals, for a total of nine orbitals in the valence space. The $^4B_1$ state, with a GVB(2/4) description, has a valence space consisting of the two C–H HF MO's, two Cr–C bond pairs (four NO's), and three singly occupied 3d-orbitals, for a total of nine orbitals again. Therefore we have a balanced orbital description of the two states at the two levels described above.

F. Ru Carbene Calculations. All calculations on the various electronic states of $RuCH_2^+$ are described in paper 2 of this series.[1b]

Acknowledgment. Partial support of this work is gratefully acknowledged from the Shell Development Co., Houston, TX, and the National Science Foundation (Grant CHE83-18041).

Chapter 2.D. The text of this section is an Article coauthored with William A. Goddard III and is to be submitted to the *Journal of Chemical Physics.*

Early versus Late Transition Metal-Oxo Bonds: the Electronic Structure of VO^+ and RuO^+

Emily A. Carter and William A. Goddard III*

Contribution No. 7580 from the Arthur Amos Noyes Laboratory of Chemical Physics, California Institute of Technology, Pasadena, California 91125

Abstract: We have carried out all-electron ab initio multiconfiguration self-consistent field with configuration interaction (MC-SCF/CI) calculations on two transition metal oxo cations MO^+ (M = V, Ru). We find that accurate theoretical descriptions of the metal-oxo bonding are obtained only when important resonance configurations are included self-consistently in the wavefunction. The ground state of VO^+ ($^3\Sigma^-$) has a triple bond similar to that of CO, with D_e^{calc}(V-O) = 128.3 kcal/mol [D_e^{expt}(V-O) = 131$\pm$5 kcal/mol], while the ground state of RuO^+ ($^4\Delta$) has a double bond similar to that of O_2, with D_e^{calc}(Ru-O) = 67.1 kcal/mol. Vertical excitation energies for a number of low-lying electronic states of VO^+ and RuO^+ are also reported. These quantitative results indicate fundamental differences in the nature of the oxo ligand in early and late metal oxo complexes. We suggest that the differences in M-O bond character are responsible for the observed trends in reactivity (e.g., the thermodynamic stability of early metal oxides versus the highly reactive oxidizing power of late metal-oxo complexes).

I. Introduction

While the electronic structure of neutral transition metal oxides has been examined by several authors,[1] the only cationic transition metal oxide (TMO) which has been studied with correlated wavefunctions is CrO^+.[2] With the growing availability of experimental bond energy and reactivity data for TMO cations,[3] physical descriptions of the molecular bonding in such systems are sorely needed. Hence we have undertaken an ab initio MCSCF/CI (multiconfiguration self-consistent field/configuration interaction) study of two TMO's, VO^+ and RuO^+, as representatives of early and late transition metal-oxo bonding, with the goal of understanding the differences in bonding and reactivity as one proceeds across the periodic table.

Examination of empirical properties of transition metal oxides reveals that early metal-oxo compounds exhibit high stability, are relatively inert, and are characterized by very strong M-O bonds, while late TMO's tend to be highly reactive oxidizing agents and possess much weaker M-O bonds.[4] For example, while VO^{2+} is used as an inert ESR-active probe of protein reactive sites,[5] oxides such as CrO_3, MnO_4^-, and OsO_4 rapidly oxidize olefins and alcohols to epoxides, diols, aldehydes, ketones, and carboxylic acids.[6] Late transition metal-oxo porphyrin complexes (models for active sites of enzymes) are effective oxygen atom transfer reagents[7] and are catalysts for hydrocarbon oxidation (cytochrome P-450 analogues).[8] The trends in reactivity are consistent with their relative thermodynamic stabilities, exemplified by the bond energies of metal-oxo diatomics (Table I). The early metal-oxo diatomics have bond strengths roughly twice as strong as their late metal counterparts. We believe that differences in the metal-oxo *bond character* are responsible for the sharp contrast in bond energies and reactivities of early and late transition metal-oxo complexes. In the present work, we show that an oxo ligand is quite versatile: oxygen atom is capable of forming (at least) three distinct types of terminal metal-oxo bonds.[9]

Experimental data for TMO cations include thermochemical measurements

to obtain bond energies and heats of formation,[3a-e] photoelectron spectra to determine the equilibrium properties of ground and excited electronic states (e.g., vibrational frequencies, bond lengths, excitation energies, and ionization potentials),[3f,g] and gas phase studies of their chemical reactivity.[3a,h-j]

Much attention has been focused on VO^+, due to its presence in interstellar space[10] and its possible relationship to vanadium oxide-catalyzed hydrocarbon oxidations.[11] Aristov and Armentrout used guided ion beam techniques to directly measure the bond energy of VO^+, obtaining $D^o(V^+-O) = 131\pm5$ kcal/mol.[3e] These authors speculated that the ground state of VO^+ might be $^3\Delta$, similar to the ground state of TiO.[1c] However Dyke *et al.* later recorded the photoelectron spectrum of VO,[3g] assigning the ground state of VO^+ to be $^3\Sigma^-$, with the $^3\Delta$ state lying at least 1.15 eV higher in energy. From a Franck-Condon analysis of the vibrational fine structure of the $VO^+(X^3\Sigma^-) \leftarrow VO(X^4\Sigma^-)$ envelope, Dyke *et al.* obtained values of $\omega_e = 1060\pm40$ cm^{-1} and $R_e = 1.54\pm0.01$ Å for VO^+ ($^3\Sigma^-$). From the first ionization potential of VO (7.25±0.01 eV), they derived an indirect value of $D^o(V^+-O) = 138\pm2$ kcal/mol.

The reactivity of several metal-oxo cations (M = V, Cr, and Fe) has been studied by Freiser and co-workers[3h,i] and by Kang and Beauchamp.[3a,j] VO^+ is found to be rather unreactive, with the strongly bound oxo ligand uninvolved in the chemistry observed.[3i] In contrast, FeO^+, with its much weaker bond (Table I), is very reactive and nonselective, forming H_2O by hydrogen abstraction from alkanes.[3h,12] The reactivity of CrO^+ is intermediate in nature,[3a,j] reflecting its moderate bond strength. The oxo ligand in CrO^+ is reactive, but selective, producing aldehydes from olefins and alcohols from alkanes, without hydrogen abstraction. RuO^+ has not yet been observed experimentally.

The only quantitative theoretical study which has been published concerns CrO^+,[2] where Harrison predicts [from multireference singles and doubles CI calculations (MRCI-SD)] the ground state to be $^4\Pi$ with the following properties:

$D_e(Cr^+–O)$ = 57.1 kcal/mol, ω_e = 915 cm^{-1}, and R_e = 1.630 Å. These results are in serious disagreement with the observations of the photoelectron spectrum of CrO.[3f] Franck-Condon analysis of the vibrational envelope yields ω_e = 640±30 cm^{-1} and R_e = 1.79±0.01 Å for the ground state of CrO^+, which was predicted by limited CI calculations to be $^4\Sigma^-$. In addition, Harrison's bond energy is low from the best experimental determination of Kang and Beauchamp[3a] by nearly 30 kcal/mol. Further examination of the electronic structure of CrO^+ may be warranted, although it is not the focus of the work presented here.

Normally when we consider how oxygen may form terminal bonds to other atoms, we think of double bonds consisting of one σ and one π bond (e.g., carbonyl groups within organic molecules). However, there are two other types of covalent bonding involving oxygen. First, triple bonds can be formed as in carbon monoxide, in which three valence bond (VB) resonance structures (two covalent bonds and one donor bond) participate in the bonding of C (^3P) to O (^3P)

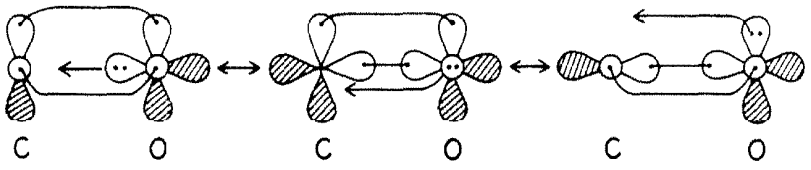

(1)

where we have indicated the locations of the valence p-electrons on carbon and oxygen in Eq. (1).[13] Second, double bonds can be formed as in O_2, in which two VB resonance structures (one σ bond and two three-electron π bonds) contribute to the bonding between two ground state oxygen atoms (^3P).

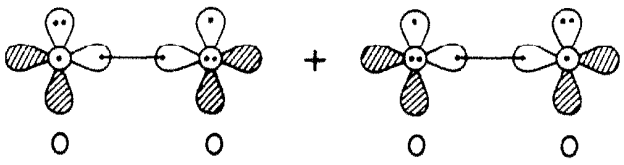

(2)

(Equivalently, molecular orbital theory describes the double bond in O_2 as filled π bonding levels and half-filled π antibonding levels, leading to one σ bond and two half-order bonds in the π system.)

In the two next sections, we discuss MCSCF/CI predictions for properties of VO^+ and RuO^+, drawing analogies from CO and O_2 in order to understand the variations in metal-oxo bond character. Section IV concludes with general predictions of properties and reactivity of transition metal-oxygen bonds from a simple analysis of the expected bond character (based on the electronic state of the metal center and the nature of its ancillary ligands).

II. VO^+

The outcome for metal-oxo bond character depends primarily on the electronic state of the metal center. Since V^+ has a ground state valence electronic configuration of $3d^4$, it has an empty d-orbital similar to carbon's empty p-orbital. As a result, oxygen forms a triple bond to V^+ in the same manner as in CO, except that the oxygen p lone pair forms the third bond by donating into an empty d-orbital on V instead of an empty p-orbital on C. The other two bonds are covalent in nature, i.e., each bond is composed of one electron from each atom.

Calculational Details

In order to treat the bonding in VO^+ properly, it is imperative to include the three possible contributing resonance structures [Eq. (1)]. This is accomplished using an MCSCF approach in which all three resonance structures are optimized self-consistently at the **GVB-RCI** level. We begin with the **GVB(3/6)-PP** wavefunction [generalized valence bond with the perfect (singlet) pairing restriction] which allows each of the six electrons involved in the three bonds to occupy its own orbital, with each bond pair described by two orbitals.[14] The **GVB(3/6)-RCI** wavefunction includes, for each GVB bond pair, the configurations corresponding to the three possible occupations of two electrons in two orbitals (3^3 configura-

tions). Physically, the **GVB(3/6)-RCI (opt)** calculation solves self-consistently for the best orbitals of the resonating wavefunction, optimizing the spin-coupling between the electrons involved in the triple bond, the charge transfer effects, and the inter-pair correlations. For the purposes of calculating bond energies, the above wavefunctions for VO^+ and CO dissociate to HF fragments (i.e., any correlation present at R_e is gone at $R = \infty$), where the fragments are ground state V^+ (^5D), C (^3P), and O (^3P).

Higher level correlations were also included self-consistently in the **RCI(3/6)*S_{corr} (opt)** calculation, in which one extra correlating orbital was optimized for each GVB bond pair by allowing single excitations to those correlating orbitals from the RCI reference states [keeping the RCI(3/6)(opt) valence orbitals fixed]. The largest CI expansion we carried out allowed all single excitations from all valence orbitals (excluding the oxygen and carbon 2s orbitals) to all virtual (unoccupied) orbitals from the GVB-RCI(3/6)(opt) reference state, denoted as **RCI(3/6)(opt)*S_{val}**. Single excitations correspond to orbital shape changes,[15] which are important for describing rehybridization effects which may occur during bond cleavage. The latter two wavefunctions dissociate to HF*S_{corr} and HF*S_{val} fragments at $R = \infty$, since all other correlations present at R_e disappear when the bond breaks. HF*S_{corr} is simply the HF wavefunction for the ground state atom, where single excitations to the (corresponding) correlating orbitals are optimized self-consistently, with the occupied orbitals fixed. HF*S_{val} involves all single excitations from all valence orbitals (excluding the O and C 2s) to all virtuals from the HF wavefunction.

No higher levels of correlation were included beyond what the CI calculations described above. For example, double excitations to virtual orbitals were not allowed, since the bonds of VO and CO are partially donor/acceptor in character and thus do not dissociate correctly using a singles and doubles CI (i.e., CI-SD requires triple and quadruple excitations at R_e).

We used the Dunning valence double-ζ contraction[16] of the Huzinaga (9s5p) primitive gaussian basis set[17] for O, augmented by one set of 3d polarization functions ($\zeta^d = 0.95$),[18] and the Rappé and Goddard valence double-ζ basis set for vanadium (Table II).[19] The ground state bond distance and the vertical excitation energies were optimized at the RCI(3/6)(opt) level.

Results

The ground state of VO^+ is predicted to be $^3\Sigma^-$, with a bond length of $R_e(V^+–O) = 1.56$ Å and $\omega_e = 1108$ cm^{-1}, in excellent agreement with the experimental results of Dyke *et al.* [$R_e(V^+–O) = 1.54\pm0.01$ Å and $\omega_e = 1060\pm40$ cm^{-1}].[3g] Two of the four d electrons on V are involved in bonding to the oxygen, with the remaining two nonbonding d electrons in δ orbitals (to reduce electron repulsion). The bond character is found to be a triple bond, but Mulliken population analysis (1.46 electrons in each oxygen pπ orbital and 1.33 electrons in the oxygen pσ orbital) suggests that the two resonance structures of Eq. (1) which have covalent σ bonds (with an average of 1.5 electrons in each O pπ orbital and 1.0 electron in the O σ orbital) dominate the bonding. If each of the resonance structures contributed equally, each oxygen p-orbital would have an occupation of $1\frac{1}{3}$ electrons. Thus, since the occupations are inequivalent, the bonds in VO^+ are best viewed as one covalent σ bond, one covalent π bond, and one donor π bond,

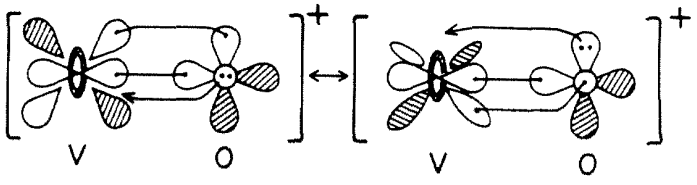

(3)

with 0.33 electron transferred from V^+ to O in the σ system and 0.07 electron transferred back to V^+ in the π system. This is consistent with the net charge

of -0.26 electron on oxygen. Similarly, Mulliken population analysis of CO finds 1.22 electrons in O pσ and 1.46 electrons in each pπ. Therefore, although all three resonance structures participate to some degree in both VO^+ and CO, the dominant resonance structures are those involving covalent σ bonding. For a qualitative view of their triple bond character, the GVB-RCI(3/6)(opt) orbitals for VO^+ and CO are compared in Fig. 1, where we see that the bonding in CO and VO^+ is indeed very similar.[20]

The triple bond character for both VO^+ and CO results in very strong bonds. Table III compares their bond strengths as a function of increasing electron correlation. The correlation problem is much more severe for transition metals than for organic molecules, as is indicated by the disparity between the Hartree-Fock (HF) and the experimental values for D_e [$\Delta D_e(VO^+) = 142$ kcal/mol whereas $\Delta D_e(CO) = 88$ kcal/mol]. VO^+ is unbound by 11 kcal/mol at the HF level, due to the inability of HF theory to describe the low overlap (π) bonds present in multiply-bonded metal-ligand complexes.[21] Once static correlation is built into the wavefunction, properly describing the low overlap π bonds ($S_\pi = 0.7$) by the GVB-PP approach, VO^+ is stabilized by almost 60 kcal/mol. Another large increase in stability occurs at the RCI level (53 kcal/mol more stable than GVB-PP) in which proper spin coupling (important for high spin metal atoms)[21] and all three resonance structures are taken into account.

Including self-consistent optimization of the resonance and spin-coupling effects, along with single excitations to virtual orbitals to account for orbital shape changes along the dissociation pathway, leads to bond energies close to experiment for both CO and VO^+. Since the bond energy of CO is known to far greater accuracy[22] than the bond energy of VO^+, we can estimate the residual correlation error expected in VO^+ by $\Delta_{corr} = D_e^{expt}(CO) - D_e^{calc}(CO) = 9.6$ kcal/mol at the highest level of correlation, RCI(3/6)(opt)*S_{val}. Adding Δ_{corr} to $D_e(VO^+)$ at the same level of theory yields our best estimate for the V–O bond energy, 118.7 +

9.6 = 128.3 kcal/mol, in excellent agreement with the experimental value of 131±5 kcal/mol.[3e]

Finally, we examined two other triplet states at the predicted equilibrium bond distance for the ground $^3\Sigma^-$ state (R_e = 1.56 Å). We find a vertical excitation energy of 40.7 kcal/mol to the $^3\Delta$ state, which has a CO-type bond with only one resonance structure.

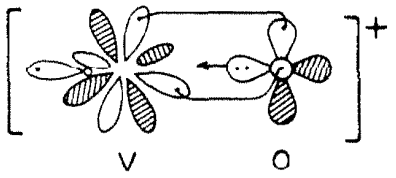

(4)

Two d electrons on V^+ form π bonds to oxygen, with the nonbonding electrons residing in δ and σ orbitals. The large vertical state splitting may be understood in terms of the difference in bond character between the $^3\Sigma^-$ and $^3\Delta$ states. While the $^3\Sigma^-$ ground state forms one donor π bond, one covalent σ bond, and one covalent π bond, the $^3\Delta$ state is forced to form two covalent π bonds and one donor σ bond. Covalent π bonds are weak relative to covalent σ bonds, with the small 3d-orbitals of V^+ enhancing this effect. Thus, the bond in the $^3\Delta$ state is weaker than in the ground state because of the tradeoff between covalent σ and π bonds. However, if the 3d-orbitals were more diffuse so that stronger π bonds could be formed (due to higher overlap), then the $^3\Delta$ state might be competetive. Indeed, the ground state of the isoelectronic TiO is $^3\Delta$,[1c,22] perhaps because the covalent π bonds are stronger for Ti(0) than for V(I).

A $^3\Phi$ state is found to be only 1.9 kcal/mol above the $^3\Delta$ state, with a nonbonding electron configuration of $\delta^1\pi^1$. This state has only a double bond between V^+ and O due to the presence of three electrons in one of the π planes.

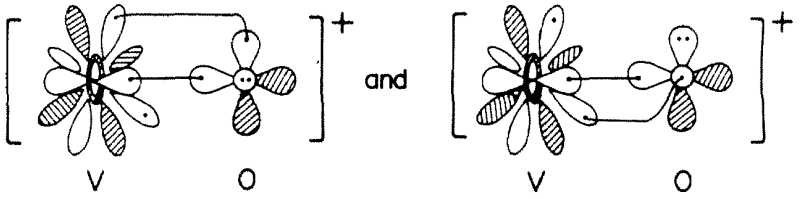

(5)

These vertical excitation energies are considerably higher than the 1.15 eV found by Dyke *et al.*[3g] from the peak to peak distances in the photoelectron spectrum of VO. However, we believe that the first IP of VO may be lower in energy than 7.25 eV as reported by Dyke, since the bond energy Dyke derives for VO^+ (137.9±2.3 kcal/mol) is higher than the directly measured value (131±5 kcal/mol)[3e] by ~ 7 kcal/mol. The direct VO^+ bond energy implies an adiabatic IP for VO of 6.95 eV (7 kcal/mol lower than Dyke's 7.25 eV), resulting in a higher experimental $^3\Delta - {}^3\Sigma^-$ state splitting for VO^+ (33±5 kcal/mol), in closer agreement with the theory (40.7 kcal/mol). However, an analysis of the ionization thresholds and an optimization of the excited state potential curves are necessary for any quantitative statement concerning adiabatic state splittings. Since we are primarily concerned with ground state properties of metal oxides, we will eschew this issue for the present.

III. RuO^+

Group VIII transition metals have doubly-occupied d-orbitals for all low-lying electronic states. The lack of empty d-orbitals decreases the favorability of forming triple bonds to oxygen (unless the metal is in a low spin electronic state). The presence of doubly-occupied d-orbitals makes metallaketone structures with covalent σ and π bonds unlikely due to electron-electron repulsion between a doubly-occupied metal dπ-orbital and the doubly-occupied oxygen pπ-orbital. For Ru, the large 4dπ orbital overlaps the O 2pπ orbital to such an extent that the "metallaketone" type of double bond is 16.9 kcal/mol higher in energy than the ground

state.

Instead of triple or traditional double bonds in RuO^+, we find a $^4\Delta$ ground state with a biradical double bond analogous to the bond in O_2. Four of the d-electrons in high spin d^7 Ru^+ are involved in the $^3\Sigma^-$ type bonding to oxygen (as in ground state O_2), forming a covalent σ bond and two three electron π bonds.

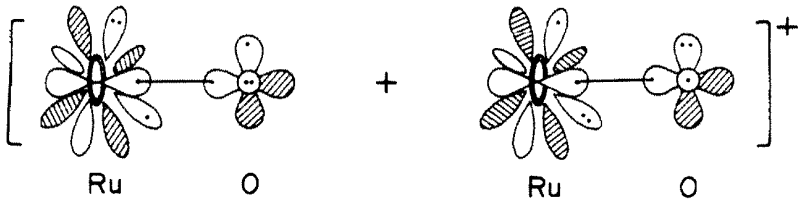

(6)

Since the Ru dσ and dπ orbitals are involved in bonds to oxygen, the other three Ru 4d electrons occupy the dδ orbitals. High spin coupling of the $^3\Sigma^-$ Ru-O bonding and the δ^3 nonbonding electrons on Ru gives rise to the ground $^4\Delta$ state. However, just as in O_2, there are other low-lying electronic states ($^1\Delta_g$ and $^1\Sigma_g^+$ for O_2) with resonance structures containing conventional double bonds (one σ and one π). These O_2-type bonding configurations, when coupled high spin or low spin to the δ^3 Ru electrons, give rise to the spectrum of states shown in Table IV.

Calculational Details

The resonance present in RuO^+ necessitates an MCSCF treatment similar to VO^+ in which both resonance structures of Eq. (6) are optimized self-consistently. This **GVBCI(opt)** calculation consists of a self-consistent RCI(1/2) treatment of the Ru-O σ bond, a full six electron CI among the four orbitals of the Ru-O π system and simultaneous inclusion of the two possible configurations of the three electrons in the Ru δ orbitals. The GVBCI(opt) wavefunction, with its full CI in the π system, is capable of describing any electronic state that is determined by the occupation and spin-coupling of the π orbitals. Thus the vertical excitation energies to just such states ($^3\Sigma_g^-$, $^1\Delta_g$, and $^1\Sigma_g^+$ bonds) were calculated at this level (Table

IV).

One higher level MCSCF calculation was performed in which the valence orbitals from the GVBCI(opt) calculation were kept fixed, while allowing single $\pi \rightarrow \pi^*$, $\delta \rightarrow \delta^*$, $\sigma \rightarrow \sigma^*$ excitations from the GVBCI reference states. This **GVBCI*S$_{corr}$(opt)** calculation optimizes the shapes of seven important, low-lying correlating orbitals (with σ_{z^2}, π_{ux}, π_{uy}, π_{gx}, π_{gy}, δ_{xy}, and $\delta_{x^2-y^2}$ symmetries). Moss and Goddard used an analogous CI treatment to accurately predict the bond energy and the electronic state spectrum of O_2.[24]

Three CI calculations involving excitations to the whole virtual space were performed. First, single excitations from all valence orbitals (excluding the oxygen 2s) to all virtuals from the GVBCI(opt) wavefunction, **GVBCI(opt)*S$_{val}$**, allows the orbital shape changes important during bond rupture. Second, the presence of a covalent σ bond allows a dissociation consistent[15,21,25,26] calculation to be performed, in which all single and double excitations from the σ bond pair to all virtuals are allowed from the GVBCI reference states. This CI incorporates full correlation of the two electrons involved in the breaking bond. We have carried out these single and double excitations (using the GVBCI reference states) from both the GVBCI*S$_{corr}$(opt) wavefunction (denoted **GVBCI*[S$_{corr}$ + SD$_\sigma$]**) and from the GVBCI(opt) wavefunction, where singles from the Ru 4d and O 2p valence space were also allowed (denoted **GVBCI(opt)*[S$_{val}$ + SD$_\sigma$]**). This latter wavefunction has been shown to yield bond energies accurate to 1-5% for both organic and organometallic molecules.[15,21,26]

The wavefunctions described above dissociate to ground state Ru^+ (^4F) and ground state O (^3P). The HF, GVB(1/2)PP, and GVBCI(opt) wavefunctions dissociate to HF fragments. The wavefunctions involving optimization of correlating orbitals dissociate to HF*S$_{corr}$, while the wavefunctions involving single excitations to virtuals from the valence space (excluding the O 2s) dissociate to HF*S$_{val}$ (see Section II). (Note that single and double excitations out of the breaking bond pair

dissociates to just singles out of a singly-occupied orbital on each fragment.)

We used the same oxygen basis as described in Section II, along with the Rappé and Goddard valence double-ζ basis for Ru.[19a,26a] The Ru-O bond length was optimized for the ground $^4\Delta$ state at the GVBCI(opt) level.

Results

The ground state of RuO^+ is predicted to be $^4\Delta$, with an equilibrium bond length of $R_e = 1.75$ Å and an equilibrium vibrational frequency of $\omega_e = 787$ cm^{-1}. Although RuO^+ has not yet been observed, these values may be compared with those of a terminal Ru=O porphyrin complex, in which the bond length is 1.765 Å and the Ru=O stretching frequency is 855 cm^{-1}.[27] The Ru=O bond is very covalent, with no charge transfer to the oxygen. In fact, the total electronic charge (from Mulliken population analysis) indicates 0.04 electron transferred to Ru^+ from O. The GVB-CI(opt) orbitals for both RuO and O_2 are shown in Fig. 2, where we see that the Ru-O σ bond is just as covalent as the O-O σ bond. The three electron π systems of both RuO^+ and O_2 look very similar, with the Ru-O π_u and π_g orbitals delocalized over both centers as in O_2.

The vertical electronic state spectrum shown in Table IV reveals the same ordering of bond types as in O_2, with the $^4\Delta$ state with $^3\Sigma^-$ biradical bonding lowest in energy, followed by the $^2\Gamma$ state with $^1\Delta$ metallaketone bonding (i.e., covalent σ and π bonds) 16.9 kcal/mol up. This $^1\Delta - {}^3\Sigma^-$ splitting of 16.9 kcal/mol for RuO^+ may be compared with the $^1\Delta_g - {}^3\Sigma_g^-$ splitting of 22.6 kcal/mol for O_2.[22] The energy splitting between these two states corresponds to twice the exchange term between the singly-occupied π_{gx} and π_{gy} orbitals, K_{xy}; thus we find $K_{xy}(RuO^+) = 8.45$ kcal/mol and $K_{xy}(O_2) = 11.3$ kcal/mol. The exchange term is larger for O_2 since exchange energy is proportional to the square of the overlap between the two orbitals [R_e(O-O) = 1.21 Å versus R_e(Ru-O) = 1.75 Å].

The $^2\Delta$ state with the $^1\Sigma^+$ bonding configuration, which should be $\sim 4K_{xy}$ higher in energy than the $^3\Sigma^-$ bonding ground state, is 37.1 kcal/mol above $^4\Delta$

instead of $\sim$ 34 kcal/mol. A lower $^2\Delta$ state, along with a nonequilibrium bond length, destabilizes the high-lying $^2\Delta$ state. In sum, the ordering of states in the O_2-type manifold is determined by a combination of two factors: (i) lower electron-electron repulsion favors $^3\Sigma^-$ over $^1\Delta$ and $^1\Delta$ over $^1\Sigma^+$ and (ii) high-spin coupling between the Ru-O bond and the nonbonding δ^3 electrons is favored over low-spin coupling. Thus the low-lying states which have O_2-type bonds are (in order of increasing energy): $^4\Delta$, $^2\Gamma$, $^2\Delta$, $^2\Sigma^{\pm}$, and $^2\Delta$.

We also calculated the energy of a $^2\Sigma^+$ state of RuO^+ with a CO-type triple bond and a nonbonding $d\delta^4$ configuration on Ru^+. This state involves only one resonance structure of Eq. (1)

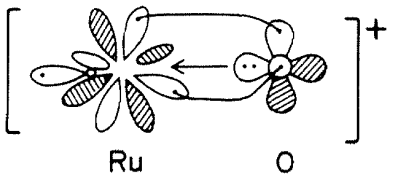

(7)

since the other resonance structures would require promotion of Ru^+ to an intermediate spin s^1d^6 excited state. We did not investigate $^2\Pi$ CO-type bonding, in which three electrons in one π plane would destroy the triple bond. While Eq. (7) has three electrons in the σ system, the triple bond may still form, since $d\sigma$ orbitals rehybridize away from the donor bond more easily (mixing in s-character) than $d\pi$ orbitals (mixing in higher energy p-character). At the GVB-RCI(2/4)(opt) level,[28] this state lies 29.7 kcal/mol above the ground state. As expected, the lack of empty d-orbitals on the metal destabilizes triple bonds to oxygen, and the biradical double bond is preferred.

The bond energies for the ground state of RuO^+ ($^4\Delta$) and the ground state of O_2 ($^3\Sigma_g^-$) are shown in Table V as a function of increasing electron correlation. We see that HF and GVB-PP are inadequate descriptions of metal-ligand multiple

bonds. Although it is only a valence level calculation, the GVBCI(opt) description stabilizes both RuO^+ and O_2 considerably. As single and (selected dissociation-consistent) double excitations are included in the wavefunction, we converge to a bond energy for O_2 of 115.5 kcal/mol at the GVBCI(opt)*[S_{val} + SD_σ] level, 4.7 kcal/mol lower than the experimental value of 120.2 kcal/mol.[22] The analogous calculation on RuO^+ yields $D_e(Ru^+{=}O)$ = 62.4 kcal/mol. Using the difference in the experimental and predicted $D_e(O{=}O)$ = 4.7 kcal/mol as an estimate of the correlation error endemic to this level of calculation, we obtain $D_e(Ru^+{=}O)$ = 67.1 kcal/mol as our best estimate for the bond energy of RuO^+. Although the bond energy of RuO^+ is not known, it is very close to the measured bond energy of FeO^+ [$D°(Fe^+{=}O)$ = 69±3 kcal/mol].[3d] Bond strengths are usually thought to increase going down a column of the periodic table, although measurements of Fe^+ and Ru^+ bonds to hydrogen and methyl have recently disputed that intuitive notion, with second row bond energies found to be about 15 kcal/mol weaker than their first row counterparts.[29] Since the bond strengths in O_2-type bonds are dependent on lowering the electron-electron repulsion in the π system, we might have expected RuO^+ to have a weaker bond than FeO^+, since the 4d orbitals of Ru may cause more π repulsion than the small 3d orbitals of Fe.

IV. Discussion and Summary

We have presented results of ab initio calculations on representative early and late transition metal oxo cations, in an effort to understand the fundamental nature of their bonding and reactivity differences. The contrasts in ground state properties of VO^+ and RuO^+ are fully evident in Table VI. The early metal forms a CO-type triple bond with no unpaired electrons on the oxygen ligand, while the late metal forms a biradical O_2-type double bond with one unpaired electron on the oxo group. The charge on oxygen in the two systems reflects the tendency toward ionic bonding for early metal oxides and toward more covalent structures for the late metal oxo compounds. The equilibrium properties of the ground state

of VO^+ are in excellent agreement with the values derived from the photoelectron spectrum of VO.[3g] The ground state properties for RuO^+ are in accord with both RuO porphyrin complexes[27] and FeO^+.[3h] The early metal oxide is characterized by a bond nearly twice as strong as the late metal oxide, with vibrational frequencies and bond lengths commensurate with their relative bond strengths.

These contrasts in properties we have predicted for the simple metal-oxo diatomics are consistent with known reactivity and stability trends. The triply-bonded oxygen of VO^+ has no unpaired electrons on the oxygen and hence VO^+ is expected to be relatively inert. Freiser and co-workers[3i] observed precisely this behavior, with the oxo ligand unreactive toward a variety of hydrocarbon substrates. Further testimony of the unreactive nature of a triply-bonded metal-oxo is provided by the vanadyl cation, VO^{2+}, which is used as an ESR-active probe of proteins because it does not react with substrates.[5] On the other hand, we expect RuO species to be reactive due to the radical character on the oxygen. Consistent with this hypothesis, isoelectronic FeO complexes are known to oxidize hydrocarbons to alcohols,[8b]FeO^+ in the gas phase forms H_2O from reaction with alkanes,[3h,12] RuO bipyridyl complexes are active oxygen atom transfer catalysts,[7] and RuO_4 is an exceedingly powerful oxidizing agent.[4] Sample reactions expected for RuO/FeO systems are shown below.

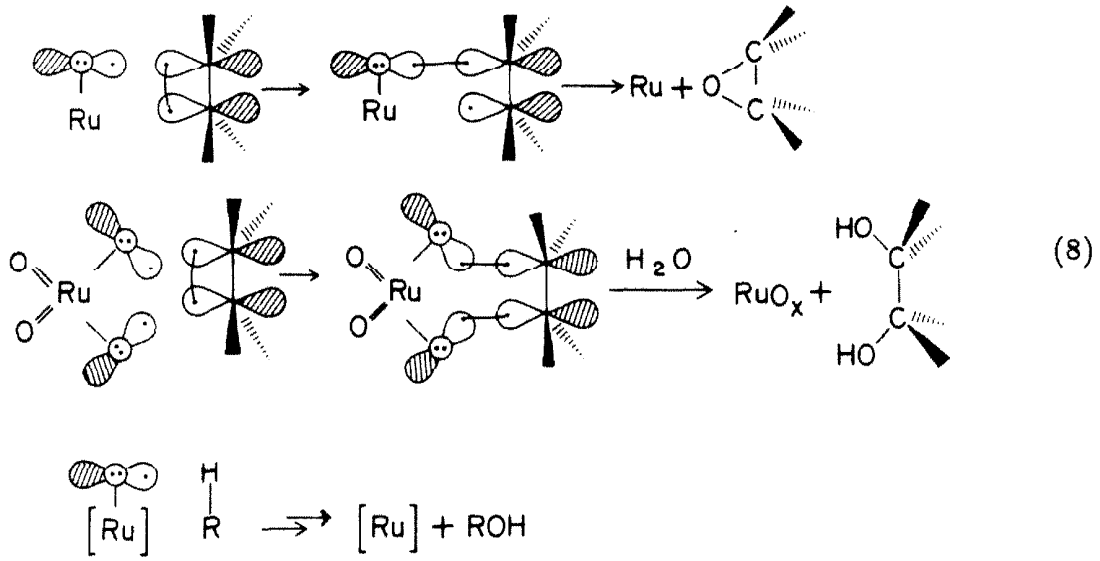

(8)

The reactivity discussed above can be understood entirely in terms of the metal-oxo bond character. If we can predict the M-O bond character as a function of the metal, then we can predict its reactivity. We divide the transition metals into three groups based on their expected behavior:

(i) Due to their empty d-orbitals, early transition metals (e.g., Sc, Ti, and V) can form triple CO-type bonds in which all of the electrons at O are paired up with the metal, rendering the oxygen inert. The early metals cannot form the biradical O_2-type bond since they have no doubly-occupied d-orbitals necessary for resonance.

(ii) The Cr and Mn triads have no empty d-orbitals and no doubly-occupied orbitals. As a result, these metals have no choice but to form conventional double bonds involving one σ and one π bond and are expected (and found experimentally[3a]) to be moderate in their reactivity.[30]

(iii) The group VIII metals cannot readily form triple bonds since they have no empty d-orbitals for the oxygen lone pair to donate into. However, the group VIII metals can form the very reactive, biradical O_2-type double bonds since they have doubly-occupied d-orbitals available for the π resonance. The O_2-type double bond should be preferred over conventional σ and π bonds due to π-π repulsion between doubly-occupied metal d-orbitals and the doubly-occupied oxygen p-orbital.

Thus we have shown that the reactivity of metal-oxo systems can be explained in a simple manner by considering how the d-orbital occupation on the metal dictates the type of metal oxygen bond formed, with early metals forming strong unreactive triple bonds and late metals forming weak, reactive biradical double bonds. These are appropriate descriptions of *terminal* metal-oxo bonding only. Future research will focus on the bonding and properties of *bridging* oxides, the preference between terminal and bridging sites, and the relationship between molecular and bulk oxides.

Acknowledgments. This work was supported by the National Science Foundation (Grant No. CHE83-18041) and the Shell Companies Foundation. EAC acknowledges a National Science Foundation predoctoral fellowship (1982-1985), a research grant award from the International Precious Metals Institute and Gemini Industries (1985-1986), and a SOHIO fellowship in Catalysis (1987).

References

(1) a) K. D. Carlson and C. Moser, J. Chem. Phys. **44**, 3259 (1966); b) S. P. Walch and W. A. Goddard III, J. Am. Chem. Soc. **100**, 1338 (1978); c) C. W. Bauschlicher, Jr., P. S. Bagus, and C. J. Nelin, Chem. Phys. Lett. **101**, 229 (1983); d) P. S. Bagus, C. J. Nelin, and C. W. Bauschlicher, Jr., J. Chem. Phys. **79**, 2975 (1983); e) C. W. Bauschlicher, Jr., C. J. Nelin, and P. S. Bagus, J. Chem. Phys. **82**, 3265 (1985); f) C. J. Nelin and C. W. Bauschlicher, Jr., Chem. Phys. Lett. **118**, 221 (1985); g) M. Krauss and W. J. Stevens, J. Chem. Phys. **82**, 5584 (1985); h) C. W. Bauschlicher, Jr. and S. R. Langhoff, J. Chem. Phys. **85**, 5936 (1986); i) M. Dolg, U. Wedig, H. Stoll, and H. Preuss, J. Chem. Phys. **86**, 2123 (1987).

(2) J. F. Harrison, J. Phys. Chem. **90**, 3313 (1986); we note that $\pi \rightarrow \pi*$ transitions using UHF (Unrestricted Hartree-Fock) wavefunctions for TMO cations have been examined by K. Yamaguchi, Y. Takahara, Y. Toyoda, T. Fueno, and K. N. Houk, preprint.

(3) a) H. Kang and J. L. Beauchamp, J. Am. Chem. Soc. **108**, 5663 (1986) and references therein; b) D. L. Hildenbrand, Chem. Phys. Lett. **34**, 352 (1975); c) E. Murad, J. Geophys. Res. **83**, 5525 (1978); d) *idem*, J. Chem. Phys. **73**, 1381 (1980); d) P. B. Armentrout, L. F. Halle, and J. L. Beauchamp, J. Am. Chem. Soc. **103**, 6501 (1981); e) N. Aristov and P. B. Armentrout, J. Am. Chem. Soc. **106**, 4065 (1984); f) J. M. Dyke, B. W. J. Gravenor, R. A. Lewis, and A. Morris, J. Chem. Soc., Faraday Trans. 2, **79**, 1083 (1983); g) J. M. Dyke, B. W. J. Gravenor, M. P. Hastings, and A. Morris, J. Phys. Chem. **89**, 4613 (1985); h) T. C. Jackson, D. B. Jacobson, and B. S. Freiser, J. Am. Chem. Soc. **106**, 1252 (1984); i) T. C. Jackson, T. J. Carlin, and B. S. Freiser, J. Am. Chem. Soc. **108**, 1120 (1986); j) H. Kang and J. L. Beauchamp, J. Am. Chem. Soc. **108**, 7502 (1986).

(4) F. A. Cotton and G. Wilkinson, "Advanced Inorganic Chemistry" (Wiley,

New York, 1980).

(5) a) J. Selbin, Coord. Chem. Rev. **1**, 293 (1966); b) N. D. Chasteen, R. J. DeKoch, B. L. Rogers, and M. W. Hanna, J. Am. Chem. Soc. **95**, 1301 (1973).

(6) A. Streitweiser, Jr. and C. H. Heathcock, "Introduction to Organic Chemistry" (MacMillan, New York, 1976).

(7) a) D. J. Gulliver and W. Levason, Coord. Chem. Rev. **46**, 1 (1982); b) G. J. Samuels and T. J. Meyer, J. Am. Chem. Soc. **103**, 307 (1981).

(8) a) J. P. Collman, J. I. Brauman, B. Meunier, T. Hayashi, T. Kodadek, and S. A. Raybuck, J. Am. Chem. Soc. **107**, 2000 (1985); b) M. J. Nappa and C. A. Tolman, Inorg. Chem. **24**, 4711 (1985).

(9) Covalent metal-oxo bonding configurations for Cr, Mo, and Fe complexes have been discussed previously by: a) A. K. Rappé and W. A. Goddard III, Nature **285**, 311 (1980); b) *idem*, J. Am. Chem. Soc. **102**, 5114 (1980); c) *ibid.* **104**, 448 (1982); d) *ibid.* **104**, 3287 (1982); e) W. A. Goddard III and B. D. Olafson, Ann. New York Acad. Sci. **367**, 419 (1981).

(10) H. Spinrad and R. F. Wing, Annu. Rev. Astron. Astrophys. **7**, 249 (1969).

(11) R. A. Sheldon and J. A. Kochi, "Metal Catalyzed Oxidations of Organic Compounds" (Academic, New York, 1981).

(12) A preliminary study of the reactions of FeO^+ appeared earlier: M. M. Kappes and R. H. Staley, J. Am. Chem. Soc. **103**, 1286 (1981).

(13) This type of triple bond has been proposed for Cr and Mo oxo bonds by Rappé and Goddard (see Ref. 9).

(14) The details of the generalized valence bond method may be found in: (a) W. J. Hunt, T. H. Dunning, Jr., and W. A. Goddard III, Chem. Phys. Lett. **3**, 606 (1969); W. A. Goddard III, T. H. Dunning, Jr., and W. J. Hunt, Chem. Phys. Lett. **4**, 231 (1969); W. J. Hunt, W. A. Goddard III, and T.

H. Dunning, Jr., Chem. Phys. Lett. **6**, 147 (1970); W. J. Hunt, P. J. Hay, and W. A. Goddard III, J. Chem. Phys. **57**, 738 (1972); F. W. Bobrowicz and W. A. Goddard III in "Methods of Electronic Structure Theory", H. F. Schaefer, ed., Plenum Publishing Corporation, 1977, pp 79-127; (b) L. G. Yaffe and W. A. Goddard III, Phys. Rev. A **13**, 1682 (1976).

(15) E. A. Carter and W. A. Goddard III, *Chem. Phys. Lett.*, submitted for publication.

(16) T. H. Dunning, J. Chem. Phys. **53**, 2823 (1970).

(17) S. Huzinaga, J. Chem. Phys. **42**, 1293 (1965).

(18) The oxygen d-exponent was optimized for H_2O by R. A. Bair and W. A. Goddard III, submitted for publication.

(19) a) A. K. Rappé and W. A. Goddard III, to be published. This basis set was optimized for the d^n configuration of the metal as discussed in A. K. Rappé, T. A. Smedley, and W. A. Goddard III, J. Phys. Chem. **85**, 2607 (1981). b) The HF ^5F - ^5D state splitting for V^+ with this basis is 7.3 kcal/mol, which may be compared with the NHF value of -3.5 kcal/mol [R. L. Martin and P. J. Hay, J. Chem. Phys. **75**, 4539 (1981)] and the experimental value (averaged over J-states) of 7.6 kcal/mol (C. E. Moore, "Atomic Energy Levels", NSRDS-NBS-35, 1971).

(20) We obtained one-electron orbitals from the RCI-MCSCF natural orbitals by freezing all orbitals other than GVB pairs and running one GVB-PP iteration to obtain the GVB-PP CI coefficients which tranform the natural orbitals to one electron orbitals. We did not allow any mixing to occur between GVB pairs.

(21) E. A. Carter and W. A. Goddard III, J. Phys. Chem. **88**, 1485 (1984).

(22) K. P. Huber and G. Herzberg, "Constants of Diatomic Molecules" (Van Nostrand, New York, 1979).

(23) J. Sugar and C. Corliss, J. Phys. Chem. Ref. Data **7**, 1191 (1978).

(24) B. J. Moss and W. A. Goddard III, J. Chem. Phys. **63**, 3523 (1975).

(25) a) R. A. Bair and W. A. Goddard III, submitted for publication; b) R. A. Bair, Ph. D. Thesis, California Institute of Technology, 1981.

(26) a) E. A. Carter and W. A. Goddard III, J. Am. Chem. Soc. **108**, 2180 (1986); b) *ibid.*, to be submitted.

(27) a) C.-M. Che, K.-Y. Wong, and T. C. W. Mak, J. Chem. Soc., Chem. Commun., 546 (1985); b) C.-M. Che, T.-W. Tang, and C.-K. Poon, J. Chem. Soc., Chem. Commun., 641 (1984).

(28) The GVB-RCI(2/4)(opt) wavefunction for the CO-type bonding in RuO^+ ($^2\Sigma^+$) is a self-consistently optimized RCI within the two GVB π pairs (two natural orbitals per pair), simultaneously allowing both occupations of the three σ electrons in the Ru dσ and the O pσ orbital. This level of calculation maintains the same degrees of freedom (e.g., the same number of orbitals and the same correlations) as the GVBCI(opt) wavefunction for the O_2-type bonding in RuO^+.

(29) M. L. Mandich, L. F. Halle, and J. L. Beauchamp, J. Am. Chem. Soc. **106**, 4403 (1984).

(30) If metals from the Cr or Mn triads are oxidized, it is then possible to form triple bonds due to the vacated metal d-orbitals. See Ref. 9.

Table I. First Row Transition Metal-Oxo Bond Strengths (kcal/mol).[a]

metal	$D^o(M^+–O)$	$D^o(M–O)$
Sc	159±7	161.5±3
Ti	161±5	158.4±2
V	131±5	146±4
Cr	85.3±1.3	110±2
Mn	57±3	85±4
Fe	69±3	93±3
Co	64±3	87±4
Ni	45±3	89±5

a) Taken directly from Ref. 3a.

Table II. The Valence Double-ζ Basis Set (Ref. 19) for Vanadium: Cartesian Gaussian Functions with Exponents (α_i) and Contraction Coefficients (C_i).

type	α_i	C_i
s	6713.0	0.0201562
s	1013.0	0.1395721
s	228.5	0.4823097
s	62.12	0.4967414
s	88.72	−0.1201452
s	13.91	0.4562692
s	5.277	0.6323929
s	8.688	−0.2174606
s	1.517	0.5246311
s	0.5481	0.6086236
s	0.8189	−0.3913214
s	0.07869	1.1016545
s	0.03017	1.0000000
p	281.1	0.0313639
p	65.29	0.1952724
p	19.81	0.5207761
p	6.575	0.4320400
p	4.293	0.0553142
p	1.928	0.5331482
p	0.5894	0.5245114
p	1.462	−0.2289791
p	0.09538	1.0105803
p	0.02774	1.0000000
d	21.18	0.0416242
d	5.566	0.2040699
d	1.753	0.4524271
d	0.5256	0.5663618
d	0.1336	1.0000000

Table III. Comparison of Adiabatic Bond Energies (D_e) for VO^+ and CO (kcal/mol).[a]

	total energies (hartrees)				
calculation	VO^+ ($^3\Sigma^-$)	CO ($^1\Sigma^+$)	O (^3P)[b]	$D_e(V^+ \equiv O)$[c]	$D_e(C \equiv O)$[d]
HF	−1016.38880 (1/1)	−112.75712 (1/1)	−74.80059 (1/1)	−11.1	170.6
GVB(3/6)-PP	−1016.48099 (6/6)	−112.81849 (6/6)	"	46.8	209.1
GVB-RCI(3/6)	−1016.56530 (27/126)	−112.87721 (27/37)	"	99.7	246.0
GVB-RCI(3/6) (opt)	−1016.57823 (27/126)	−112.87909 (27/37)	"	107.8	247.2
RCI(3/6)*S_{corr} (opt)	−1016.59051 (81/582)	−112.88198 (81/139)	−74.80148 (5/9)	115.0	248.4
RCI(3/6)(opt)*S_{val}	−1016.59666 (747/4778)	−112.88343 (351/649)	−74.80161 (33/53)	118.7	249.2
Experiment				131±5[e]	258.8[f]
$D_e + \Delta^g_{corr}$				128.3	—

a) Calculational details are given in Section II. The corresponding number of spatial configurations/spin eigenfunctions for each wavefunction is listed beneath each total energy. *b*) Total energies for ground state O (^3P) are calculated at the level consistent for R = ∞ for each calculation: HF, HF*S_{corr}, and HF*S_{val}. *c*) The wavefunctions for VO^+ all dissociate to HF ground state V^+ (^5D) (total energy = −941.60584 hartrees). *d*) The wavefunctions for CO all dissociate to HF ground state C (^3P) (total energy = −37.68462 hartrees). *e*) Ref. 3e. *f*) Ref. 22. *g*) $\Delta_{corr} = D_e^{expt}(CO) - D_e^{calc}(CO) = 9.6$ kcal/mol.

Table IV. GVBCI(opt) Vertical Excitation Energies for RuO^+ at $R_e(^4\Delta\ RuO^+) = 1.75$ Å (kcal/mol).[a]

state	character[b]	total energy (hartrees)	ΔE
$^2\Delta$	**($^1\Sigma^+$ bond)×(Ru δ^3)** + low spin ($^3\Sigma^-$ bond)×(Ru δ^3)	−4511.97615	37.1
$^2\Sigma^+$	CO-type bond	−4511.98788	29.7[c]
$^2\Sigma^+$, $^2\Sigma^-$	($^1\Delta$ bond)×(Ru δ^3)	−4511.99187	27.2
$^2\Delta$	**low spin ($^3\Sigma^-$ bond)×(Ru δ^3)** + ($^1\Sigma^+$ bond)×(Ru δ^3)	−4512.00239	20.6
$^2\Gamma$	($^1\Delta$ bond)×(Ru δ^3)	−4512.00828	16.9
$^4\Delta$	high spin ($^3\Sigma^-$ bond)×(Ru δ^3)	−4512.03521	0.0

a) Calculational details are given in Section III. *b*) Character of each state describes the coupling between the Ru nonbonding electrons (δ^3) and the Ru-O bond (described by the analogous state of O_2 to indicate the type of Ru-O bond). The dominant character for each $^2\Delta$ state is shown in **boldface**. *c*) The consistent calculation for the CO-type bond in RuO^+ is the RCI(2/4)(opt) calculation described in Ref. 28.

Table V. Comparison of Adiabatic Bond Energies (D_e) for RuO^+ ($^4\Delta$) and O_2 ($^3\Sigma_g^-$) (kcal/mol).[a]

	total energies (hartrees)					
calculation	RuO^+ ($^4\Delta$)	O_2 ($^3\Sigma_g^-$)	Ru^+ (^4F)[b]	O (^3P)[b]	$D_e(Ru^+{=}O)$	$D_e(O{=}O)$
HF	−4511.91327 (1/1)	−149.62855 (1/1)	−4437.18354 (1/1)	−74.80059 (1/1)	−44.5	17.2
GVB(1/2)-PP	−4511.96279 (2/2)	−149.65663 (2/2)	"	"	−13.4	34.8
GVBCI(opt)	−4512.03521 (22/40)	−149.73456 (6/10)	"	"	32.1	83.7
GVBCI*S_{corr}(opt)	−4512.07610 (288/916)	−149.77879 (54/130)	−4437.18429 (5/11)	−74.80148 (5/9)	56.7	110.3
GVBCI(opt)*S_{val}	−4512.08099 (1218/3964)	−149.78138 (154/390)	−4437.18450 (21/48)	−74.80161 (33/53)	59.5	111.8
GVBCI*[S_{corr}(opt) + SD_σ]	−4512.08316 (1990/5300)	−149.78571 (378/846)	−4437.18429 (5/11)	−74.80148 (5/9)	61.1	114.7
GVBCI(opt)*[S_{val} + SD_σ]	−4512.08549 (2656/7616)	−149.78736 (426/966)	−4437.18450 (21/48)	−74.80161 (33/53)	62.4	115.5
Experiment					—	120.2[c]
$D_e + \Delta_{corr}^d$					67.1	—

a) Calculational details are given in Section III. The associated number of spatial configurations/spin eigenfunctions for each calculation is given in parentheses under each total energy. *b*) Total energies for the fragments are calculated at levels consistent for R = ∞ for each calculation (Section III). *c*) Ref. 22. *d*) $\Delta_{corr} = D_e^{expt}(O_2) - D_e^{calc}(O_2) = 4.7$ kcal/mol.

Table VI. Comparison of Properties of VO^+ and RuO^+.

	VO^+		RuO^+	
property	theory[a]	expt	theory[a]	expt
ground state	$^3\Sigma^-$	$^3\Sigma^-$[b]	$^4\Delta$	—
bond order	3	3[c]	2	—
net charge on oxygen[d]	−0.26	—	+0.04	—
R_e(Å)	1.56	1.54±0.01[b]	1.75	1.765[e]
$\omega_e(cm^{-1})$	1108	1060±40[b]	787	855[e]
D_e(kcal/mol)	128.3	131±5[c]	67.1	—

a) This work. *b*) Ref. 3g. *c*) Ref. 3e. *d*) Based on Mulliken populations of the RCI(opt) for VO^+ and GVBCI(opt) for RuO^+ wavefunctions. *e*) The experimental R(Ru=O) and ω(Ru=O) are from a Ru=O porphyrin complex (Ref. 27).

Figure Captions

Fig. 1. The GVB one-electron orbitals for the σ and one π bond (the other is identical) of VO^+ ($^3\Sigma^-$) and CO ($^1\Sigma^+$): a) the V-O σ bond; b) the V-O π bond; c) the CO σ bond; and d) the CO π bond. Contours are from -0.6 to 0.6 a.u. incremented by 0.06 a.u.

Fig. 2. The GVB one-electron orbitals for the σ bond, a doubly-occupied π_u orbital, and a singly-occupied π_g orbital of RuO^+ ($^4\Delta$) and O_2 ($^3\Sigma_g^-$): a) the Ru-O σ bond; b) an Ru-O π_u orbital; c) an Ru-O π_g orbital; d) the O_2 σ bond; e) an O_2 π_u orbital; and f) an O_2 π_g orbital. Contours are from -0.6 to 0.6 a.u. incremented by 0.06 a.u.

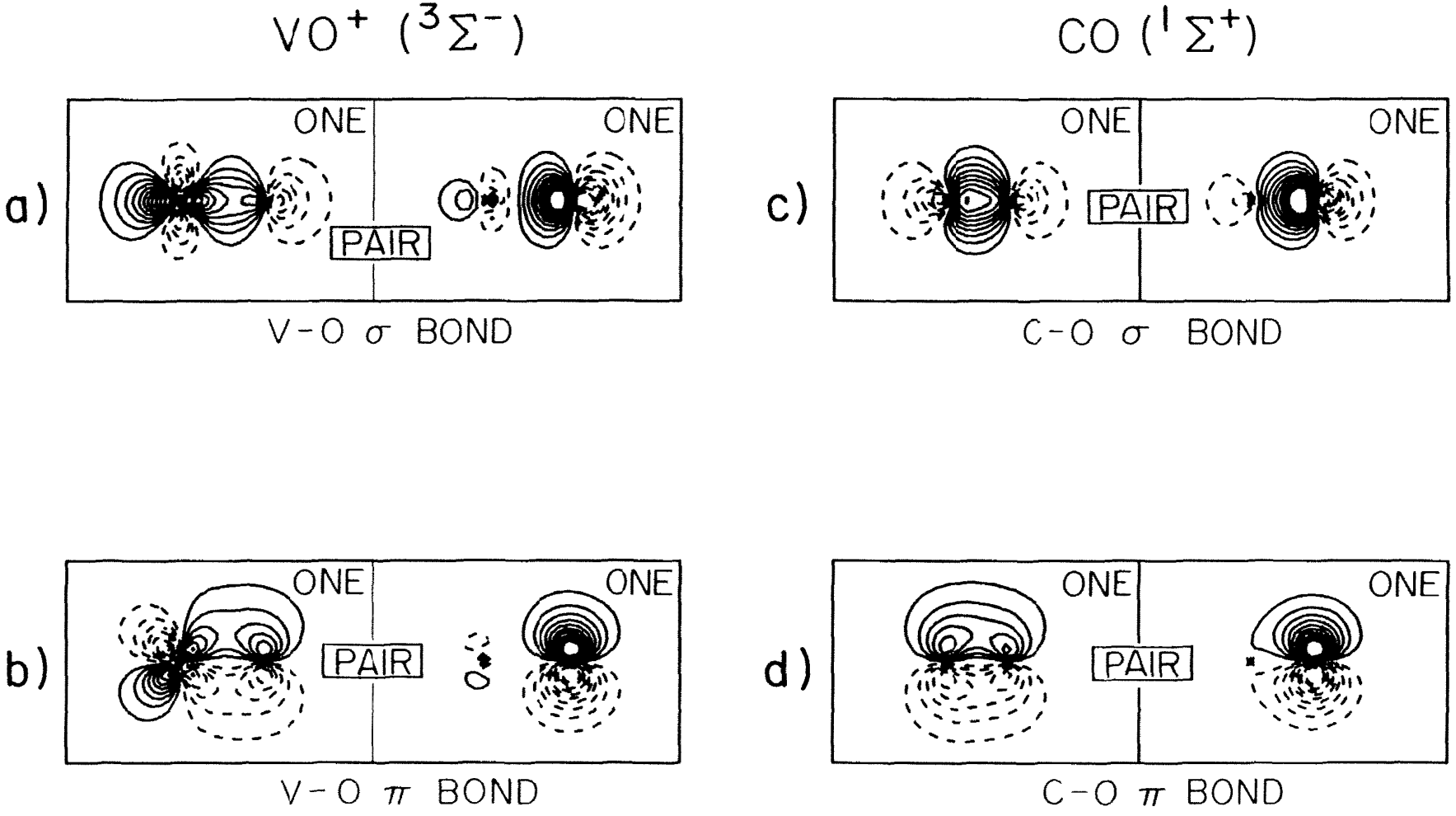
VO+ (3Σ−)
CO (1Σ+)
a)
ONE
ONE
PAIR
V-O σ BOND
c)
ONE
ONE
PAIR
C-O σ BOND
b)
ONE
ONE
PAIR
V-O π BOND
d)
ONE
ONE
PAIR
C-O π BOND

Figure 1.

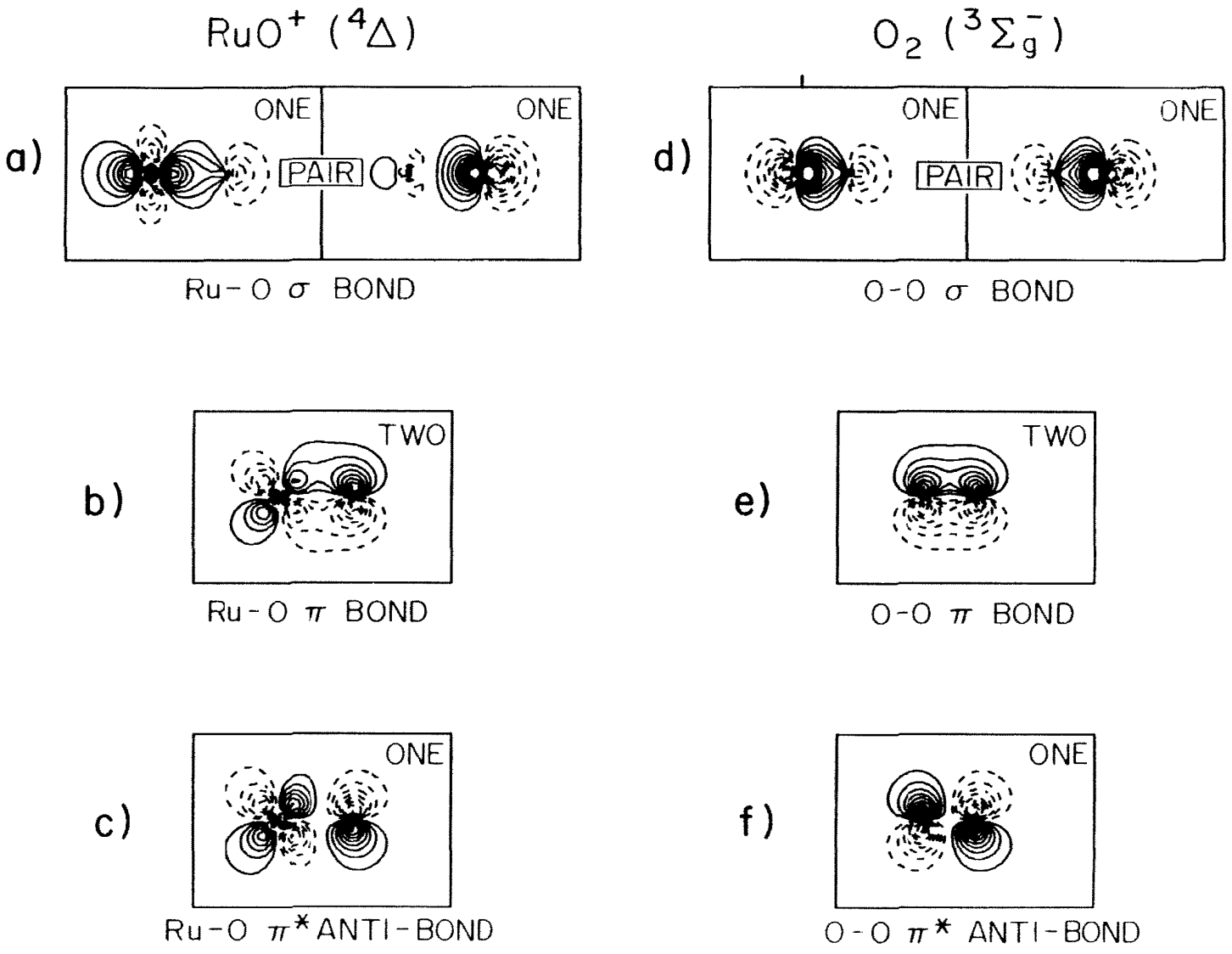
RuO+ (4Δ)
O2 (3Σg−)
a)
ONE
PAIR
ONE
Ru-O σ BOND
d)
ONE
PAIR
ONE
O-O σ BOND
b)
TWO
Ru-O π BOND
e)
TWO
O-O π BOND
c)
ONE
Ru-O π* ANTI-BOND
f)
ONE
O-O π* ANTI-BOND

Figure 2.

Chapter 2.E. The text of this section is an Article coauthored with William A. Goddard III which has been submitted to the *Journal of the American Chemical Society*.

Relationships between Bond Energies in Coordinatively Unsaturated and Coordinatively Saturated Transition Metal Complexes: A Quantitative Guide for Single, Double, and Triple Bonds

Emily A. Carter and William A. Goddard III*

Contribution No. 7567 from the Arthur Amos Noyes Laboratory of Chemical Physics, California Institute of Technology, Pasadena, California 91125

Abstract: A prescription is presented for converting M^+-X bond energies (from experiment or theory) in *unsaturated* complexes to M^+-X bond energies appropriate for coordinatively *saturated* organometallic compounds. The theoretical basis for the predicted conversion factors originates from quantitatively evaluating the consequences of: (i) the loss of high spin coupling (exchange energy) between valence electrons on the unsaturated transition metal ion subsequent to the formation of covalent metal-ligand bonds; (ii) the cost (promotional energy) of bonding to a low-lying excited state of the metal ion (either s^1d^{n-1} or d^n) instead of the ground electronic state; and (iii) the loss of high spin coupling in coordinatively saturated transition metal complexes upon bond formation (assuming a d^n valence electron configuration). These predictions should be most useful for *covalent* metal-ligand bonds in complexes where the metal has at least a +1 oxidation state and where the ligands of interest have electronegativities comparable to carbon or hydrogen. This method is *not* appropriate for prediction of bond strengths where the bonds are primarily of ionic or donor-acceptor character.

I. Introduction

Thermochemical data for organotransition metal compounds are sparse, especially for the coordinatively saturated complexes which are often the important players in transition metal-catalyzed reaction chemistry. However, a growing list of metal-ligand bond energies is becoming available for gas phase metal ions with one ligand attached (M^+–X).[1–4] The bond energies have been determined in a variety of ways, including: (i) the translational energy dependence of endothermic reactions in ion beam experiments;[1] (ii) ion cyclotron resonance (ICR) measurements of proton affinities to derive metal-hydrogen bond strengths;[2] (iii) bracketing bond energies by using Fourier Transform mass spectrometry (FTMS) to study chemical reactions;[3] and (iv) photodissociation studies which yield bond energies from photoappearance thresholds.[4]

While bond energies derived from the above techniques are useful for interpreting the chemistry of gas phase, highly *un*saturated, metal ion complexes, it is unclear how these values can be used for predicting the thermochemistry of the majority of organometallic species, namely for coordinatively saturated, "18-electron" complexes. In order to clarify this relationship, we present a prescription for the conversion of the experimentally or theoretically observed values for coordinatively *unsaturated* transition metal-ligand bond energies to those appropriate for coordinatively *saturated* transition metal-ligand bond strengths, based on examining the differential exchange and promotional costs (vide infra) inherent to bond breaking/making events. For main group X-H bond energies, Goddard and Harding[5] showed that a similar approach using only differential exchange leads to excellent quantitative predictions of trends in the bond strengths of XH_n as a function of n.

We commence with some background on the energetics of bonding to high spin metal ions, concentrating on the costs due to loss of high-spin coupling between valence electrons on the metal center. We also consider whether it is energetically feasible to form bonds to low-lying excited states of the metal ions (either s^1d^{n-1}

or d^n). The energetics involved in forming single, double, and triple bonds to first and second row transition metals (Sc-Ni and Y-Pd) are computed from ab initio calculations of intraatomic exchange integrals and from experimental excitation energies for both the s^1d^{n-1} and d^n states of M^+. We then predict, taking the lowest cost for a given metal and a given bond multiplicity, the quantity ΔK which must be added to bond energies found for the completely unsaturated M^+–X species

$$D^{\text{sat}}_{\text{M}-\text{X}} = D^{\text{unsat}}_{\text{M}-\text{X}} + \Delta K \tag{1}$$

in order to obtain estimates for the corresponding bond energies in coordinatively saturated organometallic complexes. Finally, we conclude by comparing our predictions from this method with some of the few metal-ligand bond energies available for 18-electron complexes.

II. Description of the Method

In a recent paper, Carter and Goddard[6] compared the $M{=}CH_2$ bond energy found for a completely unsaturated molecule, $RuCH_2^+$, with that of a (model) coordinatively saturated complex, $(Cl)(H)Ru^{I}CH_2$. While the metal-carbon bond character is essentially identical in both complexes, the bond energies for the unsaturated and saturated complexes are predicted to differ by 16 kcal/mol. This is typical; as discussed below, the correction term ΔK can be as large as 60 kcal/mol, yet we find that changes in metal valence electron spin coupling and (possible) promotional energies adequately account for the trends in transition metal-ligand bond energies.

For isolated metal ions (or atoms), the ground electronic state always has the singly-occupied valence orbitals coupled to form the highest spin state, as predicted by Hund's rule (e.g., Ru^+ in its ground state configuration of $4d^7$ has $S = \frac{3}{2}$). The quantitive basis for Hund's rule is the energy lowering contributed by exchange interactions in the electronic energy expression:[7]

$$E_{\text{ex}} = -\sum_{i>j} K_{i\alpha,j\alpha} - \sum_{i>j} K_{i\beta,j\beta}. \tag{2}$$

These exchange terms are only nonzero between electrons of the same spin. Therefore, the lowest energy state of M^+, whether it be s^1d^{n-1} or d^n, is always high spin.

For m high spin-coupled electrons, there are $\frac{m(m-1)}{2}$ exchange terms, each leading to a lowering of the electronic energy. However, upon covalent bond formation, some of this exchange energy is lost, weakening the intrinsic metal-ligand bond. This loss of exchange energy results from necessarily singlet-coupling the electrons in each metal-ligand bond pair. On average, then, the metal electrons involved in covalent bonding have α (up) spin half of the time and β (down) spin half of the time. This results in partial quenching of intraatomic exchange stabilization. The magnitude of this effect depends on the number of other (non-bonding) singly-occupied orbitals on the metal (as well as the magnitude of each exchange term) and therefore it depends on the degree of saturation at the metal center.

For example, a two electron triplet ($\chi_{spin} = \alpha\alpha$) has one exchange term (-K) in its energy expression. Making a single bond to one of these electrons changes the spin coupling between the two formerly high spin electrons to

$$\chi_{spin} = \frac{1}{2}[\alpha\alpha + \alpha\beta], \tag{3}$$

due to the averaged spin of the bonding electron. This spin function results in an exchange contribution of only -$\frac{1}{2}$K and a net energy destabilization of +$\frac{1}{2}$K. A three electron quartet ($\chi_{spin} = \alpha\alpha\alpha$) has a -3K exchange energy. Forming a single covalent bond to the quartet results in the spin function

$$\chi_{spin} = \frac{1}{2}[\alpha\alpha\alpha + \alpha\alpha\beta], \tag{4}$$

with an exchange energy now of only -2K, a destabilization of +1K. Thus, we see that the exchange loss grows as the number of unpaired electrons grows (or as the degree of unsaturation grows).

In this manner, it is easy to compute the loss of exchange energy upon covalent bond formation for single, double, and triple bonds by merely considering the effect

of averaged spin-coupling for bonding electrons. In the case of transition metals, d-d exchange terms are nearly always much larger than s-d exchange terms. Thus, for metals with a high spin d^n ground state, it may be advantageous to promote an electron from a valence d-orbital to the valence s-orbital (forming the s^1d^{n-1} state), since bonding to an s-electron will result in less exchange loss. Therefore, we shall consider the costs for forming single, double, and triple covalent bonds to the first and second row metal ions in both the high spin s^1d^{n-1} and d^n electronic states.

Table I symbolically displays the cost of covalent bond formation in these cases, where E_{lost} is the sum of the exchange and any promotional (excitation) energy destabilization. Exchange loss peaks in the middle of each row and hence we expect the Cr and Mn triads to have the weakest bonds (in completely unsaturated metal ion complexes), consistent with many experimental[1-4] and theoretical[8-10] observations. Table II provides ab initio values of $sd \equiv K_{sd}^{avg}$ and $dd \equiv K_{dd}^{avg}$ from averaged-field Hartree-Fock calculations on each ion (Sc^+-Ni^+ and Y^+-Pd^+)[11] and excitation energies, $E_p(s^1d^{n-1} \rightarrow d^n$ and $d^n \rightarrow s^1d^{n-1})$.[12] These numbers are used to evaluate each entry in Table I, with the results displayed in Table III. For the remaining discussion, we will utilize the values in **boldface**, which represent the lowest energy cost to form a particular bond to a particular metal ion.

In order to predict metal-ligand bond strengths for saturated systems, we first must define an *intrinsic* (exchangeless) bond energy

$$D_{int} = D^{unsat} + E_{lost}^{unsat}, \tag{5}$$

where D^{unsat} is the observed bond strength of the unsaturated complex and E_{lost} is taken from Table III. D_{int} is the bond energy one would observe if no promotional or exchange losses were incurred. To obtain the bond energy of a corresponding saturated complex, D^{sat}, we must subtract from D_{int} the exchange and/or promotional costs associated with forming covalent bonds in the *saturated system*. Therefore, we obtain

$$\begin{aligned} D^{\mathbf{sat}} &= D_{int} - E^{\mathbf{sat}}_{\mathbf{lost}} \\ &= D^{\mathbf{unsat}} + (E^{\mathbf{unsat}}_{\mathbf{lost}} - E^{\mathbf{sat}}_{\mathbf{lost}}) \\ &= D^{\mathbf{unsat}} + \Delta K. \end{aligned} \tag{6}$$

In order to calculate $E^{\mathbf{sat}}_{\mathbf{lost}}$, we assume that the metal prefers a d^n configuration in a saturated complex, since repulsive interactions between the metal and its ligands should disfavor occupation of the valence s-orbital. Bonding to a d^n configuration in a saturated complex leads to the following exchange losses (and no promotional costs since we assume a d^n ground state):

$$E^{\mathbf{sat}}_{\mathbf{lost}} = K^{\mathbf{sat}}_{\mathbf{lost}} = \begin{cases} 0K_{dd}, & \text{single bond} \\ 0.5K_{dd}, & \text{double bond} \\ 1.5K_{dd}, & \text{triple bond.} \end{cases} \tag{7}$$

Using Eq. (7) and the values listed in Table III, we can calculate ΔK of Eq. (6) to determine the conversion factors which transform unsaturated bond energies into saturated bond energies, for each bond multiplicity and for each first and second row transition metal. These differential exchange energies are listed in Table IV. Adding these values to gas phase M^+–X bond energies allows one to estimate metal-ligand bond strengths in 18-electron, coordinatively saturated complexes (or in singlet states of unsaturated complexes). To this end, Table V lists observed unsaturated bond strengths and predicted saturated bond strengths for a number of M^+–H, M^+=CH_2, and M^+ ≡CH bonds. We have not included values for gas phase M^+–CH_3 bond energies, which are much larger than those expected for saturated M-CH_3 bond strengths. This result has been attributed by Mandich *et al.*[1d] to the anomalously large stabilization of the metal methyl cation due to the high polarizability of the (approximately spherical) methyl group. In contrast, we believe that the *planar* CH_2 and CH ligands are not as easily polarizable and no extra stabilization is expected in the bare metal cation complexes. The gross trends in Table V are correct for the saturated systems, with the bond energies

decreasing as we go across a row and increasing as we go down a column. Some exceptions exist, but given current experimental uncertainties we believe that these discrepancies tag systems worthy of additional experimental study.

The predictions for saturated bond energies mostly await experimental verification. However, a few bond energies have been measured, and these are compared to our predicted values in Table VI. The agreement is generally quite good, but as this model does *not* account for changes at the metal center due to the electron withdrawing or electron-donating character of the ancillary ligands, we see variations in the experimentally observed bond strengths as the ligand set is altered.

The largest discrepancies occur for $(CO)_5Fe^+$-H and $(CO)_4Ni^+$-H, where the most recent experiments yield 72.4±3.6 and 52.8±2.2 kcal/mol, respectively, whereas the theory yields 57.0±4 and 38.5±1.4 kcal/mol. On the other hand, the binary carbonyl hydride bond energies for Cr and Mo agree well with our predictions (55.9±2.4 versus 60.7±2 kcal/mol for Cr and 63.1±2.2 versus 67.8±3 kcal/mol for Mo). Experimental bond energy determinations in these cationic systems rely on the accuracy of the ionization potentials (IP's) of the neutral carbonyls. Experimental IP data always provide upper bounds to the true adiabatic IP's, since structural relaxation of the resultant cations is not always observed on the time scale of the experiments. (If vibrational fine structure is observed, it is still difficult to determine the 0-0 transition.) Thus, for those cations which have the ability to relax geometrically, the observed IP's of the corresponding neutrals are upper bounds, leading to upper bounds on the bond energies. Since $Cr(CO)_6$ and $Mo(CO)_6$ are low spin octahedral with $(t_{2g})^6$ configurations, they are unlikely to change geometries upon ionization. Hence, the measured IP's are close to the adiabatic IP's, leading to adiabatic bond energies. For $Fe(CO)_5$ and $Ni(CO)_4$, however, structural relaxation upon ionization is likely, due to the change in occupation of d-orbitals overlapping the ligands [in contrast to $Cr(CO)_6$ and $Mo(CO)_6$]. Indeed, recent analysis of the photoelectron spectrum of $Ni(CO)_4$ led to a decrease in the experimental $(CO)_4Ni^+$-H bond energy by 7.4 kcal/mol (due to the decrease in the measured IP)

and revealed a distortion from T_d to D_{2d} symmetry upon ionization.[13] With such structural relaxation occurring, the observed IP's are upper bounds, leading to bond energies which are also upper bounds for Fe and Ni carbonyl hydride cations. To bring the experimental values in line with the theoretically predicted bond energies would require decreasing the observed IP's of $Fe(CO)_5$ and $Ni(CO)_4$ by 0.67 eV and 0.62 eV, respectively.

III. Summary

A simple method has been derived which accurately predicts bond strengths in *coordinatively saturated* organotransition metal complexes from values currently available for coordinatively unsaturated M^+–X bond strengths. The analysis is based on calculating the differential exchange and promotional losses which necessarily accompany covalent bond formation. The assumptions made in the derivation are: (i) that exchange and promotional energy effects dominate orbital hybridization and overlap contributions to the determination of bond strength conversion factors (inaccuracies in the method are no doubt due to this simplifying assumption)[14] and (ii) that metal centers in coordinatively saturated complexes have d^n electronic ground states.

The prescription as outlined above should be appropriate for 18-electron (or singlet states of even electron) metal complexes with oxidation states of at least +1. The approach is designed for predicting metal-ligand bond energies where the ligand is either a hydrocarbon moiety or hydrogen (i.e., where covalent bonding prevails). It is *not* designed to predict bond strengths for ionic (e.g., cyclopentadienyl, oxo, halide) or donor-acceptor (e.g., CO or Fischer carbene) metal-ligand interactions.

Acknowledgments. This work was supported by the National Science Foundation (Grant No. CHE83-18041) and the Shell Companies Foundation. EAC acknowledges a National Science Foundation predoctoral fellowship (1982-1985), a research grant award from the International Precious Metals Institute and Gemini Industries (1985-1986), and a SOHIO fellowship in Catalysis (1987). We also thank J. L. Beauchamp for providing experimental data prior to publication.

References

(1) a) Armentrout, P. B.; Beauchamp, J. L. *J. Am. Chem. Soc.* **1981**, *103*, 784; b) Armentrout, P. B.; Halle, L. F.; Beauchamp, J. L. *J. Am. Chem. Soc.* **1981**, *103*, 6501; c) Halle, L. F.; Armentrout, P. B.; Beauchamp, J. L. *Organometallics* **1982**, *1*, 963; d) Mandich, M. L.; Halle, L. F.; Beauchamp, J. L. *J. Am. Chem. Soc.* **1984**, *106*, 4403; e) Tolbert, M. A.; Beauchamp, J. L. *J. Am. Chem. Soc.* **1984**, *106*, 8117; f) Aristov, N.; Armentrout, P. B. *J. Am. Chem. Soc.* **1986**, *108*, 1806; g) Elkind, J. L.; Armentrout, P. B. *Inorg. Chem.* **1986**, *25*, 1078.

(2) a) Beauchamp, J. L.; Stevens, A. E.; Corderman, R. R. *Pure & Appl. Chem.* **51**, pp. 967-978; b) Stevens, A. E.; Beauchamp, J. L. *J. Am. Chem. Soc.* **1981**, *103*, 190.

(3) Jacobsen, D. B.; Freiser, B. S. *J. Am. Chem. Soc.* **1985**, *107*, 5870.

(4) a) Hettich, R. L.; Jackson, T. C.; Stanko, E. M.; Freiser, B. S. *J. Am. Chem. Soc.* **1986**, *108*, 5086; b) Hettich, R. L.; Freiser, B. S. *J. Am. Chem. Soc.* **1986**, *108*, 2537.

(5) Goddard III, W. A.; Harding, L. B. *Ann. Rev. Phys. Chem.* **1978**, *29*, 363.

(6) Carter, E. A.; Goddard III, W. A. *J. Am. Chem. Soc.* **1986**, *108*, 2180.

(7) The changes in electrostatic energy from configuration to configuration involve changes in both coulomb and exchange integrals and hence it is not strictly correct to imply that only exchange interactions are responsible for high spin ground states. However, use of averaged exchange terms (weighted by the number of terms of a given type, e.g., one $\delta\bar{\delta}$ versus four $\pi\delta$) from averaged-field orbitals (see ref. 11 below), leads to sufficiently accurate results for our considerations (and keeps the method simple enough to apply easily).

(8) Carter, E. A.; Goddard III, W. A. *J. Phys. Chem.* **1984**, *88*,1485.

(9) Brusich, M. J.; Goddard III, W. A., unpublished results.

(10) a) Schilling, J. B.; Goddard III, W. A.; Beauchamp, J. L. *J. Am. Chem. Soc.*

1986, *108*, 582; b) *idem*, submitted.

(11) Carter, E. A.; Brusich, M. J.; Schilling, J. B.; Goddard III, W. A., unpublished results. "Averaged-field" means we solve for equivalently-shaped d-orbitals (i.e., if n is the number of d-electrons, then each orbital is constrained to have an occupation of $\frac{n}{5}$ electrons).

(12) Excitation energies (weighted over J-values) are taken from Moore, C. E. *Atomic Energy Levels*, NSRDS-NBS-35, 1971.

(13) Reutt, J. R.; Wang, L. S.; Lee, Y. T.; Shirley, D. A. *Chem. Phys. Lett.* **1986**, *126*, 399.

(14) A possible improvement to this method would involve a quantitative assessment of the relative preference for *d* versus *s* bonding to each metal, based on the intrinsic (exchangeless) bond strengths. However, such intrinsic bond strengths for *s* versus *d* are difficult to extract accurately (see ref. 10b), and application of the method would be considerably more complicated.

Table I. Symbolic Exchange and Promotional Costs for the Formation of Single, Double, and Triple Covalent Bonds to s^1d^{n-1} and d^n Metal Ions.[a]

M^+	ground state	E_{lost}(single bond)		E_{lost}(double bond)		E_{lost}(triple bond)	
		s^1d^{n-1}	d^n	s^1d^{n-1}	d^n	s^1d^{n-1}	d^n
Sc^+	s^1d^1	$\frac{1}{2}sd$	$E_p + \frac{1}{2}dd$	$\frac{1}{2}sd$	$E_p + \frac{1}{2}dd$	—	—
Y^+	s^2	$E_p(s^1d^1) + \frac{1}{2}sd$	$E_p(d^2) + \frac{1}{2}dd$	$E_p(s^1d^1) + \frac{1}{2}sd$	$E_p(d^2) + \frac{1}{2}dd$	—	—
Ti^+, Zr^+	s^1d^2	$1sd$	$E_p + 1dd$	$1sd + \frac{1}{2}dd$	$E_p + \frac{3}{2}dd$	$1sd + \frac{1}{2}dd$	$E_p + \frac{3}{2}dd$
V^+, Nb^+	d^4	$E_p + \frac{3}{2}sd$	$\frac{3}{2}dd$	$E_p + \frac{3}{2}sd + 1dd$	$\frac{5}{2}dd$	$E_p + \frac{3}{2}sd + \frac{3}{2}dd$	$3dd$
Cr^-, Mo^+	d^5	$E_p + 2sd$	$2dd$	$E_p + 2sd + \frac{3}{2}dd$	$\frac{7}{2}dd$	$E_p + 2sd + \frac{5}{2}dd$	$\frac{9}{2}dd$
Mn^+, Tc^+	s^1d^5	$\frac{5}{2}sd$	$E_p + \frac{3}{2}dd$	$\frac{5}{2}sd + 2dd$	$E_p + \frac{5}{2}dd$	$\frac{5}{2}sd + \frac{7}{2}dd$	$E_p + 3dd$
Fe^+	s^1d^6	$2sd$	$E_p + 1dd$	$2sd + \frac{3}{2}dd$	$E_p + \frac{3}{2}dd$	$2sd + \frac{5}{2}dd$	$E_p + \frac{3}{2}dd$
Ru^+	d^7	$E_p + 2sd$	$1dd$	$E_p + 2sd + \frac{3}{2}dd$	$\frac{3}{2}dd$	$E_p + 2sd + \frac{5}{2}dd$	$\frac{3}{2}dd$
Co^+, Rh^+	d^8	$E_p + \frac{3}{2}sd$	$\frac{1}{2}dd$	$E_p + \frac{3}{2}sd + 1dd$	$\frac{1}{2}dd$	$E_p + \frac{3}{2}sd + \frac{3}{2}dd$	—
Ni^+, Pd^+	d^9	$E_p + 1sd$	$0dd$	$E_p + 1sd + \frac{1}{2}dd$	—	$E_p + 1sd + \frac{1}{2}dd$	—

a) E_{lost} = total energy lost upon forming single, double, or triple bonds to the high spin valence states of M^+, in the form of promotional energy (E_p) and exchange energy $K_{sd} \equiv sd$ and $K_{dd} \equiv dd$.

Table II. Exchange (K_{sd}^{avg} and K_{dd}^{avg}) and Promotional (E_p) Energies in s^1d^{n-1} and d^n Metal Ions (kcal/mol).[a]

M^+	state	valence electron configuration	$K_{sd}^{avg} \equiv sd$	$K_{dd}^{avg} \equiv dd$	E_p
Sc^+	^3D	s^1d^1	7.3	—	0.0
	^3F	d^2	—	11.3	13.8
Ti^+	^4F	s^1d^2	5.7	15.2	0.0
	^4F	d^3	—	13.3	2.5
V^+	^5D	d^4	—	15.0	0.0
	^5F	s^1d^3	5.5	16.8	7.8
Cr^+	^6S	d^5	—	16.5	0.0
	^6D	s^1d^4	5.0	18.4	35.1
Mn^+	^7S	s^1d^5	4.8	19.8	0.0
	^5D	d^6	—	17.6	41.7
Fe^+	^6D	s^1d^6	5.0	20.9	0.0
	^4F	d^7	—	18.8	5.8
Co^+	^3F	d^8	—	20.0	0.0
	^5F	s^1d^7	4.8	22.1	9.9
Ni^+	^2D	d^9	—	21.2	0.0
	^4F	s^1d^8	4.8	23.3	25.1
Y^+	^3D	s^1d^1	9.9	—	3.7
	^3F	d^2	—	9.3	24.0
Zr^+	^4F	s^1d^2	9.2	11.6	0.0
	^4F	d^3	—	10.8	7.1
Nb^+	^5D	d^4	—	12.2	0.0
	^5F	s^1d^3	8.9	13.0	7.6
Mo^+	^6S	d^5	—	13.4	0.0
	^6D	s^1d^4	8.5	14.2	36.7
Tc^+	^7S	s^1d^5	8.3	15.3	0.0
	^5D	d^6	—	14.3	11.8
Ru^+	^4F	d^7	—	14.6	0.0
	^6D	s^1d^6	7.5	15.6	25.1
Rh^+	^3F	d^8	—	16.1	0.0
	^5F	s^1d^7	7.5	17.1	49.1
Pd^+	^2D	d^9	—	17.1	0.0
	^4F	s^1d^8	7.3	18.0	73.6

a) K_{sd}^{avg} and K_{dd}^{avg} are ab initio values for the *sd* and *dd* exchange integrals from averaged-field Hartree-Fock calculations (ref. 11). The *dd* exchange terms have been averaged over the five types of interactions (i.e., $\sigma\delta$, $\sigma\pi$, $\delta\pi$, $\pi\bar{\pi}$, and $\delta\bar{\delta}$). E_p is the (J-weighted) relative energy of the M^+ excited state (ref. 12).

Table III. Exchange and Promotional Costs (kcal/mol) for the Formation of Single, Double, and Triple Covalent Bonds to s^1d^{n-1} and d^n Metal Ions.[a]

M^+	ground state	E_{lost}(single)		E_{lost}(double)		E_{lost}(triple)	
		s^1d^{n-1}	d^n	s^1d^{n-1}	d^n	s^1d^{n-1}	d^n
Sc^+	s^1d^1	**3.7**	19.5	**3.7**	19.5	—	—
Ti^+	s^1d^2	**5.7**	17.8	**13.3**	22.5	**13.3**	22.5
V^+	d^4	**16.1**	22.5	**32.9**	37.5	**41.3**	45.0
Cr^+	d^5	45.1	**33.0**	72.7	**57.8**	91.1	**74.3**
Mn^+	s^1d^5	**12.0**	68.1	**51.6**	85.7	**81.3**	94.5
Fe^+	s^1d^6	**10.0**	24.6	41.4	**34.0**	62.3	**34.0**
Co^+	d^8	17.1	**10.0**	39.2	**10.0**	**50.3**	—
Ni^+	d^9	29.9	**0.0**	**41.6**	—	**41.6**	—
Y^+	s^2	**8.7**	28.7	**8.7**	28.7	—	—
Zr^+	s^1d^2	**9.2**	17.9	**15.0**	23.3	**15.0**	23.3
Nb^+	d^4	21.0	**18.3**	34.0	**30.5**	40.5	**36.6**
Mo^+	d^5	53.7	**26.8**	75.0	**46.9**	89.2	**60.3**
Tc^+	s^1d^5	**20.8**	33.3	51.4	**47.6**	74.4	**54.7**
Ru^+	d^7	40.1	**14.6**	63.5	**21.9**	79.1	**21.9**
Rh^+	d^8	60.4	**8.1**	77.5	**8.1**	**86.1**	—
Pd^+	d^9	80.9	**0.0**	**89.9**	—	**89.9**	—

a) E_{lost} = total energy lost upon forming single, double, or triple bonds to the high spin valence states of $M^+ = E_p + K_{lost}$ (promotional energy and exchange energy losses). The values in **boldface** correspond to the least energy cost for M^+ to form a given type of covalent bond.

Table IV. Predicted Differential Exchange Energies in kcal/mol ($\Delta K = E_{lost}^{unsat} - K_{lost}^{sat}$) for the Formation of Single, Double, and Triple Covalent Bonds in Coordinatively Saturated Metal Complexes.[a] [Adding ΔK to unsaturated $D(M^+\text{-}X)$ gives estimates for saturated $D(M^I\text{-}X)$.]

	$\Delta K = E_{lost}^{unsat} - K_{lost}^{sat}$		
M^+	single bond	double bond	triple bond
Sc^+	3.7	-2.0	—
Ti^+	5.7	6.7	-6.7
V^+	16.1	25.4	18.8
Cr^+	33.0	49.6	49.6
Mn^+	12.0	42.8	54.9
Fe^+	10.0	24.6	5.8
Co^+	10.0	0.0	20.3
Ni^+	0.0	31.0	9.8
Y^+	8.7	4.1	—
Zr^+	9.2	9.6	-1.2
Nb^+	18.3	24.4	18.3
Mo^+	26.8	40.2	40.2
Tc^+	20.8	40.5	33.3
Ru^+	14.6	14.6	0.0
Rh^+	8.1	0.0	62.0
Pd^+	0.0	81.4	64.3

a) E_{lost}^{unsat} values are taken from Table III. K_{lost}^{sat} = 0 K_{dd} for a single bond, $\frac{1}{2}K_{dd}$ for a double bond, and $\frac{3}{2}K_{dd}$ for a triple bond (assuming the saturated complex has a local metal electron configuration of d^n). K_{dd} values (for d^n M^+) are taken from Table II.

Table V. Predicted Coordinatively Saturated M-X Bond Energies from Coordinatively Unsaturated M-X Bond Energies [D^{sat}_{pred} (M^I–X) = D^{unsat}(M^+–X) + ΔK] in kcal/mol.

M^+	$D^{unsat}(M^+–H)$	$D^{sat}_{pred}(M^+–H)$	$D^{unsat}(M^+=CH_2)$	$D^{sat}_{pred}(M^+=CH_2)$	$D^{unsat}(M^+ \equiv CH)$	$D^{sat}_{pred}(M^+ \equiv CH)$
Sc^+	55.3±2[a]	59.0±2	97±6[d]	95±6		
Ti^+	55.1±2[a]	60.8±2	85±6[d]	91.7±6		
V^+	47.3±1.4[a]	63.4±1.4	76±2[d]	101.4±2	114±2[d]	132.8±2
Cr^+	27.7±2[a]	60.7±2	49.6,[e]52±3[d]	99.2,101.6±3		
Mn^+	47.5±3.4[a]	59.5±3.4	58.4[f]	101.2		
Fe^+	47.0±4[a]	57.0±4	69.2,[f]82±5[g]	93.8,106.6±5	101±7[g]	106.8±7
Co^+	45.5±2.3[a]	55.5±2.3	84±5[g]	84±5	100±7[g]	120.3±7
Ni^+	38.5±1.4[a]	38.5±1.4	(86±6)[h]	(117±6)		
Y^+	58±3[a]	66.7±3				
Zr^+	54±3[a]	63.2±3				
Nb^+	53±3[a]	71.3±3				
Mo^+	41±3[a]	67.8±3				
Tc^+	46.3[b]	67.1				
Ru^+	41±3[c]	55.6±3	73.6[i]	88.2		
Rh^+	42±3[c]	50.1±3	94±5[j]	94±5		
Pd^+	45±3[c]	45±3				

a) ref. 1g. *b*) ref. 10b. *c*) ref. 1d. *d*) ref. 1f. *e*) ref. 8. *f*) ref. 9. *g*) ref. 4b. *h*) ref. 1b. The value is placed in parentheses to emphasize its uncertainty. *i*) ref. 6. *j*) ref. 3.

Table VI. Comparison of Observed and Predicted Coordinatively Saturated (18-Electron) Metal-Ligand Bond Energies (kcal/mol).

complex	$D^{sat}_{obs}(L_nM^+ - X)^a$	$D^{sat}_{pred}(M^+ - X) = D^{unsat}(M^+ - X)^b + \Delta K^c$
$(CO)_6Cr^+$–H	55.9±2.4,[d] 58±3[e]	60.7±2
$(CO)_6Mo^+$–H	63.1±2.2,[d] 65±3[e]	67.8±3
$(CO)_5(CH_3)Mn^+$–H	64.8±2.6,[d] 67±3[e]	59.5±3.4
$(CH_3C_5H_4)(CO)_3Mn^+$–H	68.6±3.1,[d] 71±3[e]	59.5±3.4
$(CO)_5(CH_3)Re^+$–H	71.2±3.1,[d] 73±3[e]	67.1[f]
$(CO)_5Fe^+$–H	72.4±3.6,[d] 74±5[e]	57.0±4
$Cp(CO)_2(CH_3)Fe^+$–H	51.2±3.3,[d] 53±3[e]	57.0±4
Cp_2Fe^+–H	52.4±5,[d] 54±5,[e] 56±5[g]	57.0±4
Cp_2Ru^+–H	65.7±3.6,[d] 68±5,[h] 79±5[e]	55.6±3
$Cl(CH_3)Ru$–H	54.1[i]	55.6±3
$Cp(CO)_2Co^+$–H	57±5,[h] 59.5±2.9,[d] 73±5[e]	55.5±2.3
$[(CN)_5Co$–$H]^{3-}_{aq}$	58[j]	55.5±2.3
$Cp(CO)_2Rh^+$–H	55±5,[h] 69.6±2.9,[d] 80±5[e]	50.1±3
$(CO)_4Ni^+$–H	52.8±2.2,[k] 60.2±2.2,[d] 62±3[e]	38.5±1.4
$(CO)_5Mn^+ = CH_2$	104±3[l]	101.2
$(Cl)(H)Ru{=}CH_2$	90.3[i]	88.2

a) Observed M^+–X bond energy in coordinatively saturated complexes (*cs*). *b*) Observed M^+–X bond energy in coordinatively unsaturated complexes (*cu*). *c*) ΔK = the differential cost in exchange and promotional energies between *cs* and *cu*. *d*) Simões, J. A. M.; Beauchamp, J. L., to be published. *e*) Stevens, A. E.; Beauchamp, J. L. *J. Am. Chem. Soc.* **1981**, *103*, 190. *f*) value for $D^{sat}_{pred}(Tc^+$-H) which should be comparable to $D^{sat}_{pred}(Re^+$-H). *g*) Foster, M. S.; Beauchamp, J. L. *J. Am. Chem. Soc.* **1975**, *97*, 4814. *h*) revised version (Beauchamp, J. L., private communication) of reference *e*). *i*) theoretical value: Carter, E. A. and Goddard, W. A., in preparation. *j*) de Vries, B. *J. Catal.* **1962**, *1*, 484. *k*) revised according to new value of the adiabatic IP for $Ni(CO)_4$ from PES spectra (Reutt, J. E.; Wang, L. S.; Lee, Y. T.; Shirley, D. A. *Chem. Phys. Lett.* **1986**, *126*, 399). *l*) Stevens, A. E., Ph.D. Thesis, California Institute of Technology, 1981.

Chapter 3

Modeling Fischer-Tropsch Chemistry: Kinetic and Thermodynamic Predictions

Chapter 3.A. The text of this section is a Communication coauthored with William A. Goddard III which appeared in the *Journal of the American Chemical Society.*

Reprinted from the Journal of the American Chemical Society, 1987, *109*, 579.

Methylidene Migratory Insertion into an Ru–H Bond

Emily A. Carter and William A. Goddard III*

Contribution No. 7409
Arthur Amos Noyes, Laboratory of Chemical Physics
California Institute of Technology
Pasadena, California 91125
Received May 5, 1986

The migratory insertions of CH_x fragments into transition-metal–hydrogen and transition-metal–alkyl bonds have long been proposed as chain initiation and propagation steps in the Fischer–Tropsch synthesis of hydrocarbons.[1] Particularly for ruthenium, an effective heterogeneous catalyst for the production of high molecular weight polymethylenes,[2] there is strong indirect evidence that the chain growth mechanism involves methylidene insertion into growing alkyl chains.[1,3] Several experiments on homogeneous systems point to the facility of direct CH_2 insertions into both M–H and M–R bonds.[4] Thorn and Tulip[5a] proposed that acidification of a hydrido hydroxymethyliridium complex proceeds via a hydridomethyleneiridium intermediate which undergoes CH_2 insertion into the Ir–H bond to yield an iridium methyl complex. Upon hydrogen abstraction from mononuclear metal dimethyl complexes, Thorn and Tulip,[5b] as well as Cooper,[6] Maitlis,[7] and Werner,[8] have postulated the intermediacy of methyl methylidene metal complexes which insert CH_2 into M–CH_3 and then β-hydride eliminate en route to the formation of ethylene hydride complexes. Thus these studies suggest that both the chain initiation and propagation steps in Fischer–Tropsch synthesis may be facile even at a single metal center.

As a model for these important elementary reactions, we have used ab initio quantum mechanical techniques to investigate the migratory insertion of CH_2 into an adjacent Ru–H bond. To our knowledge, these calculations provide the first quantitative description of the energetics of such a reaction, including evaluations of both the activation barrier to insertion as well as the relative stabilities of the reactant and product. The reaction pathway is depicted below

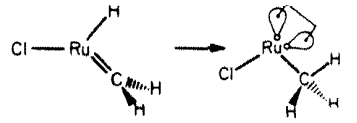

1 2

where **1** is a model for 18-electron complexes such as $(C_5H_5)(PPh_3)Ru(R)(CH_2)$ (**3**) or $[(C_6Me_6)(PPh_3)Ru(CH_3)(CH_2)]^+$ (**4**), the intermediate postulated by Werner.[8] As discussed previously,[9] **1** conforms to the valence bond (VB) view of oxidation states in which electronegative ligands may remove no more than two units of charge from the metal (the easily ionized s-electrons), leaving the other ligands to form covalent bonds to unpaired d-electrons (or to form donor bonds into empty metal valence orbitals). Thus ligands with large electron affinities[10] such as Cp (η^5-C_5H_5) and Cl form rather ionic bonds with the metal valence electrons, while neutral π-donor ligands (e.g., π-aryls) and phosphines require empty metal valence orbitals. Finally, ligands with unpaired electrons (and small electron affinities, e.g., CH_2, CH_3, H, NO, etc.) require unpaired metal d-electrons with which to form covalent bonds. As a result, we believe the singlet state of **1** is a good model for **3** and **4**, since all three complexes have a metal VB oxidation state of +1. Ru(I) is d^7, with three unpaired d-electrons to form covalent bonds to R and CH_2 in **1**, **3**, and **4**.

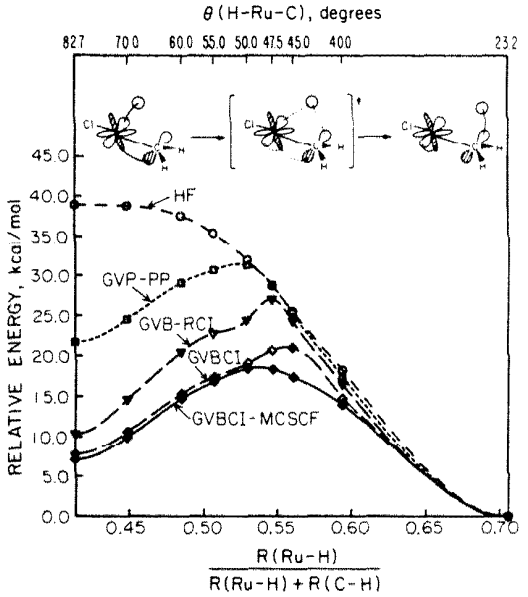

Figure 1. Reaction coordinate for the insertion of CH_2 into Ru–H in **1** to form $ClRu(CH_3)$ (**2**) at the HF, GVB-PP(3/6), GVB-RCI(3/6), GVBCI(3/6), and GVBCI(3/6)-MCSCF levels. Energy (kcal/mol) is plotted relative to the total energy for **2** vs. R(Ru–H)/[R(Ru–H) + R(C–H)] (normalized reaction coordinate). Also shown at the top are the corresponding H–Ru–C angles (deg). The full GVBCI-MCSCF leads simultaneously to a proper description of both the reactant-like and product-like configurations important at the transition state and hence to a smooth potential curve. Some lower level calculations lead to a less smooth transition, the wave function being less capable of simultaneous description of both reactant and product channels.

Consider the process of inserting the CH_2 ligand into the Ru–H bond to form an Ru–CH_3 species. We begin with an Ru–H bond and two Ru–C in-plane bonds (one σ and one π) which are converted to a C–H bond, one Ru–C bond and an Ru d lone pair. Notice that the *presence of the in-plane π-bond*[11] suggests a

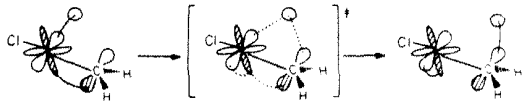

(1) Biloen, P.; Sachtler, W. M. H. *Adv. Catal.* **1981**, *30*, 165.
(2) (a) Anderson, R. B. In *Catalysis*; Emmett, P. H., Ed.; Reinhold: New York, 1956; Vol. IV, pp 237–242. (b) Pichler, H.; Buffleb, H. *Brennst.-Chem.* **1940**, *21*, 257, 273, 285.
(3) (a) Brady, R. C., III; Pettit, R. *J. Am. Chem. Soc.* **1980**, *102*, 6181. (b) *Ibid.* **1981**, *103*, 1287. (c) Baker, J. A.; Bell, A. T. *J. Catal.* **1982**, *78*, 165–181.
(4) The first observation of general alkylidene insertions into M–R bonds was by: Sharp, P. R.; Schrock, R. R. *J. Organomet. Chem.* **1979**, *171*, 43.
(5) (a) Thorn, D. L.; Tulip, T. H. *Organometallics* **1982**, *1*, 1580. (b) Thorn, D. L.; Tulip, T. H. *J. Am. Chem. Soc.* **1981**, *103*, 5984.
(6) Hayes, J. C.; Pearson, G. D. N.; Cooper, N. J. *J. Am. Chem. Soc.* **1981**, *103*, 4648.
(7) Isobe, K.; Andrews, D. G.; Mann, B. E.; Maitlis, P. M. *J. Chem. Soc., Chem. Commun.* **1981**, 809.
(8) Kletzin, H.; Werner, H.; Serhadli, O.; Ziegler, M. L. *Angew. Chem., Int. Ed. Engl.* **1983**, *22*, 46.
(9) Carter, E. A.; Goddard, W. A., III *J. Am. Chem. Soc.* **1986**, *108*, 2180.
(10) The electron affinities of Cp and Cl are 2.2 eV (Rosenstock, H. M.; Draxl, K.; Steiner, B. W.; Herron, J. T. *J. Phys. Chem. Ref. Data* **1977**, *6*, 736–772) and 3.62 eV (Hotop, H.; Lineberger, W. C. *J. Chem. Phys. Ref. Data* **1975**, *4*, 539–576), respectively.
(11) This conformation is the lowest energy orientation for **1**: Carter, E. A.; Goddard, W. A., III, manuscript in preparation.

0002-7863/87/1509-0579$01.50/0

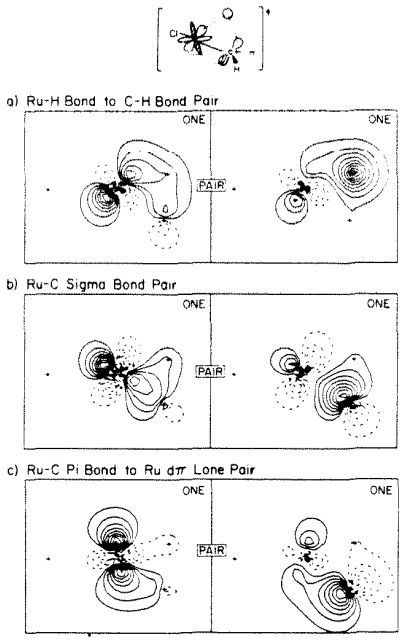

Figure 2. GVB(3/6)PP one-electron orbitals near the transition state (θ(H–Ru–C) = 50.0°). (a) Orbital pair describing the Ru–H bond of the reactant **1** and the C–H bond of the product **2**; (b) orbital pair describing the Ru–C σ-bond for both **1** and **2**; (c) orbital pair describing the Ru–C π-bond of **1** and the Ru dπ lone pair of **2**. Contours are shown at intervals of 0.05 au.

smooth transition from an Ru–H to a C–H bond may be possible, since the in-plane carbon p-orbital is oriented correctly for formation of the in-plane C–H bond. Indeed, at the highest level of theory examined, we find that the CH_2 insertion into Ru–H proceeds with a low activation barrier (11.5 kcal/mol) and is thermodynamically favorable, with an exothermicity of 7.1 kcal/mol, as displayed in the reaction coordinate of Figure 1. Notice that the transition state occurs approximately halfway between reactants and products, as expected for a reaction which is nearly thermoneutral (Hammond postulate).

Figure 2 shows the orbitals near the transition state [θ(H–Ru–C) = 50°]. Here we see that the Ru–H bond smoothly converts into the C–H bond (Figure 2a), while the Ru–C σ-bond (Figure 2b) does not change significantly. At the transition state, the Ru–C π-bond (Figure 2c) has begun to move out of the way of the incipient C–H bond and already has substantial Ru d lone-pair character.[12] The Ru–C and Ru–H bonds at the transition state have lengthened significantly from their values in **1**, increasing from 1.87 to 1.93 Å for Ru–C and from 1.65 to 1.77 Å for Ru–H.

The exothermicity, activation barrier, and transition-state geometry were calculated at five levels of theory, as shown in Figure 1.[13] The geometries along the reaction coordinate were predicted by analytic gradients of Hartree–Fock wave functions,[14] with all geometrical parameters optimized at each H–Ru–C angle.[15] In the highest level of theory considered (the bottom curve of Figure 1), we optimize the six active orbitals (the orbitals actively involved in the insertion, namely, the Ru–H and the Ru–C σ- and π-bond pairs) self-consistently for a full six-electron CI within those six orbitals (all occupations of six electrons in six orbitals—the GVB(3/6)CI-MCSCF level). This level allows a balanced description of the three bond pairs changing during the reaction. Higher level, extended basis dissociation-consistent CI calculations[16] on various dissociation processes involving these species[13] suggest that the true exothermicity is 10.4 kcal/mol, in good agreement with our MCSCF calculations.

In conclusion, we have shown that alkylidene migratory insertions can be quite facile, proceeding with a low activation barrier. These calculations provide the first quantitative evidence for the feasibility of this elementary reaction (previously postulated based on experimental results,[4-8] but never directly observed). These results suggest that for Ru, the reverse reaction of α-hydrogen elimination is subject to a barrier of 18.6 kcal/mol. This is consistent with the fact that α-H eliminations most often occur for the early transition metals. Work in progress on the related reaction of CH_2 insertion into an Ru–alkyl bond suggests an exothermicity of 4.9 kcal/mol. The activation barrier will probably be higher than that for H due to the necessary reorientation of the alkyl upon migration from Ru to CH_2.[17] The alkyl migration differs primarily from the hydride energetics because the incipient C–C bond is weaker than the incipient C–H bond. While our calculations suggest that late transition metals undergo CH_2 insertion with relative ease, early metal alkylidenes have been observed that do *not* insert into M–R bonds. We believe that this is due to the much greater strength of the M–C π-bond for the early transition metals.[18]

Acknowledgment. This work was supported by the Shell Development Co., Houston, TX, and the National Science Foundation (Grant CHE83-18041). E.A.C. gratefully acknowledges the support of a National Science Foundation Predoctoral Fellowship (1982–1985).

(12) By the point at which θ(H–Ru–C) = 40.0°, the Ru d lone pair is fully formed. (The equilibrium geometry of $ClRuCH_3$ has an H–Ru–C angle of 23.2°.)

(13) Full details to be published elsewhere. A valence double ζ quality basis was used.

(14) Hartree–Fock (HF) calculations are known to predict accurate geometries. As a test, we optimized the geometry of **1** at both the HF and GVB-RCI(3/6) levels and found that the two geometries were very similar (e.g., all bond lengths and angles differed by at most 0.03 Å and 11.9°, respectively); see ref 11.

(15) The geometries of **1** and **2** were optimized with no restrictions except the retention of C_s symmetry (lower symmetry cases were found to be higher in energy; ref 11).

(16) Bair, R. A.; Goddard, W. A., III, unpublished results. Bair, R. A. Ph.D. thesis, Caltech, 1980. Carter, E. A.; Goddard, W. A., III *J. Phys. Chem.* **1984**, *88*, 1485. Reference 9.

(17) Low, J. J.; Goddard, W. A., III *Organometallics* **1986**, *5*, 609.

(18) Carter, E. A.; Goddard, W. A., III *J. Am. Chem. Soc.* **1986**, *108*, 4746.

Chapter 3.B. The text of this section is an Article coauthored with William A. Goddard III and is to be submitted to *Organometallics*.

Modeling Fischer-Tropsch Chemistry: the Thermochemistry and Insertion Kinetics of $ClRuH(CH_2)$

Emily A. Carter and William A. Goddard III*

Contribution No. 7583 from the Arthur Amos Noyes Laboratory of Chemical Physics, California Institute of Technology, Pasadena, California 91125

Abstract: The insertions of metal-bound CH_x into M-H and M-CH_3 bonds have been proposed as the chain initiation and propagation steps, respectively, in the Fischer-Tropsch reductive polymerization of CO to form alkanes. As a model for this important elementary reaction, we have examined the properties and migratory insertion reactivity of a prototypical coordinatively saturated complex $ClRuH(CH_2)$ using ab initio methods (generalized valence bond + configuration interaction). The $Ru{=}CH_2$ double bond is covalent, with $D_e(Ru{=}C)$ = 84.7 kcal/mol. The optimum geometry has the CH_2 plane perpendicular to the ClRuH plane, with a rotational barrier of $\geq$13.6 kcal/mol. The lowest energy conformer of the $^1A'$ state of $ClRuH(CH_2)$ has an in-plane π bond, which facilitates the insertion of the CH_2 ligand into the adjacent Ru-H bond. Using analytic gradient techniques combined with MCSCF wavefunctions to find the minimum energy pathway, we find that the insertion proceeds with a moderate barrier (11.5 kcal/mol) and is exothermic by 7.1 kcal/mol. From a thermodynamic cycle designed to probe basis set and electron correlation deficiencies, we estimate an actual barrier to insertion of 10.9$\pm$1.7 kcal/mol and an exothermicity of 10.5$\pm$1.0 kcal/mol (using predicted values of D_e(Ru-H) = 54.1 kcal/mol, $D_e(CH_2\text{-H})$ = 112.9 kcal/mol, and D_e(Ru-CH_3) = 54.3 kcal/mol).

I. Introduction

Ruthenium complexes containing hydrido, alkyl, alkylidene, and alkylidyne ligands have been proposed as intermediates in metal-catalyzed heterogeneous and homogeneous C-H and C-C bond forming processes. In homogeneous reactions, both CH_2 insertion into M-H and M-R bonds to make new metal alkyls[1] and intramolecular alkylidene coupling in binuclear Ru systems to make olefins, have been observed.[2] Catalytic reduction of CO to methanol, ethanol, and ethylene glycol by soluble Ru complexes have also been observed.[3] In the particular heterogeneous case of the Fischer-Tropsch (FT) synthesis of hydrocarbons from CO and H_2, Ru metal is the most active undoped catalyst, readily producing high molecular weight polymethylenes.[4] The insertions of metal-bound CH_x fragments into metal-hydrogen and metal-alkyl bonds are thought to be responsible for the chain initiation and growth steps of the FT reaction.[5]

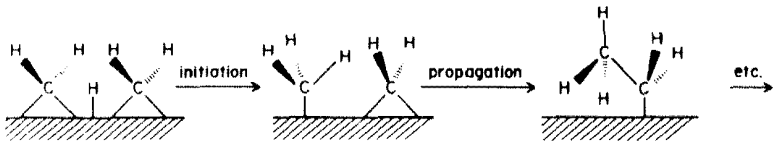

(1)

The mechanism shown in eq 1 is particularly applicable to Ru catalysts since polymethylene may be produced simply through repeated CH_2 insertions into a growing alkyl chain. While methylene on the clean Ru(001) surface has been observed in bridging coordination sites at low temperature,[6] the actual insertion step of eq 1 may well require both reacting species to be coordinated to the same metal atom. Indeed, Thorn and Tulip[1c,1f] have provided evidence for both H and CH_3 migration to CH_2 at an Ir(I) center, while Cooper,[1a,b,g,i,j] Maitlis,[1e] and Werner[1h] have proposed methyl methylidene metal complexes as intermediates during dimethyl rearrangements to olefin hydrides (subsequent to hydrogen abstraction). These studies suggest that both chain initiation and growth may be

achieved at a single metal center. Hence, we have studied a model for the first step of eq 1, in which CH_2 inserts into an adjacent Ru-H bond to form a metal-methyl bond, in the mononuclear organometallic complex shown in eq 2.

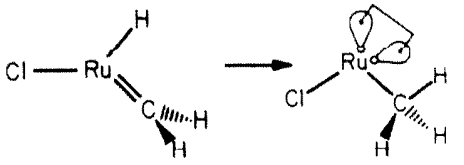

(2)

1 2

As outlined previously,[7] the electronic structure of **1** may be understood using the valence bond (VB) description of oxidation states in which electron-withdrawing ligands such as Cp (η^5-C_5H_5), Cl, or oxo may collectively ionize the metal center up to a maximum of two units of charge (i.e., only the easily ionized valence *s*-electrons), with the rest of the metal valence *d*-electrons forming covalent bonds to less electronegative ligands such as alkyl, aryl, or hydrogen. Donor-acceptor bonds involve donation into empty metal valence *d*, *s*, or *p* orbitals, in order to saturate the metal to eighteen electrons. These bonding rules imply that Cl and Cp will form ionic bonds, π-aryls, phosphines, and CO will make donor bonds, and open shell ligands such as R·, :CH_2, H·, and ·NO will form covalent bonds to unpaired metal *d*-electrons.

Thus, the singlet state of $ClRu(CH_2)H$ (**1**) is a model for 18-electron, coordinatively saturated complexes such as $Cp(PR_3)Ru(R)(CH_2)$, in which the Cp and PR_3 groups are mimicked by the Cl and the low spin state of **1** (the metal must be low spin so that PR_3 and Cp^- have four empty metal orbitals to donate into). $[(C_6Mc_6)(PPh_3)Ru(CH_3)(CH_2)]^+$ (**3**) is another complex for which low spin **1** serves as a prototype, where the phosphine and the π-aryl group again force the metal to a low spin state in order to have empty orbitals available for ligand donation and where the positive charge is mimicked by the chlorine ligand in **1**. Complex **3** has been postulated as an intermediate in the isomerization of a ruthenium dimethyl complex to a ruthenium ethylene hydride via the insertion of CH_2 into an adjacent

Ru-CH_3 bond.[1h]

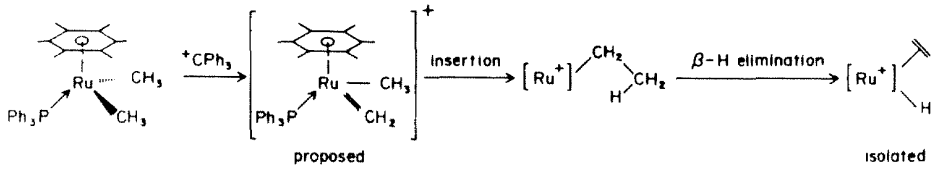

(3)

While CH_2 insertions into adjacent M-H(R) bonds have been indirectly observed for a number of homogeneous organometallic systems,[1] direct observation has eluded researchers until very recently. Magnetization transfer experiments of Bercaw and co-workers[8] directly monitored the insertion of CH_2 into the Ta-H bond of $Cp^*_2Ta(H)(CH_2)$ above room temperature, yielding the 16-electron $Cp^*_2Ta\text{-}CH_3$ complex. The VB oxidation state[7] of Ta in this complex is +2, since the Cp* ligands ($Cp^* = \eta^5\text{-}C_5Me_5$) form ionic bonds to Ta (achieving the aromatic structure of Cp^-), leaving three unpaired *d*-electrons on Ta to form covalent bonds to H and CH_2. The situation is analogous in **1**, where we find that the Cl of Cl-Ru ties up approximately one valence electron from the Ru in an ionic bond, leaving the Ru in a d^7 Ru(I) configuration having three singly-occupied d orbitals available for bonding to H and CH_2.

To date, no direct measurements of kinetic parameters or thermodynamic properties for the migratory insertion of CH_2 into M-H have been reported. Thus, the goal of this work is to examine the nature of this reaction at one metal center, characterizing the qualitative features of the metal-ligand bonding which favor (or disfavor) migratory insertions of CH_2 and predicting the quantitative aspects of the insertion potential energy surface (e.g., the activation barrier and the exothermicity). In the next section, we discuss the equilibrium properties of the hydrido methylidene **1**. Section III presents detailed theoretical results on the migratory insertion itself,[9] while Section IV discusses an independent way of estimating the energetics of the insertion event. Using the newly-developed method of correlation-consistent configuration interaction (CCCI),[10] we obtain the exothermicity and activation barrier to

insertion as a function of both basis set and level of electron correlation via a thermodynamic cycle which utilizes metal-ligand bond energies obtained from CCCI calculations. Section V concludes with some speculations regarding other insertion steps in FT chemistry, while Section VI provides the calculational details.

II. Properties of $ClRu(CH_2)H$

To understand the electronic structure of the $^1A'$ state of **1**, we consider how the ClRu fragment may bond to H and CH_2. As mentioned in the Introduction, the Cl ligand of $ClRu(CH_2)H$ ties up the Ru s-electron (the ground state of Ru atom is s^1d^7) in an ionic bond, leaving a high spin d^7 electronic configuration on Ru. Classifying the five d orbitals with respect to the final molecular plane as σ or π, there are two important configurations of ClRu,

$$(d\sigma_1)^1(d\sigma_2)^1(d\sigma_3)^1(d\pi_1)^2(d\pi_2)^2, \text{ which we denote as } \sigma^3$$

and

$$(d\sigma_1)^1(d\sigma_2)^1(d\sigma_3)^2(d\pi_1)^1(d\pi_2)^2, \text{ which we denote as } \pi\sigma^2.$$

Two high symmetry conformers of **1** exist:[11] a twisted structure **1a** and a planar structure **1b**.

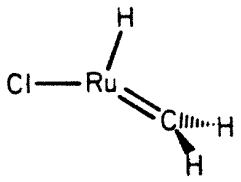

1a

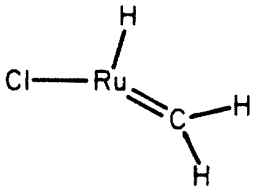

1b

Geometry **1a** has all three M-H and M-C bonds in the H-Ru-C plane, requiring the ClRu σ^3 configuration, while geometry **1b** has an out-of-plane M-C π bond, requiring $\pi\sigma^2$ ClRu.[12]

The one-electron generalized valence bond (GVB) orbitals for both conformers are shown in Figures 1 and 2, where we see that the Ru-H and Ru-C bonds are quite covalent, with each bond pair involving one electron localized in an Ru d

orbital spin-paired with one electron localized on the ligand. In both cases, the CH_2 fragment is best viewed as a *neutral* triplet CH_2 having one electron in each of the σ and π nonbonding orbitals

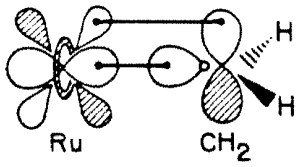

spin-paired with singly-occupied $d\sigma$ and $d\pi$ (or $d\bar{\pi}$, for the in-plane π bond) orbitals on Ru, forming an Ru=C covalent double bond as in ethylene.[7]

The GVB orbital overlaps, metal orbital hybrid character, and electron populations for the metal and the ligand for the three correlated bond pairs for both geometries are listed in Table I. We see that the metal bonding orbitals have 74 to 98% 4d character, with less than 11% ionic character in each bond pair.[13] Approximately 0.5 electron is transferred from the Ru 5s to the Cl in both **1a** and **1b**, so that one should visualize the Ru-Cl bond as partially covalent, involving 5s-5p hybrid character on Ru.

The orbital overlaps for all three bonds in geometry **1a** are larger than the overlaps in geometry **1b**. These differential overlaps are not due to changes in bond length, since the optimum bond lengths for both **1a** and **1b** are very similar (Table II). Geometry **1a** is expected to be more stable than geometry **1b**, since bond overlaps should correlate with stability. Indeed, we find that geometry **1a** (σ^3 bonding) is favored by 13.6 kcal/mol with respect to geometry **1b** ($\sigma^2\pi$ bonding). Thus we predict a lower limit of 13.6 kcal/mol on the Ru=CH_2 rotational barrier.

Denoting the Ru=C and Ru-H axes as z and y, the Ru-C $\bar{\pi}$ bond (π bond in the plane) in **1a** involves the $4d_{yz}$ orbital, while the Ru-C σ and Ru-H bonds involve orbitals that are mainly $4d_{z^2}$ and $4d_{y^2}$. Since the $\bar{\pi}$ bond involves the $4d_{yz}$ orbital, we expect a 90° H-Ru-C bond angle so that the Ru-H and Ru-C σ bond orbitals will be orthogonal to the Ru-C $\bar{\pi}$ bond.

The optimum structural parameters[14] for geometry **1a** are listed in Table II

and depicted below:

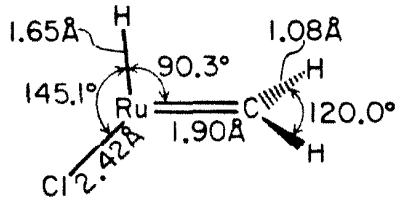

As mentioned in the Introduction, d^3 Ta(II) should form bonds similar to d^7 Ru(I), since both metals have three unpaired d-electrons which can bond to H(R) and CH_2. Thus, the Ru-H and Ru=CH_2 bonds in **1a** should be quite analogous to the Ta-CH_3 and Ta=CH_2 bonds in Schrock's complex $Cp_2Ta(CH_3)(CH_2)$ (**4**).[15] In fact, the Ru=C bond length, the H-Ru-C bond angle, and the perpendicular orientation of CH_2 ligand, all compare well with the values R(Ta=C) = 2.03 Å, θ(CTaC) = 95.6°, and the out-of-plane orientation of the CH_2 ligand found in **4**.[15] Another electronically similar complex to **1** is $Cl(NO)(PPh_3)_2Os(CH_2)$ (**5**), in which the NO and PPh_3 ligands are simulated by the H ligand and the low spin state in **1**. The X-ray structure of **5** reveals an Os=C bond length of 1.92Å and an orientation for the CH_2 ligand which is perpendicular to the N-Os-C plane,[16] in excellent agreement with our results for **1**.

The Ru=CH_2 stretching frequencies are in the range of 740-800 cm^{-1}, which may be compared with 623.6 cm^{-1} for matrix-isolated $FeCH_2$.[17] (No other M=CH_2 vibrational frequencies have been identified.) The Ru=C stretching frequency of **1b** is larger than in **1a** by $\sim$ 50 cm^{-1}. This may be understood in terms of the larger steric repulsions in **1b** relative to **1a**, since the methylidene hydrogens are coplanar with the rest of the molecule in **1b**, whereas they are out of the plane in **1a**. Such steric repulsions induce a harder inner wall of the local potential, leading to an increased Ru=C vibrational frequency. The decrease in the Ru-H vibrational frequency going from **1a** to **1b** may be attributed to the decrease in the overlap in the Ru-H bond (Table I), indicating a shallower potential and thus a lower vibrational frequency in **1b**.

The calculated rotational barrier of 13.6 kcal/mol for **1a** $\rightarrow$ **1b** is smaller than

the lower bound of 21.4 kcal/mol estimated for **4**.[15] This is to be expected, since the Cp ligands in the Ta complex should destabilize the π orbitals required to make the out-of-plane π-bond in **4**, thereby increasing the rotational barrier. In the Ru case, the $d\pi$'s are accessible in energy, leading to a lower rotational barrier for the Ru complex. In a related system, Brookhart[18] has measured the rotational barrier in $Cp(Ph_2PCH_2CH_2PPh_2)FeCH_2^+$ ($Ph = C_6H_5$) to be 10.4 kcal/mol, in reasonable agreement with our results.

The structural coordinates and vibrational frequencies for geometry **1b** (see Table II) are similar except that the H-Ru-C angle opens up to 111.7°, and the H-Ru-Cl angle drops to 93.6°.

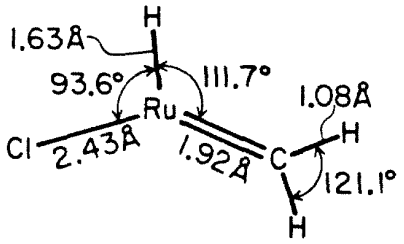

In this case, there is a doubly-occupied dσ orbital bisecting the H-Ru-C bond angle (see Figure 2), and the Ru-H and Ru-C dσ orbitals must stay orthogonal to this orbital, forcing a larger H-Ru-C bond angle. The Cl ligand must also stay orthogonal to the in-plane dσ orbital and thus moves away, resulting in a smaller Cl-Ru-H angle.

As the Ru-C bond distance is increased to break the $Ru{=}CH_2$ bond, **1a** correlates with the ClRuH complex **6a** in the $(\sigma_1)^1(\sigma_2)^1$ triplet state $^3A'$ (σ^3 configuration of ClRu), while **1b** correlates with **6b** in the $(\sigma_1)^1(\pi)^1$ triplet state $^3A''$ ($\pi\sigma^2$ configuration of ClRu).

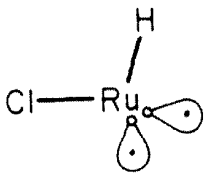

6a

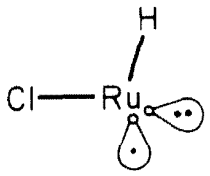

6b

These states of ClRuH are separated by at least 4.2 kcal/mol, with $^3A''$ lower.[19] Thus, even though the lowest triplet state of ClRuH is $\pi\sigma^2$,[11] the favored geometry

of $ClRuH(CH_2)$ ($^1A'$) corresponds to the σ^3 state. This means that the stabilization enjoyed by the σ^3 state of **1a** over the $\sigma^2\pi$ state of **1b** is determined by the Ru-C bonds rather than by the intrinsic energies of the ClRuH fragment. That is, the *in-plane* $\bar{\pi}$ *bond* of **1a** versus the out-of-plane π bond of **1b** contributes to the stabilization of **1a** over **1b**. Consistent with this idea, Table I indicates that the most dramatic increase in orbital overlaps occurs for the out-of-plane π bond (**1b**) converting to an in-plane $\bar{\pi}$ bond (**1a**). Another factor which destabilizes **1b** relative to **1a** is the higher steric (or nuclear) repulsion in **1b**, since all of the atoms are coplanar.

III. Migratory Insertion Kinetics

For the methylidene insertion step (1) relevant to Fischer-Tropsch catalysis, we find the structure **1a**, with the *in-plane* π *bond,* to be the relevant conformation. Consider the transformation of the Ru-H bond and the Ru=C double bond (prior to insertion) to a C-H bond, an Ru-C single bond and an Ru 4d lone pair. We envision a sequence involving the rearrangement of the three in-plane bonding pairs,[20]

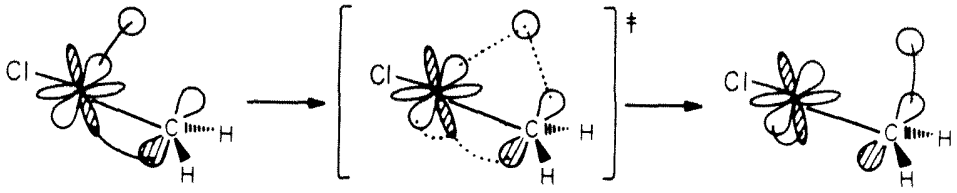

where the Ru-C $\bar{\pi}$ bond must be mixed with the Ru-H σ bond in order to make the new C-H σ bond and an Ru 4d lone pair. Structure **1a** (σ^3) has a carbon *p*-orbital in the H-Ru-C plane (part of the $\bar{\pi}$ bond) which is oriented such that a smooth conversion from Ru-H to C-H is possible, whereas structure **1b** ($\sigma^2\pi$) has a π bond perpendicular to the H-Ru-C plane such that the carbon *p*-orbital needed for the incipient C-H bond is orthogonal to the insertion pathway. This suggests that *only systems containing alkylidenes oriented perpendicular to adjacent bonds* (with an in-plane π bond as in **1a**) will have low barriers to migratory insertion.

In a preliminary report of this work,[9] we showed that the insertion reaction of eq

2 (involving **1a** with its in-plane π bond) is indeed favorable, proceeding with a low barrier of 11.5 kcal/mol and an exothermicity of 7.1 kcal/mol. Figure 3 displays the five levels of theory for which the reaction path was calculated. Analytic gradients of Hartree-Fock (HF, variational molecular orbital theory) wavefunctions were used to optimize the geometries at the nine points shown along the insertion pathway. The H-Ru-C angle was taken to be the reaction coordinate, with each successive H-Ru-C angle held fixed while all other geometrical parameters were optimized (within C_s symmetry). The geometries of **1a** and **2** were optimized using HF gradients with no constraints except the retention of C_s symmetry.[11,21]

Table III, in conjunction with Figure 3, displays the trends in exothermicity and activation energy as a function of increasing electron correlation. Notice that Hartree-Fock theory, while reliable for structural predictions,[21] is in serious disagreement with the highest quality wavefunction, GVBCI-MCSCF (see Section VI), where reaction energetics are concerned. HF predicts a highly exothermic reaction ($\Delta E_{rxn} = -38.9$ kcal/mol) with no barrier, while GVBCI-MCSCF predicts a much more moderate exothermicity of 7.1 kcal/mol and a moderate barrier of 11.5 kcal/mol. The reason HF describes the reaction energetics so poorly is due to the inability of HF theory to properly describe transition metal-ligand multiple bonds. As explained previously,[22] the restriction in HF which forces all orbitals to be doubly-occupied results in a charge-separated species, which is very high in energy. Thus, the metal-carbene bond in **1a** is ill-described and the reactant is therefore highly destabilized, leading to an artificially large exothermicity. HF-Slater transition state theory predictions of large exothermicities for migratory insertion of CH_2 into a Mn-H bond must therefore be considered suspect.[23] Recent HF predictions of the energetics of CO insertion at Mn should also be interpreted with caution.[24]

Once each of the six electrons involved in the insertion reaction (two in the Ru-H bond and four in the Ru=C bond) are allowed the freedom to each occupy their own orbitals [as in all of the GVB(3/6) wavefunctions], the description of metal-ligand multiple bonds improves tremendously.[7,22,25] Thus, we find a large

reactant stabilization relative to HF, leading to a decrease in the exothermicity by 17.2 kcal/mol and the appearance of a barrier (9.7 kcal/mol), even with the lowest level of GVB theory (GVB-PP). Another significant drop of 11.4 kcal/mol in the exothermicity, with a concomitant increase of 7 kcal/mol in the activation barrier, occurs when the spin-coupling restriction of the perfect singlet pairing (GVB-PP) wavefunction is lifted and interpair correlation terms are included by the GVB-RCI calculation, allowing a reasonable description of the metal-carbon double bond.[7,22] The exothermicity drops still further when these six electrons are allowed full freedom within the six active orbitals involved in the insertion in the GVBCI(3/6) calculation (a full valence CI, i.e., all occupations of the six electrons in the six orbitals). The activation barrier now drops at the GVBCI level, since the six active orbitals are now allowed to overlap in the transition state. Optimizing the orbitals self-consistently at the GVBCI level reduces the barrier and the exothermicity to their final values of 11.5 and −7.1 kcal/mol, respectively.

Figures 1, 4, and 5 show the progression of the six active orbitals from reactant **1a** in Figure 1 through the transition state in Figure 4 to product **2** in Figure 5. The Ru-C σ bond does not change very much during the insertion, but the other two bond pairs change smoothly from reactants to products, converting the Ru-H bond of **1a** into the C-H bond of **2** and the Ru-C $\bar{\pi}$ bond of **1a** into the Ru 4d lone pair of **2**. At the transition state, the Ru-C $\bar{\pi}$ bond (Figure 4c) is beginning to move out of the way of the incipient C-H bond, with some 4d lone pair character evident. The barrier to reaction is kept moderate by the ability of the active orbitals to maintain high overlap in the transition region so that no bonds are weakened significantly.[26] Finally, we note that the orbitals in Figure 5 [θ(H-Ru-C) = 40.0°] are presented as product orbitals, merely to emphasize that once past the transition region, the orbitals quickly adopt the characteristics of product, even just 10° past the transition state geometry [θ(H-Ru-C)$^{\dagger} \sim 50°$]. (The H-Ru-C "bond angle" in the product **2** is 23.2°.)

The changes in the geometry as the insertion proceeds are shown in Table IV.

The Ru-H bond length smoothly increases from 1.65 Å in **1a** to 2.63 Å in **2**, while the incipient C-H bond decreases smoothly in length from the nonbonded distance of 2.33 Å in **1a** to the equilibrium distance of 1.10 Å in **2**. The Ru=C double bond length of 1.87 Å in **1a** also smoothly increases to the Ru-C single bond length of 2.06 Å. Other geometrical parameters change also, but with less marked differences.

In the next section, we discuss higher level calculations aimed at determining the effect of extended basis sets and of higher electron correlation on the barrier and exothermicity of the insertion process.

IV. Insertion Thermochemistry

Theoretical calculations usually produce predictions with no independent means of estimating the associated error or degree of accuracy. In addition to the five levels of theory used above to map out the potential energy surface of the insertion shown in eq 2, we have undertaken a study using a larger basis set than used for the work of Section III, along with the inclusion of higher order correlations in the configuration interaction (CI) calculation. The goal of the work presented in this section is to provide an independent assessment of the activation barrier and exothermicity for the insertion reaction.

Calculating the bond energies for the metal-ligand bonds in **1a** and **2**, we can construct a thermodynamic cycle to predict the exothermicity of eq 2, as shown in Figure 6. The energetics for each step in the cycle were calculated using the CCCI method[10] (see Section VI) within both a valence double-ζ (VDZ) basis and polarized VDZ bases (VDZD, VDZP and VDZDP). The CCCI method has proven to be an extremely accurate technique for the prediction of energetics, predicting single and double bond dissociation energies and excitation energies for both organic and organometallic molecules to within 5 kcal/mol of the experimental values.[10,25,27]

We have calculated the steps leading to ClRu ($^2A'$) + H (^2S) + CH_2 ($^3B_1$) at the top of Figure 6, starting from the reactant **1a** at the bottom left or from the product **2** at the bottom right and following the cycle upward, in order to obtain

the relative energies of **1a** and **2**. Tables V - IX display results for D_e(Ru=C), ΔE_{ST}(ClRuH), D_e(Ru-H), D_e(Ru-C), and D_e(H_2C-H), as a function of basis set and increasing level of electron correlation. The CCCI results listed in each table correspond to the values shown in Figure 6.

Table V lists the adiabatic Ru=C bond energies in ClRuH(CH_2) (**1a**), dissociating the optimized geometry of **1a** (Table II) to the optimum structure for the $^3A'$ state of ClRuH [R_e(Ru-H) = 1.64 Å, R_e(Ru-Cl) = 2.38 Å, and θ_e(Cl-Ru-H) = 104.8°] and the equilibrium geometry of CH_2 ($^3B_1$) [R_e(C-H) = 1.08 Å and θ_e(H-C-H) = 133°]. We see that HF theory grossly underestimates the Ru=C bond strength, consistent with the discussion in Section III regarding the inability of HF theory to describe multiple metal-ligand bonds properly. The GVB-PP wavefunction stabilizes the Ru=C bond by 32 kcal/mol (VDZ basis), indicating the importance of allowing each electron in the Ru=C bond to occupy its own orbital (allowing for less than unit overlap in the bond pair). Higher order CI calculations up through CCCI serve to increase the bond strength by allowing up to full correlation of each breaking bond pair and allowing for valence orbital shape readjustments important for fragment rehybridization which occurs upon bond cleavage. The final CCCI value within the VDZD basis, D_e(ClHRu=CH_2) = 84.7 kcal/mol, should be representative of Ru=CH_2 bond energies in coordinatively saturated systems.[7,28] Our best estimate for D_e(ClHRu=CH_2), and hence Ru=C bond energies in other coordinatively saturated (or low spin unsaturated) complexes, is 89.6±2.5 kcal/mol, based on the correlation error inherent to the CCCI description of double bonds (4.9±2.5 kcal/mol).[10]

Table VI displays the adiabatic singlet-triplet splittings [ΔE_{ST} = E($^1A'$) − E($^3A''$)] for ClRuH. The equilibrium geometry of the $^3A''$ state of ClRuH is listed above and the equilibrium structure of the $^1A'$ state of ClRuH is found to be R_e(Ru-H) = 1.59 Å, R_e(Ru-Cl) = 2.35 Å, and θ_e(Cl-Ru-H) = 101.3°. ΔE_{ST} changes only slightly among all the levels listed, with the final CCCI result of 16.9 kcal/mol found to be the same for polarized and unpolarized basis sets.

Table VII presents adiabatic Ru-H bond energies for ClRuH ($^1A'$), using the equilibrium geometry described above for ClRuH and the equilibrium bond distance of 2.39 Å for RuCl ($^2A'$). At the highest level of correlation (CCCI) and basis (VDZP), we find an Ru-H bond energy of 54.1 kcal/mol. Since the model complex is low spin and does not suffer exchange losses during bond formation, this value should be representative of coordinatively saturated Ru-H bond energies.[28] Furthermore, D_e(ClRu–H, $^1A'$) should be higher than the bond energy in the coordinatively unsaturated complex Ru^+-H by 14.6 kcal/mol,[28] leading to a predicted bond energy for $D_e(Ru^+–H)$ = 39.5 kcal/mol, in excellent agreement with the experimental value of 41±3 kcal/mol[29] and in good agreement with a theoretical value of 34.5 kcal/mol.[30]

Adiabatic bond energies for $ClRuCH_3$ ($^1A'$) (**2**) are shown in Table VIII, using the equilibrium geometry for **2** shown in the last column of Table IV, the optimum bond length for ClRu ($^2A'$) of 2.39 Å, and the experimental geometry for CH_3 ($^2A''$) of R_e(C-H) = 1.079 Å and θ_e(H-C-H) = 120.0°.[31] At the CCCI level, the bond energy is 54.3 kcal/mol within the VDZD basis, essentially identical to the Ru-H bond energy. While this result is contrary to the trends in coordinatively saturated complexes, where M-CH_3 bond strengths are thought to be weaker than the corresponding M-H bond energies by 10-15 kcal/mol,[32] the result is in excellent agreement with the experimental Ru^+-CH_3 bond energy of 54±5 kcal/mol. This agreement is probably due to a cancellation of two effects: (i) the differential exchange loss incurred when bonds are formed in a saturated versus an unsaturated complex[7,28] (leading to a bond *weakening* of ~ 15 kcal/mol going from saturated to unsaturated Ru complexes) and (ii) the extra stabilization of $RuCH_3^+$ due to the polarizability of the methyl ligand (resulting in a bond *strengthening*, relative to a neutral system, of ~15 kcal/mol).[29] Thus, the Ru-CH_3 bond energy predicted here should be representative of coordinatively saturated (or low spin unsaturated) $RuCH_3$ bonds.[28]

The adiabatic C-H bond energies in CH_3 are shown in Table IX for three different basis sets and five levels of theory. As we have seen for all of the bond energies calculated herein, the bond strengths increase dramatically upon the inclusion of electron correlation. The final value for the CCCI C-H bond strength with the VDZDP basis is 112.9 kcal/mol, in good agreement with the experimental $D_e(CH_2\text{–}H) = 115.8 \pm 1.4$ kcal/mol.[33]

The exothermicities calculated using the CCCI values from Tables V - IX are shown at the bottom of Figure 6 for three different basis sets. The VDZ basis set result of $\Delta E_{rxn} = -9.4$ kcal/mol is in good agreement with the GVBCI-MCSCF result of -7.1 kcal/mol (Table III), suggesting that the dominant correlations important in the reaction are already included at the valence level (GVBCI). Considering the number of calculations required to complete the thermodynamic cycle of Figure 6, the agreement is excellent. Increasing the basis as well as the electron correlational level serves to increase the exothermicity slightly, to a final value of $\Delta E_{rxn} = -11.5$ kcal/mol.

Figure 6 yields thermodynamic estimates for the feasibility of eq 2, but yields no kinetic information about the height of the barrier. For an independent prediction of the barrier height as a function of electron correlation, we carried out CCCI calculations (Section VI) on the reactant **1a**, the transition state geometry [θ(H-Ru-C)$^\dagger = 50°$], and the product **2**, for both the VDZ and the VDZDP basis sets. The results are shown in Table X, where we see an across-the-board decrease in the activation energy and an increase in the exothermicity going from VDZ to VDZDP bases. A slight overall decrease in the activation energy and the exothermicity is seen going from the valence level CI [RCI(3/6)] to the higher order CI's. Our best estimates for E_a and ΔE_{rxn} are obtained simply by averaging the results from the two higher order CI's within the extended basis (VDZDP).

Thus we have used two different techniques to arrive at independent estimates of the energetics of the migratory insertion reaction of CH_2 into an adjacent Ru-H bond. The exothermicities and activation barriers are in close agreement from all

three methods [ΔE_{rxn} = −7.1 (GVBCI-MCSCF), −11.5 (Figure 6), and −10.6±1.0 (Table X) kcal/mol; E_a = 11.5 (GVBCI-MCSCF) and 10.9±1.7 (Table X) kcal/mol], lending credence to the reliability of these methods for the prediction of energetics in organometallic systems.

V. Discussion and Summary

The migratory insertion of a terminal CH_2 ligand into an adjacent ruthenium-hydrogen bond is predicted to be exothermic by 10.5±1.0 kcal/mol and to proceed with a small barrier (10.9±1.7 kcal/mol), with a preferred orientation of the CH_2 ligand *perpendicular* to the bond into which it will insert. We have thus demonstrated the feasibility of the FT chain initiation step (eq 1) to occur at one metal center. Group VIII metals are by far the most active for FT synthesis; perhaps another reason for their higher activity (aside from their ability to readily dissociate carbon monoxide) is this low barrier for chain initiation. Early metals are not good catalysts for FT synthesis, presumably because the M=CH_2 bond strength is too strong, leading to an endothermic process.[34]

The analogous insertion of CH_2 into an adjacent Ru-CH_3 bond can be predicted using the bond energies and excitation energies in Figure 6, along with an estimate for the C-C bond strength of ethyl radical. The methyl migration thermodynamic cycle will be identical to that of Figure 6, except for two steps:

(i) instead of the Ru-H bond in ClRuH ($^1A'$) breaking, we now break an Ru-CH_3 bond in the $^1A'$ state of $ClRuCH_3$ [D_e(Ru-CH_3) = 54.3 kcal/mol; see Figure 6] and

(ii) instead of breaking the C-H bond of methyl radical, we break the C-C bond of ethyl radical [$D_e(H_3C–CH_2\cdot)$ = 105.8±3.4 kcal/mol[35]].

We assume here that the singlet-triplet splittings of ClRuH and $ClRuCH_3$ are the same (we expect that the singlet-triplet splitting is more a function of the metal than of the ancillary ligands) and that D_e(Ru-Et) is the same as D_e(Ru-Me). Given these two assumptions, we find that the insertion of CH_2 into an Ru-CH_3 bond

is downhill by 4.2±3.4 kcal/mol. This insertion is less exothermic than for the insertion into an Ru-H bond because the incipient C-C bond is 7.1±3.4 kcal/mol weaker than the incipient C-H bond. Furthermore, steric factors would suggest that D_e(Ru-Et) should be less than D_e(Ru-Me), which would lead to an even less exothermic reaction (perhaps even endothermic). A higher barrier is expected for methyl migration over hydrogen migration due partly to the smaller exothermicity (the Hammond postulate) and partly to the essential reorientation of the methyl group (with its directed sp^3 hybrid orbital) during the migration from Ru to CH_2 (H has no such reorientation problems due to the spherical nature of its 1s orbital).[36] Hence we predict that chain propagation should be the rate-determining step in FT synthesis. Indeed, for some group VIII metals (e.g., Ni), the chain propagation step is so unfavorable that the only product of FT synthesis is methane.[37]

The present work yields the following conclusions:

(i) methylidene insertions into metal-hydrogen bonds should be facile, with low barriers ($\sim$ 10.9 kcal/mol) and moderate exothermicities ($\sim$ 10.5 kcal/mol) for late transition metals (since the M=C double bonds are relatively weak compared to those of early metals) *only if the orientation of the CH_2 ligand is perpendicular to bond into which it will insert*;

(ii) the reverse reaction of α-hydride elimination is predicted to be uphill by $\sim$ 21 kcal/mol, consistent with the lack of evidence for α-hydride eliminations among late transition metals;

(iii) The analogous insertion of CH_2 into a Ru-CH_3 bond is predicted to be less exothermic ($\Delta E_{rxn} \sim -4$ kcal/mol) than for insertion into Ru-H, due to the weaker incipient bond formed (C-C versus C-H). The activation barrier should be higher due to the lower exothermicity and the reorientation of the sp^3 hybrid on CH_3 during its migration; and

(iv) the implications for FT synthesis from (i) and (iii) are that chain initiation should proceed readily with a low barrier while chain propagation is predicted to be the rate-determining step for late transition metals.

VI. Calculational Details

All of the electrons of Ru, C, and H were treated explicitly, while the Cl atom was described using the SHC effective potential to represent the core electrons[38a] and a valence minimal basis molecularly contracted for $TiCl_4$.[38b] The VDZ basis consisted of a valence double-ζ basis for Ru,[7,39] the Dunning valence double-ζ contractions[40] of the Huzinaga (9s5p) and (4s) primitive gaussian bases for carbon and hydrogen[41] (exponents for H scaled by 1.2). The VDZP basis added one set of unscaled 2p-polarization functions for the migrating hydrogen to the VDZ basis. The VDZD basis added one set of carbon 3d-polarization functions ($\zeta^d = 0.64$) to the VDZ basis. The VDZDP basis added the two polarization functions above to the VDZ basis.

The geometries of **1a**, **1b**, and **6a** were optimized at the GVB-RCI level [RCI(3/6) for **1a** and **1b**; RCI(1/2) for **6a**, leaving the Ru-Cl bond at the HF level]. The RCI (restricted configuration interaction) starts from the GVB-PP wavefunction (generalized valence bond with perfect-pairing restriction) in which each correlated bond pair (Ru-H, Ru-Cσ, Ru-Cπ) is described with two orbitals, so that each electron involved in the insertion process has its own orbital. All other electron pairs were left uncorrelated (but solved for self-consistently). The GVB-RCI wavefunction allows all configurations arising from the three possible occupations of two electrons in two orbitals for each GVB bond pair. [The rotational barrier in **1** was calculated at the GVB-RCI(3/6) level.] The geometries of **2**, the $^1A'$ state of ClRuH, and the $^2A'$ state of RuCl were optimized using Hartree-Fock (HF) gradient techniques.

The reaction pathway was followed at the HF, the GVB-PP(3/6), the GVB-RCI(3/6), the GVBCI(3/6), and the GVBCI(3/6)-MCSCF levels. The GVBCI(3/6) allows a full CI within the six "active" orbitals (e.g., the Ru-C bond pairs and the Ru-H bond pair), while the GVBCI(3/6)-MCSCF self-consistently optimizes the orbitals for the GVBCI(3/6) wavefunction.

The bond and excitation energies of the various species in Tables V - IX were calculated at the HF, GVB-PP, GVB-RCI, and higher order CI levels described below:

(i) RCI*S_{val} allows all single excitations from all valence orbitals (except Cl) to all virtual (unoccupied) orbitals from the RCI reference configurations.

(ii) RCI*[$SD_{pair\ 1} + SD_{pair\ 2} + \cdots$] allows all single and double excitations to all virtuals from pair 1 and pair 2, etc. (but *not* simultaneously) from the RCI reference configurations.

(iii) CCCI adds the configurations of (ii) to the configurations of (i), allowing for full correlation of the changing bonds (RCI*SD) along with orbital shape readjustments for the other valence orbitals (RCI*S_{val}).[10]

Acknowledgments. This work was supported by the National Science Foundation (Grant No. CHE83-18041) and the Shell Companies Foundation. EAC acknowledges a National Science Foundation predoctoral fellowship (1982-1985), a research grant award from the International Precious Metals Institute and Gemini Industries (1985-1986), and a SOHIO fellowship in Catalysis (1987).

References

(1) (a) Cooper, N. J.; Green, M. L. H. *J. C. S. Dalton Trans.* **1979,** 1121; (b) Hayes, J. C.; Pearson, G. D. N.; Cooper, N. J. *J. Am. Chem. Soc.* **1981,** *103,* 4648-4650; (c) Thorn, D. L.; Tulip, T. H. *ibid.* 5984-5986; (d) Canestrari, M.; Green, M. L. H. *J. C. S. Dalton Trans.* **1982,** 1789; (e) Isobe, K.; Andrews, D. G.; Mann, B. E.; Maitlis, P. M. *J. Chem. Soc., Chem. Commun.* **1981,** 809; (f) Thorn, D. L.; Tulip, T. H. *Organometallics* **1982,** *1,* 1580; (g) Hayes, J. C.; Cooper, N. J. *J. Am. Chem. Soc.* **1982,** *104,* 5570; (h) Kletzin, H.; Werner, H.; Serhadli, O.; Ziegler, M. L. *Angew. Chem. Int. Ed. Engl.* **1983,** *22,* 46; (i) Jernakoff, P.; Cooper, N. J. *J. Am. Chem. Soc.* **1984,** *106,* 3026; (j) Jernakoff, P.; Cooper, N. J. *Organometallics* **1986,** *5,* 747; (k) Thorn, D. L. *ibid.* 1897.

(2) (a) Cooke, M.; Davies, D. L.; Guerchais, J. E.; Knox, S. A. R.; Mead, K. A.; Roué, J.; Woodward, P. *J. Chem. Soc., Chem. Commun.* **1981,** 862; (b) Herrmann, W. A. *Adv. Organomet. Chem.* **1981,** *20,* 249. Other C-C couplings at $\mu - CH_2Ru_2$ centers include: Colborn, R. E.; Dyke, A. F.; Knox, S. A. R.; MacPherson, K. A.; Orpen, A. G. *J. Organomet. Chem.* **1982,** *239,* C15 and Adams, P. Q.; Davies, D. L.; Dyke, A. F.; Knox, S. A. R.; Mead, K. A.; Woodward, P. *J. Chem. Soc., Chem. Commun.* **1983,** 222.

(3) (a) Bradley, J. S. *J. Am. Chem. Soc.* **1979,** *101,* 7419; (b) Dombek, B. D. *ibid.* **1980,** *102,* 6855; (c) Daroda, R. J.; Blackborrow, J. R.; Wilkinson, G. *J. Chem. Soc., Chem. Commun.* **1980,** 101; (d) Knifton, J. R. *ibid.* **1981,** 188; (e) Warren, B. K.; Dombek, B. D. *J. Catal.* **1983,** *79,* 334.

(4) (a) Anderson, R. B. "Catalysts for the Fischer-Tropsch Synthesis", in "Catalysis: Hydrocarbon Synthesis, Hydrogenation, and Cyclization", Emmett, P. H., Ed.; Reinhold Publishing Corporation: New York, 1956; Vol. IV, pp 237- 242; (b) Pichler, H.; Buffleb, H. *Brennst. Chem.* **1940,** *21,* 257, 273, 285.

(5) (a) Biloen, P; Sachtler, W. M. H. *Adv. Catal.* **1981,** *30,* 165; (b) Brady, R. C., III; Pettit, R. *J. Am. Chem. Soc.* **1980,** *102,* 6181; (c) *ibid.* **1981,** *103,*

1287; (d) Baker, J. A.; Bell, A. T. *J. Catal.* **1982**, *78*, 165.

(6) George, P. M.; Avery, N. R.; Weinberg, W. H.; Tebbe, F. N. *J. Am. Chem. Soc.* **1983**, *105*, 1393-1394.

(7) Carter, E. A.; Goddard, W. A., III *J. Am. Chem. Soc.* **1986**, *108*, 2180.

(8) van Asselt, A.; Burger, B. J.; Gibson, V. C.; Bercaw, J. E. *J. Am. Chem. Soc.* **1986**, *108*, 5347.

(9) A preliminary account of the insertion results has already appeared: Carter, E. A.; Goddard, W. A., III *J. Am. Chem. Soc.* **1987**, **109**, 579.

(10) (a) Carter, E. A.; Goddard, W. A., III *Chem. Phys. Lett.*, submitted for publication; (b) *idem*, *J. Chem. Phys.*, submitted for publication.

(11) The lowest energy structure of **1a** retains C_s symmetry (i.e., lower symmetry structures for both **1a** and **1b** were found to be higher in energy) but the CH_2 ligand is bent 4.1° out of the idealized $RuCH_2$ plane, toward the Cl ligand. However, the cost to make Ru and the CH_2 ligand coplanar is only 0.08 kcal/mol, and hence we consider the $RuCH_2$ unit to be coplanar for simplicity.

(12) Complexes **1a** and **1b** are taken to be singlet spin states as models for coordinatively saturated organometallic complexes. Similar low spin models with only a few ligands have recently been used in ab initio studies of CO insertion (Dedieu, A.; Sakaki, S.; Strich, A.; Siegbahn, P. E. M. *Chem. Phys. Lett.* **1987**, *133*, 317). Since $^1A'$ spin states are used for **1**, we consider only the triplet spin states of ClRuH (obtained when the bond of Ru=C bond is broken). However, the actual ground state of $ClRuH(CH_2)$ is a $^3A''$ state wherein all three bonds to H and CH_2 are maintained. The singlet "σ^3" state we have chosen to examine lies (at least) 16.8 kcal/mol higher in energy at the GVBCI(4/8) level of theory [which consists of a full CI among the six orbitals of the three bond pairs and the two high spin orbitals for $ClRu(CH_2)H$ ($^3A''$), and of a full CI among the eight orbitals corresponding to the three bond pairs plus the singlet Ru 4d lone pair for $ClRu(CH_2)H$ ($^1A'$)]. We did not optimize the structure of the $^3A''$ state of $ClRu(CH_2)H$, so that 16.8 kcal/mol is a lower bound on the

$^1A'$ - $^3A''$ energy difference.

The $^3A''$ ground state of $ClRu(CH_2)H$ may be understood as follows. In the $^1A'$ state, the σ and $\bar{\pi}$ bonds to H and CH_2 (choosing the H-Ru-C plane as yz) utilize $4d_{yz}$, $4d_{z^2}$, $4d_{y^2}$, and some 5s character on the metal, while $4d_{x^2}$ character is not used at all. In the triplet state, the $4d_{x^2}$ and $4d_{xz}$ orbitals are singly-occupied, gaining favorable exchange terms between the high spin electrons *without losing any of the metal-ligand bonding*, leading to a triplet ground state. Correspondingly, the ground state of ClRuH is actually a linear $^5\Delta$ state, derived from the (excited state) s^2d^6 valence electron configuration on Ru.

(13) The electron populations were calculated by summing over Mulliken populations for the first and second natural orbitals of each GVB pair. The electron transfer to the Cl was calculated by summing over Mulliken populations of the Cl Hartree-Fock orbitals.

(14) All angles and bond lengths were optimized at the GVB-RCI(3/6) level (Section VI) in complexes **1a** and **1b**, except for R(C-H), which was fixed at 1.08 Å.

(15) Guggenberger, L. J.; Schrock, R. R. *J. Am. Chem. Soc.* **1975,** *97,* 6578.

(16) Hill, A. F.; Roper, W. R.; Waters, J. M.; Wright, A. H. *J. Am. Chem. Soc.* **1983,** *105,* 5939.

(17) Chang, S.-C.; Kafafi, Z. H.; Hauge, R. H.; Billups, W. E.; Margrave, J. L. *J. Am. Chem. Soc.* **1985,** *107,* 1447.

(18) Brookhart, M.; Tucker, J. R.; Flood, T. C.; Jensen, J. *J. Am. Chem. Soc.* **1980,** *102,* 1203.

(19) The optimum geometry [at the GVB(1/2)-PP level] of $^3A'$ has Θ (Cl-Ru-H) = 104.8°, R(Ru-H) = 1.64 Å, and R(Ru-Cl) = 2.38 Å. The $^3A' - {}^3A''$ energy splitting of 4.2 kcal/mol is a lower bound since the geometry of the $^3A''$ state was kept fixed at the optimum geometry for the $^3A'$ state (only the equilibrium geometry of the $^3A'$ state was needed in later calculations).

(20) For spin-conserved processes, the resultant insertion product is $^1A'$ $ClRuCH_3$,

not $^3A'$ $ClRuCH_3$.

(21) HF wavefunctions are reliable for predicting accurate geometries. The HF and the RCI(3/6) optimum geometries of **1a** are very similar, with the Ru-Cl, Ru-H, and C-H bond lengths identical for both levels of theory. The other HF geometrical parameters for **1a** are R(Ru=C) = 1.87 Å, θ(H-Ru-C) = 82.7°, θ(H-Ru-Cl) = 157.0°, and θ(H-C-H) = 113.3°. These values differ from the RCI(3/6) optimum geometry by no more than 0.03 Å and 11.9° (where the latter difference is large due to the flat potential felt by the Cl ligand). The HF energies for these two geometries are: −4936.36310 and −4936.35958 hartrees for the HF gradient and the RCI(3/6) optimizations, respectively. These small changes in energy (2.2 kcal/mol) and structure between the two geometries support the use of HF gradient-optimized geometries in this study. Future work using gradients of correlated wavefunctions will be necessary to test this assertion.

(22) Carter, E. A.; Goddard, W. A., III *J. Phys. Chem.*, **1984**, *88*, 1485.

(23) Ziegler, T.; Versluis, L.; Tschinke, V. *J. Am. Chem. Soc.* **1986**, *108*, 612.

(24) Axe, F. U.; Marynick, D. S. *Organometallics*, **1987**, *6*, 572.

(25) Carter, E. A.; Goddard, W. A., III *J. Chem. Phys.*, submitted for publication.

(26) (a) Steigerwald, M. L.; Goddard, W. A., III *J. Am. Chem. Soc.*, **1984**, *106*, 308; (b) *idem*, submitted for publication.

(27) Hanratty, M. A.; Carter, E. A.; Beauchamp, J. L., Goddard, W. A., III *Chem. Phys. Lett.* **1986**, *123*, 239.

(28) The difference in Ru-H bond energies in singlet ClRuH and triplet Ru^+-H may be attributed to differential exchange loss suffered by Ru when the Ru-H bond is formed. Here the difference amounts to one d-d exchange term, $K_{dd}(Ru^+)$ = 14.6 kcal/mol. (Carter, E. A.; Goddard, W. A., III *J. Am. Chem. Soc.*, submitted for publication.)

(29) Mandich, M. L.; Halle, L. F.; Beauchamp, J. L. *J. Am. Chem. Soc.* **1984**,

106, 4403.

(30) Schilling, J. B.; Goddard, W. A., III; Beauchamp, J. L. *J. Am. Chem. Soc.*, submitted for publication.

(31) Herzberg, G. *Proc. Roy. Soc.*, **1961**, *A262*, 291.

(32) Martinho Simões, J. A.; Beauchamp, J. L. *Chem. Rev.*, submitted for publication.

(33) (a) The total energies for CH_2 differ slightly from the values listed in Table V, due to one change in the basis set between complex **1** (where the 3s combination of the 3d-polarization functions on carbon was included in the calculation) and CH_3 [where the 3s combination was omitted (ref 10a)]; (b) the experimental D_e was derived from $\Delta H^o_{f,0}$ in "JANAF Thermochemical Tables", NSRDS-NBS **1971**, *37* and supplements to JANAF in *J. Phys. Chem. Ref. Data* **1975**, *4*, 1; *ibid.*, **1982**, *11*, 695, with zero point energy corrections from Jacox, M. E. *J. Phys. Chem. Ref. Data* **1984**, *13*, 945 for CH_3 and from Bunker, P. R.; Jensen, P.; Kraemer, W. P.; Beardsworth, R. *J. Chem. Phys.* **1986**, *85*, 3724 for CH_2.

(34) Carter, E. A.; Goddard, W. A., III *J. Am. Chem. Soc.* **1986**, *108*, 4746.

(35) $D_e(H_3C–CH_2\cdot)$ was estimated from $D_{298}(H_3C–CH_2\cdot) = 101.3\pm2.2$ kcal/mol [$\Delta H^o_{f,298}$ was taken from JANAF (ref 33b) for $:CH_2$ (92.35±1 kcal/mol) and $CH_3\cdot$ (34.82±0.2 kcal/mol) and $\Delta H^o_{f,298}$ for $C_2H_5\cdot$ (25.9±1 kcal/mol) was taken from McMillen, D. F.; Golden, D. M. *Ann. Rev. Phys. Chem.*, **1982**, *33*, 493]. Temperature corrections for the heat capacity changes going to T = 0 K were taken equal to $4R\Delta T$ = 2.4 kcal/mol, leading to $D_0(H_3C–CH_2\cdot) = 98.9\pm2.2$ kcal/mol. Finally, $D_e(H_3C–CH_2\cdot) = 105.8\pm3.4$ was obtained from zero point energy corrections to D_0 ($\Delta ZPE = 6.9\pm1.2$ kcal/mol from ref 10a and references therein).

(36) Low, J. J.; Goddard, W. A., III *Organometallics*, **1986**, *5*, 609.

(37) Kelley, R. D.; Goodman, D. W. in "The Chemical Physics of Solid Surfaces and Heterogeneous Catalysis" (Elsevier, Amsterdam, 1982) Vol. 4, 427-453.

(38) (a) Rappé, A. K.; Smedley, T.A.; Goddard, W. A., III *J. Phys. Chem.* **1981,** *85,* 1662; (b) Rappé, A. K.; Goddard, W. A., III, unpublished.

(39) a) Rappé, A. K.; Goddard, W. A., III, to be published. This basis set was optimized for the d^n configuration of the metal as discussed in A. K. Rappé, T. A. Smedley, and W. A. Goddard III, *J. Phys. Chem.*, **1981**, *85*, 2607.

(40) Dunning, Jr., T. H. *ibid.* **1970,** *53,* 2823.

(41) Huzinaga, S. *J. Chem. Phys.* **1965,** *42,* 1293.

Table I. Orbital overlaps, metal orbital hybridization, and bond populations for the GVB bond pairs in **1a** and **1b**.[a]

			Ru hybridization		bond populations[b]	
complex	bond	overlap	% 5sp	% 4d	Ru	X
1a (σ^3)	Ru-C σ	0.73	18.8	81.2	0.96	1.03
"	Ru-C π	0.50	4.4	95.6	1.10	0.88
"	Ru-H	0.69	25.6	74.4	1.02	0.95
1b ($\sigma^2\pi$)	Ru-C σ	0.71	17.8	82.2	0.93	1.03
"	Ru-C π	0.41	2.2	97.8	1.07	0.93
"	Ru-H	0.63	15.6	84.4	1.08	0.91

a) Ref. 13. *b*) A perfectly covalent bond has a bond population of 1.00 for Ru and 1.00 for X (X = CH_2 or H).

Table II. Optimized structural parameters and harmonic vibrational frequencies for **1a** and **1b**.[a]

parameter	complex **1a** (σ^3)	complex **1b** ($\sigma^2\pi$)
R_e(Ru-C) (Å)	1.90	1.92
R_e(Ru-H) (Å)	1.65	1.63
R_e(Ru-Cl) (Å)	2.42	2.43
θ_e(H-Ru-C) (deg)	90.3	111.7
θ_e(H-Ru-Cl) (deg)	145.1	93.6
θ_e(H-C-H) (deg)	120.0	121.1
ω_e(Ru=C) (cm^{-1})	746	798
ω_e(Ru-H) (cm^{-1})	2013	1825
ω_e(Ru-Cl) (cm^{-1})	420	353
ω_e(HCH scissors) (cm^{-1})	1487	1416

a) Optimized at the GVB-RCI(3/6) level (Section VI).

Table III. Energetics (kcal/mol) for the CH_2 insertion into the Ru-H bond in $ClRuH(CH_2)$ within a VDZ basis.[a]

	spatial config./	total energies (hartrees)[b]					
calculation	SEF[c]	**1a**	T.S.[d]	**2**	ΔE_{rxn}	E_a[e]	Θ(H-Ru-C)†[e]
HF	(1/1)	−4936.36311	−4936.36311	−4936.42511	−38.9	0.0	82.7°
GVB(3/6)-PP	(8/8)	−4936.43966	−4936.42443	−4936.47422	−21.7	9.7	51.2°
RCI(3/6)	(27/37)	−4936.46372	−4936.43708	−4936.48020	−10.3	16.7	47.7°
GVBCI(3/6)	(141/175)	−4936.46940	−4936.44821	−4936.48174	−7.7	13.4	45.2°
GVBCI(3/6)-MCSCF	(141/175)	−4936.47118	−4936.45301	−4936.48242	−7.1	11.5	48.8°

a) Calculational details are provided in Sections III and VI. *b*) 1 hartree = 627.5096 kcal/mol. *c*) The number of spatial configurations/ spin eigenfunctions associated with each calculation. *d*) T.S. = transition state. The total energies listed under T.S. are values for points calculated nearest the true T.S. and its associated θ(H-Ru-C)† (i.e., HF energy is for $\theta^\dagger$ = 82.7°, GVB-PP for 50.0°, RCI for 47.5°, GVBCI for 45.0°, and GVBCI-MCSCF for 50.0°). *e*) The proper method of calculating the activation barrier is by fitting the data points to a potential maximum; the values listed for E_a and θ(H-Ru-C)† are obtained in this manner. Using the differences in total energies for the nearest points to the T. S. leads to a decrease in E_a by 0.1 kcal/mol for the GVB-PP and the two GVBCI calculations.

Table IV. Changes in the Hartree-Fock geometry along the reaction coordinate.

θ(H-Ru-C) (deg)	82.7[a]	70.0	60.0	55.0	50.0	47.5	45.0	40.0	23.2[b]
R_e(Ru-H) (Å)	1.65	1.68	1.72	1.75	1.77	1.83	1.85	1.94	2.63
R_e(C-H) (Å)	2.33	2.05	1.82	1.70	1.57	1.51	1.45	1.33	1.10
R_e(Ru-C) (Å)	1.87	1.89	1.91	1.92	1.93	1.93	1.93	1.94	2.06
R_e(Ru-Cl) (Å)	2.42	2.41	2.40	2.40	2.38	2.39	2.38	2.37	2.36
R_e(C-H')[c] (Å)	1.09	1.08	1.08	1.08	1.09	1.08	1.08	1.08	1.09
θ_e(H'CH') (deg)	113.3	112.4	112.2	112.2	110.9	112.4	112.5	112.5	108.6
θ_e(Cl-Ru-C) (deg)	120.3	130.2	134.3	138.9	142.0	135.4	135.5	132.1	105.4
θ_e(H'-C-Ru) (deg)	123.4	123.7	123.7	123.8	124.4	123.8	123.6	122.9	110.5

a) The optimum angle for **1a** at the HF level. *b*) The optimum angle for **2** at the HF level. *c*) Unprimed hydrogen is the migrating hydrogen.

Table V. Adiabatic Ru = CH_2 Bond Energies (D_e) in $^1A'$ ClHRu=CH_2 (kcal/mol).[a]

calculation	basis set[b]	total energies (h)[c] $^1A'$ ClRuH(CH_2)	$^3A'$ ClRuH	$^3B_1$ CH_2	D_e(Ru=C)
HF	VDZ	-4936.35958 (1/1)	-4897.42464 (1/1)	-38.91349 (1/1)	13.5
GVB-PP	"	-4936.44192 (8/8)	-4897.45542 (2/2)	"	45.8
RCI	"	-4936.46669 (27/37)	-4897.45736 (3/5)	"	60.1
RCI*S_{val}	"	-4936.51258 (1899/3997)	-4897.46850 (117/295)	-38.92067 (14/28)	77.4
CCCI[d]	"	-4936.51676 (4979/9725)	"	"	80.1
GVB-PP	VDZD	-4936.45422 (8/8)	-4897.45542 (2/2)	-38.92331 (1/1)	47.4
RCI	"	-4936.47749 (27/37)	-4897.45736 (3/5)	"	60.8
RCI*[$SD_{Ru-C\sigma}$ + $SD_{Ru-C\pi}$]	"	-4936.50089 (5465/9619)	-4897.46142 (67/109)	"	72.9
CCCI	"	-4936.53849 (7127/13895)	-4897.46850 (117/295)	-38.93503 (22/44)	84.7

a) Details of the calculations are provided in Section VI. *b*) VDZ: Valence double-ζ bases were used for all atoms except Cl [treated using an SHC-EP for the core electrons and an MBS (minimum basis set) description of the valence electrons]; VDZD: same basis set as VDZ except one set of d-polarization functions was added to the C basis (ζ= 0.64). See Section VI. *c*) 1 h = 1 hartree = 627.5096 kcal/mol. The number of spatial configurations/spin eigenfunctions associated with each calculation is given in parentheses under each total energy. *d*) CCCI ≡ RCI*[$SD_{Ru-C\sigma}$ + $SD_{Ru-C\pi}$ + S_{val}].

Table VI. Adiabatic Singlet-Triplet Splittings (ΔE_{ST}) in ClRuH (kcal/mol).[a]

calculation[b]	basis set[c]	total energies (h) $^1A'$	$^3A'$	ΔE_{ST}
GVB-PP	VDZP	-4897.42851 (4/4)	-4897.45650 (2/2)	17.6
RCI	"	-4897.42855 (9/10)	-4897.45841 (3/5)	18.7
RCI*$SD_{Ru\ d\sigma's}$	"	-4897.43829 (389/490)	-4897.46436 (348/550)	16.4
CCCI[d]	"	-4897.44504 (555/760)	-4897.47204 (408/778)	16.9
CCCI	VDZ	-4897.44320 (425/581)	-4897.47013 (304/584)	16.9

a) $\Delta E_{ST} = E_{singlet} - E_{triplet}$. *b*) Calculational details provided in Section VI. *c*) VDZP: VDZ Ru, SHC-EP + MBS Cl, and DZP H; VDZ: same as VDZP but the unscaled p-function on H was removed (Section VI). *d*) CCCI $\equiv$ RCI*[$SD_{Ru\ d\sigma's}$ + S_{val}].

Table VII. Adiabatic Ru-H Bond Energies (D_e) in $^1A'$ ClRuH (kcal/mol).[a]

		total energies (h)[c]		
calculation	basis set[b]	$^1A'$ ClRuH	$^2A'$ ClRu	D_e(Ru-H)
HF	VDZ	-4897.39340 (1/1)	-4896.85740 (1/1)	23.0
GVB-PP	"	-4897.42733 (4/4)	-4896.86188 (2/2)	41.5
RCI	"	-4897.42737 (9/10)	-4896.86188 (3/4)	41.5
RCI*SD_{Ru-H}	"	-4897.43014 (289/361)	-4896.86197 (32/42)	43.2
CCCI[d]	"	-4897.44147 (425/581)	-4896.86258 (76/152)	50.0
HF	VDZP	-4897.39505 (1/1)	-4896.85740 (1/1)	24.1
GVB-PP	"	-4897.42851 (4/4)	-4896.86188 (2/2)	42.3
RCI	"	-4897.42855 (9/10)	-4896.86188 (3/4)	42.3
RCI*SD_{Ru-H}	"	-4897.43616 (389/490)	-4896.86197 (32/42)	47.0
CCCI	"	-4897.44812 (555/760)	-4896.86258 (76/152)	54.1

a) Calculational details provided in Section VI. *b*) See Table VI, footnote c. *c*) The total energy of the H atom within the DZ (and DZP) basis is -0.49928 hartree. *d*) CCCI $\equiv$ RCI*[SD_{Ru-H} + S_{val}].

Table VIII. Adiabatic Ru – CH_3 Bond Energies (D_e) in $^1A'$ ClRu-CH_3 (kcal/mol).

		total energies (hartrees)			
calculation[a]	basis set[b]	$^1A'$ $ClRuCH_3$	$^2A'$ ClRu	$^2A_2''$ CH_3	D_e(Ru-C)
HF	VDZ	-4936.42511 (1/1)	-4896.85740 (1/1)	-39.54946 (1/1)	11.5
GVB-PP	"	-4936.47422 (8/8)	-4896.86188 (2/2)	-39.56471 (2/2)	29.9
RCI	"	-4936.48019 (27/37)	-4896.86188 (3/4)	-39.56620 (3/4)	32.7
RCI^*SD_{Ru-C}	"	-4936.48672 (1843/3191)	-4896.86197 (32/42)	-39.56943 (6/8)	34.7
CCCI[c]	"	-4936.52800 (3457/7113)	-4896.86258 (76/152)	-39.58120 (42/104)	52.9
HF	VDZD	-4936.43668 (1/1)	-4896.85740 (1/1)	-39.56032 (1/1)	11.9
GVB-PP	"	-4936.48692 (8/8)	-4896.86188 (2/2)	-39.57549 (2/2)	31.1
RCI	"	-4936.49312 (27/37)	-4896.86188 (3/4)	-39.57677 (3/4)	34.2
RCI^*SD_{Ru-C}	"	-4936.50339 (2545/4462)	-4896.86197 (32/42)	-39.58737 (25/44)	33.9
CCCI	"	-4936.54580 (4510/9272)	-4896.86258 (76/152)	-39.59667 (58/143)	54.3

a) Calculations discussed in detail in Section VI. *b*) See Table V, footnote b. *c*) CCCI $\equiv$ $RCI^*[SD_{Ru-C} + S_{val}]$.

Table IX. Adiabatic $CH_2 - H$ Bond Energies (D_e) in $^2A_2''$ CH_3 (kcal/mol).[a]

		total energies (h)[c]		
calculation	basis set[b]	$^2A_2''$ CH_3	$^3B_1$ CH_2	$D_e(CH_2 - H)$
HF	VDZ	-39.54946 (1/1)	-38.91349 (1/1)	85.8
GVB-PP	"	-39.56471 (2/2)	"	95.3
RCI	"	-39.56620 (3/4)	"	96.3
RCI*SD_{C-H}	"	-39.57066 (36/60)	"	99.1
CCCI[d]	"	-39.58487 (65/140)	-38.92067 (14/28)	103.5
HF	VDZD	-39.56032 (1/1)	-38.92254 (1/1)	86.9
GVB-PP	"	-39.57549 (2/2)	"	96.4
RCI	"	-39.57677 (3/4)	"	97.2
RCI*SD_{C-H}	"	-39.58743 (61/104)	"	103.9
CCCI	"	-39.60548 (102/215)	-38.93425 (20/40)	107.9
HF	VDZDP	-39.56282 (1/1)	-38.92254 (1/1)	88.5
GVB-PP	"	-39.57750 (2/2)	"	97.7
RCI	"	-39.57874 (3/4)	"	98.5
RCI*SD_{C-H}	"	-39.59498 (80/138)	"	108.7
CCCI	"	-39.61340 (130/271)	-38.93425 (20/40)	112.9
Experiment[e]				115.8±1.4

a) Calculational details provided in Section VI. *b*) VDZ and VDZD: see Table V, footnote b; VDZDP: one set of unscaled p-polarization functions for the hydrogen atom involved in the breaking C-H bond was added to the VDZD basis. *c*) The total energy of the H atom within the DZ (and DZP) basis is -0.49928 hartree. *d*) CCCI ≡ RCI*[SD_{C-H} + S_{val}]. *e*) Ref. 33.

Table X. Direct calculations of the insertion activation barrier (E_a) and exothermicity (ΔE_{rxn}) within both VDZ and VDZDP bases as a function of electron correlation (kcal/mol).[a]

	total energies (hartrees)									
	VDZ basis[b]			VDZDP basis[c]			E_a		ΔE_{rxn}	
calculation	**1a**	T.S.[d]	**2**	**1a**	T.S.	**2**	VDZ	VDZDP	VDZ	VDZDP
RCI(3/6)[e]	−4936.46372	−4936.44119	−4936.48020	−4936.47494	−4936.45713	−4936.49508	14.1	11.2	−10.3	−12.6
RCI(3/6)*SD[f]	−4936.48731	−4936.47086	−4936.49752	−4936.51191	−4936.49718	−4936.52711	10.3	9.2	−6.4	−9.5
CCCI[g]	−4936.51729	−4936.49542	−4936.53167	−4936.54521	−4936.52510	−4936.56373	13.7	12.6	−9.0	−11.6
best estimate[h]							10.9±1.7		−10.6 ± 1.0	

a) Details of the calculations are provided in Section VI. *b*) VDZ: See Table V, footnote *b*. *c*) VDZDP: VDZ + one set of d-polarization functions on C ($\zeta = 0.64$) and one set of unscaled p-polarization functions on the migrating H. *d*) T. S. = geometry at transition state where θ(H-Ru-C)[1] = 50.0 degrees (Section III). *e*) 27 spatial configurations/37 spin eigenfunctions. *f*) RCI(3/6)*SD ≡ RCI(3/6)*[$SD_{Ru-H\ bond/C-H\ bond}$ + $SD_{Ru-C\ \sigma\ bond}$ + $SD_{Ru-C\ \pi\ bond/Ru\ 4d\ lone\ pair}$]. VDZ: 5475 spatial configurations/9499 spin eigenfunctions; VDZDP: 9084 spatial configurations/16048 spin eigenfunctions. *g*) CCCI ≡ [$SD_{Ru-H\ bond/C-H\ bond}$ + $SD_{Ru-C\ \sigma\ bond}$ + $SD_{Ru-C\ \pi\ bond/Ru\ 4d\ lone\ pair}$ + S_{val}]. VDZ: 6501 spatial configurations/12337 spin eigenfunctions; VDZDP: 10488 spatial configurations/19950 spin eigenfunctions. *h*) Based on the average of the RCI(3/6)*SD and CCCI values using the VDZDP basis.

Figure Captions

Fig. 1. GVB(3/6)PP one-electron orbitals for **1a**, the σ^3 state of $ClRu(CH_2)H$ at its optimum geometry: (a) the Ru-H bond; (b) the Ru-C σ bond; (c) the Ru-C $\bar{\pi}$ bond; (d) the Ru doubly-occupied $4d_{xz}$ orbital; and (e) the Ru doubly-occupied $4d_{xy}$ orbital. Long dashes indicate zero amplitude and the spacing between contours is 0.05 a.u.

Fig. 2. GVB(3/6)PP one-electron orbitals for **1b**, the $\sigma^2\pi$ state of $ClRu(CH_2)H$ at its optimum geometry: (a) the Ru-H bond; (b) the Ru-C σ bond;(c) the Ru-C π bonds; (d) the Ru doubly-occupied $4d_{z^2}$ orbital; and (e) the Ru doubly-occupied $4d_{xy}$ orbital.

Fig. 3. Reaction coordinate for the insertion of CH_2 into Ru-H in **1a** to form **2** at the HF, GVB(3/6)-PP, GVB-RCI(3/6), GVBCI(3/6), and GVBCI(3/6)-MCSCF levels of theory. Energy (kcal/mol) is plotted relative to the total energy of **2** vs. the normalized reaction coordinate R(Ru-H)/[R(Ru-H) + R(C-H)]. The corresponding H-Ru-C angles (deg) are indicated at the top. The full GVBCI-MCSCF wavefunction yields simultaneously a proper description of reactant, transition state, and product, resulting in a smooth potential curve. Some lower level wavefunctions lead to less smooth transitions, since they are less capable of describing both reactant and product channels.

Fig. 4. GVB(3/6)PP one-electron orbitals near the transition state [θ(H-Ru-C)† = 50.0°]: (a) orbital pair describing the Ru-H bond of reactant **1a** and the C-H bond of product **2**; (b) the Ru-C σ bond; (c) orbital pair describing the Ru-C $\bar{\pi}$ bond of **1a** and the Ru 4d lone pair of **2**. (Nodal lines have been omitted for clarity.)

Fig. 5. GVB(3/6)PP one-electron orbitals in the product channel [θ(H-Ru-C)† = 40.0°]: (a) the C-H bond of product **2**; (b) the Ru-C σ bond; (c) the Ru 4d lone pair of **2**. (Nodal lines have been omitted for clarity.)

Fig. 6. The thermodynamic cycle used to derive ΔE_{rxn} (kcal/mol) for eq 2. The bond and excitation energies shown are from CCCI calculations (Sections IV and VI) using the VDZ, VDZD, and VDZDP basis sets (Table V, footnote b and Table VI, footnote c; Section VI). The predicted exothermicities (ΔE_{rxn}) are shown at the bottom.

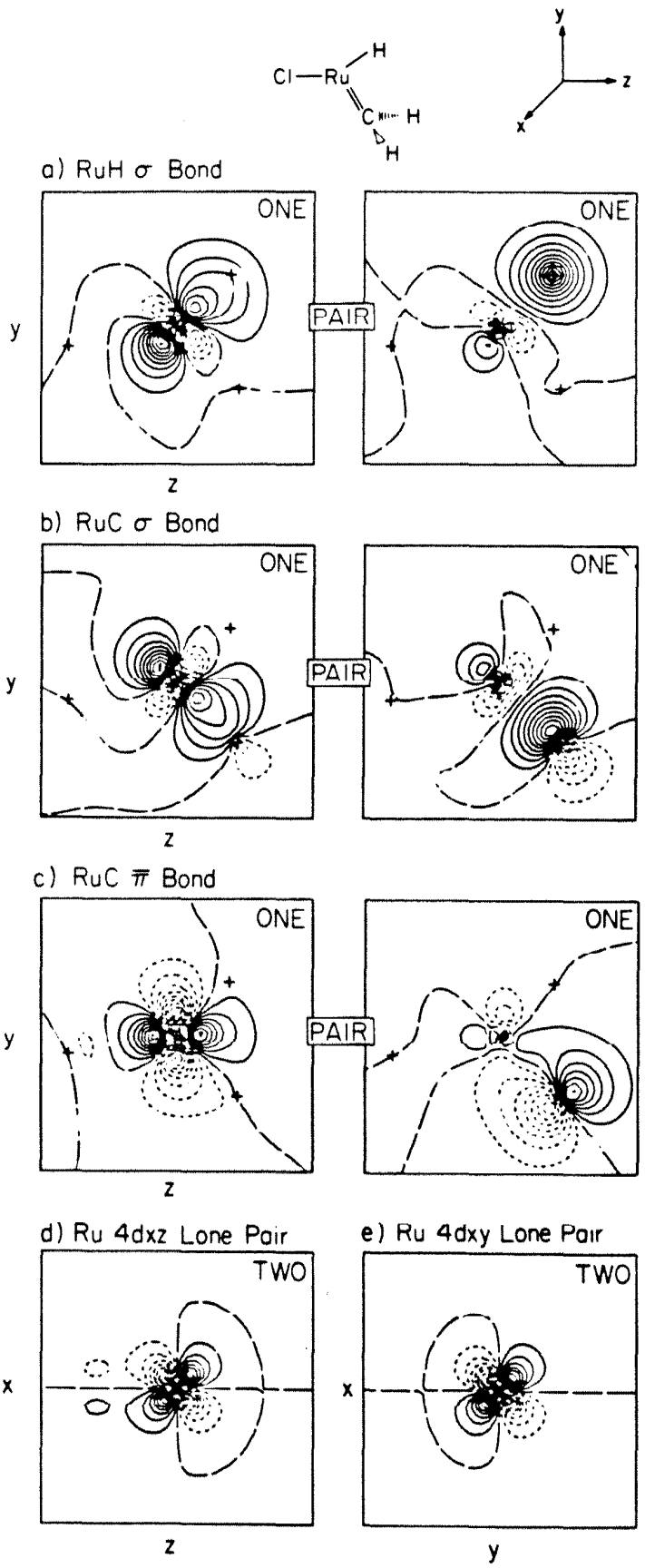
Cl—Ru
H
C
H
H
y
z
x
a) RuH σ Bond
ONE
PAIR
ONE
y
z
b) RuC σ Bond
ONE
PAIR
ONE
y
z
c) RuC π Bond
ONE
PAIR
ONE
y
z
d) Ru 4dxz Lone Pair
TWO
x
z
e) Ru 4dxy Lone Pair
TWO
x
y

Figure 1.

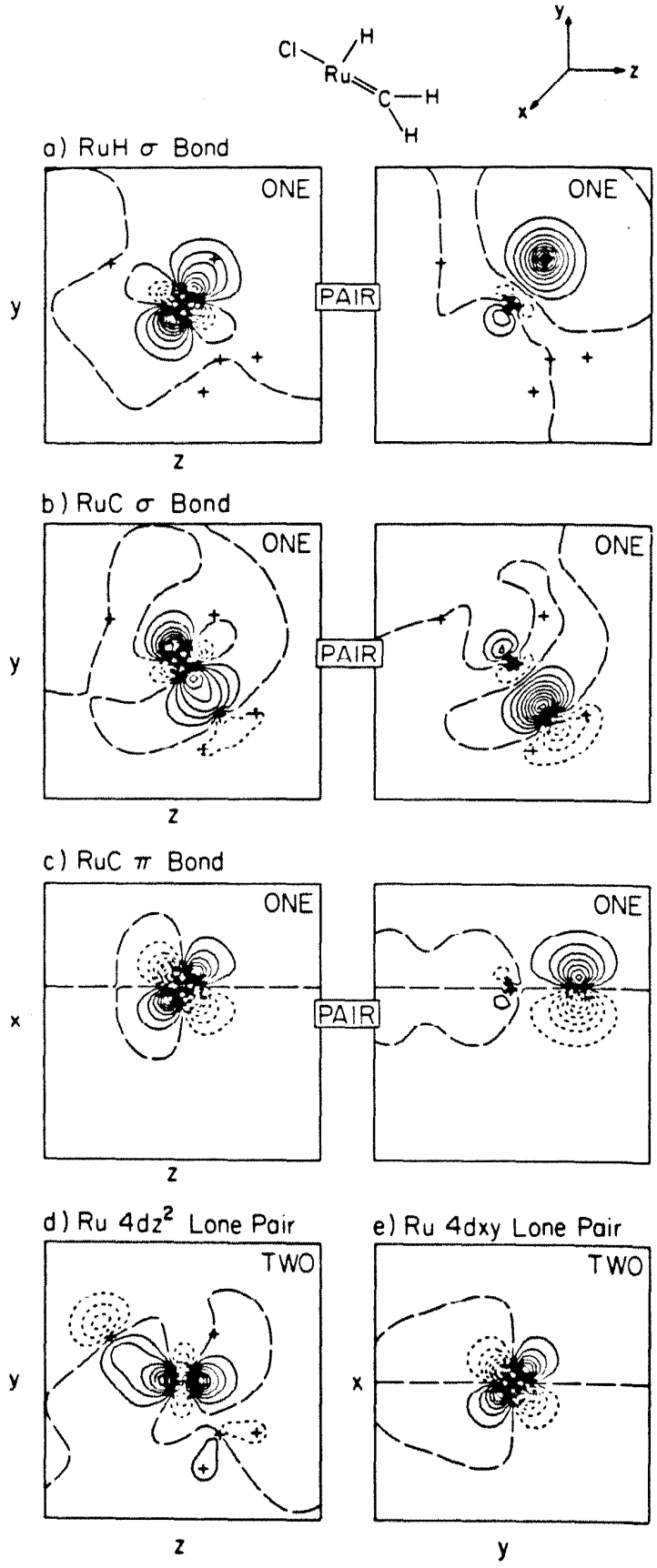
Cl
H
Ru
C
H
H
y
z
x
a) RuH σ Bond
ONE
ONE
PAIR
y
z
b) RuC σ Bond
ONE
ONE
PAIR
y
z
c) RuC π Bond
ONE
ONE
PAIR
x
z
d) Ru 4dz² Lone Pair
TWO
y
z
e) Ru 4dxy Lone Pair
TWO
x
y

Figure 2.

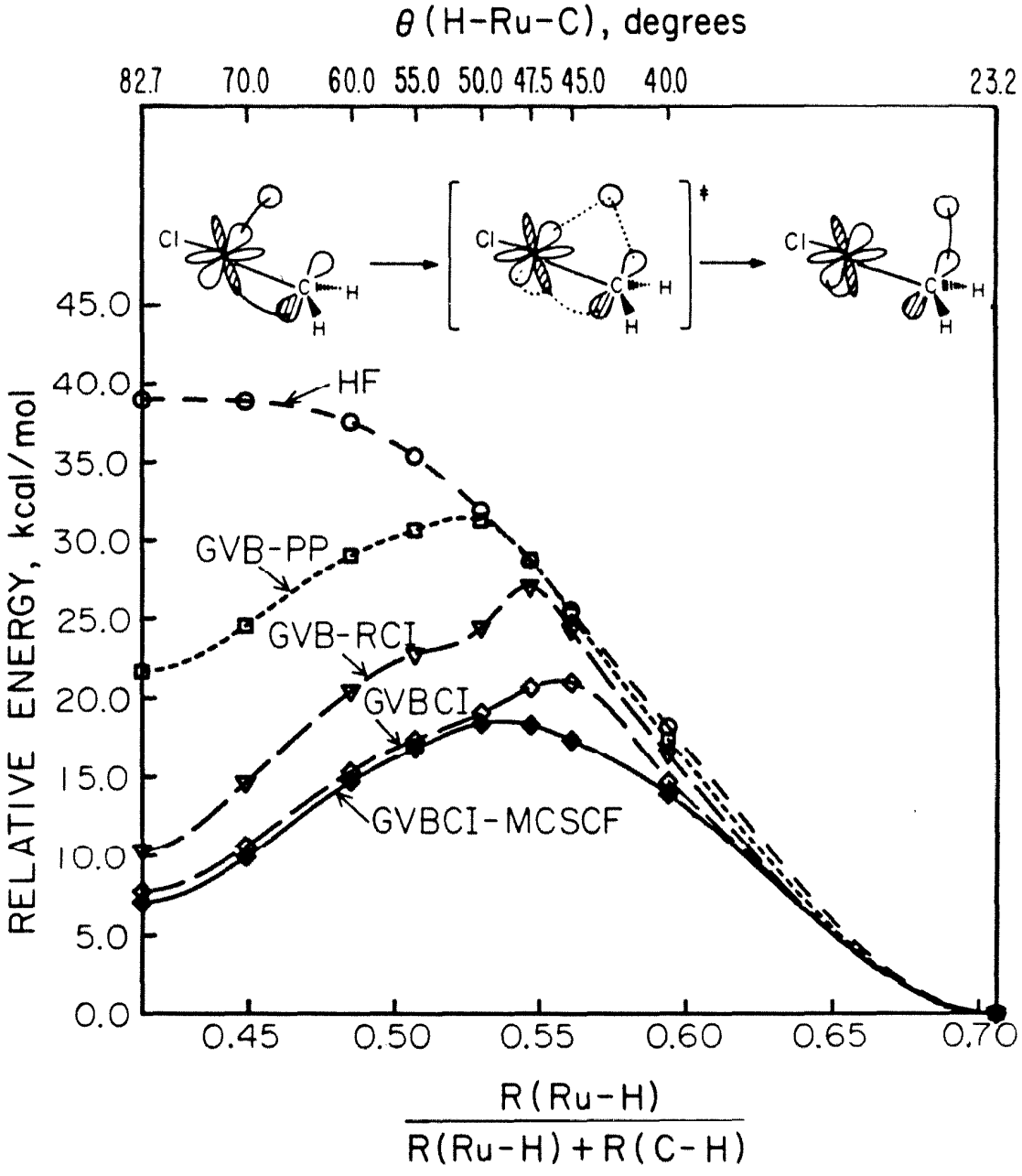
θ (H-Ru-C), degrees
82.7
70.0
60.0
55.0
50.0
47.5
45.0
40.0
23.2
Cl
C
H
H
‡
HF
GVB-PP
GVB-RCI
GVBCI
GVBCI-MCSCF
RELATIVE ENERGY, kcal/mol
45.0
40.0
35.0
30.0
25.0
20.0
15.0
10.0
5.0
0.0
0.45
0.50
0.55
0.60
0.65
0.70
R(Ru-H)
R(Ru-H)+R(C-H)

Figure 3.

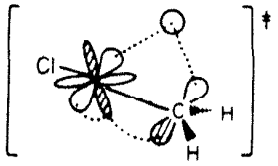

a) Ru-H Bond to C-H Bond Pair

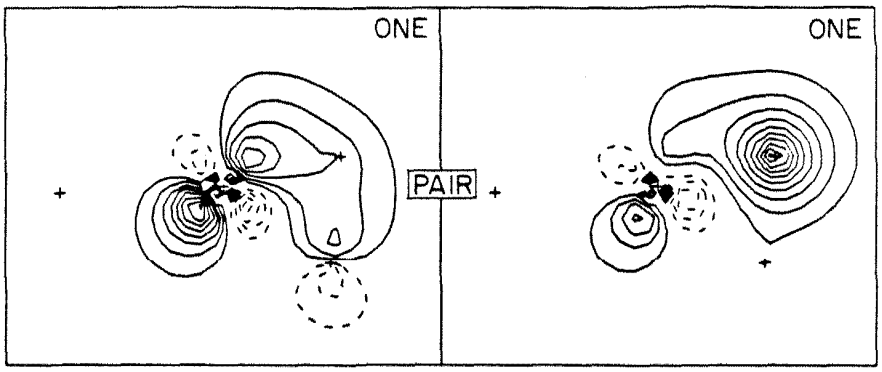

b) Ru-C Sigma Bond Pair

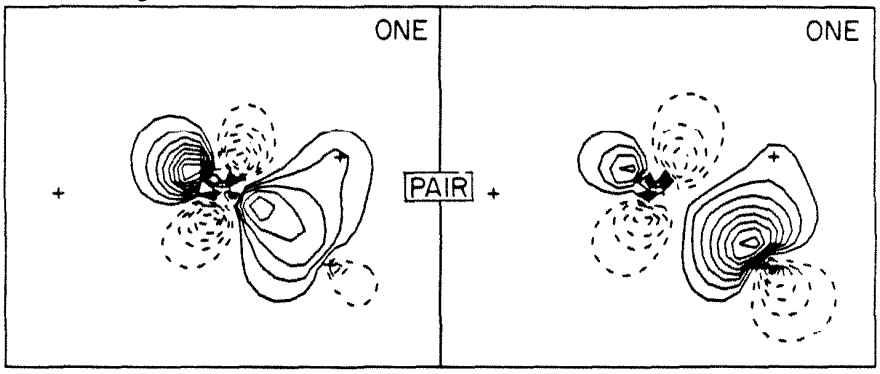

c) Ru-C Pi Bond to Ru dπ Lone Pair

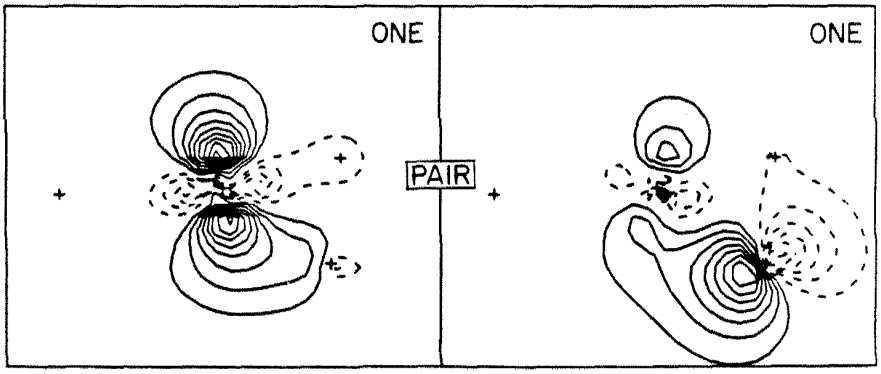

Figure 4.

$ClRu-CH_3$

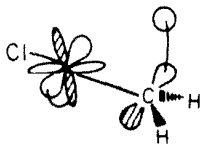

a)

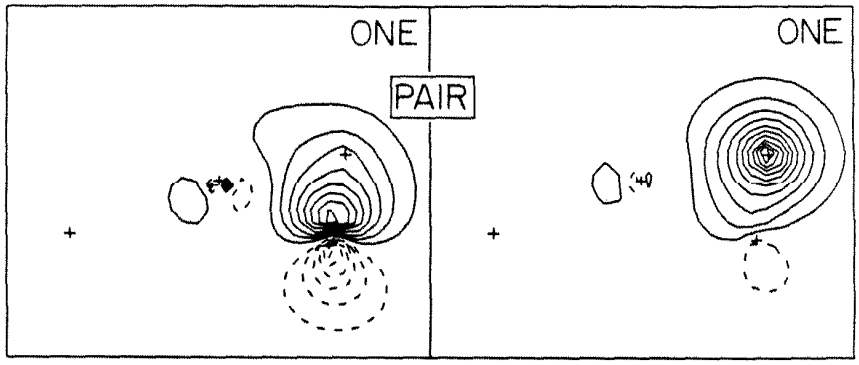

C-H Bond

b)

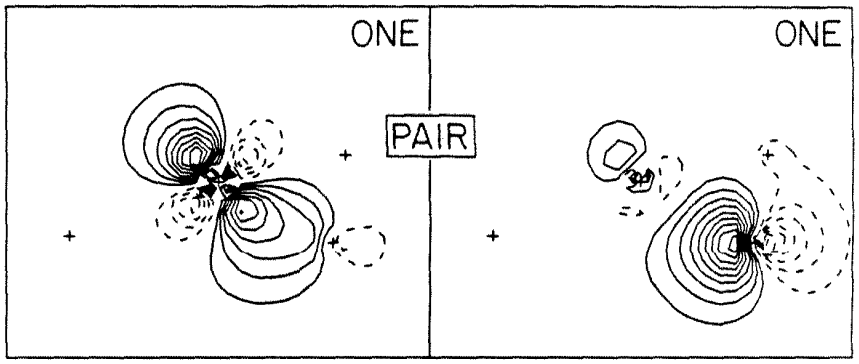

Ru-C Bond

c)

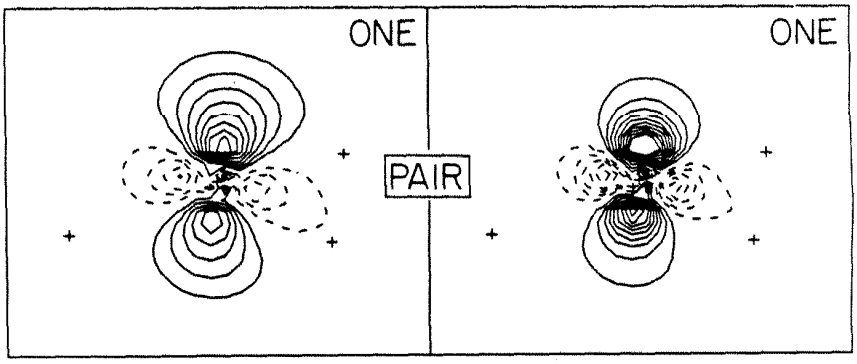

Ru d Lone Pair

Figure 5.

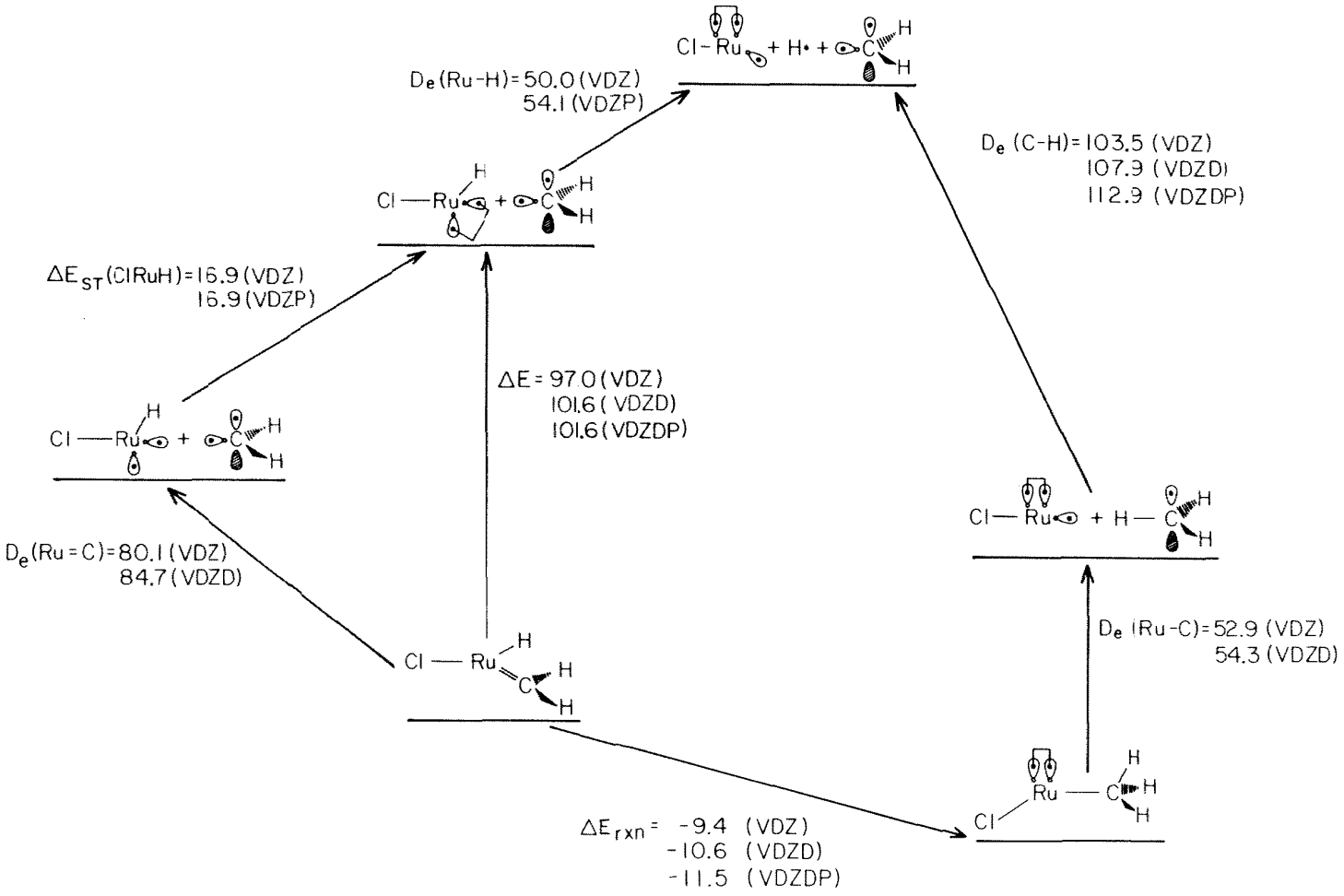

*Energy in kcal/mol

Figure 6.

Chapter 4

Chemisorption of Oxygen, Chlorine, Hydrogen, Hydroxide, and Ethylene on Silver Clusters: A Model for the Olefin Epoxidation Reaction

The text of this chapter is an Article coauthored with William A. Goddard III and is to be submitted to *Surface Science*.

Chemisorption of Oxygen, Chlorine, Hydrogen, Hydroxide, and Ethylene on Silver Clusters: A Model for the Olefin Epoxidation Reaction

Emily A. Carter and William A. Goddard III*

Contribution No. 7582 from the Arthur Amos Noyes Laboratory of Chemical Physics, California Institute of Technology, Pasadena, California 91125.

Abstract: The mechanism of the silver-catalyzed olefin epoxidation reaction is still far from understood, despite extensive experimental investigation. In order to sort out the feasibility of various postulated pathways, we have undertaken an ab initio quantum mechanical study of the key role players in this reaction. In particular, we have predicted preferred binding sites, geometries, vibrational frequencies, and binding energies for O, O_2, Cl, H, OH, and C_2H_4 on Ag_3, a model for Ag aggregates present on actual supported catalysts. A primary prediction of this work is the existence of two near-degenerate states of O_{ad}, with binding energies of 77.8 and 78.7 kcal/mol [in excellent agreement with TDS data for O/Ag(110) and O/Ag(111)], but with only one predicted to be active for olefin epoxidation. These states are proposed to be unique forms of oxygen occupying distinctly different adsites on Ag. Implications for other mechanistic aspects of this reaction (e.g., the role of promoters and the combustion pathway) are discussed, with new interpretations offered of recent single-crystal studies of the epoxidation reaction in terms of monatomic oxygen as the active oxidizing agent.

I. Introduction

The selective oxidation of ethylene to ethylene oxide (EO) is an exceedingly important industrial catalytic reaction, providing the feedstock chemical for the production of ethylene glycol, which is in turn used to synthesize antifreeze and polyesters.[1] The industrial reaction is usually carried out at pressures of 10-12 atm and at temperatures of about 540°K, with a catalyst consisting of silver dispersed on α-alumina,

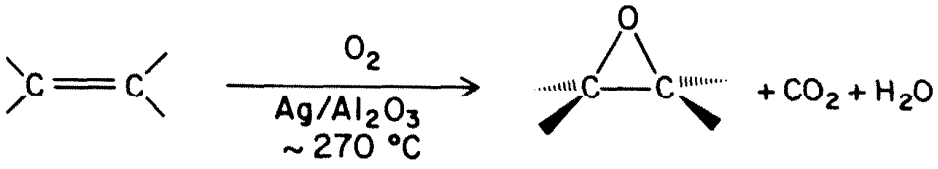

(1)

with trace quantities of chlorine (usually in the form of 1,2-dichloroethane), cesium (in the form of aqueous solutions of CsOH, $CsNO_3$, or Cs_2CO_3[2]), and other promoters added in order to increase the activity and selectivity of the catalyst. Total combustion of the olefin to CO_2 and H_2O is a competetive process, with alkali metals and chlorine (as well as other electronegative elements) known to inhibit this latter route.

The unique aspects of this partial oxidation are the following:[3-5]

(i) silver is especially active, with other transition metals yielding only products of total combustion;

(ii) chlorine, calcium, potassium, and cesium are among the known promoters of the reaction; and

(iii) epoxidation is only efficient for ethylene, with higher olefins combusted to CO_2 and H_2O.

It is not known why silver is so exceptional nor is it fully understood why olefins other than ethylene are combusted rather than epoxidized. In addition, despite the

relative simplicity of this system, there remains great controversy over the precise nature of the active form of oxygen (atomic versus molecular[3-6]) and over the mechanism by which alkali metals and chlorine act to promote the formation of EO.[7]

Much emphasis has been placed on achieving maximum selectivity to EO (i.e., minimal combustion), since the production of EO from ethylene is such a lucrative industry. Proponents of molecular $O_{2,ad}$ as the active species claim that selectivities higher than 6/7 are unattainable, due to a postulated mechanism in which an adsorbed peroxy radical reacts with ethylene, forming EO with the outside oxygen and forming CO_2 with the oxygen which remains behind. The stoichiometry of the two competing reactions would then fix the maximum selectivity at 6/7:[6]

$$C_2H_4 + O_{2,ad} \longrightarrow C_2H_4O + O_{ad} \tag{2}$$

$$C_2H_4 + 6O_{ad} \longrightarrow 2CO_2 + 2H_2O \tag{3}$$

(This scheme assumes that the outer oxygen exclusively forms EO and the surface-bound oxygen exclusively combusts ethylene.) A mechanism involving atomic oxygen, however, sets no maximum on the selectivity to EO. While unpromoted catalysts normally achieve selectivities in the range of 45%,[6] a recent report indicates selectivities as high as 85-87% (at or slightly above the theoretical maximum from the above mechanism) when NaCl was added to the catalyst.[8] Thus it is not at all clear whether 6/7 is a true theoretical limit on the selectivity of the partial oxidation of ethylene.

Detailed experimental data exist to support either O_{ad} or $O_{2,ad}$ as the active precursor to ethylene oxide.[7f,9-13] However, all evidence supporting molecular oxygen is indirect,[7f,9-12] while there does exist direct evidence for the evolution of EO in the presence of O_{ad}.[13] The most recent experiments to be interpreted in terms of molecular oxygen as the active agent are due to Campbell,[7f,12] who found no direct correlation between the steady-state coverage of monatomic oxygen (by varying the crystal face, the temperature, or the coverage of chlorine) and the rate of EO

production. He concluded from these negative results that diatomic oxygen must be the active species for epoxidation. We have a different interpretation consistent with his data (Section IV), invoking O_{ad} as the active site for expoxidation.

The most convincing evidence to date supporting monatomic oxygen was recently reported by van Santen and de Groot.[13f] $^{16}O_2$ was initially adsorbed on Ag powder at high temperature (475°K) to produce monatomic $^{16}O_{ad}$ [c.g., O_2 adsorbs dissociatively above 150°K on Ag(110)[14]], with an adsorbed oxygen to surface Ag ratio of $\sim$ 1. (Separate experiments showed that this precovered oxygen surface yielded epoxide when reacted with ethylene.) Then a mixture of gaseous $^{18}O_2$ and C_2H_4 was introduced at room temperature to the ^{16}O-precovered surface, and the temperature was increased at a rate of 2.3°K/min. Under conditions where gaseous oxygen scrambling was slow, ethylene first reacted to form exclusively $C_2H_4{}^{16}O$, followed later by the ^{18}O analog. Unless the oxygen adatoms recombine immediately prior to reaction (which has not been ruled out), these experiments indicate that O_{ad} is the direct precursor to EO.

The promoters which have been studied most thoroughly experimentally are Cl and Cs.[7,8] Since they observed an increase in rate of EO production at high Cl coverages, Campbell and Koel have concluded that Cl promotes EO formation by site-blocking, with CO_2 production suppressed due to its site requirement for formation presumed larger than for EO formation.[7a-c] While this may be one service Cl provides, we believe it is the *specific sites blocked by Cl* which are crucial to the formation of the oxidant active for EO synthesis (Section IV). Concerning Cs and other alkali metals, Lambert has demonstrated that Cs inhibits isomerization and hence the secondary combustion of EO on Ag(111).[7g,h,15] On the same surface, Campbell found that cesium is converted to a surface cesium oxide with the approximate composition CsO_3, under the reaction conditions for producing EO. Again, Campbell proposes a site-blocking mechanism for the role Cs plays as a promoter.[7d] We prefer (Section IV) to consider the electronic rather than the steric effect that cesium may induce when aggregated with oxygen.

The present work is concerned with calculating qualitative features (e.g, the nature of the adsorbate-silver bond) and quantitative features (e.g., binding energies, vibrational frequencies, and equilibrium geometries) of the interaction of a silver cluster with various adsorbates postulated or known to play a role in the epoxidation chemistry. We have focused this first study on Ag_3, as a model for the close-packed (111) plane of silver, which should be the primary surface on supported catalysts (due to its thermodynamic stability). We begin by discussing the qualitative aspects of bonding atomic and molecular species to the Ag_3 cluster in Section II. Reported in Section III are results for H, Cl, O, O_2, OH, and C_2H_4 interacting with the 1-fold (1F), 2-fold (2F), and 3-fold (3F) sites of Ag_3. Section IV discusses these results in terms of their impact on interpreting experimental data from extended surfaces and on the various controversial mechanisms outlined above. We propose our own view of the epoxidation reaction, in terms of the active oxygen species, the role promoters play in stabilizing it, and other contributions by promoters which enhance the production of EO. Section V concludes with a summary of the cluster findings and their impact on the mechanistic details of the epoxidation reaction over Ag. Section VI provides calculational details.

II. Qualitative Bonding of X to Ag_3

When an gaseous atom or molecule adsorbs on a perfect surface, the infinite two-dimensional periodicity is broken, with the subsequent interactions expected to be localized. Thus we believe that the chemical bonding between an adsorbate and a substrate is a localized phenomenon, and therefore may be well-represented by the interaction of an adsorbate on a finite cluster. The cluster model we have chosen is three silver atoms in an equilateral triangle with a Ag-Ag distance equal to the nearest neighbor distance in bulk Ag [R(Ag-Ag) = 2.89Å]. The cluster geometry is kept fixed, while the adsorbate degrees of freedom are optimized, in order to mimic the interaction of an adsorbate with an unreconstructed surface.

With a valence electron configuration for Ag of $4d^{10}5s^1$, the closed shell Ag d-

electrons do not participate directly in metal-metal bonding, while the s-electrons on Ag form the Ag-Ag bonds. Ag_3 has three valence s-electrons, with the ground $^2E'$ state (D_{3h} symmetry) having two electrons spin-paired to form the Ag-Ag bond, leaving one s-electron in a singly-occupied orbital. The valence orbitals for one component of the $^2E'$ state are shown in fig. 1 ($^2A_1$ for this C_{2v} resonance structure). We find, as in alkali metals,[16] that the electrons localize in interstitial sites, bond midpoints in this case, due to the greater strength of one-electron bonds over two-electron bonds in systems where the orbitals have low overlap (S$\sim$0.4) [e.g., $D_0(Li_2^+) = 1.44$ eV whereas $D_0(Li_2) = 1.05$ eV]. These localized electrons then spin-pair to form a low spin ground state, often causing geometric distortions.[16] However, since we are not concerned here with predicting the ground state structure of Jahn-Teller-distorted Ag_3,[17] but instead are interested in modeling a surface, we constrain Ag_3 to the equilateral triangle geometry to model the (111) face.

The presence of the radical orbital on Ag_3 (fig. 1a) is in contrast to the electronic structure of bulk Ag, which is diamagnetic (no unpaired spins). Thus, we expect that adsorbate-cluster bonds in the 2F site (where the radical orbital has the greatest amplitude) will be especially strong, with binding energies larger than that expected for an extended surface. On an actual surface of Ag, some coupling energy (probably fairly small) will have to be expended in order to unpair Ag spins (breaking Ag-Ag bonds) so that bonds to the adsorbates may be formed. The 1F site on Ag_3 is generally next lowest in energy, since the radical orbital has considerable amplitude there. The 3F site should give a lower bound to the binding energy of most species, since the electron density of this cluster is centered around the bond midpoints, leaving the center of the cluster (the 3F site) electron-deficient.

Fig. 2 schematically depicts the binding of H, Cl, and O to the 2F site of Ag_3. Both H (^2S) and Cl (^2P) have one unpaired electron which can be spin-paired to the Ag_3 radical electron, as shown in figs. 2a and 2b. The bond to Cl is in reality very ionic, so fig. 2b is not meant in any way to imply that covalent bonding occurs (see Section III.B). Oxygen atom (^3P), with its two unpaired electrons can either

form one σ and one π bond (fig. 2c) to the $^4A_2$ state of Ag_3 (30.1 kcal/mol above the ground $^2A_1$ state) or it can form ionic bonds to the $^2A_1$ state, pulling the radical electron off the cluster to form $Ag_3^+O^-$. O^- (^2P) has two possible orientations with respect to the C_2 axis, with either the unpaired electron along the C_2 axis (denoted $^2\Sigma$ in fig. 2d) or with the unpaired electron perpendicular to this axis (denoted $^2\Pi$ in fig. 2e). Similar bonding configurations are found for adsorbate bonding in the 1F site (retaining C_{2v} symmetry) and in the 3F site (C_{3v} symmetry). The bonding of the molecular adsorbates (OH, O_2, and C_2H_4) is somewhat more complex and discussion of them is deferred to the next section.

III. Results

Although configurations involving adsorption in the 1F site are of theoretical interest, they are less important for comparison to experimental results than the ground states of each Ag_3X system, along with the 3F binding sites expected to be prevalent on aggregated Ag. Hence we will emphasize results for the ground state of each complex and for the electronic states arising from interaction of the adsorbate with the 3F binding site.

A. Ag_3H

The simplest adsorbate to interact with the Ag_3 cluster is hydrogen. The three adsorption sites are shown schematically below, for the singlet states of Ag_3H.

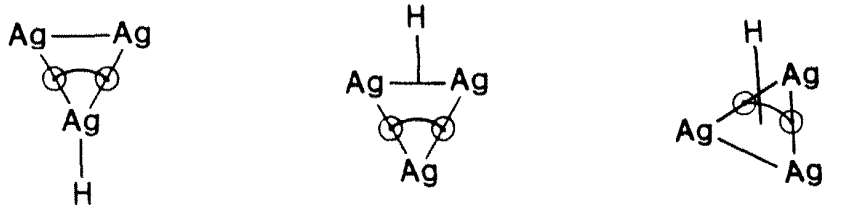

(4)

1F **2F** **3F**

Predicted properties are listed in Table I for Ag_3H as a function of adsorption site and electronic state. The ground state ($^1A_1$) involves hydrogen bonding to the radical orbital on Ag_3 (fig. 2a), leading to the planar 2F site as the lowest energy

configuration (nonplanar configurations of the cluster were found to be higher in energy). The Ag_3-H bond strength of 56.8 kcal/mol is similar to second row, late transition metal-hydrogen diatomic bond strengths (54 - 59 kcal/mol[18]) presumably because of the similarly large amounts of metal s-character involved in both the bond to the cluster and to the metal atom in M-H (90% s-character in the Ag_3 radical orbital).[18]

The one-electron GVB orbitals for the Ag-Ag and Ag_3-H bonds are shown in fig. 3, where we see that the Ag-Ag bond (fig. 3b) has moved out of the way of the 2F site to avoid interaction with the Ag_3-H bond. Fig. 3a indicates that the Ag_3-H bond is essentially covalent, with one electron localized on the cluster and one electron in a 1s orbital on hydrogen, spin-paired to form the Ag_3-H bond. The degree of ionic character is assessed quantitatively in Table II, where Mulliken population analysis indicates that hydrogen actually pulls 0.2-0.4 electron off of the cluster, resulting in a substantial dipole moment for H in the 1F and 3F sites. The dipole moment is nearly zero for the 2F site because the negative image charge on the "bulk" Ag atom (the atom not directly attached to the adsorbate) cancels out the effect of the charge shift to H. We have also indicated the shift expected in the Ag 4d-band upon adsorption of H, with the 3F $H_{(ad)}$ shifting the d-band the most (downward by 0.4 eV). The large charge transfer to hydrogen is due to the small vertical ionization potential (IP) for Ag_3 of 4.18 eV (in good agreement with 4.26 eV for the work function of bulk Ag[19]).

Examining the excited states in Table I, we see that the 1F binding site lies above the ground state by 4.4 kcal/mol. In the 1F geometry, the H is attached to only one of the Ag atoms, within the plane of the cluster. Although the distance to the cluster, $R_\perp$, is shorter for the 2F site, the actual Ag-H distance is longer for 2F [R(Ag-H) = 2.02 Å] than for 1F [R(Ag-H) = 1.77 Å], leading to a lower vibrational frequency for the 2F Ag_3-H. The binding energy for the 1F site is found to be weaker than the 2F binding energy by 6 kcal/mol. (The relative total energies reported are from GVB-PP calculations, whereas the bond energies are calculated

at the CCCI level; this results in slightly different energy splittings when comparing the two levels of calculation.)

Two triplet states lie next highest in energy, with the $^1A'$ state of the 3F site lying 39.1 kcal/mol up from the 2F ($^1A_1$) ground state. The binding energy of H to the 3F site is less than half that predicted for the ground state of the cluster [D(Ag-H) = 28.5 kcal/mol for the $^3A''$ state and D(Ag-H) = 19.5 kcal/mol for the $^1A'$ state]. For adsorbates such as H, where covalent bonding is expected, the 3F site suffers from a lack of electron density in the center of the cluster, leading to low overlap in the Ag_3-H bond, and hence a low binding energy. On an extended surface, however, we expect much larger electron density in the 3F hollows,[16] with larger binding energies as a result. Thus the 3F binding energy for H is a lower bound on the actual Ag surface-H bond energy.

Dissociative adsorption of H_2 has not been observed on Ag and is known to be activated on Cu and Au.[20] Therefore, either the process is activated or endothermic (and thus activated) on Ag. If it is an endothermic reaction, then the binding energy of H to Ag must be less than 52 kcal/mol (half of the bond energy in H_2). Consistent with this expectation, the 2F site bond energy of 56.8 kcal/mol is an upper bound, since no unpairing energy present on an extended surface is incurred for Ag_3. However, the 2F site binding energy may reflect the stability of H bound at a step or kink, where unpaired Ag electrons may be present (as in Ag_3). The Ag-H binding energy is thus bracketed to an upper bound of 57 kcal/mol near sites of unsaturation and a lower bound of 20 kcal/mol for a 3F site. We expect that larger clusters will have higher binding energies to 3F sites as a result of more density present in the 3F faces. Indeed, results for tetrahedral Ag_4 from pseudopotential local density functional (LDF) calculations[21] indicate binding energies to the 3F face of 49.8 kcal/mol and to the 2F bridge of 54.6 kcal/mol, the latter in good agreement with our CCCI result of 56.8 kcal/mol. (We have also calculated the binding energy of H to the 2F bridge site of tetrahedral Ag_4 using CCCI methods, yielding a binding energy of 55.2 kcal/mol, again in good agreement with the LDF

work of ref. 21.)

B. Ag_3Cl

The three possible high symmetry adsorption sites for Cl on Ag_3 are shown below.

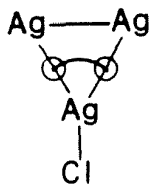

1F

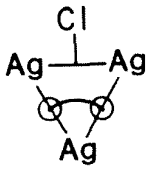

2F

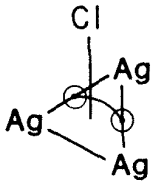

3F

(5)

Table III lists predicted properties of Cl bonding to both the $^2A_1$ ground state of Ag_3 and to the $^4A_2$ excited state (30.1 kcal/mol up), resulting in a spectrum of low-lying singlet and triplet states. Unlike H, the singlet states are all lower in energy than the triplet states. The bond between Ag_3 and Cl is much more ionic (Table II) than the Ag_3-H bond. Thus the relative stabilities of the triplet and singlet states of Ag_3Cl are due primarily to the triplet-singlet splitting in Ag_3^+ (ΔE_{ST} = 50.5 kcal/mol).

The ground state has Cl in the 2F site ($^1A_1$), with a Ag-Cl distance of 2.72 Å ($R_\perp$ = 2.23 Å), an Ag_3-Cl vibrational frequency of 211 cm^{-1} and a bond energy of 91.0 kcal/mol. The bond distance is very close to that observed for Cl on Ag(111) from SEXAFS experiments, in which the Cl was found to reside in 3F sites with R(Ag-Cl) = 2.70±0.01Å.[22] Although Cl_2 dissociates readily on Ag, no binding energies for Cl on Ag have been reported, primarily because there is some uncertainty as to whether Cl desorbs as Cl_2 or as AgCl.[23]

The orbitals for the ground state of Ag_3Cl (fig. 4) indicate a large amount of ionic character in the Ag_3-Cl bond, with the Ag-Ag bond again moving out of the way of the Ag_3-Cl bond (as for Ag_3H). Table II supports the assertion that the bonding is ionic, with approximately 0.6 electron removed from the cluster by Cl for all three sites. Significant dipole moments and d-band shifts are predicted

for all three sites of Ag_3Cl, with a very large dipole moment of 12.5 debye and d-band shift of 0.8 eV predicted for the 1F site. The dipole moments as a function of adsite for electronegative groups such as Cl and O (vide infra) show the following trend: 1F exhibits the largest dipole moment, 2F a moderate dipole moment, and 3F the smallest dipole moment. Since the 1F site has the most dispersive charge distribution, with the adsorbate negatively-charged and all three Ag atoms positively-charged, it exhibits the largest dipole moment. The 2F site has the next most wide-spread charge distribution, but the small negative image charge on the "bulk" Ag atom induces a dipole moment less than half the size of the 1F dipole moment. The closest approach of the adsorbate is in the 3F site, leading to the smallest dipole moment. A trend is also apparent in the d-band shifts: for clusters where the "bulk" Ag atoms are positively-charged, the d-band shifts are quite large (i.e., for the 1F site). Decreasing the occupation of the sp-band (the valence Ag orbitals) stabilizes the d-band by lowering electron-electron repulsion.

The 1F site lies 9.3 kcal/mol above the 2F site, with the 3F site 22.0 kcal/mol up (Table III). The 3F site has an Ag-Cl bond length of 2.90 Å ($R_\perp$ = 2.38 Å) and a bond energy of 79.7 kcal/mol. This is 0.18 Å longer than for the 2F site and 0.20 Å longer than the experimental value for Cl/Ag(111). This suggests that Cl adsorbed on Ag(111) is held more tightly than the theoretical 3F site properties would imply. The bond energy of Cl to Ag_3 in the 3F site is therefore expected to be a lower bound on the surface-Cl binding energy (as with Ag_3H). Thus, we have been able to bracket the Ag-Cl surface bond energy to within $\sim$ 10 kcal/mol, since the Ag-Cl bond for the 2F site (91.0 kcal/mol) should be an upper bound (see Section II) and the Ag-Cl 3F site provides the lower bound of 79.7 kcal/mol. Since no experimental values are available, these values may only be compared to results from semi-empirical SW-Xα calculations for Cl on an Ag_5 cluster, which yielded a binding energy of 72.2 kcal/mol.[24]

C. Ag_3O

The low-lying states of oxygen on Ag_3 adsorbed on a 2F site are indicated in figs. 2c - e, while we show the three low-lying states of oxygen on a 3F site of Ag_3 below.

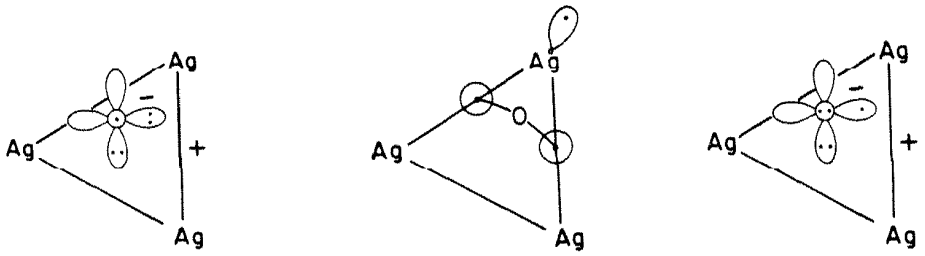

$^2\Sigma$ di-σ $^2\Pi$ (6)

Instead of a σ and π double bond as found for the 1F and 2F sites for O/Ag_3 (fig. 2), we obtain two equivalent σ bonds for the double-bonded state of the 3F site, denoted as di-σ bonding.

Table IV displays the properties for the three low-lying states of Ag_3O binding to all three sites. Again, the 2F site is favored, with the ionic bonding configurations of figs. 2d and 2e separated by only 2.7 kcal/mol, while the $\sigma\pi$ double-bonded state lies 29.8 kcal/mol higher in energy. The ground state has an Ag-O bond length of 2.26 Å ($R_\perp$ = 1.74 Å), an Ag_3–O vibrational frequency of 332 cm^{-1}, and a bond strength of 92.9 kcal/mol. Again, this bond energy is expected to be an upper bound to the surface-O binding energy, because both the slightly smaller (vertical) IP of Ag_3 (4.18 eV) relative to the bulk work function of Ag (4.26 eV) and the localized hole (positive charge) on the cluster work to create a stronger ionic bond. The $^2\Pi$ state (2.7 kcal/mol up) has a longer bond length [$R_\perp$ = 1.91 Å or R(Ag-O) = 2.55 Å], a smaller vibrational frequency (289 cm^{-1}), and a slightly smaller bond energy (90.2 kcal/mol) than the ground state. This is due to the doubly-occupied O pσ orbital which prevents a close approach of O to the cluster. The ground state, on the other hand, can form a shorter, stronger bond to the cluster because the O pσ orbital is singly-occupied. In contrast, the 1F $^2\Pi$ state is much lower in energy (3.1 kcal/mol above the ground state) than the 1F $^2\Sigma$ state (23.4 kcal/mol). The

bonding for 1F resembles AgO diatomic, since the oxygen is bound to only one Ag atom. AgO has a similar ordering of states, with a $^2\Pi$ ground state and a $^2\Sigma$ excited state $\sim$ 15 kcal/mol higher.[25]

The two lowest states of oxygen in the 3F site are of primary importance to the discussion in Section IV, since they represent the most realistic binding site on Ag_3 to compare with an extended surface. We see from Table IV that the two lowest states in the 3F site are nearly degenerate, separated by 0.9 kcal/mol (up 14 kcal/mol from the 2F ground state). These near degenerate states have very different properties, however, with the $^2\Sigma$ radical state exhibiting a long bond length ($R_\perp$ = 1.80 Å) and a small vibrational frequency (299 cm^{-1}), while the di-σ state (0.9 kcal/mol higher) has a much shorter bond length ($R_\perp$ = 1.37 Å) and a higher vibrational frequency (412 cm^{-1}). The vibrational frequency for O/Ag(110) is known from electron energy loss spectroscopy (EELS) to be 315 cm^{-1}, in good agreement with the 3F radical state.[26] The bond energies for the two 3F states are predicted to be 78.7 and 77.8 kcal/mol. This is in excellent agreement with thermal desorption data from O/Ag(110) and O/Ag(111) where O desorbs at temperatures between 565 and 600°K (depending on the crystal face and the coverage), implying a surface-oxygen binding energy of $\sim$ 80 kcal/mol.[26,27] Our results are in contrast to Hartree-Fock calculations reported for O on Ag_{26}, where, although good agreement was obtained for the vibrational frequency and distance from the surface, a Ag-O bond energy of 9 kcal/mol was predicted for the 4-fold bridge site on Ag(110).[28]

The $^2\Pi$ radical state in the 3F site is $\sim$5 kcal/mol higher than the two 3F states discussed above, with the oxygen much less tightly bound, as indicated by the long bond length ($R_\perp$ = 1.92 Å) and the low vibrational frequency (252 cm^{-1}). Even higher in energy are the $^2\Sigma$ radical state for the 1F site and the two $\sigma\pi$ double-bonded states for the 1F and 2F sites. The $\sigma\pi$ double-bonded states in the 2F and 1F sites are destabilized because they involve very weak π bonds due to the low overlap between the cluster valence b_2 orbital and the oxygen pπ orbital: for the 2F site (discussed below), the π bond resolves this problem by ionizing the cluster,

while the π bond in the 1F site involves two weakly-coupled singly-occupied orbitals with an overlap of 0.06! This explains why the 1F $\sigma\pi$ double-bonded state is so high in energy (53.9 kcal/mol up). The 3F analog, the di-σ state, forms ionic σ bonds (1.60 electrons on O in each bond) with some back-donation bonding from the O lone pair, leading to a large stabilization of the di-σ state over the $\sigma\pi$ double-bonded states.

In sum, we predict that the radical states are preferred for the 1F and 2F sites, while two very different states [with stark contrasts in both predicted properties and reactivity (Section IV)] are competetive for the 3F site, one with radical character on oxygen and one with the O 2p electrons tied up in bonds to the cluster, leaving no unpaired electrons on oxygen.

The orbitals for the three states of O on Ag_3 in the 2F site are shown in figs. 5 - 7. Fig. 5 shows the ground state ($^2A_1$) of Ag_3O, with fig. 5a depicting the singly-occupied O 2p radical [oriented perpendicular to the cluster "surface" (i.e., the two Ag atoms)], fig. 5b shows the in-plane, doubly-occupied O 2pπ lone pair, and fig. 5c displays the Ag-Ag bond. Fig. 6 shows the $^2B_2$ excited state, in which the radical orbital (fig. 6b) now is oriented parallel to the cluster surface, with the doubly-occupied O 2p orbital perpendicular to the surface. Comparison of the Ag-Ag bonds in figs. 5c and 6c reveal that the Ag-Ag bond delocalizes towards the surface of the 2F site more in the $^2A_1$ (or $^2\Sigma$) radical state than in the $^2B_2$ (or $^2\Pi$) radical state, presumably because the O 2p orbital of the $^2A_1$ radical is only singly-occupied. This delocalization may explain why the $^2\Sigma$ orientation is preferred over the $^2\Pi$ orientation for the 2F site.

The orbitals for the "$\sigma\pi$ double-bonded" state (also $^2A_1$) are shown in fig. 7, where we see that the π bond (fig. 7b) is very ionic and strongly resembles the doubly-occupied oxygen pπ in the $^2A_1$ ground state (fig. 5b). Hence, although this $^2A_1$ excited state is derived from a $\sigma\pi$ double bond, the π bond is extremely ionic (with 1.67 electrons on the oxygen and only 0.33 on the cluster). This excited state is very high in energy (29.8 kcal/mol up), since the Ag-Ag bond has been broken

in the cluster. It is also destabilized because it must be orthogonal to the ground state, which has the same symmetry ($^2A_1$). The major difference between these two $^2A_1$ states is the location of the unpaired electron: the ground state has a radical electron on the oxygen, while the excited state has radical character on the cluster.

In Table II we see that all of the low-lying states of oxygen pull 0.6 - 0.7 electron off the cluster, leading to large dipole moments which follow the same trend as discussed above for Cl and H (i.e., the 1F site has the largest dipole moment due to the larger distance over which charge is distributed, the 2F states have more moderate dipoles due to the negative image charge on the "bulk" Ag atom, and the 3F states have the smallest dipoles since they have the most compact charge distributions). The Ag d-band is largely unaffected by adsorption of O, except for the 1F site, where the large polarization of the s-electrons induces the d-band shift, as discussed for Cl.

D. Ag_3O_2

The two lowest energy configurations for O_2 on Ag_3 are shown below, with the ground state having the parallel O_2^- structure (denoted as η^2 to indicate that both oxygen atoms are bound to the surface), with the η^1 peroxy (only one oxygen bound to the surface) lying 4.1 kcal/mol higher.

(7)

Except for the 2F peroxy species, only high symmetry orientations of O_2 on all three sites were considered (Table V). For the 2F site, we examined the following orientations:

(i) η^2 ***2-fold.*** O_2^- is bound parallel to the 2F surface and in the Ag_3 plane (ground state);

(ii) η^1 ***peroxy.*** One oxygen is bound to the surface with the other oxygen free [the

optimum C_s symmetry geometry, assuming the attached oxygen binds above the Ag-Ag bond midpoint, has $R_{\perp}(Ag_2\text{-}O) = 2.24$ Å, R(O-O) = 1.33 Å, and the outer oxygen displaced by 1.7° degrees off the horizontal and toward the cluster) (4.1 kcal/mol up);

(iii) η^1 *end-on.* All atoms are coplanar with one oxygen bound to the surface, and the O-O axis perpendicular to the Ag-Ag 2F site and along the C_2 axis of the molecule (9.8 kcal/mol up); and

(iv) η^2 *2-fold* $\perp$ *bridge.* The O-O axis is perpendicular to the Ag-Ag axis, with the oxygen atoms above and below the Ag_3 plane (the O-O bond midpoint is coplanar with Ag_3 and lies on the C_2 axis of the molecule) (16.2 kcal/mol up). Two orientations were examined for each of the 1F and 3F sites:

(v) η^2 *1-fold.* All atoms are coplanar, with the O-O axis parallel to the two "bulk" Ag atoms and the O-O bond midpoint lies along the C_2 axis, with the O atoms equidistant from the "surface" Ag atom (13.2 kcal/mol up);

(vi) η^1 *end-on 1-fold.* All atoms are coplanar, with the O-O axis perpendicular to the "bulk" Ag atoms and along the C_2 axis of the molecule (25.9 kcal/mol up);

(vii) η^2 *3-fold.* The O-O axis is parallel to the Ag_3 plane, lying directly above a perpendicular bisector of the Ag_3 triangle, with the O-O bond midpoint directly above the center of the cluster (26.4 kcal/mol up); and

(viii) η^1 *end-on 3-fold.* The O-O axis is perpendicular to the Ag_3 plane and directly above the center of the cluster (29.7 kcal/mol up).

The properties of geometries (i) - (viii) are listed in Table V. The ground state ($^2A_2$) has an O-O bond length and vibrational frequency of 1.32 Å and 1264 cm^{-1}, respectively, with a very large bond energy of 46.9 kcal/mol. The peroxy state, which has been proposed as a possible intermediate in the synthesis of EO, has a similar O-O bond length of 1.33 Å but with a lower vibrational frequency of 921 cm^{-1} and a smaller bond energy of 36.3 kcal/mol. These values differ sharply from observed binding energies for O_2 on Ag (ranging from 11 - 13 kcal/mol,[14,27b] depending on crystal face) and from the observed O-O vibrational frequency of 639

cm^{-1} on Ag(110).[26,29]

For all geometries examined, we find that the bond between O_2 and Ag_3 is very ionic (e.g., 0.70 electron is transferred from the cluster to O_2 in the ground state). Thus Ag_3O_2 is best thought of as $Ag_3^+O_2^-$, with binding energies much larger than those found on extended surfaces because the localized positive charge on the cluster (not present on the surface) induces an anomalously strong ionic bond. The average O-O vibrational frequency of all the geometries listed in Table V is 1036 cm^{-1}, which is close to the O-O stretch in O_2^- (ω_e = 1090 cm^{-1}).[30] The O-O bond length for O_2 on Ag(110) has recently been estimated from NEXAFS experiments to be 1.47±0.05 Å,[31] very close to the bond length of 1.48 Å in $(CH_3)_3CO\text{-}OC(CH_3)_3$,[32] but very much longer than the 1.32 - 1.39 Å range which we find for O_2 on Ag_3.

While our model clearly does not describe the states of dioxygen observed on extended Ag surfaces, we at least may conclude that O_2 prefers a symmetric configuration rather than η^1 peroxy or end-on orientations. This is consistent with XPS data for O_2 on Ag(110), in which only one sharp O 1s peak is observed, indicating that the O_2 is lying parallel to the surface.[33] A recent XPS study of O_2 on Ag(111) indicates the oxygens may not be equivalent,[34] which could be interpreted either as O_2 being tilted with respect to the surface (as in the η^1 peroxy species) or as the O_2 lying parallel to the surface but with each oxygen sitting over inequivalent sites.

In order to successfully model the interaction of dioxygen with the Ag(110) surface, at least four Ag atoms will be needed to mimic the 4-fold trough site. Future work will require examining O_2 on a bent rhombus Ag_4 cluster in order to model the four-fold site of the (110) face.

E. Ag_3OH

Table VI displays properties for OH binding to the 1F, 2F, and 3F sites on Ag_3. We find that OH prefers to bind in a linear fashion, rather than bent or tilted with respect to the surface. This is due to the ionic character of the Ag_3-OH bond,

in which 0.6 - 0.8 electron (depending on the site) is transferred to OH from the cluster. Therefore the bonding in Ag_3OH is best viewed as OH^- interacting with Ag_3^+. The 2F site is again lowest in energy, with the bond energy of 78.9 kcal/mol providing an upper bound to the bond energy on an extended surface. The 3F site is 18.8 kcal/mol higher in energy, with the bond energy of 59.1 kcal/mol expected to reflect that of OH bound in a 3F site on a single crystal face of Ag. The 1F site lies slightly higher in energy (20.2 kcal/mol up) and has a bond energy of 69.4 kcal/mol.

As before, the relative energies are calculated at a different level than the bond energies (Section VI). Since the bond energies were calculated using CI methods and the relative energies shown in Table VI are from the lower level GVB-PP calculations, it may be that a more reliable ordering of states is obtainable from the relative bond energies. This would lead to the 3F site being 19.8 kcal/mol above the 2F site (in good agreement with the GVB-PP result) and to the 1F site being only 9.5 kcal/mol above the ground state. The GVB-PP energies for 1F and 3F are close in energy, so that the dynamic correlations included in a CI calculation could very well change the ordering of the excited states.

The vibrational frequencies for Ag_3OH may be compared to values for OH adsorbed on Pt(111),[35] where the O-H stretch is 3480 cm^{-1} and the Pt-O stretch is 430 cm^{-1}. The predicted Ag_3-O stretch in the 1F site (445 cm^{-1}) is closest to the experimental value, while the O-H stretch in the 3F site (3637 cm^{-1}) most closely resembles the experimental result. A strong intensity bending frequency is also observed on Pt, which was interpreted as a tilted OH group on the surface. However, if the OH group is linear and perpendicular to the surface, the bending (or frustrated rotational) mode is dipole allowed, so that our findings are still consistent with the observations on Pt(111).

Since OH is valence isoelectronic with Cl, and Cl is known to sit in 3F sites on Ag(111), we suggest that OH also adsorbs in 3F sites. The binding energy of OH to the 3F site (59 kcal/mol) along with the predicted binding energy of O_{ad} (79

kcal/mol) may then be used to estimate the thermodynamics of hydroxyl disproportionation to $H_2O_{ad} + O_{ad}$. Assuming a binding energy for water in the presence of O on Ag(110) of 15 kcal/mol (H_2O desorbs at 240°K under such conditions[36]) and assuming that the O-H bond strength in adsorbed water is the same as the O-H bond strength in adsorbed OH (vide infra), we estimate that hydroxyl disproportionation is endothermic by $\sim$ 24 kcal/mol. This is in good agreement with recent work by Madix and co-workers who followed the kinetics of hydroxyl disproportionation on oxygen-covered Ag(110) and found an activation energy of 22.2⊥0.3 kcal/mol.[37] Thus our binding energy for the 3F site of 59.1 kcal/mol provides a good estimate of the true binding energy of OH to Ag.

F. $Ag_3(C_2H_4)^+$

Calculations on ethylene interacting with neutral Ag_3 yielded only repulsive potential curves. This is consistent with the low probability for adsorption of ethylene on clean Ag surfaces.[38] On oxygen-precovered surfaces, however, the more electrophilic Ag atoms readily adsorb C_2H_4.[38] As a model for these electrophilic sites, we have examined five high-symmetry orientations of ethylene bound to Ag_3^+, shown schematically in fig. 8. They are listed in terms of decreasing energy, with the 3-fold bridge being the least-favored and with both 1-fold sites being nearly degenerate in energy, so that the ground state should have essentially no barrier to rotation about the Ag-C_2H_4 bond.

Table VII shows the properties predicted for these five orientations, with the primary result being the prediction of an 8.7 kcal/mol bond energy for ethylene in the 1-fold site. This is in excellent agreement with the experimental heat of adsorption of $\sim$10 kcal/mol for C_2H_4 adsorption on an oxygen precovered Ag(110) surface.[38] (It is known that ethylene binds directly to Ag, since no change in the Ag-O stretch is observed in the EEL spectrum; thus this is heat of adsorption for ethylene on Ag, not ethylene on O_{ad}.) The good agreement between experiment and theory for the Ag-(C_2H_4) bond energy suggests that C_2H_4 may prefer to bind

in 1-fold sites on the Ag surface (as found for the cluster).

The bond lengths for the five adsorption sites increase for less favored binding sites, with the vibrational frequencies tracking the bond lengths consistently. Only a π-bonded form of ethylene was considered, since EEL spectra for C_2H_4 and C_2D_4 on Ag(110) reveal no change in the out-of-plane bending vibrations when compared to the gas phase values. This indicates that no substantial rehybridization occurs upon adsorption.[38a]

In sum, the predictions of this section are mostly in good agreement with experimental data, lending credence to the use of a metal cluster to represent the *localized* interactions present on an extended metal surface.

IV. Implications for Olefin Epoxidation

In this section we will address the major reaction steps involved in the partial oxidation of olefins, predicting both the thermodynamic feasibility and the qualitative nature of each reaction. We will develop a perspective which allows a reinterpretation of a series of experimental studies, leading to a global view of the types of oxygen which exist on the surface, how promoters work to stabilize the active form of oxygen, and how decomposition pathways occur.

Thermodynamics of Olefin Oxidation on Silver

From the experimental and theoretical heats of adsorption of oxygen, we conclude that O_2 dissociation is facile, proceeding through a chemisorbed O_2^- species (heat of adsorption $\sim$ 10 kcal/mol[27b]) which decomposes above 170°K to form a monatomic oxide.[26] From the results of Section III.C, we predict that two near-degenerate states of oxygen can populate high coordination sites on Ag surfaces. One we refer to as "di-σ" bonding, with both singly-occupied 2p-orbitals on O (^3P) spin-paired to the surface, forming two σ bonds. The other we refer to as "$^2\Sigma$ radical" bonding, to indicate the presence of a singly-occupied pσ orbital on O^-.

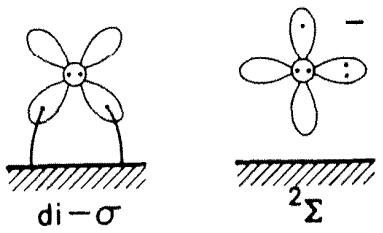

(8)

The di-σ species is predicted to have a short bond length ($R_\perp$ = 1.37 Å), a vibrational frequency of 412 cm^{-1}, and a binding energy of 77.8 kcal/mol. Since all of the electrons of the di-σ oxygen are intimately involved with the surface, we expect this species to be relatively inert and it should *not* be active for the formation of EO. In contrast, the $^2\Sigma$ radical species is expected to have a much longer bond length ($R_\perp$ = 1.80 Å), a smaller Ag-O vibrational frequency (299 cm^{-1}), but essentially the same binding energy to the surface (78.7 kcal/mol). We propose that the radical character of the $^2\Sigma$ oxygen nominates this species as the active oxidizing agent for EO formation. The oxygen radical orbital can easily break into the C=C π bond of an olefin, forming a radical center on the outer olefinic carbon, followed by rapid collapse to the epoxide. (The extra electron on O_{ad} is transferred to the surface upon reaction, i.e., the surface is reduced when the olefin is oxidized).

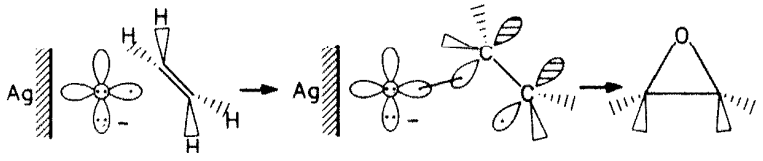

(9)

The mechanism shown in eq. 9 implies a loss of stereochemistry at one of the carbon atoms. In fact, stereospecific ethylene-1,2-d_2 does randomize (although not 100%) when oxidized to EO under actual catalytic reaction conditions,[39] lending support to the above mechanism. The production of epoxide is predicted to be thermodynamically favorable for both ethylene and propylene (ΔH_{rxn} = −6 and −8 kcal/mol for C_2H_4 and C_3H_6, respectively), where we have used the theoretical

value for the Ag-O binding energy (79 kcal/mol) in conjunction with the heats of formation of the olefins ($\Delta H^o_{f,298}$ = 12.5 kcal/mol for C_2H_4 and 4.9 kcal/mol for C_3H_6), epoxides [$\Delta H^o_{f,298}$ = −12.6 kcal/mol for EO and −22.6 kcal/mol for propylene oxide (PO)], and oxygen atom ($\Delta H^o_{f,298}$ = 59.6 kcal/mol) to predict the heats of reaction.[40]

Although the reaction is thermodynamically favorable, it is well-known that PO is produced in yields ranging from 0 - 5% from propene over Ag catalysts.[41] PO is formed in such small amounts due to the competing reaction of total combustion to CO_2 and H_2O. The rate-limiting step for total oxidation is presumably the first hydrogen atom abstraction from the olefin to form OH_{ad} on the surface, since the subsequent olefinic radical should be highly reactive and decompose rapidly. Hydrogen abstraction from ethylene is endothermic by ~28 kcal/mol, inhibiting combustion.[42]

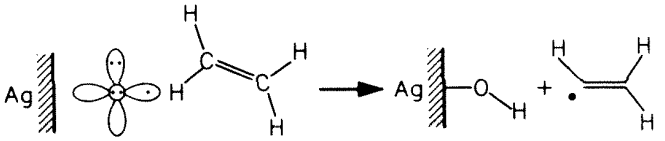

(10)

For propylene, however, the hydrogen abstraction reaction is predicted to be exothermic by ~ 3 kcal/mol.[43] Combustion of propylene competes significantly with partial oxidation, while ethylene combustion is unfavorable. The difference in energetics is merely due to the difference in C-H bond strengths for the two olefins. In the case of ethylene, the vinylic C-H bond strength is extremely strong, recently determined by Lee and co-workers[42] to be D^o_0 = 116.7±1.2 kcal/mol (D_{298} = 118 kcal/mol[42]), whereas the allylic C-H bond is much weaker (D_{298} = 87 kcal/mol[43]). The difference in C-H bond strengths may be understood in terms of the stability of the subsequent radical formed: in the case of C_2H_4, a highly unstable vinyl radical would be formed, while for C_3H_6, a resonance-stabilized allyl radical is formed, as shown below.

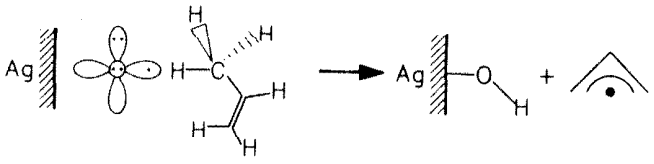

(11)

Thus any olefin with allylic hydrogens will combust; this explains why the epoxidation reaction over Ag is specific to ethylene. It would be interesting to know whether blocking the allylic sites, such as in styrene or *t*-butylethylene, leads to greater selectivity. Certainly such experiments would help determine whether the hydrogen abstraction occurs preferentially from the olefin or whether subsequent intermediates in the partial oxidation reaction are more susceptible to combustion.

After hydrogen abstraction from the olefin occurs to form surface-bound hydroxyls (H_{ad} is not formed, since the incipient Ag-H bond is weaker than the incipient O-H bond), water is produced as one of the final products of combustion. As discussed in Section III.E, the energetics for the formation of H_2O from surface-bound hydroxyl groups can be predicted from the theoretical values for the binding energies of OH (59 kcal/mol) and O (79 kcal/mol) and an estimate for the heat of adsorption of H_2O on Ag ($\sim$ 15 kcal/mol).[36] We assumed that the O-H bond strengths do not change significantly going from H_2O to OH_{ad}. This assumption is reasonable, since the average bond strength in water is 110.8 kcal/mol[40] and the bond strength in OH^- (similar to adsorbed OH, as discussed in Section III.E) is 110.6 kcal/mol.[30] These values lead to a predicted endothermicity of 24 kcal/mol to disproportionate two surface-bound hydroxyls to one adsorbed oxygen atom and one adsorbed molecule of H_2O. This is in good agreement with the activation energy of 22.2$\pm$0.3 kcal/mol observed for OH disproportionation on Ag(110).[37]

Identification of the Active Oxygen

As discussed in the Introduction, many investigations have been carried out to try to determine the nature of the oxygen which produces epoxide, in order to find

ways to optimize its concentration. Van Santen's recent labelling study involving an Ag surface pre-covered with $^{16}O_{ad}$ and exposed to a gaseous mixture of C_2H_4 and $^{18}O_2$ provides compelling evidence that adsorbed oxygen atoms are responsible for the production of EO, since initially only ^{16}O-labeled EO is formed.[13f] However, Campbell has shown that the rate of EO production is uncorrelated with the overall concentration of atomic oxygen, a conclusion based on the following two facts:

(i) for low coverages of oxygen ($\theta_O \leq 0.5$), the probability for dissociative adsorption is about two orders of magnitude smaller on Ag(111) than on Ag(110) at 490°K.[27b] Thus the steady-state coverage of O_{ad} is a factor $\sim$ 18 smaller on Ag(111) than on Ag(110), while the activities for EO production on the two surfaces differ only by a factor of two;[12c] and

(ii) coadsorption of Cl and O on Ag(110) and Ag(111) produced EO at rates dependent on chlorine coverage but independent of the steady-state concentration of O_{ad}.[7a-c]

Since the rate was found to be independent of the overall coverage of monatomic oxygen, Campbell concluded that diatomic oxygen must be the active precursor to EO.

Herein we present a new interpretation of the kinetic trends discussed above, in terms of atomic oxygen as the active species for epoxidation. The difference in steady-state coverages of O_{ad} between the (110) and (111) faces of Ag is due to the presence of more than one binding site for O on Ag(110). While the close-packed (111) surface has only 3-fold binding sites available (assuming the energy differences between the *hcp* and *fcc* sites are negligible), the corrugated (110) surface has *two distinctly different binding sites with undoubtedly different stabilities.* These two sites are shown in fig. 9, in which fig. 9a depicts the 4-fold site in the bottom of troughs (between the first and second layer Ag atoms), while fig. 9b displays the 3-fold site located on the side of the troughs. This 3-fold site is analogous to the 3-fold site present on the (111) plane of Ag.

At oxygen coverages below 0.5, p($n \times 1$) (n decreasing continuously from 7 to

2 as the oxygen coverage increases) low-energy electron diffraction (LEED) patterns form, which have been interpreted as oxygens residing in the 4-fold sites of the troughs.[6,44] At a pressure of 50 torr and a temperature of 485°K, a new high coverage ($\theta_O = 0.67$) form of oxygen has been recently observed on the (110) surface, exhibiting a c(6×2) LEED pattern.[27a] This high coverage form was shown to be reactive for CO oxidation to CO_2, but once the oxygen coverage dropped to 0.5 [p(2×1) LEED pattern], the reaction probability for CO oxidation dropped precipitously.

Several conclusions may be drawn from these observations:

(i) the 4-fold site on Ag(110) (fig. 9a) is filled first and thus is probably the most stable site for oxygen adatoms;

(ii) higher dosages of oxygen allow another site to fill which we interpret to be the 3-fold site (fig. 9b); and

(iii) the 4-fold site is less reactive than the 3-fold site as indicated by the CO titration studies.[27a]

Thus the difference in coverage of O_{ad} between Ag(110) and Ag(111) is due to the fact that the unreactive 4-fold sites on Ag(110) fill first, followed by filling the reactive 3-fold sites on Ag(110). Ag(111) only has 3-fold sites and therefore the activity per adsorbed oxygen atom is higher than that found for Ag(110). We believe that the crucial concentration is *not* the overall concentration of O_{ad} but rather the concentration of O_{ad} in 3-fold sites, and that perhaps these latter concentrations are similar on both crystal faces, resulting in similar activities for the formation of EO.

We predict on the basis of the present ab initio study that the oxygen species in the 3-fold site has the $^2\Sigma$ radical O^- character shown in eq. 8, since this species is predicted to be the most stable (by 1 kcal/mol) type of oxygen in the 3-fold site of Ag_3. This radical oxygen is set up to react with olefinic substrates, as indicated in eq. 9. The oxygen in the 4-fold site is expected to have di-σ-type bonding (eq. 8), resulting in an unreactive oxide, since all of the oxygen electrons are tied up with the

surface. The oxygens in the 4-fold hollows of Ag(110) have binding energies of $\sim$ 82 kcal/mol, whereas the 3-fold oxygens on Ag(111) are bound by $\sim$ 80 kcal/mol.[27b] Thus the di-σ bonding in the 4-fold site is slightly stronger than the di-σ bonding in the 3-fold site of Ag_3 (77.8 kcal/mol). The O^- radical in the 3-fold site of Ag_3 has a binding energy of 78.7 kcal/mol, in excellent agreement with the stability found for oxygen in the 3-fold sites on Ag(111) and Ag(110).[27]

In sum, a key to increasing the activity of the catalyst is to saturate the 4-fold, unreactive sites, and then maximize the oxygen concentration in the reactive 3-fold sites. Consistent with this idea is the observation that a 1:1 ratio of O/Ag is needed to obtain EO on Ag powders;[13f] i.e., a high coverage of oxygen is necessary to form the active oxygen species.

The Role of Promoters

Chlorine is the prototypical promoter for a reaction in which other electronegative elements also act to increase the activity and selectivity to EO formation.[3-5] Campbell and Koel have observed that high coverages of Cl ($\theta_{Cl} \geq 0.4$) inhibit the formation of CO_2.[7b] They have interpreted this result as an ensemble effect, where the number of open surface sites required for total combustion is presumed higher than the number of sites necessary for epoxidation. While the relative site requirements may indeed differ, we believe there is significant evidence that it is the ***specific sites blocked by chlorine which increase the activity of the catalyst.***

In particular, a p(2×1) structure is observed by LEED above $\theta_{Cl} = 0.4$ on Ag(110), coinciding with the dramatic increase in reactivity towards ethylene. A comparison of the ab initio binding energies of Cl versus O indicate (Tables III and IV) that Cl may be slightly more stable than O, with predicted binding energies of 79.7 kcal/mol for Cl and and 78.7 kcal/mol for O in 3-fold sites. Thus Cl may displace O, binding to the most stable site on the (110) surface (the 4-fold site in the troughs). The p(2×1)-Cl LEED pattern is consistent with this analysis, since the p(2×1)-O LEED pattern is interpreted as binding in those 4-fold sites. Furthermore, Winograd and co-workers used angle-resolved secondary ion mass

spectrometry (SIMS) to show that as the Cl coverage increases, the surface-Cl distance decreases significantly, indicating that Cl probably falls into the troughs (occupying the 4-fold sites) at high coverage.[45]

Our interpretation of Campbell and Koel's results is that Cl saturates the 4-fold hollows, forcing O to occupy the slightly less stable but reactive 3-fold sites. Thus the role of Cl (or S, Se, Br, etc.) is simply to block the unreactive 4-fold hollows to increase the population of reactive oxygen species in the 3-fold sites.

Salts of alkali metals and alkaline earths are also known promoters of the EO reaction.[3-5] Cesium is one of the most common dopants and has been studied on single crystals by both Lambert and Campbell.[7d,e,g,h] Thermal desorption and LEED studies of the coadsorption of Cs and O on Ag(111) have revealed that aggregates are formed with the approximate stoichiometry CsO_3. The promotional effect of Cs was attributed in this work by Campbell[7d] to be exactly analogous to the role he proposed for Cl: that of a site-blocker such that CO_2 formation was suppressed.

As in the case of Cl, we offer a new interpretation of the role of Cs, based on our results for the interaction of ethylene with Ag_3 and Ag_3^+. Since Cs (and the other electropositive promoters) are added as salts, they are likely to be present as Cs^+. Aggregates such as Cs^+O_3 should be favorable, since the oxygen adatoms are partially negatively charged (Section III.C). Ethylene binds only weakly to the clean Ag surface,[38] consistent with our results of a repulsive interaction with the neutral Ag_3 cluster (Section III.F). However, we find that the positively-charged Ag_3 cluster does bind ethylene with a bond energy of $\sim$ 9 kcal/mol. We propose that Cs^+ sits on top of the oxygens present in the 4-fold trough sites (since they may be more negatively charged than the radical oxygens in the 3-fold sites), and then helps to direct olefins down to the Ag surface via a Lewis acid-Lewis base interaction, increasing the overall sticking probability for ethylene to Ag. If ethylene adsorption occurs on Cs^+ in the troughs, nearby oxygen radicals in the 3-fold sites on the sides of the troughs may be more readily accessible to the ethylene, increasing the rate

of reaction, as shown schematically below for a generic surface.

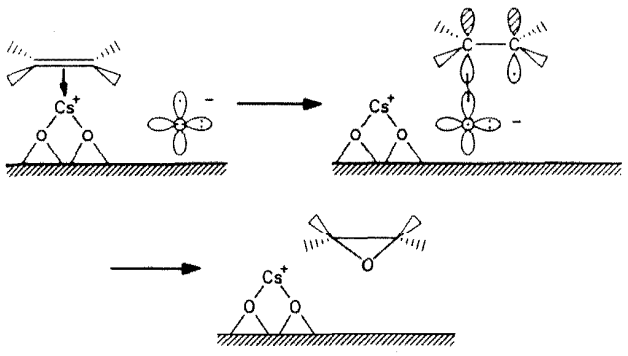

(13)

In this section we have addressed many of the issues involved in the olefin epoxidation reaction as catalyzed by silver. In the next section we summarize our findings.

V. Conclusions

Ab initio GVB-CI calculations of the interaction of various adsorbates on Ag_3 indicate the following:

(i) all adsorbates except ethylene (which prefers 1-fold coordination) favor binding to the 2-fold, in-plane site of the cluster, with bond energies much stronger than those expected for adsorbate surface bond energies. The unpaired electron on this cluster helps to preserve the Ag-Ag bonds (bulk diamagnetic Ag should incur some Ag-Ag bond weakening upon adsorption); and

(ii) adsorbate binding energies to the 3-fold site of the cluster provide realistic estimates of the actual binding energies on an extended surface, with values reported for H (29 kcal/mol as a lower bound), Cl (80 kcal/mol), O (79 kcal/mol), O_2 (17 kcal/mol as an upper bound), and OH (59 kcal/mol). The binding energy of ethylene to Ag_3^+ was found to be 9 kcal/mol in the 1-fold site. The values for C_2H_4 and O are in excellent agreement with experiment.

Implications from this work for understanding the detailed mechanistic aspects of the Ag-catalyzed olefin epoxidation reaction are as follows:

(iii) two near-degenerate states of O_{ad} are predicted to have drastically different properties and reactivity, with a $^2\Sigma$ radical O^- species predicted to be the active precursor to epoxide. This suggests that *the control of catalyst activity is directly related to the relative populations of the reactive oxygen radical and the inactive, di-σ-bound oxygen*;

(iv) these two oxygen species are used in Section IV to propose new interpretations of the trends observed in single crystal studies of EO formation, with the result that the radical oxygen is predicted to reside on 3-fold sites on both Ag(111) and Ag(110), while the unreactive di-σ oxygen is expected to prefer the 4-fold binding site in the valleys of the (110) surface;

(v) the role of electronegative promoters such as Cl is attributed to blocking the 4-fold sites, forcing the formation of the radical oxygen, while the role of electropositive promoters is to enhance the probability for adsorption of ethylene;

(vi) epoxide formation is exothermic for both ethylene and propylene, but olefins larger than ethylene combust due to the ease with which allylic hydrogens may be abstracted from the olefin to form surface-bound hydroxyl groups. This disproportionation of OH_{ad} to adsorbed O and H_2O is predicted to be endothermic by 24 kcal/mol, in good agreement with experiment;

(vii) the combustion of ethylene may actually occur after EO is formed, since the primary C-H bonds in EO are weaker than the vinylic C-H bonds of ethylene; and, lastly,

(viii) we suggest that the reason Ag is the only transition metal which successfully catalyzes the selective oxidation of ethylene is because ethylene dehydrogenates rapidly on most other transition metal surfaces.[46] Indeed, the low affinity of the Ag surface for ethylene and the low binding energy of H to Ag must play a significant role in inhibiting ethylene decomposition on Ag.

VI. Calculational Details

Basis Sets

The eleven valence electrons of Ag ($4d^{10}5s^1$) were treated explicitly within the (3s3p4d/3s2p2d) gaussian basis of Hay and Wadt, with the core electrons represented by an effective core potential.[47] The Dunning valence double-ζ contractions[48] of the Huzinaga gaussian primitive bases[49] for hydrogen (4s; exponents scaled by 1.2), oxygen (9s5p), and carbon (9s5p) were used, with a 3d-polarization function added to oxygen ($\zeta^d = 0.95$). For Ag_3H, the more extensive triple-ζ contraction of Huzinaga's 6s primitive basis[49] along with a 2p-polarization function ($\zeta^p = 0.6$) were used on H. Cl was described using the SHC effective core potential and valence double-ζ basis set of Rappé *et al.*,[50] along with one 3d polarization function ($\zeta^d = 0.6$) and one set of s and p diffuse functions ($\zeta^s = \zeta^p = 0.49$). For Ag_3O and Ag_3OH, one set of s and p diffuse functions[51] was added to the O basis described above ($\zeta^s = 0.088$ and $\zeta^p = 0.60$) and the (6s/3s) basis used on H in Ag_3H was also used on Ag_3OH.

GVB and CCCI Calculations

All geometries and vibrational frequencies were optimized for all molecules [with the Ag_3 cluster constrained to be an equilateral triangle with side length 2.89Å (the nearest neighbor value in bulk Ag[52]) and the ethylene molecular geometry fixed at the experimental geometry[53]] at the GVB-PP level (two pairs were correlated for Ag_3H, Ag_3Cl, Ag_3OH, Ag_3O_2, while three bond pairs were correlated for O and C_2H_4 bound to Ag_3).[54] The relative energies reported in each table were calculated at the GVB-PP level. The bond energies for H, Cl, and the doubly-bonded states of O were calculated using the correlation-consistent configuration interaction (CCCI) approach,[55] which allows full correlation (single and double excitations) from the bond that is breaking, along with single excitations from all valence orbitals to all unoccupied orbitals, to account for orbital shape changes important during bond breakage. These excitations are allowed from the RCI reference states, in which

all three occupations of two electrons in the two orbitals of each GVB pair are included. The doubly-bonded states of Ag_3O dissociate diabatically to the $^4A_2$ excited state of Ag_3. We calculate the diabatic bond energy, then subtract the $^4A_2$ - $^2A_1$ energy splitting in Ag_3 [30.1 kcal/mol at the GVB(1/2)PP level] to obtain the adiabatic bond energy. The bond energies for the ionic radical states of O on Ag_3 were determined indirectly by subtracting or adding the GVB-PP energy difference between the radical state and the double-bonded state for each adsite. The binding energies for O_2 to Ag_3 were determined using a valence level CI to describe the resonance in the π orbitals of O_2. Since O_2 on Ag_3 is best described as O_2^-, we calculated the ionic bond energy, then subtracted the theoretical IP(Ag_3) = 4.18 eV and added the experimental EA(O_2) = 0.44 eV[30] to obtain a covalent bond energy. The valence level CI consisted of an RCI within the Ag-Ag and O-O σ bond pairs simultaneous with both configurations of the O_2^- three-electron π system ($\pi_u^2\pi_g^1$ and $\pi_u^1\pi_g^2$). The bond energies for Ag_3OH were calculated by allowing all single and double excitations out of the O s and p lone pairs from the RCI configurations for the O-H and Ag-Ag GVB bond pairs, dissociating to the ionic limit, followed by subtracting the cluster IP and adding EA(OH) = 1.83 eV.[56] The ethylene binding energies to Ag_3^+ were calculating at the GVB(3/6)-PP level (Ag-Ag and the two C-C bonds were correlated as GVB pairs).

Acknowledgments. This work was supported by the National Science Foundation (Grant No. CHE83-18041) and the Shell Companies Foundation. EAC acknowledges a National Science Foundation predoctoral fellowship (1982-1985), a research grant award from the International Precious Metals Institute and Gemini Industries (1985-1986), and a SOHIO fellowship in Catalysis (1987).

References

(1) A. M. Brownstein, "Trends in Petroleum Technology" (Petroleum Publishing Co., Tulsa, 1976).

(2) (a) R. P. Nielsen and J. H. LaRochelle, Shell Oil Co., U. S. Patent 3 962 136; (b) M. M. Bhasin, P. C. Ellgen and C. D. Hendrix, Union Carbide, U. K. Patent Application GB 2 043 481 A; (c) W.-D. Mross, Catal. Rev. - Sci. Eng. 25 (1983) 591.

(3) H. H. Voge and C. R. Adams, Adv. Catal. 17 (1967) 1515.

(4) X. E. Verykios, F. P. Stein and R. W. Coughlin, Catal. Rev. - Sci. Eng. 22 (1980) 197.

(5) W. M. H. Sachtler, C. Backx and R. A. van Santen, Catal. Rev. - Sci. Eng. 23 (1981) 127.

(6) M. Barteau and R. J. Madix, in: "The Chemical Physics of Solid Surfaces and Heterogeneous Catalysis", Vol. 4, Eds. D. A. King and D. P. Woodruff (Elsevier, Amsterdam, 1982), Ch. 4.

(7) (a) C. T. Campbell and M. T. Paffett, Appl. Surf. Sci. 19 (1984) 28; (b) C. T. Campbell and B. E. Koel, J. Catal. 92 (1985) 272; (c) C. T. Campbell, J. Catal. 99 (1986) 28; (d) C. T. Campbell, J. Phys. Chem. 89 (1985) 5789; (e) C. T. Campbell and K. A. Daube, Surf. Sci., in press; (f) C. T. Campbell, in: "Catalyst Characterization Science", Eds. M. L. Deviney and J. L. Gland (American Chemical Society, Washington, D. C., 1985), ACS Symposium Series, No. 288, p. 210; (g) R. B. Grant and R. M. Lambert, J. Catal. 93 (1985) 92; (h) R. B. Grant and R. M. Lambert, Langmuir 1 (1985) 29.

(8) (a) A. Ayame, N. Takeno, and H. Kanoh, J. Chem. Soc., Chem. Comm. (1982) 617; (b) A. Ayame, T. Kimura, M. Yamaguchi, H. Miura, N. Takeno, H. Kanoh, I. Toyoshima, J. Catal. 79 (1983) 233.

(9) W. Herzog, Ber. Bunsenges. Phys. Chem. 74 (1970) 216.

(10) R. B. Clarkson and A. C. Cirillo, J. Catal. 33 (1974) 392.

(11) P. A. Kilty, N. C. Rol, and W. H. M. Sachtler, Proc. 5th Int. Cong. Catal., Palm Beach (1972) paper 64.

(12) (a) C. T. Campbell and M. T. Paffett, Surface Sci. 139 (1984) 396; (b) C. T. Campbell, J. Vac. Sci. Technol. A2 (1984) 1024; (c) C. T. Campbell, J. Catal. 94 (1985) 436.

(13) (a) E. L. Force and A. T. Bell, J. Catal. 38 (1975) 440; (b) E. L. Force and A. T. Bell, J. Catal. 40 (1975) 356; (c) C. Backx, J. Moolhuysen, P. Geenen, R. A. van Santen, J. Catal. 72 (1981) 364; (d) R. B. Grant and R. M. Lambert, J. Chem. Soc., Chem. Comm. (1983) 662; (e) R. B. Grant and R. M. Lambert, J. Catal. 92 (1985) 364; (f) R. A. van Santen and C. P. M. de Groot, J. Catal. 98 (1986) 530.

(14) M. A. Barteau and R. J. Madix, Surface Sci. 97 (1980) 101.

(15) R. B. Grant and R. M. Lambert, J. Catal., submitted for publication.

(16) (a) M. H. McAdon and W. A. Goddard III, J. Non-Cryst. Solids 75 (1985) 149; (b) M. H. McAdon and W. A. Goddard III, Phys. Rev. Lett. 55 (1985) 2563; (c) M. H. McAdon and W. A. Goddard III, J. Phys. Chem., in press.

(17) Distortion from D_{3h} symmetry leads to an obtuse-angle geometry for the $^2B_2$ state and an acute-angle geometry for the $^2A_1$ state of Ag_3. ESR studies have yielded conflicting results, with the $^2B_2$ state lower in a C_6D_6 matrix [J. A. Howard, K. F. Preston, and B. Mile, J. Am. Chem. Soc. 103 (1981) 6226], while the $^2A_1$ state prevails in an N_2 matrix [K. Kernisant, G. A. Thompson, and D. M. Lindsay, J. Chem. Phys. 82 (1985) 4739], indicating that all three structures are very close in energy. [The equilateral triangle is the low-lying saddle point (~ 400 cm^{-1}) between these two near-degenerate, C_{2v} symmetry structures.] For a recent theoretical study of this distortion, see S. P. Walch, J. Chem. Phys. 85 (1986) 5900.

(18) M. A. Tolbert and J. L. Beauchamp, J. Phys. Chem. 90 (1986) 5015.

(19) "CRC Handbook of Chemistry and Physics", R. C. Weast, Ed. (CRC Press, Boca Raton, 1981), E-79.

(20) (a) M. Balooch, M. J. Cardillo, D. R. Miller, and R. E. Stickney, Surface Sci. 46 (1974) 358; (b) A. G. Sault, R. J. Madix, and C. T. Campbell, Surface Sci. 169 (1986) 347.

(21) J. Flad, G. Igel-Mann, M. Dolg, H. Preuss and H. Stoll, Surface Sci. 163 (1985) 285.

(22) G. M. Lamble, R. S. Brooks, S. Ferrer, and D. A. King, Phys. Rev. B15 34 (1986) 2975.

(23) (a) M. Bowker and K. C. Waugh, Surface Sci. 134 (1983) 639; (b) D. E. Taylor, E. D. Williams, and R. L. Park, preprint.

(24) T. Zeng-ju, Z. Kai-ming, and X. Xi-de, Surface Sci. 163 (1985) 1.

(25) E. A. Carter and W. A. Goddard III, unpublished results.

(26) C. Backx, C. P. M. de Groot, and P. Biloen, Surface Sci. 104 (1981) 300.

(27) (a) C. T. Campbell and M. T. Paffett, Surface Sci. 143 (1984) 517; (b) C. T. Campbell, Surface Sci. 157 (1985) 43.

(28) R. L. Martin and P. J. Hay, Surface Sci. 130 (1983) L283.

(29) B. A. Sexton and R. J. Madix, Chem. Phys. Lett. 76 (1980) 294.

(30) K. P. Huber and G. Herzberg, "Constants of Diatomic Molecules" (Van Nostrand, New York, 1979).

(31) D. A. Outka, J. Stöhr, W. Jark, P. Stevens, J. Solomon, and R. J. Madix, Phys. Rev. B15, in press.

(32) J. Marsden, L. S. Bartell, and P. Diodati, J. Mol. Struct. 39 (1977) 253.

(33) K. C. Prince, G. Paolucci, and A. M. Bradshaw, Surface Sci. 175 (1986) 101.

(34) C. T. Campbell, Surface Sci. 173 (1986) L641.

(35) P. R. Norton, in: "The Chemical Physics of Solid Surfaces and Heterogeneous Catalysis", Vol. 4, Eds. D. A. King and D. P. Woodruff (Elsevier, Amsterdam, 1982), Ch. 2.

(36) (a) E. J. Stuve and R. J. Madix, Surface Sci. 111 (1981) 11; (b) I. Pockrand, Surface Sci. 122 (1982) L569.

(37) S. W. Jorgensen, A. G. Sault, and R. J. Madix, Langmuir 1 (1985) 526.

(38) (a) C. Backx, C. P. M. de Groot, and P. Biloen, Appl. Surface Sci. 6 (1980) 256; (b) C. Backx, C. P. M. de Groot, P. Biloen, and W. M. H. Sachtler, Surface Sci. 128 (1983) 81.

(39) (a) A. L. Larrabee and R. L. Kuczkowski, J. Catal. 52 (1978) 72; (b) N. W. Cant and W. K. Hall, J. Catal. 52 (1978) 81.

(40) $\Delta H^{\circ}_{f,298}$ are taken from "JANAF Thermochemical Tables", J. Phys. Chem. Ref. Data 14 Suppl. 1 (1985) and from S. W. Benson, "Thermochemical Kinetics" (Wiley, New York, 1976).

(41) M. A. Barteau and R. J. Madix, J. Am. Chem. Soc. 105 (1983) 344, and references therein.

(42) $\Delta H_{rxn} = +27.6$ kcal/mol for hydrogen abstraction from ethylene is derived from $D^{\circ}_{298}(C_2H_3\text{–}H) = 118.2$ kcal/mol [obtained by correcting D°_0 by 1.5 kcal/mol ($\frac{5}{2}$RT) for finite temperature, where $D^{\circ}_0 = 116.7 \pm 1.2$ kcal/mol is from H. Shiromaru, Y. Achiba, K. Kimura, and Y. T. Lee, J. Phys. Chem. 91 (1987) 17)], $D^{\circ}_{298}(O\text{-}H^{-}) = 110.6$ kcal/mol [obtained from temperature correcting D°_0 from ref. 30 by 0.9 kcal/mol ($\frac{3}{2}$RT)], and the theoretically-predicted binding energies of OH and O to the Ag surface (59 and 79 kcal/mol).

(43) $\Delta H_{rxn} = -2.8$ kcal/mol is derived from the same quantities listed in ref. 42 except that the C-H bond energy in propene of 87.8 kcal/mol was obtained from ref. 40.

(44) H. A. Engelhardt and D. Menzel, Surface Sci. 57 (1976) 591.

(45) D. W. Moon, R. J. Bleiler, and N. Winograd, J. Chem. Phys. 85 (1986) 1097.

(46) M. M. Hills, J. E. Parmeter, C. B. Mullins, and W. H. Weinberg, J. Am. Chem. Soc. 108 (1986) 3554, and references therein.

(47) P. J. Hay and W. R. Wadt, J. Chem. Phys. 82 (1985) 270.

(48) T. H. Dunning, J. Chem. Phys. 53 (1970) 2823.

(49) S. Huzinaga, J. Chem. Phys. 42 (1965) 1293.

(50) A. K. Rappé, T. A. Smedley, and W. A. Goddard III, J. Phys. Chem. 85 (1981) 1662. Note that the second *p* exponent for the Cl basis listed in Table

I of this reference should read 0.641, not 0.691, and the s orbital energy for Cl in Table IV of this reference should read -1.0675, not -0.1068.

(51) R. A. Bair and W. A. Goddard III, submitted for publication.

(52) N. W. Ashcroft and N. David Mermin, "Solid State Physics" (Holt, Rinehart, and Winston, Philadelphia, 1976).

(53) M. D. Harmony, V. W. Laurie, R. L. Kuczkowski, R. H. Schwendeman, D. A. Ramsay, F. J. Lovas, W. J. Lafferty, and A. G. Maki, J. Phys. Chem. Ref. Data 8 (1979) 619.

(54) (a) W. J. Hunt, T. H. Dunning, Jr., and W. A. Goddard III, Chem. Phys. Lett. 3 (1969) 606; W. A. Goddard III, T. H. Dunning, Jr., and W. J. Hunt, Chem. Phys. Lett. 4 (1969) 231; W. J. Hunt, W. A. Goddard III, and T. H. Dunning, Jr., Chem. Phys. Lett. 6, (1970) 147; W. J. Hunt, P. J. Hay, and W. A. Goddard III, J. Chem. Phys. 57 (1972) 738; F. W. Bobrowicz and W. A. Goddard III in "Methods of Electronic Structure Theory", H. F. Schaefer, ed., (Plenum, New York, 1977) pp 79-127; (b) L. G. Yaffe and W. A. Goddard III, Phys. Rev. A 13 (1976) 1682.

(55) E. A. Carter and W. A. Goddard III, Chem. Phys. Lett., submitted for publication.

(56) P. S. Drzaic, J. Marks, and J. I. Brauman in: "Gas Phase Ion Chemistry", Vol. 3 (Academic, Orlando, 1984) Ch. 21.

Table I. Properties of Ag_3H as a function of adsite and electronic state.

state[a]	site	relative energy[b] (kcal/mol)	$R_{\perp,e}$(Å)[c]	$\omega_e(Ag_3\text{–}H)$ (cm^{-1})	D_e(kcal/mol)[d]
$^3B_2$	1-fold	41.3	1.75	1411	21.6
$^1A'$	3-fold	39.1	1.63	482	19.5
$^3A''$	3-fold	37.4	1.19	809	28.5
$^3B_2$	2-fold	21.4	1.21	1012	42.8
$^1A_1$	1-fold	4.4	1.77	1357	50.8
$^1A_1$	2-fold	0.0	1.41	913	56.8

a) Electronic state symmetry of the GVB wavefunction. *b*) GVB(2/4)-PP energy relative to the ground state total energy of −112.82983 hartrees (1 hartree = 627.5096 kcal/mol = 27.21162 eV). *c*) $R_\perp$ = the perpendicular distance from H to the center of the cluster site (e.g., to the Ag-Ag bond midpoint for the 2-fold site, to the Ag atom for the 1-fold site, and to the center of the triangle for the 3-fold site). *d*) Adiabatic bond energies from CCCI calculations (Section VI).

Table II. Charge transfer to atomic adsorbate X on Ag_3, as a function of adsite and bond character.

	state/bond		excess charge[b]			dipole	
X	character[a]	site	X	$Ag_{surface}$	Ag_{bulk}	moment (debye)[c]	d-band shift (eV)[d]
H	$^1A_1$[e]	2-fold	−0.30	+0.26	−0.22	0.08	+0.09
H	"	1-fold	−0.23	+0.03	+0.10	7.60	−0.20
H	$^1A'$	3-fold	−0.39	+0.13	—	2.06	−0.39
Cl	$^1A_1$[e]	2-fold	−0.61	+0.36	−0.12	5.19	−0.36
Cl	"	1-fold	−0.64	+0.38	+0.13	12.50	−0.80
Cl	$^1A'$	3-fold	−0.55	+0.18	—	3.61	−0.44
O	$^2\Sigma$ radical[e]	2-fold	−0.70	+0.40	−0.09	4.14	−0.05
O	$^2\Pi$ radical	2-fold	−0.69	+0.41	−0.13	3.95	−0.05
O	$^2\Pi$ radical	1-fold	−0.61	+0.39	+0.11	10.83	−0.51
O	$^2\Sigma$ radical	3-fold	−0.60	+0.20	—	1.75	+0.04
O	di-σ double bond	3-fold	−0.78	+0.26	—	3.03	+0.02

a) See Table IV for Ag_3O. *b*) Obtained from Mulliken populations. "Surface" Ag = Ag atoms directly attached to adsorbate and "bulk" Ag = Ag atoms beneath the surface atoms. *c*) Magnitude of the dipole moment along bond axis. *d*) Averaged shift of Ag d-orbital energies upon adsorption. *e*) Ground state.

Table III. Properties of Ag_3Cl as a function of adsite and electronic state.

state	site	relative energy[a] (kcal/mol)	$R_{\perp,e}$(Å)	$\omega_e(cm^{-1})$	D_e(kcal/mol)[b]
$^3B_2$	1-fold	50.7	2.43	258	50.0
$^3A''$	3-fold	44.4	2.21	203	55.2
$^3B_2$	2-fold	35.1	2.15	230	61.8
$^1A'$	3-fold	22.0	2.38	161	79.7
$^1A_1$	1-fold	9.3	2.45	246	85.0
$^1A_1$	2-fold	0.0	2.23	211	91.0

a) GVB(2/4)-PP energy relative to the ground state total energy of −571.82622 hartrees. *b*) See Table I, footnote d.

Table IV. Properties of Ag_3O as a function of adsite and bond character.

bond character[a]	site	relative energy[b] (kcal/mol)	$R_{\perp,e}$(Å)	$\omega_e(cm^{-1})$	D_e(kcal/mol)[c]
$\sigma\pi$ double bond	1-fold	53.9	2.11	415	39.0
$\sigma\pi$ double bond	2-fold	29.8	1.54	380	63.1
$^2\Sigma$ radical	1-fold	23.4	2.13	378	69.5
$^2\Pi$ radical	3-fold	19.9	1.92	252	72.8
di-σ double bond	3-fold	14.9	1.37	412	77.8
$^2\Sigma$ radical	3-fold	14.0	1.80	299	78.7
$^2\Pi$ radical	1-fold	3.1	2.14	399	89.8
$^2\Pi$ radical	2-fold	2.7	1.91	289	90.2
$^2\Sigma$ radical	2-fold	0.0	1.74	332	92.9

a) Bond character refers to either two bonds from O to Ag_3 ($\sigma\pi$ or di-σ) or an ionic bond between O^- and Ag_3^+ ($^2\Sigma$ for radical electron along the symmetry axis or $^2\Pi$ for radical electron perpendicular to the symmetry axis); see Section III.C. *b*) GVB(2/4)-PP energy relative to the ground state total energy of −187.10445 hartrees. *c*) Bond energies for the double-bonded states are from CCCI calculations (Section VI); bond energies for the radical states are obtained by adding the difference in relative GVB-PP energies (column 3) of the radical and double-bonded states (for a given adsite) to the CCCI bond energy for the double-bonded state.

Table V. Properties of Ag_3O_2 as a function of adsite and orientation.

bond orientation[a]	site	relative energy[b] (kcal/mol)	$R_{\perp,e}$(Å)[c]	R(O-O) (Å)	$\omega_e(cm^{-1})$ Ag_3–O_2	O-O	D_e(kcal/mol)[d]
η^1 end-on	3-fold	29.7	1.85	1.39	195	856	17.1
η^2	3-fold	26.4	2.24	1.34	211	912	20.4
η^1 end-on	1-fold	25.9	2.10	1.35	303	1005	20.9
η^2 $\perp$ bridge	2-fold	16.2	1.99	1.34	226	1179	30.6
η^2	1-fold	13.2	2.22	1.33	290	1200	33.7
η^1 end-on	2-fold	9.8	1.76	1.37	251	949	37.1
η^1 peroxy	2-fold	4.1	2.22	1.33	306	921	36.3
η^2	2-fold	0.0	2.18	1.32	286	1264	46.9

a) High symmetry orientations except for η^1 peroxy (see Section III.D. for details of peroxy geometry). η^1 and η^2 refer to the number of oxygen atoms directly bound to the cluster. End-on has only one oxygen bound to the cluster, with O_2 oriented straight up from the 1-, 2-, or 3-fold sites. 1- and 2-fold Ag_3O_2 orientations are all planar except for the 2-fold perpendicular bridge (O_2 in 2-fold site, oxygens equivalent with O-O axis perpendicular to Ag-Ag axis). *b*) GVB(2/4)-PP energy relative to the ground state total energy of −261.94443 hartrees. *c*) Perpendicular distance from the center of the cluster site to the bond midpoint of O_2 for η^2 and to the nearest O for η^1. *d*) Adiabatic bond energies from a valence level CI (Section VI).

Table VI. Properties of Ag_3OH as a function of adsite.[a]

site	relative energy[b] (kcal/mol)	$R_{\perp,e}$(Å)[c]	R(O-H) (Å)	$\omega_e(cm^{-1})$ Ag_3–O	O–H	D_e(kcal/mol)[d]
1-fold	20.2	2.07	0.96	445	3796	69.4
3-fold	18.8	1.72	0.97	295	3637	59.1
2-fold	0.0	1.70	0.96	363	3740	78.9

a) Linear geometries for OH are global minima, with tilted OH orientations found to be higher in energy. *b*) GVB(2/4)-PP energy relative to the ground state total energy of −187.75179 hartrees. *c*) $R_{\perp,e}$ = perpendicular distance from the center of the cluster site to O. *d*) Adiabatic bond energies from CCCI calculations (Section VI).

Table VII. Properties of $Ag_3^+(C_2H_4)$ as a function of adsite and orientation.

orientation[a]	site	relative energy[b] (kcal/mol)	$R_{\perp,e}$(Å)[c]	$\omega_e(Ag_3\text{–}C_2H_4)$ (cm^{-1})	D_e(kcal/mol)[d]
C-C ∥	3-fold	7.6	4.95	21	1.0
C-C ⊥	2-fold	6.1	3.64	34	2.5
C-C ∥	2-fold	5.8	3.58	37	2.8
C-C ∥	1-fold	0.1	2.71	107	8.6
C-C ⊥	1-fold	0.0	2.70	110	8.7

a) Gives orientation of C-C axis relative to the Ag_3 plane, where the C-C bond midpoint lies in the Ag_3 plane for the 1- and 2-fold sites. *b*) GVB(3/6)-PP energy relative to the ground state total energy of −190.15705 hartrees. *c*) $R_{\perp,e}$ = perpendicular distance from the center of the cluster site to C-C bond midpoint. *d*) Adiabatic bond energies from GVB(3/6)PP calculations (Section VI).

Figure Captions

Fig. 1. The GVB one-electron valence orbitals of Ag_3 ($^2A_1$): (a) the Ag_3 singly-occupied orbital and (b) the Ag-Ag bond pair. Contours range from -0.5 to $+0.5$ a.u., incremented by 0.01 a.u.

Fig. 2. Schematic of possible bonding configurations for X/Ag_3 (the 2-fold bridge site): (a) X = H; (b) X = Cl; (c) X = O (σ and π double bond); (d) X = O (ionic $^2\Sigma$ state); and (e) X = O (ionic $^2\Pi$ state).

Fig. 3. The GVB one-electron orbitals of Ag_3H ($^1A_1$) (for the 2-fold bridge site): (a) the Ag_3-H bond pair and (b) the Ag-Ag bond pair.

Fig. 4. The GVB one-electron orbitals of Ag_3Cl ($^1A_1$) (for the 2-fold bridge site): (a) the Ag_3-Cl bond pair; (b) the Ag-Ag bond pair; and (c) the Cl doubly-occupied, in-plane p-orbital.

Fig. 5. The GVB one-electron orbitals of ground state Ag_3O ($^2A_1$) with $^2\Sigma$ O^- character (for the 2-fold bridge site): (a) the O 2pσ radical; (b) the O in-plane 2p lone pair; and (c) the Ag-Ag bond pair.

Fig. 6. The GVB one-electron orbitals of Ag_3O ($^2B_2$) with $^2\Pi$ O^- character (for the 2-fold bridge site): (a) the O 2pσ pair; (b) the O 2pπ radical; and (c) the Ag-Ag bond pair.

Fig. 7. The GVB one-electron orbitals of excited state Ag_3O ($^2A_1$) with $\sigma\pi$ double bond character (for the 2-fold bridge site): (a) the Ag_3-O bond pair; (b) the Ag_3-O π bond; and (c) the Ag_3 singly-occupied orbital.

Fig. 8. Adsorption sites for C_2H_4 on Ag_3^+: (a) the 3-fold site; (b) the 2-fold perpendicular bridge site; (c) the 2-fold parallel bridge site; (d) the 1-fold parallel site; and (e) the 1-fold perpendicular site (the ground state). The + signs for Ag_3^+ have been omitted for clarity.

Fig. 9. The two high-symmetry adsorption sites on Ag(110): (a) the 4-fold site down in the trough and (b) the 3-fold site along the sides of the trough.

Ag_3 $(^2A_1)$

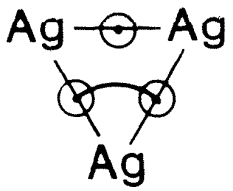

a)

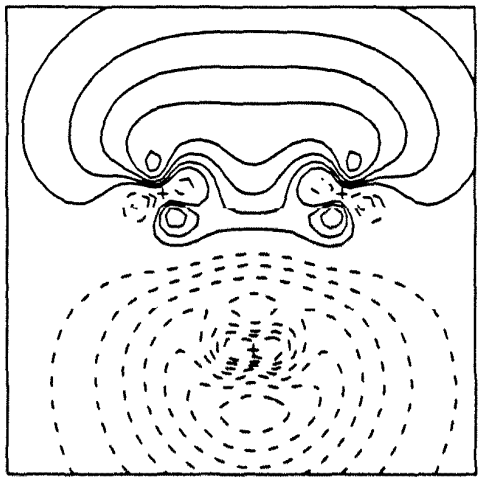

Ag RADICAL

b)

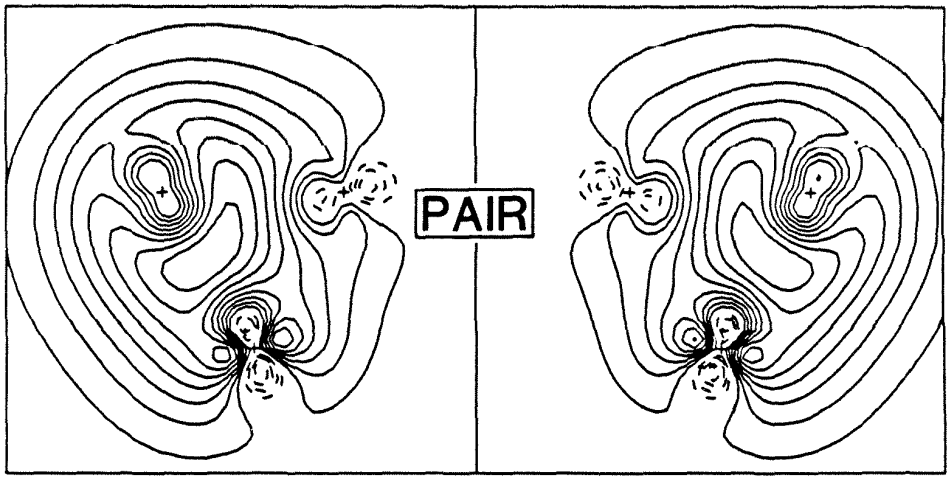

Ag-Ag BOND

Figure 1.

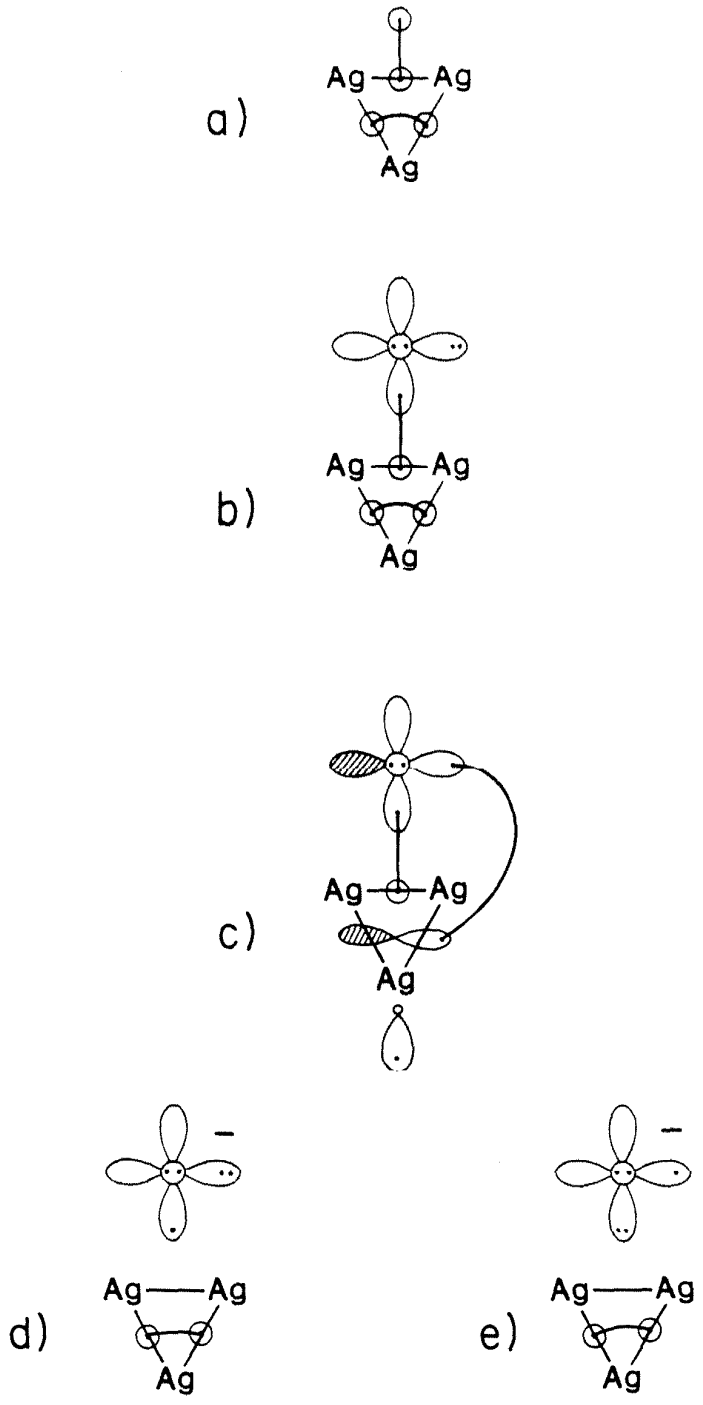

Figure 2.

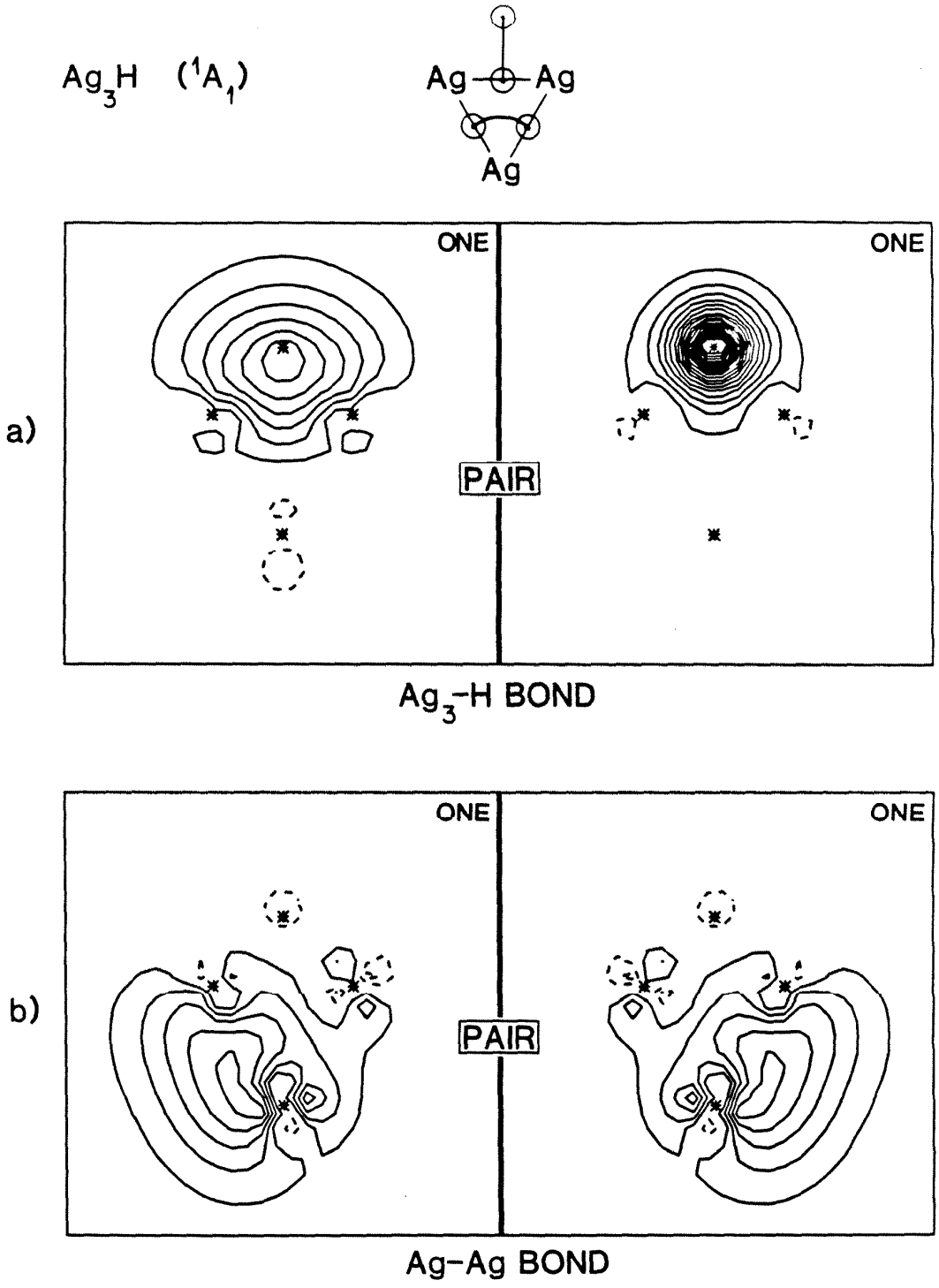
Ag_3H ($^1A_1$)
Ag
Ag
Ag
a)
ONE
ONE
PAIR
Ag_3-H BOND
b)
ONE
ONE
PAIR
Ag-Ag BOND

Figure 3.

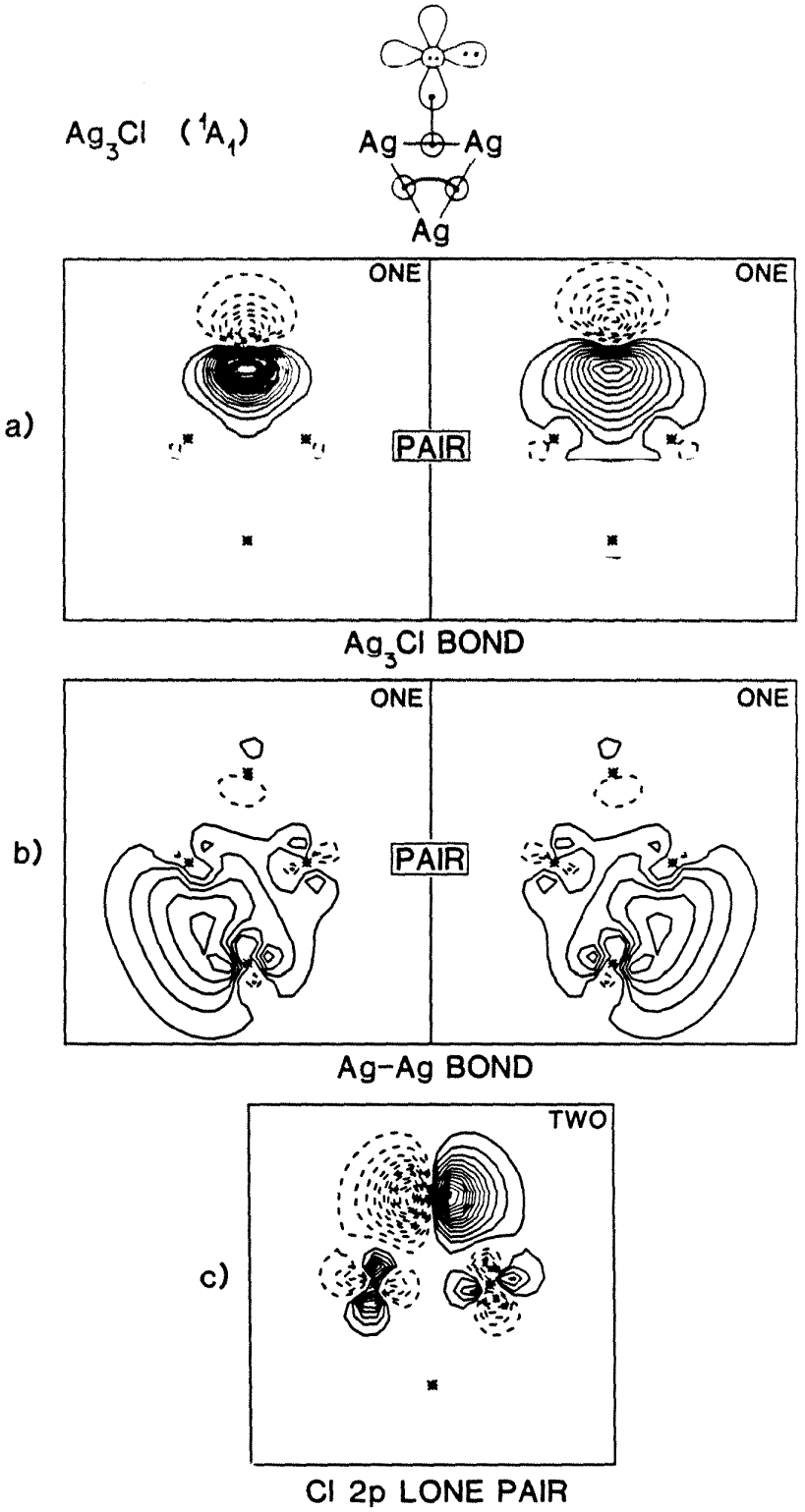
Ag3Cl (1A1)
Ag
Ag
Ag
a)
ONE
ONE
PAIR
Ag3Cl BOND
b)
ONE
ONE
PAIR
Ag-Ag BOND
c)
TWO
Cl 2p LONE PAIR

Figure 4.

Ag_3O $(^2A_1)$

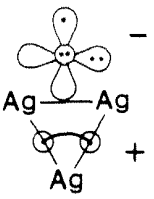

a)

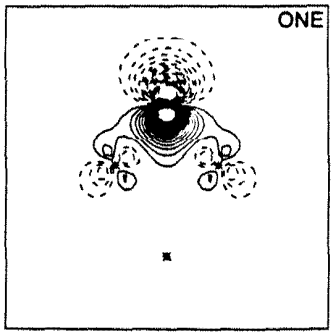

O 2p σ RADICAL

b)

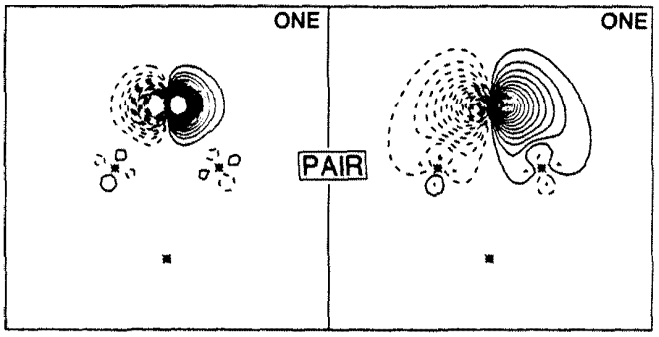

O 2p LONE PAIR

c)

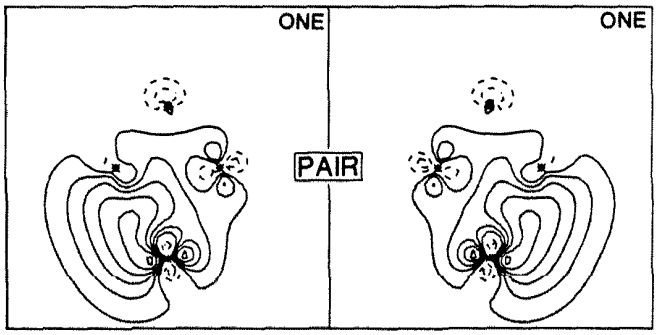

Ag-Ag BOND

Figure 5.

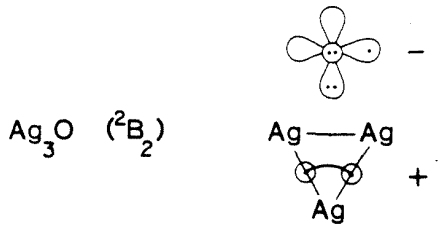

a)

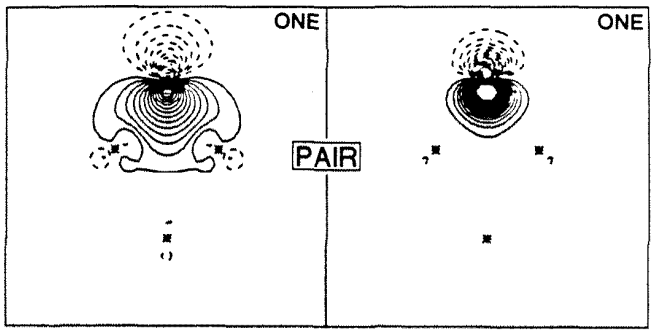

O 2pσ PAIR

b)

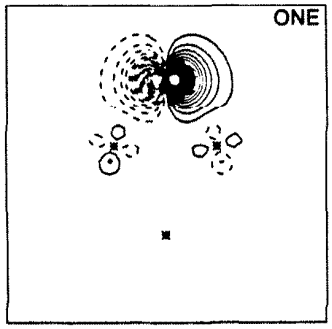

O 2p π RADICAL

c)

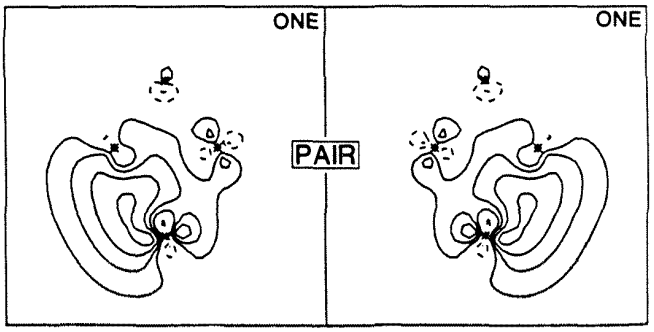

Ag-Ag BOND

Figure 6.

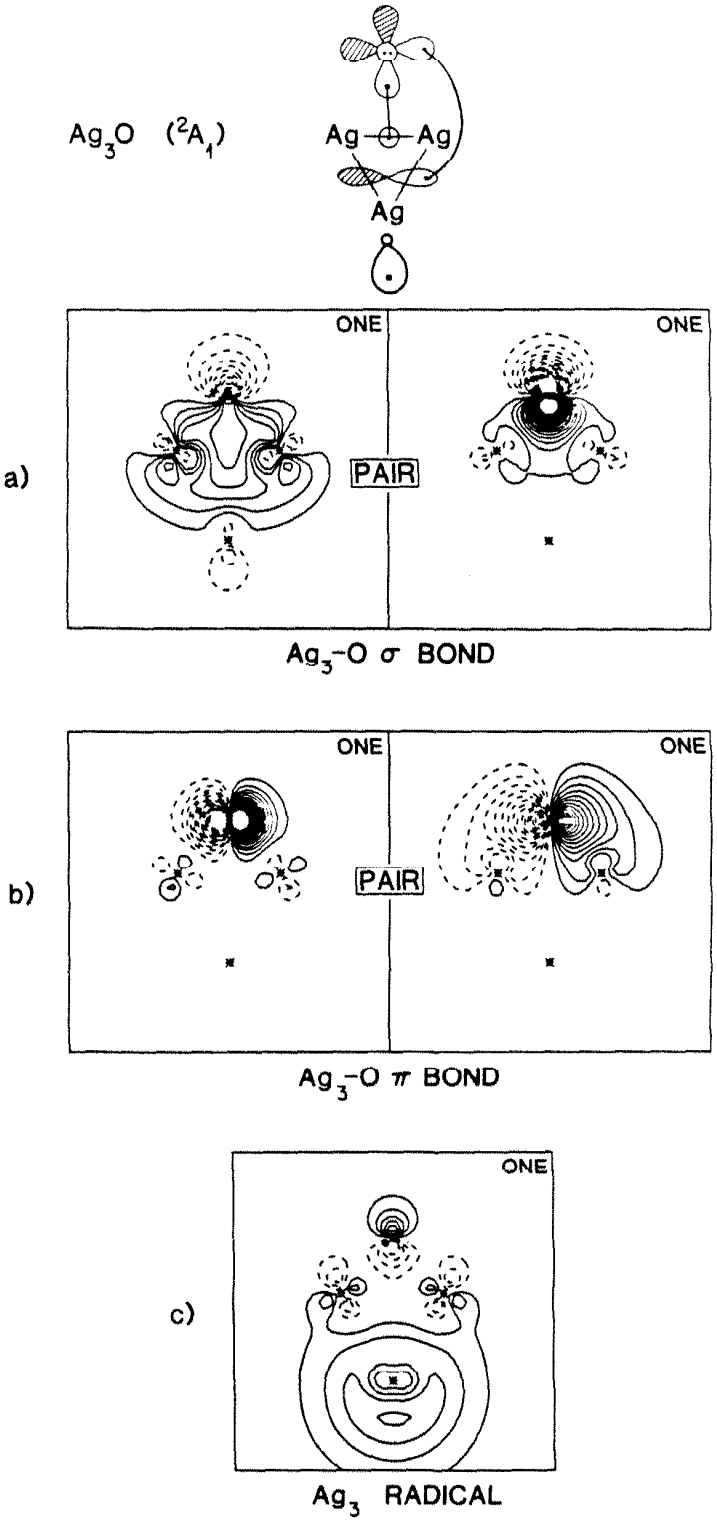
Ag3O (2A1)
Ag
Ag
Ag
a)
ONE
ONE
PAIR
Ag3-O σ BOND
b)
ONE
ONE
PAIR
Ag3-O π BOND
c)
ONE
Ag3 RADICAL

Figure 7.

a)

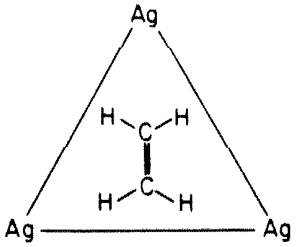

b)

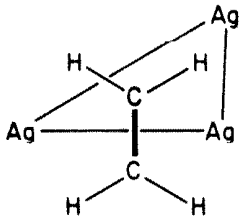

c)

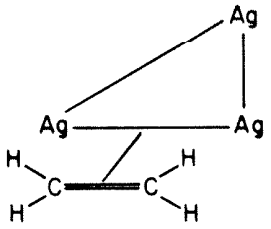

d)

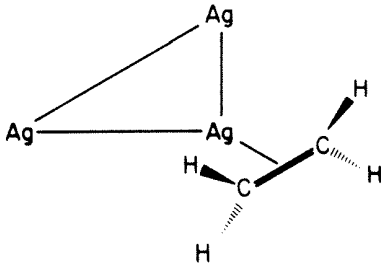

e)

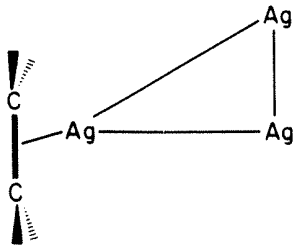

Figure 8.

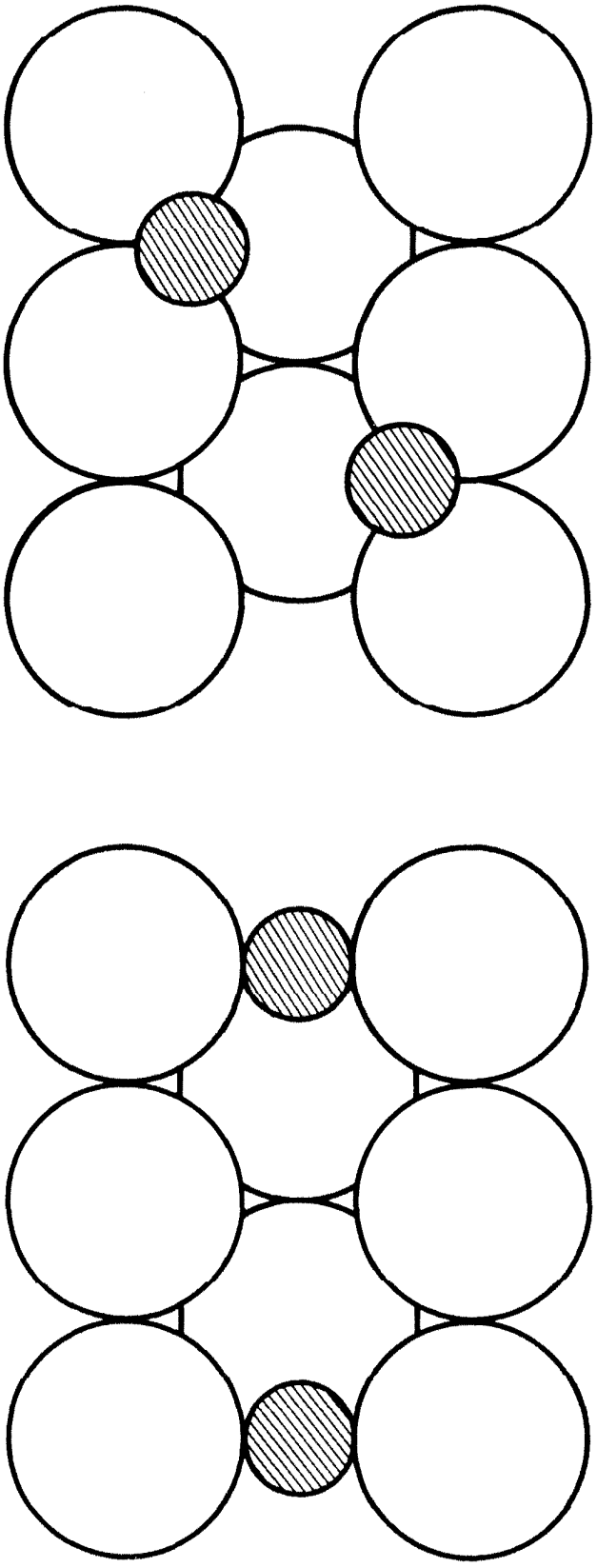

Figure 9.

Conclusions of the Thesis

This thesis has presented an ab initio method for the prediction of accurate energetics for events of chemical interest. The correlation-consistent configuration interaction (CCCI) technique is based on the generalized valence bond (GVB) first order wavefunction, whose orbitals form the basis for the CCCI calculation. The uniqueness of the method is due to the choice of the CI expansion, which incorporates the same electron correlations at both endpoints of a process, but includes only the dominant correlations dictated by the physics (or chemistry) of the system. This results in a rapid truncation of the CI expansion, so that the energetics for processes involving fairly large molecules can be easily assessed by this approach.

The accuracy of the CCCI method has been demonstrated by predicting the following quantities (for both organic and inorganic compounds):

(i) chemical bond dissociation energies;

(ii) electronic excitation energies;

(iii) activation barriers for chemical reactions; and

(iv) thermochemical heats of formation and heats of reaction.

The goal of this thesis was not merely to provide quantitatively accurate energetic information, but also to use these quantities to distill simple conceptual rules for predicting the relative stabilities and reactivity of organic and transition metal-containing molecules. In particular, we have shown that:

(a) the dominant contribution to the relative bond strengths in substituted olefins and methanes is the singlet-triplet energy splittings of the substituted carbenes from which they are comprised;

(b) the relationship between molecular bond energies and electronic excitation energies in the subsequent fragments establishes a new connection between thermochemistry and spectroscopy;

(c) the ground electronic states of substituted carbenes are determined by the electronegativities of the substituents (relative to carbon), the presence of pπ

lone pairs on the substituents, and the size of the substituents, with highly electronegative groups with $p\pi$ lone pairs favoring singlet ground states, while bulky electropositive groups favor triplet ground states;

(d) the bond character, reactivity, and stability of transition metal carbenes is dictated partially by whether the ground state of the carbene is singlet or triplet, with singlet carbenes [e.g., CF_2, CCl_2, $CR(OR')$] preferring a terminal configuration involving a donor/acceptor bond and triplet carbenes [e.g., CH_2, CRR', $CR(SiR'_3)$] favoring covalent alkylidene bonding;

(e) the bond character, reactivity, and stability of transition metal carbenes is also determined by the valence electronic configuration at the metal, with early metals favoring covalent, terminal alkylidene-type bonding (since the π bonds are strong for early metals) and late metals favoring donor/acceptor carbene-type bonding or bridging alkylidene bonding (since the π bonds are weak and doubly-occupied orbitals on the metal allow for π-backbonding);

(f) the character, reactivity, and stability of transition metal oxygen bonds may be predicted solely by knowing the valence electronic state of the metal, with early metals forming inert triple bonds as in CO (since an empty metal d-orbital allows O to be a four-electron donor) and late metals forming reactive biradical double bonds as in O_2 (since the doubly-occupied d-orbitals on the metal allow an O_2-type π resonance);

(g) coordinatively unsaturated (*cu*) metal-ligand bonds are generally weaker than coordinatively saturated (*cs*) metal-ligand bonds, because the coordinatively unsaturated metal prefers to be high spin (resulting in maximum exchange losses upon bonding); and

(h) additive conversion factors for converting from *cu* M-X bond strengths to *cs* M-X bond strengths have been derived, so that organometallic chemists will be able to estimate the thermochemistry of *cs* metal complexes.

Finally, we have used CCCI to elucidate mechanistic information about two very important catalytic reactions, the Fischer-Tropsch reductive polymerization of

CO and the Ag-catalyzed selective oxidation of ethylene, with these results:

(i) the chain initiation step of the Fischer-Tropsch synthesis of hydrocarbons is found to be exothermic by $\sim$ 10 kcal/mol and possess a barrier of $\sim$ 11 kcal/mol, while the chain propagation step is predicted to be less exothermic ($\Delta E_{rxn} \approx -4.2$ kcal/mol) and possess a higher barrier;

(j) control of epoxidation catalyst activity is related to deactivating 4-fold sites on Ag(110) facets and adsorbing oxygen in 3-fold sites (the oxygen species in the 3-fold site has radical O^- character and should be active for ethylene epoxidation); and

(k) electronegative promoters are predicted to fill 4-fold hollows so that increasing concentrations of active oxygen will form in 3-fold sites, while electropositve promoters are expected to enhance the probability for adsorption of ethylene.

In sum, the CCCI method is a powerful, general approach which, when combined with physically reasonable models, yields both accurate energetics and new qualitative insights regarding bonding and reactivity for a diverse group of chemical systems.

Appendix 1

The text of this appendix is a Letter coauthored with M. A. Hanratty, J. L. Beauchamp, W. A. Goddard III, A. E. Illies, and M. T. Bowers which appeared in *Chemical Physics Letters.*

Volume 123, number 4 CHEMICAL PHYSICS LETTERS 17 January 1986

ELECTRONIC STATES OF CHROMIUM CARBENE IONS CHARACTERIZED BY HIGH-RESOLUTION TRANSLATIONAL ENERGY LOSS SPECTROSCOPY

M.A. HANRATTY, E.A. CARTER, J.L. BEAUCHAMP, W.A. GODDARD III

Arthur Amos Noyes Laboratory of Chemical Physics [1], California Institute of Technology, Pasadena, CA 91125, USA

A.J. ILLIES and M.T. BOWERS

Department of Chemistry, University of California, Santa Barbara, CA 93106, USA

Received 4 November 1985

The electronic states of the unsaturated organometallic carbene $CrCH_2^+$ are investigated using high-resolution translational energy loss spectroscopy. The observed energy loss feature (1.05 ± 0.2 eV) is in good agreement with theoretical calculations which predict two higher lying states, $^6B_1$ and $^6A_1$ at 0.78 and 0.82 eV respectively, above the $^4B_1$ ground state of $CrCH_2^+$.

1. Introduction

Rapid progress in experimental methodology has made it possible to generate and study highly reactive organometallic fragments in the gas phase. While experimental investigations have focused mainly on the reactivity and thermochemical stability of such species [1–7], parallel developments in ab initio theory have provided descriptions of the molecular and electronic structures of these molecules [8–10]. Transition metal carbenes, species which contain a divalent carbon bonded to a transition metal center, are an example of reactive organometallic fragments which have been the subject of both experimental and theoretical investigations.

Ion beam [1–3] and ion cyclotron resonance [4–7] techniques have recently been used to investigate the energetics and reactions of both the coordinately saturated and "bare" transition metal carbenes. In the latter category it has been observed [1,4] that the chromium carbene ion, $CrCH_2^+$, can be generated by reaction of electronically excited Cr^+ with methane:

$$Cr^+ + CH_4 \rightarrow CrCH_2^+ + H_2 \,. \qquad (1)$$

Reaction (1) is 45 kcal/mol *endothermic* for ground-state Cr^+ (^6S derived from the d^5 configuration) [11], but is 12.5 kcal/mol *exothermic* if the Cr^+ ion is in the ^4D excited state. Several experimental results [1,4] suggest that it is, in fact, the ^4D state (derived from the s^1d^4 configuration and 2.5 eV higher in energy than the ground state) [11] which is responsible for the production of $CrCH_2^+$ by reaction (1).

Recent ab initio calculations of the low-lying electronic states of $CrCH_2^+$ by Carter and Goddard [8] predict that the ground state of $CrCH_2^+$ is a $^4B_1$ state, with a directly calculated bond dissociation energy D_e = 44 kcal/mol and an estimated exact bond dissociation energy of D_{corr} = 50 kcal/mol. This can be compared with the experimentally determined [1] bond energy of 65 ± 7 kcal/mol. Earlier CI calculations by other workers [9] suggested that the $CrCH_2^+$ ground state is the $^6B_1$ state, with a significantly weaker bond, while Carter and Goddard [8] found the $^6B_1$ state to be 18 kcal/mol higher in energy than the $^4B_1$ state. In an attempt to resolve the situation, we have employed high-resolution translational energy loss spectroscopy to investigate the electronic states of $CrCH_2^+$.

[1] Contribution No. 7320.

0 009-2614/86/$ 03.50

2. Experimental

The theory and instrumentation for translational energy loss spectroscopy have appeared in detail elsewhere [12,13] and will be described only briefly. Experiments were performed at UCSB using a double focusing mass spectrometer (VG ZAB-2F). A variable temperature ion source was operated at 330 K with 6.5×10^{-3} Torr total pressure. Chromium ions are formed from 150 eV electron impact ionization of $Cr(CO)_6$. Reaction of excited-state Cr^+ with CH_4 (reaction (1)) produces $CrCH_2^+$. Ions extracted from the source are accelerated to 8 kV, mass selected by a magnetic sector and focused into a collision cell. Typically, 10^{-3} Torr of helium is used as the collision gas. Translational energy analysis of the unscattered main ion beam and its scattered components is accomplished with an electrostatic analyzer, located after the collision chamber and collinear with the incident ion beam axis. In the absence of a collision gas, the energy resolution of the main beam (Cr^+ or $CrCH_2^+$) was 0.2 eV (fwhm).

During the collision between a neutral target and an ion, which has been accelerated to several kilovolts, the internal energy of the ion may be altered in this situation, peaks at higher and/or lower energies than the unscattered ion beam (corresponding to de-excitation and excitation, respectively, of ionic states) are observed. The reported experiments are sensitive to collisions occurring at small scattering angles, for which translational energy losses of the ion correspond to changes in the ion internal energy [13]. Ions with the same nominal mass as the ion of interest may also appear in the spectrum but are easily identified with the high-resolution capabilities of the instrument. In the case of chromium carbene ($^{52}CrCH_2^+$), other ions of mass 66 were also observed in the high-resolution energy loss spectrum but did not occur in a region which would obscure the predicted electronic transitions.

3. Results and discussion

Although collisional excitation can generate states that are difficult to prepare by optical methods, processes which are optically "allowed" are generally observed to have a larger cross section for collisional excitation than those which are optically "forbidden"

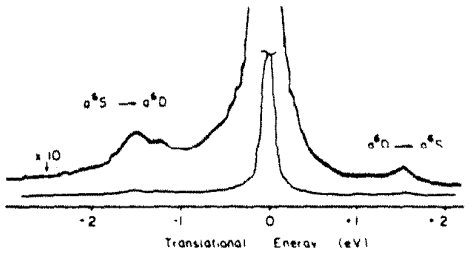

Fig. 1. Translational energy loss spectrum of Cr^+ scattered from helium ($P_{He} = 6 \times 10^{-3}$ Torr).

[12]. For transition metal systems, it is not uncommon to have numerous electronic states of the same or different spin multiplicity close in energy to the ground state. In order to determine the relative magnitudes of the collisional excitation cross sections for transition metal ions, the high-resolution translational energy loss spectrum of Cr^+ scattered from He was investigated (fig. 1). The main peak at zero translational energy loss in fig. 1 corresponds to the unscattered Cr^+ beam. Two smaller features occur 1.45 eV lower and higher in energy than the main beam. As shown in table 1, this energy change corresponds to the spin allowed $a\,^6S \rightarrow a\,^6D$ excitation and $a\,^6D \rightarrow a\,^6S$ de-excitation, respectively. Also from table 1, one can see that this is the only transition involving the ^6S ground state which would occur below 2 eV. Transitions between the quartet states of Cr^+, specifically the $a\,^4D \rightarrow b\,^4P$ and the $a\,^4G \rightarrow b\,^4P$, would appear at 1.17 and 1.23 eV, respectively, and may in fact be present but obscured by the $^6S \rightarrow {}^6D$ transition. Transitions between the $a\,^4D$ and $a\,^6S$ states at

Table 1
Low-lying electronic states of chromium ion

State	Configuration	Energy (eV) [a]
$a\,^6S$	$3d^5$	0.00
$a\,^6D$	$3d^4s^1$	1.48
$a\,^4D$	$3d^4s^1$	2.42
$a\,^4G$	$3d^5$	2.54
$a\,^4P$	$3d^5$	2.71
$b\,^4D$	$3d^5$	3.10
$b\,^4P$	$3d^4s^1$	3.71
$a\,^2P$	$3d^5$	3.74

[a] Data taken from ref. [11] refer to lowest J state.

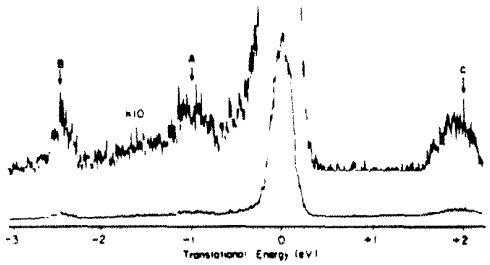

Fig. 2. Translational energy loss spectrum of $^{52}CrCH_2^+$ scattered from helium ($P_{He} = 6 \times 10^{-3}$ Torr). The feature marked "A" is from $^{52}CrCH_2^+$, while "B" and "C" are from mass impurities.

2.42 eV were not observed. The apparent collisional cross section for these excitation processes is small. This could be due to either a small value of the transition matrix elements linking these states, a small population of the initial states, or both [12,13].

The translational energy loss spectrum for $CrCH_2^+$ scattered from He is displayed in fig. 2. An excitation peak labeled "A" appears 1.05 eV lower in energy than the main beam. No superelastic (higher-energy) peaks or metastable transitions are observed. The other two peaks indicated in fig. 2 ("B" and "C") result from $^{54}CrC^+$ and $^{50}CrCH_4^+$, which have the same nominal mass as $^{52}CrCH_2^+$, but which otherwise have no bearing on the present study.

Table 2
Low-lying electronic states of $CrCH_2^+$ ion

State	Configuration	Energy (eV)
$^4B_1$	$Cr^+(^6S) + {}^3B_1\ CH_2$	0.00
$^6B_1$	$Cr^+(^6S) + {}^3B_1\ CH_2$	0.78
$^6A_1$	$Cr^+(^6S) + {}^1A_1\ CH_2$	0.82

The recent ab initio calculations of Carter and Goddard [8] for the electronic states of $CrCH_2^+$ can be used to assign the transitions observed in the translational energy loss spectrum of $CrCH_2^+$. The authors predict a $^4B_1$ ground state, which is best envisioned as a high-spin ^6S Cr^+ forming a *covalent* double bond with a $^3B_1$ CH_2 fragment. Two low-lying excited states were calculated: a $^6B_1$ state, consisting of a single covalent σ bond between ground-state (^6S) Cr^+ and CH_2, with the Cr^+ and CH_2 π electrons high-spin

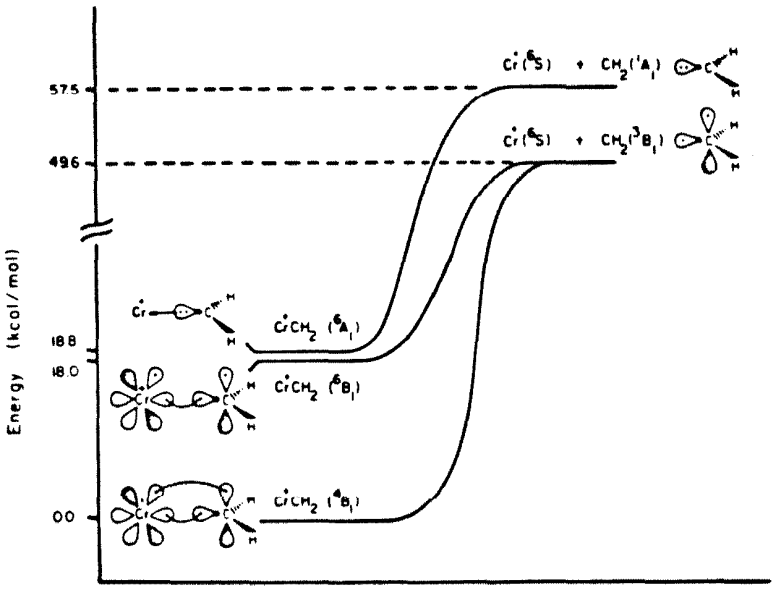

Fig. 3. Adiabatic electronic state correlation diagram for low-lying states of $^{52}CrCH_2^+$. Data from refs. [8,14].

coupled to the other valence d electrons, lies 18.0 kcal/mol (0.78 eV) above the $^4B_1$ ground state, and the $^6A_1$ state [14], composed of a single σ donor bond between the ground-state (^6S) Cr^+ and excited-state ($^1A_1$) CH_2, calculated to lie 18.8 kcal/mol (0.82 eV) above the $^4B_1$ ground state of $CrCH_2^+$. These results are summarized in table 2 and shown with schematical descriptions of the bonding orbitals in fig. 3.

The experimentally observed translational energy loss feature at 24.2 kcal/mol (1.05 ± 0.2 eV) obtained in this investigation is in good agreement with the theoretical predictions for electronic excitation of the $^4B_1$ ground state to either $^6B_1$ or $^6A_1$ states of $CrCH_2^+$. The calculations of Carter and Goddard [8] indicate that vibrational excitation (0.4 eV for the C–H stretch of the $^4B_1$ ground state and $^6B_1$ excited state) could also be resolved with this technique. There is no evidence for vibrational excitation of either the ground or excited state at this S/N ratio. In contrast to the translational energy loss spectrum of Cr^+ ions, where only spin allowed transitions are readily apparent, the $CrCH_2^+$ excitations are attributed to spin forbidden transitions, and the small cross section inferred from the weak signal is consistent with this assignment.

Unsaturated metal species such as $CrCH_2^+$ are of interest as prototypes for organometallic species implicated in numerous catalytic reactions. This study suggests that high-resolution translational energy loss spectroscopy can be successfully applied to investigations of the excited electronic states of a wide range of reactive organometallic species which can be formed in the gas phase. It is also encouraging that, in this case, the agreement between the experimental determination and the theoretical predictions is quite good.

Acknowledgement

This work was supported by the National Science Foundation under Grants No. CHE-8318041 (WAG), CHE-8020464 (MTB) and CHE-8407857 (JLB). Support from the Shell Development Company (WAG) and the Atlantic Richfield Foundation (MAH graduate fellowship) is gratefully acknowledged. EAC acknowledges a National Science Foundation predoctoral fellowship (1982–1985).

References

[1] L.F. Halle, P.B. Armentrout and J.L. Beauchamp, J. Am. Chem. Soc. 103 (1981) 962;
P.B. Armentrout and J.L. Beauchamp, J. Chem. Phys. 74 (1981) 2819.
[2] N. Aristov and P.B. Armentrout, J. Am. Chem. Soc. 106 (1984) 4065.
[3] M.L. Mandich, L.F. Halle and J.L. Beauchamp, J. Am. Soc. 106 (1984) 4403.
[4] D.P. Ridge, private communication.
[5] D. Jacobson and B.S. Freiser, J. Am. Chem. Soc. 107 (1985) 4373.
[6] D. Jacobson and B.S. Freiser, J. Am. Chem. Soc. 107 (1985) 4379.
[7] A.E. Stevens and J.L. Beauchamp, J. Am. Chem. Soc. 100 (1978) 2854, 101 (1979) 6449.
[8] E.A. Carter and W.A. Goddard III, J. Phys. Chem. 88 (1984) 1485.
[9] M.A. Vincent, Y. Yoshioka and H.F. Schaefer III, J. Phys. Chem. 86 (1982) 3905.
[10] A. Rappe and W.A. Goddard III, J. Am. Chem. Soc. 104 (1982) 448.
[11] C.E. Moore, NSRDS NBS 35 (1971) 10.
[12] A.J. Illies and M.T. Bowers, Chem. Phys. 65 (1982) 281.
[13] R.G. Cooks, ed., Collision spectroscopy (Plenum Press, New York, 1978).
[14] E.A. Carter and W.A. Goddard III, submitted for publication.